UNIVERSITÄT ZU LÜBECK

From the Institute of Chemistry
of the University of Lübeck
Director: Prof. Dr. rer. nat. Thomas Peters

Metabolic Studies and Quantification of Activated Sugar Nucleotides in Neuronal Cells, Astrocytes, and Other Mammalian Cells

Dissertation
for Fulfillment of
Requirements
for the Doctoral Degree
of the University of Lübeck

From the Department of Natural Sciences

Submitted by

Mailin Döpkens
from Osterode/Harz

Lübeck 2015

First referee: Professor Dr. Thomas Peters

Second referee: Professor Dr. Olaf Jöhren

Date of oral examination: 06.03.2015

Approved for printing. Lübeck, 09.03.2015

To my family and Niels.

Abstract

Uridine diphosphate-*N*-acetylglucosamine (UDP-GlcNAc) is an activated sugar nucleotide produced along the hexosamine biosynthetic pathway (HBP). This activated sugar is the donor substrate not only for glycosylation, but also for posttranslational *O*-GlcNAcylation of proteins. Other activated sugars are being produced in salvage pathways of the HBP. Changes in flux through the HBP either increase or decrease UDP-GlcNAc levels, affecting *O*-GlcNAcylation of many proteins. This modification not only plays an important role in many fundamental cellular processes, but also its dysregulation can lead to human diseases such as diabetes, Alzheimer's disease, and cancer. Alterations of UDP-GlcNAc levels may provide an indication of the development of metabolic disorders, making UDP-GlcNAc an ideal metabolic marker.

Perchloric acid (PCA) is widely used for extraction of water-soluble metabolites. Here I have shown that PCA extraction is not suitable for detection of activated sugar nucleotides in cell extracts, since most of these sugars are being degraded. However, methanol/chloroform (M/C) extraction is well suitable for quantitative detection of these metabolites, as shown by nuclear magnetic resonance (NMR) spectroscopy. I have identified five activated sugar nucleotides (UDP-GlcNAc, UDP-*N*-acetylgalactosamine (UDP-GalNAc), UDP-glucose (UDP-Glc), UDP-galactose (UDP-Gal), and UDP-glucuronic acid (UDP-GlcUA)) in different cell lines and primary astrocytes. Since the anomeric protons of activated sugar nucleotides resonate in a non-crowded region of the ^{1}H-NMR spectrum, quantification of corresponding nucleotides is straightforward. I determined nucleotide levels and showed that the abundance of activated sugar nucleotides is a cell-type specific feature. The highest levels of activated sugar nucleotides were found in astrocytes, indicating an important role of activated sugars in these brain cells.

Little is known about the intracellular concentration of activated sugar nucleotides involved in protein glycosylation and *O*-GlcNAcylation. Analysis of intracellular concentrations of sugar nucleotides may provide details for the understanding of protein glycosylation in different mammalian cells. In this work I investigated changes in the levels of activated sugar nucleotides after treatment with hexosamines (HexN), galactose, and in glucose-deprived cells. I showed that changes of the levels of these sugars are cell-specifically regulated and easily detectable using ^{1}H-NMR spectroscopy.

Nitric oxide (NO) is an important intercellular messenger in the brain. High concentrations of NO and its derivative peroxynitrite ($ONOO^{-}$), however, inhibit mitochondrial respiration and

the TCA cycle enzyme aconitase. It is suggested that NO plays a role in the development of neurodegenerative disorders. It was recently proposed that during inhibition of mitochondrial respiration and TCA cycle by NO, astrocytes switch into a glycolytic state to maintain energy production. In compliance with these earlier studies, I have shown, using [1-^{13}C]glucose as a precursor for selective labeling, that treatment with NO enhances glycolysis in primary cortical astrocytes. Inhibition of aconitase under these conditions was proven by massive citrate accumulation. Furthermore, NO induced a decrease in glutamate levels in astrocytes. Since normal flux through the TCA cycle is blocked because of aconitase inhibition, I assumed that glutamate serves as an alternative substrate to fuel and thereby partially maintains a segment of the TCA cycle.

UDP-GlcNAc can be easily detected in ^{1}H,^{13}C-heteronuclear single quantum coherence (^{1}H,^{13}C-HSQC) NMR spectra using [1-^{13}C]glucose as a precursor. Inhibition of mitochondrial respiration will block ^{13}C-label incorporation into UDP-GlcNAc. Although detection of enhanced glycolysis indicated that mitochondrial respiration was impaired in NO treated astrocytes, incorporation of the ^{13}C-label into UDP-GlcNAc was not affected. These results imply that mitochondrial respiration was not completely blocked in NO-treated astrocytes.

The two major hallmarks in the development of Alzheimer's disease are amyloid-ß (Aß) containing senile plaques and neurofibrillary tangles (NFTs) aggregated from hyperphosphorylated tau. Tau hyperphosphorylation involves reduced *O*-GlcNAcylation of the protein. There is strong evidence that Aß and tau pathologies are mechanistically linked. Aß is also associated with mitochondrial oxidative stress in Alzheimer's disease. It is discussed that inhibition of the mitochondrial respiratory chain by Aß is mediated by enhanced NO production. Here I report that treatment with Aß leads to significantly decreased UDP-GlcNAc levels in primary astrocytes but not in neuronal HT-22 cells. This decrease was most likely caused by inhibition of the mitochondrial respiratory chain. Following Aß exposure, I also observed an upregulation of glycolysis in astrocytes, possibly to maintain ATP-levels. I hypothesized that Aß-induced reduction in UDP-GlcNAc levels in astrocytes may be at least one possible factor contributing to decreased *O*-GlcNAcylation and thus hyperphosphorylation of tau in Alzheimer's disease. My results further corroborate that astrocytes and neurons respond differently to treatment with Aß and that astrocytes may play a major role in the pathogenesis of Alzheimer's disease. In addition, the results also confirm the assumption that accumulation of Aß precedes hyperphosphorylation of tau and thus NFT formation. Moreover, these results imply that Aß cannot exert its toxic action by enhanced

NO production alone, because a reduction in UDP-GlcNAc levels was not observed in NO-treated astrocytes.

In this thesis I have shown that experiments focussing on the detection of activated sugar nucleotides in diseases displaying aberrant *O*-GlcNAc modification profiles such as diabetes and Alzheimer's disease may provide new insights into mechanisms of disease onset and progression.

Zusammenfassung

Uridindiphosphat-*N*-Acetylglucosamin (UDP-GlcNAc) ist ein aktiviertes Zuckernukleotid, das im Hexosamin-Biosyntheseweg (HBP) synthetisiert wird. UDP-GlcNAc ist nicht nur ein Donorsubstrat für Glykosylierungen, sondern auch für die posttranslationale *O*-GlcNAcylierung von Proteinen. Weitere aktivierte Zucker werden in Wiederverwertungsstoffwechselwegen (*Salvage Pathways*) des HBP produziert. Veränderungen im Nährstofffluss durch den HBP erhöhen oder erniedrigen die Konzentration von UDP-GlcNAc, was sich wiederum auf die *O*-GlcNAcylierung vieler Proteine auswirkt. Die *O*-GlcNAc-Modifikation spielt eine wichtige Rolle bei vielen grundlegenden zellulären Prozessen und eine Fehlregulation kann zu Krankheiten wie Diabetes, Alzheimer und Krebs führen. Veränderungen des zellulären UDP-GlcNAc-Spiegels können daher Hinweise auf die Entwicklung von Stoffwechselstörungen geben, was UDP-GlcNAc zu einem idealen metabolischen Marker macht.

Perchlorsäure wird häufig zur Extraktion von wasserlöslichen Metaboliten aus Zellen verwendet. In dieser Arbeit habe ich gezeigt, dass Perchlorsäure-Extraktion nicht geeignet ist, um aktivierte Zuckernukleotide zu detektieren, da vieler dieser Zucker säurehydrolyse-empfindlich sind. Mit Hilfe von Kernspinmagnetresonanzspektroskopie (NMR-Spektroskopie) konnte ich zeigen, dass die Methanol/Chloroform-Extraktion hingegen sehr gut geeignet ist, um aktivierte Zucker zu detektieren. In verschiedenen Zelllinien als auch primären Astrozyten, konnte ich 5 verschiedene aktivierte Zucker identifizieren (UDP-GlcNAc, UDP-*N*-Acetylgalactosamin (UDP-GalNAc), UDP-Glucose (UDP-Glc), UDP-Galactose (UDP-Gal) und UDP-Glucuronsäure (UDP-GlcUA)). Da die Frequenzen der anomeren Protonen der aktivierten Zucker in einer Region des Spektrums resonieren, in denen es zu keiner Überlagerung mit Signalen anderer Metabolite kommt, ist eine quantitative Analyse der Zucker möglich. Die Quantifizierung zeigte, dass die Konzentrationen der einzelnen Zucker ein zellspezifisches Merkmal sind. Die höchsten Konzentrationen wurden in primären Astrozyten detektiert. Dies deutet darauf hin, dass aktivierte Zuckernukleotide eine wichtige Rolle in diesen Gehirnzellen spielen.

Bisher ist wenig über die Regulation intrazellulärer Konzentrationen von aktivierten Zuckernukleotiden bekannt. Die Analyse der Konzentrationen kann dazu beitragen, dass wichtige Details, die zum Verständnis von Protein-Glycosylierungen und *O*-GlcNAcylierungen beitragen, aufgedeckt werden. Im Rahmen dieser Arbeit wurden Veränderungen in den Konzentrationen der aktivierten Zuckernukleotide nach Behandlung

mit Hexosaminen (HexN) und Galactose sowie nach Glucoseentzug in verschiedenen Zelltypen untersucht. Es wurde gezeigt, dass Veränderungen der Konzentrationen dieser Zucker zellspezifisch geregelt und leicht mittels ^{1}H-NMR-Spektroskopie nachweisbar sind.

Stickstoffmonoxid (NO) ist ein wichtiger interzellulärer Botenstoff im Gehirn. Hohe Konzentrationen an NO und seinem Folgeprodukt Peroxinitrit inhibieren jedoch die mitochondriale Atmungskette sowie das TCA-Zyklus Enzym Aconitase. NO ist vermutlich an der Entstehung neurodegenerativer Krankheiten beteiligt. Es wurde kürzlich gezeigt, dass Astrozyten, während der Hemmung der mitochondrialen Atmung durch NO, ihren glykolytischen Energieumsatz erhöhen, um die Energieproduktion aufrecht zu erhalten. In Übereinstimmung mit diesen früheren Studien habe ich mit [1-^{13}C]Glucose als selektiv markierte Vorstufe gezeigt, dass die Behandlung mit NO die Glykolyserate in primären kortikalen Astrozyten erhöht. Massive Citrat-Akkumulierung unter diesen Umständen wies die Hemmung der Aconitase nach. Darüber hinaus habe ich detektiert, dass durch NO eine Abnahme des Glutamatspiegels in Astrozyten ausgelöst wird. Da der normale Fluss durch den TCA-Zyklus durch die Hemmung der Aconitase blockiert ist, vermute ich, dass Glutamat als ein alternatives Substrat in den TCA-Zyklus eingespeist wird, um zumindest den Fluss durch ein Teilsegment des Zyklus‘ aufrechtzuerhalten.

UDP-GlcNAc kann in ^{1}H,^{13}C-*Heteronuclear Single Quantum Coherence* (^{1}H,^{13}C-HSQC) NMR Spektren unter Verwendung von [1-^{13}C]Glucose als Vorstufe detektiert werden. Hemmung der Atmungskette führt dazu, dass kein weiteres ^{13}C-Label mehr in das UDP-GlcNAc Molekül eingebaut werden kann. Obwohl die erhöhte Glykolyse darauf hinwies, dass die Atmungskette durch NO in Astrozyten gehemmt ist, wurde der Einbau des ^{13}C-Labels in UDP-GlcNAc nicht beeinflusst. Diese deutet darauf hin, dass die mitochondriale Atmung in NO-behandelten Astrozyten nicht vollständig gehemmt wird.

Die zwei Hauptmerkmale bei der Entstehung von Alzheimer sind Senile Plaques, bestehend aus Ablagerungen des Amyloid-ß (Aß) Proteins sowie Neurofibrilläre Bündel (*Neurofibrillary Tangles*; NFT) aus hyperphosphoryliertem Tau-Protein. Die Hyperphosphorylierung von Tau wird durch eine Erniedrigung der *O*-GlcNAcylierung des Proteins ausgelöst. Vieles deutet darauf hin, dass Aß- und Tau-Pathologien mechanistisch verknüpft sind. Aß wird außerdem mit oxidativem Stress in Alzheimer in Verbindung gebracht. Es wird diskutiert, dass Aß die mitochondriale Atmungskette durch erhöhte NO-Produktion hemmt. In dieser Arbeit berichte ich, dass die Behandlung mit Aß zu signifikant

erniedrigten UDP-GlcNAc Konzentrationen in primären Astrozyten führt. Dieser Effekt wurde nicht in neuronalen HT-22 Zellen beobachtet. Die Erniedrigung der UDP-GlcNAc Konzentration wird höchstwahrscheinlich durch Hemmung der Atmungskette ausgelöst, da wir gleichzeitig eine Erhöhung der Glykolyserate detektiert haben - wahrscheinlich um die ATP-Synthese aufrecht zu erhalten. Ich vermute, dass die durch Aß-Behandlung ausgelöste Erniedrigung der UDP-GlcNAc Konzentration in Astrozyten zumindest ein möglicher Faktor ist, der zur Erniedrigung der *O*-GlcNAcylierung und dadurch zur Hyperphosphorylierung von Tau in Alzheimer beiträgt. Meine Ergebnisse bestätigen außerdem, dass Astrozyten und Neuronen unterschiedlich auf die Behandlung mit Aß reagieren und dass Astrozyten möglicherweise eine wichtige Rolle bei der Entstehung von Alzheimer spielen. Zusätzlich bestärken meine Ergebnisse die Annahme, dass die Akkumulierung von Aß der Hyperphosphorylierung von Tau vorausgeht. Des Weiteren deuten die Ergebnisse darauf hin, dass die durch Aß ausgelöste Toxizität nicht allein durch erhöhte NO-Produktion zustande kommt, da die Behandlung mit NO allein nicht zu einer Reduktion der UDP-GlcNAc Konzentration führte.

In dieser Arbeit konnte gezeigt werden, dass die Detektion und Quantifizierung von aktivierten Zuckernukleotiden neue Erkenntnisse über den Mechanismus von Krankheiten, die Veränderungen in der *O*-GlcNAcylierung von Proteinen aufweisen, liefern kann.

Content

Abbreviations

acetyl-CoA	acetyl-coenzyme A
ADP	adenosine diphosphate
Ala	alanine
AMPK	AMP-activated protein kinase
ANLSH	astrocyte–neuron lactate shuttle hypothesis
AP-3	clathrin assembly protein-3
APP	amyloid precursor protein
Asn	asparagine
Asp	aspartate
Aß	amyloid-ß
ATP	adenosine triphosphate
BEMAD	mild ß-elimination followed Michael addition with dithiothreitol
BH_4	tetrahydrobiopterin
CaMKII	calcium/calmodulin-dependent kinase
cGMP	cyclic guanosine monophosphate
CHO	chinese hamster ovarian cells
CIC	citrate carrier
CMP	cytidine monophosphate
CMP-NeuNAc	cytidine monophosphate-*N*-acetylneuraminic acid
CNS	central nervous system
CTP	cytidine triphosphate
Da	dalton
DCC	*N*,*N*'-Dicyclohexylcarbodiimid
dd	doublet of doublets
ddd	doublet of doublet of doublets
DETA-NONOate	(Z)-1-[N-(2-aminoethyl)-N-(2-ammonioethyl)amino]diazen-1-ium-1,2-diolate
DMEM	Dulbecco's modified Eagle's medium
DON	6-diazo-5-oxo-L-norleucine
EDTA	ethylenediaminetetraacetic acid
ENO1	enolase 1
eNOS	endothelial nitric oxide synthase
eqn	equation

ER	endoplasmatic reticulum
ETD	ion-trap mass spectrometry with electron-transfer dissociation
FAD	flavin adenine dinucleotide (oxidized form)
$FADH_2$	flavin adenine dinucleotide (reduced form)
FCS	fetal calf serum
FDG	fluorodeoxyglucose
FMN	flavin mononucleotide
Fru-1,6-BP	fructose-1,6-bisphosphate
Fru-2,6-BP	fructose-2,6-bisphosphate
Fru-6-P	fructose-6-phosphate
Fuc	fucose
Fuc-1-P	fucose-1-phosphate
GABA	γ-aminobutyric acid
GAG	glycosaminoglycan
Gal	galactose
Gal-1-P	galactose-1-phosphate
GALE	UDP-glucose 4-epimerase / UDP-galactose 4-epimerase
GALK	galactokinase
GalN	galactosamine (2-deoxy-2-amino-D-galactose)
GalN-1-P	galactosamine-1-phosphate
GalNAc	*N*-acetylgalactosamine
GALT	galactose-1-phosphate uridylyltransferase
GAPDH	glyceraldehyde-3-phosphate dehydrogenase
GDH	glutamate dehydrogenase
GDP-Fuc	guanosine diphosphate-fucose
GDP-Man	guanosine diphosphate-mannose
GFAT	glutamine-fructose-6-P aminotransferase
Glc	glucose
Glc-1,2-cyclo-P	glucose-1,2-cyclo-phosphate
Glc-1-P	glucose-1-phosphate
Glc-2-P	glucose-2-phosphate
Glc-6-P	glucose-6-phosphate
GlcN	glucosamine (2-deoxy-2-amino-D-glucose)
GlcN 6-P *N*-	glucosamine-6-P *N*-acetyltransferase

acetyltransferase	
GlcN-6-P	glucosamine-6-phosphate
GlcNAc	*N*-acetylglucosamine
GlcNAc-1-P	*N*-acetylglucosamine-1-phosphate
GlcUA	glucuronic acid
GlcUA-1,2-cyclo-P	glucuronic acid-1,2-cyclo-phosphate
GlcUA-1-P	glucuronic acid-1-phosphate
GlcUA-2-P	glucuronic acid-2-phosphate
Gln	glutamine
Glu	glutamate
GLUT	glucose transporter
GPI	glycophosphatidylinositol
GS	glutamine synthetase
GSH	glutathione (L-γ-glutamyl-L-cysteinylglycine)
GSK-3	glycogen synthase kinase-3
GSSG	glutathione disulfide
GTP	guanosine triphosphate
HBP	hexosamine biosynthetic pathway
HEK293	human embryonic kidney cells
HexN	hexosamine
HexNAc	*N*-acetylhexosamine
HIF	hypoxia-inducible factor
HK2	hexokinase 2
HMBC	heteronuclear multiple bond correlation
HPLC	high-performance liquid chromatography
HRE	hypoxia-response element
HSQC	heteronuclear single quantum coherence
HT-22	immortalized clonal mouse hippocampal neuronal cell line
IdoA	iduronic acid
iNOS	inducible nitric oxide synthase
IRP1	iron-responsive element 1
IRS-1	insulin receptor substrate-1
kDA	kilodalton
Lac	lactate

LDH	lactate dehydrogenase
LDHA	lactate dehydrogenase A
L-NAME	N_{ω}-nitro-L-arginine methyl ester
M/C	methanol/chloroform
Man	mannose
Man-1-P	mannose-1-phosphate
Man-6-P	mannose-6-phosphate
ManN	mannosamine (2-deoxy-2-amino-D-mannose)
ManNAc	*N*-acetylmannosamine
ManNAc-6-P	*N*-acetylmannosamine-6-phosphate
MAPK	mitogen-activated protein kinase
MCT	monocarboxylate transporter
MDBK	Madin-Darby bovine kidney cells
MGEA5	meningioma-expressed antigen 5
mRNA	messenger ribonucleic acid
MRS	magnetic resonance spectroscopy
mtNOS	mitochondrial nitric oxide synthase
NaCT	sodium-dependent citrate transporter
NAD^+	nicotinamide adenine dinucleotide (oxidized form)
NADH	nicotinamide adenine dinucleotide (reduced form)
$NADP^+$	nicotinamide adenine dinucleotide phosphate (oxidized form)
NADPH	nicotinamide adenine dinucleotide phosphate (reduced form)
NeuNAc	*N*-acetylneuraminic acid
NeuNAc-9-P	*N*-acetylneuraminic acid-9-phosphate
NFT	neurofibrillary tangles
NMDA	*N*-methyl-D-aspartate
NMR	nuclear magnetic resonance
nNOS	neuronal nitric oxide synthase
NO	nitric oxide
NOHA	N^{ω}-hydroxyl-arginine
NOS	NO synthase
OGA	*O*-GlcNAcase (ß-*N*-acetylglucosaminidase)
O-GlcNAc	*O*-linked-ß-*N*-acetylglucosamine
OGT	*O*-GlcNAc transferase (uridine diphospho-*N*-acetylglucosamine:

	polypeptide ß-*N*-acetylglucosaminyltransferase)
$ONOO^-$	peroxinitrite
PAG	phosphate-activated glutaminase
PAI-1	plasminogen activator inhibitor-1
PARP-1	poly(ADP-ribose) polymerase-1
PBS	phosphate buffered saline
PCA	perchloric acid
PDC	pyruvate dehydrogenase complex
PDH	pyruvate dehydrogenase
PDK1	pyruvate dehydrogenase kinase 1
PDX-1	pancreatic duodenal homeobox-1
PEP	phosphoenolpyruvate
PET	positron emission tomography
PFK	phosphofructokinase
PFKFB	6-phosphofructo-2-kinase/fructose-2,6-bisphosphatase
PGK1	phosphoglycerate kinase 1
PHD	prolyl hydroxylase
P_i	inorganic phosphate
PI3K	phosphatidylinositol-4,5-bisphosphate 3-kinase
PP2A	protein phosphatase 2A
PP_i	inorganic pyrophosphate
ppm	parts per million
PPP	pentose phosphate pathway
PTP	permeability transition pore
PUGNAC	*O*-(2-acetamido-2-deoxy-D-glucopyranosylidene) amino *N*-phenylcarbamate
qRT-PCR	quantitative real-time polymerase chain reaction
ROS	reactive oxygen species
RT	room temperature
s	singlet
Ser	serine
sGC	soluble guanylate cyclase
Sulfo-NONOate	(E)-1-sulfonatodiazen-1-ium-1,2-diolate
Tau	tubulin associated protein

TCA	trichloroacetic acid
TCA cycle	tricarboxylic acid cycle
Thr	threonine
TMS-ECD	Fourier transform mass spectrometry with electron-capture dissociation
TOM	translocase of the outer membrane
TSP	3-(trimethylsilyl)propionic-2,2,3,3-d_4 acid
UDP	uridine phosphate
UDP-Gal	uridine phosphate-galactose
UDP-GalNAc	uridine diphosphate-*N*-acetylgalactosamine
UDP-Glc	uridine diphosphate-glucose
UDP-GlcNAc	uridine diphosphate-*N*-acetylglucosamine
UDP-GlcNAc pyrophosphorylase	UDP-*N*-acetylglucosamine pyrophosphorylase
UDP-GlcUA	uridine diphosphate-glucuronic acid
UDP-Hex	uridine diphosphate-hexoses (UDP-Glc + UDP-Gal)
UDP-Hex(NAc)	uridine diphosphate-(*N*-acetyl-)hexoses (UDP-Glc + UDP-Gal + UDP-GlcNAc + UDP-GalNAc)
UDP-HexNAc	uridine diphosphate-*N*-acetyl-hexoses (UDP-GlcNAc + UDP-GalNAc)
UMP	uridine monophosphate
UTP	uridine triphosphate
α-KGDH	α-ketoglutarate dehydrogenase
$\Delta\Psi_m$	mitochondrial membrane potential

1 Introduction

1.1 Metabolic Studies Using NMR Spectroscopy

Pathological processes in a cell are reflected by changes in the metabolic pathways. Analysis and quantification of metabolites can therefore provide valuable information about the role of metabolites in normal and pathological conditions. Understanding the biochemical processes that lead to certain diseases can help to develop new therapeutic approaches or diagnostics.
Even though nuclear magnetic resonance (NMR) spectroscopy is less sensitive than other biochemical tracer studies, it has the advantages of being noninvasive, nondestructive, and does not require metabolite isolation. It also allows simultaneous nonselective metabolite detection and quantification through various metabolic pathways, such as glycolysis, tricarboxylic acid cycle (TCA cycle), and fatty acid metabolism. For this reason NMR spectroscopy has become well established for studies of metabolite levels *in vivo* and *in vitro*. Metabolites of cell and tissue extracts, body fluids (e.g. blood, urine, cerebrospinal fluid), or intact (perfused) cells can be directly detected and quantified in one single experiment.

By now, NMR spectroscopy on cellular metabolites is well established using ^{1}H, ^{13}C, ^{31}P, and ^{15}N as NMR active nuclei with biological relevance. The most widely used NMR active nuclei for studying metabolites from cells and tissues is proton- (^{1}H-)NMR spectroscopy. In general, all small metabolites (< 1 kDa) with a concentration in the mircomolar range that contain protons can be detected (Serkova & Glunde, 2009). For conventional NMR analyses, the required cells mass is usually $10^{7} – 10^{8}$ cells per cell extract. In ^{1}H-NMR spectra from body fluids and tissue extracts more than 100 metabolites can be detected (Nicholson & Wilson, 1989). The obtained spectra are complex, exhibiting overcrowded regions of overlapping signals which often prevents correct signal assignments and hampers accurate quantification of metabolites. A better signal separation can be obtained by 2D-^{1}H,^{13}C-NMR experiments, such as heteronuclear single quantum coherence (HSQC) or heteronuclear multiple bond correlation (HMBC). Since the experiments are inverse correlated (the high-sensitivity nucleus ^{1}H is excited and detected) they are not only easier to interpret, but also have higher sensitivity than standard 1D-^{13}C-NMR spectra. These 2D-^{1}H,^{13}C-NMR experiments are proven to be well suited for the identification of metabolites in cell extracts (Willker *et al.*, 1996). Furthermore, by using ^{13}C-labeled precursors (e.g. [1-^{13}C]glucose) dynamic fluxes through different metabolic pathways can be monitored (Zwingmann & Leibfritz, 2003). Moreover, NMR spectroscopy can detect unexpected aberrant metabolic

profiles that may not be observed using other methods that concentrate on a particular metabolite or enzymatic pathway. The great improvement in sensitivity due to the availability of high magnetic field strengths and the development of cryoprobes that enhance the signal-to-noise ratio of up to 4-fold allow now measurements of less concentrated samples in appropriate acquisition times (Keun *et al*., 2002).

Another considerable advantage of NMR is that metabolic markers that were discovered *in vitro* by high-resolution NMR-spectroscopy can often be translated into *in vivo* protocols using noninvasive localized magnetic resonance spectroscopy (MRS) (Serkova *et al*., 2009). Nevertheless, especially in the brain, studies of homogenous *in vitro* cell cultures are necessary. Studies using intact brain can be problematical since the tissue consists of metabolically different brain regions and cell types, such as neurons and astrocytes. *In vivo* MRS of the brain therefore unavoidably detects metabolites of different cell types exhibiting different metabolic characteristics (Michaelis *et al*., 1991). For that reason, cell lines and primary cultures of brain cells are often used to study brain metabolism before investigating their role in *in vivo* studies. In this context, the analysis of cell culture media is of particular interest to monitor metabolic trafficking and cell export processes (Willker *et al*., 1996).

In the present thesis cell extracts and media samples of mainly neuronal cells and primary astrocytes were investigated, whereby focus was laid on the metabolism of activated sugar nucleotides and in particular UDP-GlcNAc. ^{1}H-NMR, as well as, ^{1}H,^{13}C-HSQC experiments using [1-^{13}C]glucose as a precursor were performed.

1.2 Sample Preparation

Growing interest in metabolite profiling has increased the need for simple and efficient metabolite extraction methods. Thus, an essential aspect in metabolite profiling analyses has been the development and optimization of metabolite extraction methods.

Sample handling is a critical step when investigating biological material, since biochemical degradation due to enzymatic activities proceeds very rapidly. To reduce enzyme activities it is important to work at low temperatures during the whole process of sample collection and cell extraction. Not only should samples be kept on ice, solvents used should also be ice-cold.

Furthermore, to retain reproducibility it is of importance to maintain the period of time between sample collection as short as possible and at the same time of equal length.
Apart from enzymatic degradation, the extraction solvent itself can lead to decomposition of labile metabolites. These effects can also be reduced to a certain extent by working on ice and in a timely manner. In respect thereof, the selection of a suitable extraction solvent is of particular importance. The type of extraction method to be selected greatly depends on the metabolites investigated and on the analytical method employed.

The following requirements should be generally fulfilled:

- high efficiency (high metabolite yield; quantitative recovery of metabolites)
- good reproducibility
- no degradation of labile metabolites (e.g. acid hydrolysis)
- inhibition of consecutive enzymatic reactions
- low variability
- fast (high-throughput studies)

Cellular enzymes (proteins) exhibit broad signals due to their short T2 relaxation times. These signals interfere with signals of small metabolites present in water-soluble cell extracts. Therefore, unwanted proteins have to be removed by precipitation. Several methods have been developed for protein precipitation. Proteins can be precipitated by influencing pH, ionic strength, and/or temperature (Englard & Seifter, 1990). This being the case, proteins can be precipitated by using acids, organic solvents, inorganic salts, or metal ions (see Table 1) (McDowall, 1989).

Table 1. Reagents used for protein precipitation (according to Blanchard, 1981; McDowall, 1989).

Precipitant	Example
acids	trichloroacetic acid (TCA) perchloric acid (PCA)
organic solvents	acetonitrile acetone ethanol methanol
inorganic salts	ammonium sulfate
metal ions	copper ions zinc ions

Trichloroacetic acid (TCA) and perchloric acid (PCA) form insoluble salts with the cationic form of the proteins at low pH (McDowall, 1989). Both precipitants are commonly used as 5 - 20 % solutions. TCA and PCA are very efficient at precipitating proteins (McDowall, 1989). However, the main disadvantage is that the pH of the supernatant is very low and the metabolites to be investigated must be stable against acid hydrolysis. Supernatants of PCA extracts commonly exhibit a pH of < 1,5 and TCA supernatants a pH of 1,4 - 2,0 (Blanchard, 1981).

Organic solvents, such as acetonitrile, acetone, ethanol, and methanol act by lowering the solubility of proteins and thus precipitating them from the solution (Lim, 1988). Organic solvents were found to be less effective in protein precipitation compared to acids (McDowall, 1989). Nevertheless, the great advantage is that the pH remains near the physiological range.

The effectiveness in protein precipitation in descending order is as follows (McDowall, 1989):

acetonitrile > acetone > ethanol > methanol

Proteins can also be eliminated by metal ions, such as copper or zinc in alkaline solution by forming insoluble salts (McDowall, 1989). However, metal ions interfere with subsequent NMR analysis and are therefore not suitable for extraction.

Ammonium sulphate denatures proteins reversibly and has been used as a precipitant for many years. However, precipitation using ammonium sulfate is not efficient (< 75 %) (McDowall, 1989).

Of the above-mentioned methods, PCA is widely used for extraction of water-soluble metabolites. An extraction method for cellular lipids, using methanol and chloroform, was first described by Folch *et al.*, 1957. This method was later modified by Bligh and Dyer, 1959 using smaller solvent volumes. The solvent ratios (methanol/chloroform/water) were based on the water content of the sample in such a way that two phases develop; the chloroform phase containing all lipids and the methanol/water phase containing all the water-soluble metabolites. A layer of precipitated proteins develops between the two samples. Although the Bligh and Dyer method meets the requirement to extract both lipids and water-soluble metabolites it was merely used for lipid extraction. Previous lipid extraction methods, such as the Folch's method, were unsuitable because of the high salt content in the phase of the water-soluble metabolites which were added during the extraction procedure.

In 1996 Tyagi *et al*. developed a similar extraction that simultaneously and quantitatively recovers both the water-soluble metabolites from the methanol/water phase and the lipids from the chloroform phase from one single sample (dual-phase extraction). Cells were extracted with methanol, chloroform, and water at a ratio of 1:1:1 (v/v/v). Evaluation of the new procedure was done by ^{31}P- and ^{13}C-NMR spectroscopy: The metabolite content determined from the upper phase of the dual-phase extraction compared well with the metabolite yield from PCA extracted water-soluble metabolites. The lower chloroform phase containing all the lipids compared well with lipids extracted by the Folch's method (Tyagi *et al*., 1996). This method allows simultaneous monitoring of enzymatic pathways that bridge both cellular components, e.g. phospholipids and its water-soluble precursor choline, both playing an important role in the development of breast cancer (Glunde *et al*., 2004). Another great advantage of this methanol/chloroform (M/C) extraction is that the pH remains near the physiological range minimizing the degradation of (acid-)labile metabolites. There is evidence that PCA extraction leads to decomposition of water-soluble, as well as hydrophobic phosphate containing intermediates (Katyal *et al*., 1985; Hawkins *et al*., 1987; Tyagi *et al*., 1996).

PCA extracts have to be neutralized with KOH leading to formation of a huge precipitate of potassium perchlorate ($KClO_4$) which has to be removed by centrifugation. There is always continued precipitation of $KClO_4$, even in the dried residue of the extract. Repeated centrifugation to remove the precipitate results in loss of metabolite yield by co-precipitation and alterations of extract volume. Besides, not all perchlorate is precipitable and may interfere heavily with subsequent analytical investigations (Tyagi *et al*., 1996). The extract of the water-soluble phase of M/C extracts by contrast contains minimal amounts of salts, being an advantage for any subsequent analytical method. The lyophilized residue is very small and can be re-dissolved in much smaller volumes of D_2O for NMR analysis facilitating to record adequate NMR spectra in shorter acquisition times or using less cell mass (Tyagi *et al*.,1996).
Decomposition of acid-labile metabolites, formation of a huge $KClO_4$ precipitate, as well as the additional centrifugation steps to remove the precipitate certainly contribute to a higher variability in metabolite yield in the PCA method compared to the M/C technique. A higher extraction efficiency and lower variability of the M/C technique was investigated in extracts of M2R mouse melanoma cells (Tyagi *et al*., 1996), tissue of rat brain and cultured astrocytes (Le Belle *et al*., 2002), and in CHO cells (Sellick *et al*., 2010).
In M/C extractions consistently higher lactate levels were detected which may indicate that enzyme inactivation is not as efficient as in PCA extracts. However, a possible overlap of the

lactate signal with a broad signal from not completely removed protein and/or lipid in the M/C extract was also discussed (Le Belle *et al*., 2002). A schematic overview of the PCA and M/C extraction is depicted in Figure 1.

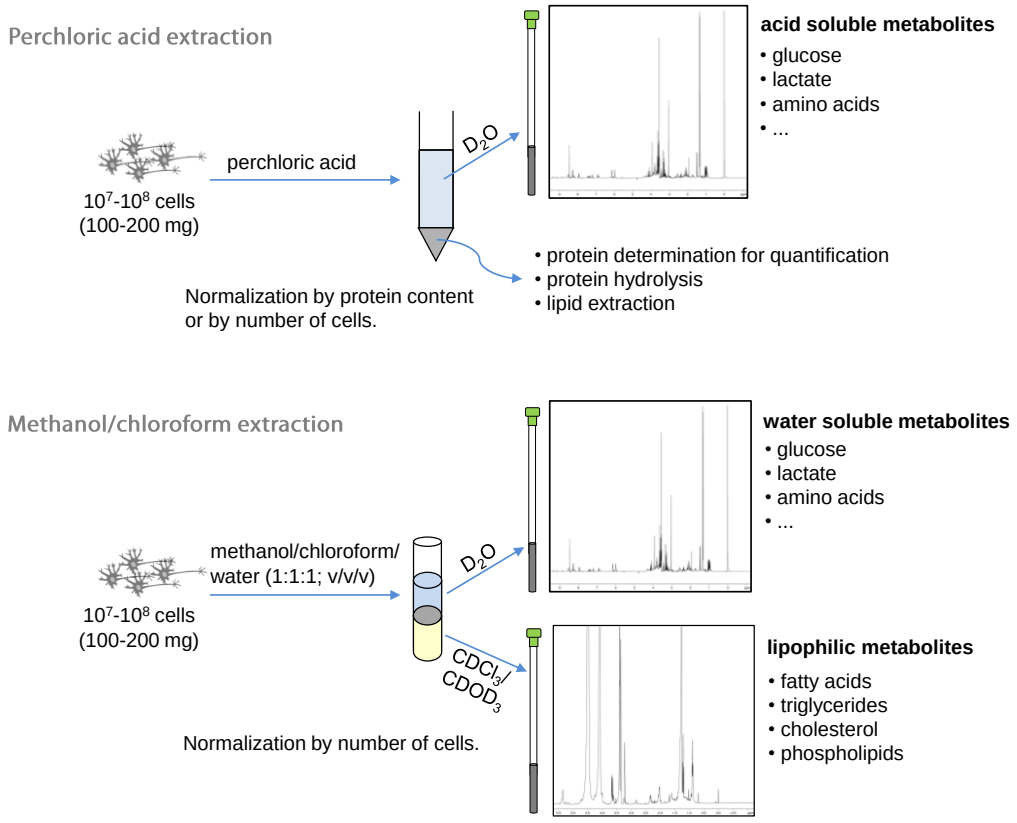

Figure 1. Sample preparation using perchloric acid and methanol/chloroform (dual-phase) extraction with subsequent analysis by NMR spectroscopy (adapted from Serkova & Glunde, 2009).

1.3 The Hexosamine Biosynthetic Pathway

Uridine diphosphate-*N*-acetylglucosamine (UDP-GlcNAc)[1] is a so called activated sugar nucleotide - or activated sugar for short - and the major product of the hexosamine biosynthetic pathway (HBP; see Figure 2). After entering the cell glucose is rapidly phosphorylated to glucose-6-phosphate (Glc-6-P) which is isomerized in a second step to fructose-6-phosphate (Fru-6-P). Fru-6-P can either be oxidized to pyruvate via glycolysis or can enter the HBP. Approximately 2 - 5 % (depending on cell type) of the intracellular glucose is diverted to HBP (Marshall *et al*., 1991a; Hawkins *et al*., 1997). The first and rate-

[1] For the sake of simplicity, the symbols D- and L- as well as α- and ß- are omitted from the names of activated sugar nucleotides and other monosaccharides. The symbols will only be used when needed for distinction.

limiting step of the HBP is the formation of glucosamine-6-phosphate (GlcN-6-P) with glutamine as the amine donor by the enzyme glutamine-fructose-6-P aminotransferase (GFAT; EC 2.6.1.16) (Kornfeld, 1967). In the next step an acetyl group which derives from acetyl-coenzyme A (acetyl-CoA) is transferred by the enzyme glucosamine-6-P *N*-acetyltransferase (GlcN-6-P *N*-acetyltransferase; EC 2.1.3.4) to yield *N*-acetylglucosamine-1-phosphate (GlcNAc-1-P) (Davidson *et al*., 1957). The last step of the pathway is the transfer of uridine triphosphate (UTP) to GlcNAc-1-P to give UDP-GlcNAc, the final product of the pathway. This step is catalyzed by the enzyme UDP-*N*-acetylglucosamine pyrophosphorylase (UDP-GlcNAc pyrophosphorylase; EC 2.7.7.23) (Strominger & Smith, 1959).

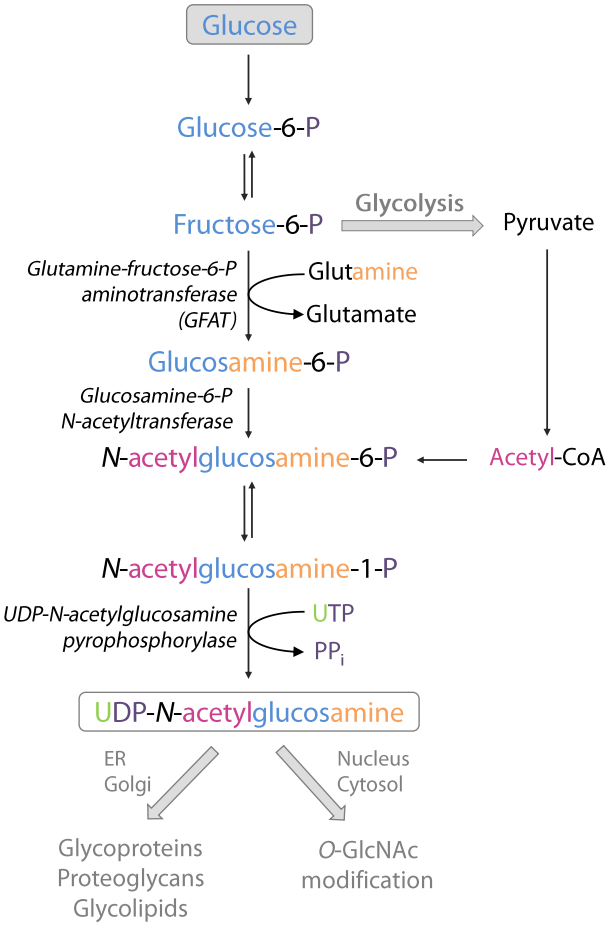

Figure 2. Synthesis of UDP-*N*-acetylglucosamine (UDP-GlcNAc) from glucose in the hexosamine biosynthetic pathway (HBP). The key enzymes involved in the HBP are shown in italics. The rate limiting enzyme of the pathway is glutamine-fructose-6-P aminotransferase (GFAT), which transfers the amine group from glutamine to fructose-6-P to generate glucosamine-6-P. Glucosamine-6-P is acetylated by glucosamine-6-P *N*-acetyltransferase (GlcN-6-P *N*-acetyltransferase) to produce *N*-acetylglucosamine-6-P. UDP-*N*-acetylglucosamine pyrophosphorylase (UDP-GlcNAc pyrophosphorylase) catalyzes the transfer of UTP to *N*-acetylglucosamine-1-P to give UDP-GlcNAc, the final product of the pathway. UDP-GlcNAc is the precursor for glycoproteins, proteoglycans, glycolipids, and *O*-GlcNAcylation of proteins (for the latter see also Chapter 1.6). CoA, coenzyme A; ER, endoplasmatic reticulum; PP_i, pyrophosphate; UDP, uridine diphosphate; UTP, uridine triphosphate.

The biosynthesis of UDP-GlcNAc is complex, as different metabolic pathways are concurrently involved (Figure 3): The ribose and uracil moieties of the nucleotide are

incorporated via pentose phosphate pathway (PPP) and pyrimidine synthesis. The utilization of glutamine potentially links the HBP with amino acid metabolism. UDP-GlcNAc derives its acetyl group from acetyl-CoA. Acetyl-CoA cannot be directly incorporated into UDP-GlcNAc via transformation of pyruvate into acetyl-CoA by the pyruvate dehydrogenase complex (PDC) in the mitochondrion, because acetyl-CoA itself cannot pass the mitochondrial membrane and the HBP happens in the cytosol. Intramitochondrial acetyl-CoA and oxaloacetate merge in the TCA cycle to form citrate, which is transported out of the mitochondria and cleaved by ATP-citrate-lyase to oxaloacetate and cytosolic acetyl-CoA. The incorporation of acetyl-CoA into UDP-GlcNAc therefore involves glycolysis (to form pyruvate), PDC to generate mitochondrial acetyl-CoA, TCA cycle, and ATP-citrate lyase. Since cytosolic acetyl-CoA is a key precursor for fatty acid biosynthesis, the incorporation into UDP-GlcNAc links the HBP to fatty acid metabolism. Fortunately, several key metabolites of these pathways, including lactate and glucose can be readily identified and quantified by NMR spectroscopy.

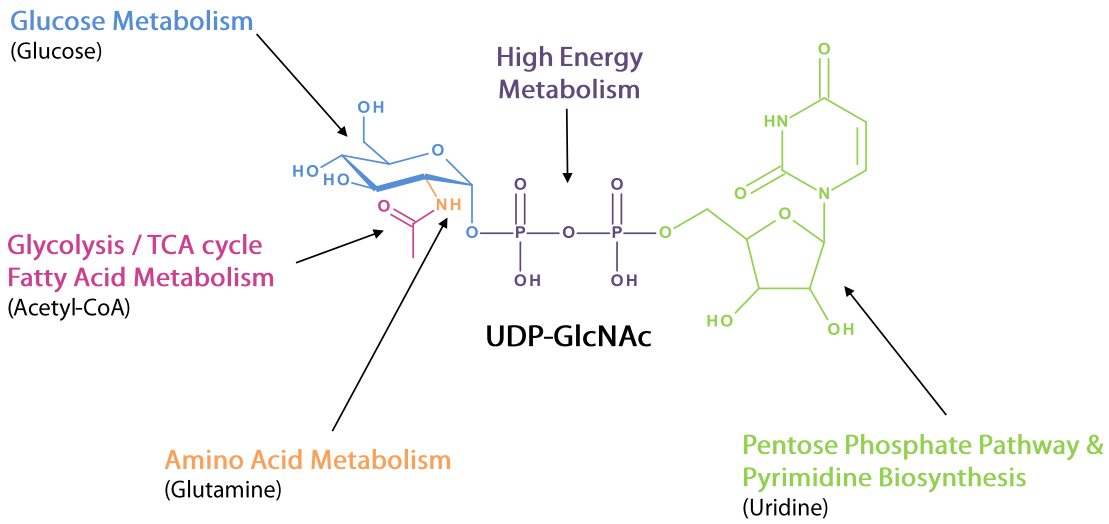

Figure 3. Chemical structure of the high-energy compound UDP-GlcNAc. UDP-GlcNAc is an ideal metabolic marker due to its chemical composition. Glucose (blue) is directly incorporated into UDP-GlcNAc. The acetyl group (pink) derives from acetyl-CoA which either originates from fatty acid metabolism or from the interface between glycolysis and TCA cycle. The nitrogen of the *N*-acetyl group (orange) is transferred from glutamine and therefore connects UDP-GlcNAc to the amino acid metabolism. The ribose moiety of uridine (green) is produced in the pentose phosphate pathway and the uracil moiety of uridine is produced in pyrimidine biosynthesis. Levels of UDP-GlcNAc in cells are affected by all metabolic pathways involved. CoA, coenzyme A; TCA, tricarboxylic acid; UDP-GlcNAc, uridine diphosphate-*N*-acetylglucosamine.

In some cells, intracellular UDP-GlcNAc concentrations can reach levels similar to ATP, thus being the second most abundant high energy metabolite in cells (Wice *et al*., 1985; Tomiya *et al*., 2001; Marshall *et al*., 2004). UDP-GlcNAc is a potent feedback inhibitor for GFAT in

mammalian cells (Kornfeld *et al*., 1964, Kornfeld, 1967), implying a tight metabolic control of the flux through HBP and UDP-GlcNAc levels.

UDP-GlcNAc is a precursor for glycoproteins, proteoglycans, glycolipids, and is the unique donor for the *O*-linkage of a single *N*-acetylglucosamine molecule (*O*-GlcNAc) to many nuclear and cytoplasmic proteins (see also Chapters 1.5 and 1.6).

1.4 Biosynthesis and Interconversion of Other Activated Sugar Nucleotides

Apart from UDP-GlcNAc, other activated sugar nucleotides exist that are important precursors for the biosynthesis of glycoconjugates. To become activated, monosaccharides are transported into the cytosol by hexose transporters, e.g. by transporters of the glucose transporter (GLUT) family (Bell *et al*., 1993). In the cytosol the monosaccharides are being phosphorylated by hexokinases. The phosphorylated sugar then either reacts with a nucleotide (UTP, guanosine triphosphate (GTP), or cytidine triphosphate (CTP)) to form an activated sugar nucleotide or it reacts with an already existing activated sugar nucleotide in exchange for the sugar moiety. Some activated sugar nucleotides are also formed by epimerization of another activated sugar nucleotide. Possible reactions of hexoses to form activated sugar nucleotides are summarized in Figure 4.

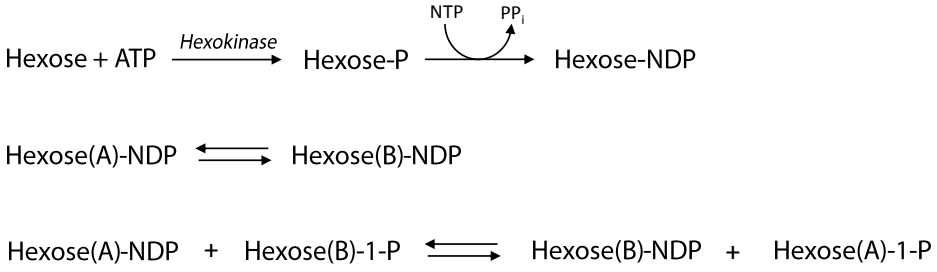

Figure 4. Possible reactions of hexoses to form activated sugar nucleotides. Adapted from (Varki *et al*., 1999). ATP, adenosine triphosphate; NDP, nucleotide diphosphate; NTP, nucleotide triphosphate; PP_i, pyrophosphate.

However, activated sugar nucleotides are not only *de novo* synthesized. These sugars can also be salvaged from degraded already existing glycoproteins and glycosaminoglycans, a process that occurs mainly in acidic lysosomes (Rome & Hill, 1986; Winchester, 2005). For example, over 50 % of *N*-acetylglucosamine (GlcNAc) and *N*-acetylgalactosamine (GalNAc) in intact cultures of human diploid fibroblasts are reincorporated into newly synthesized macromolecules as shown by incubation with [^{3}H]glucosamine (GlcN) (Rome & Hill, 1986).

In addition, inhibition of GFAT, i.e. paralyzation of the HBP, by 6-diazo-5-oxo-L-norleucine (DON) had no effect on the uridine diphosphate-*N*-acetylhexosamine (UDP-HexNAc) level in bovine thyroid gland slices. This result suggests that degradation of the carbohydrate part of thyroglobulin is used to maintain the UDP-HexNAc pool (Trujillo & Gan, 1973).
After transport into the cytoplasm the *N*-acetylated monosaccharides are rapidly phosphorylated by hexokinases (Leloir *et al*., 1958) and subsequently activated to sugar nucleotides.
The relative contribution of *de novo* synthesized and salvaged activated sugar nucleotides probably varies depending on cell type and amount of glycoprotein synthesized and salvage pathways are not restricted to *N*-acetylated sugars (Varki *et al*., 1999).

Figure 5 shows the major pathways for the biosynthesis and interconversion of activated sugar nucleotides. It is apparent that glucose can potentially generate all other activated sugar nucleotides. The formation of UDP-GlcNAc through the HBP has been described in Chapter 1.3. UDP-GalNAc can be formed by epimerization of UDP-GlcNAc by UDP-glucose 4-epimerase (also referred to as UDP-galactose 4-epimerase (GALE); EC 5.1.3.2) (Wilson & Hogness, 1964).

Cytidine monophosphate-*N*-acetylneuraminic acid (CMP-NeuNAc) is synthesized from UDP-GlcNAc. At first, UDP-GlcNAc is converted to *N*-acetylmannosamine (ManNAc) by UDP-GlcNAc 2-epimerase (EC 5.1.3.14). ManNAc is then phosphorylated at the expense of ATP by ManNAc kinase (EC 2.7.1.60) to yield ManNAc-6-P. The two reactions are actually carried out by a single bifunctional enzyme that exhibits two catalytic activities, the UDP-GlcNAc 2-epimerase/ManNAc kinase (Hinderlich *et al*., 1997). ManNAc-6-P then condenses with phosphoenolpyruvate (PEP) to form *N*-acetylneuraminic acid-9-phosphate (NeuNAc-9-P). The reaction is catalyzed by NeuNAc phosphate synthase (EC 2.5.1.57) (Lawrence *et al*., 2000). After that NeuNAc-9-P is dephosphorylated and free NeuNAc is activated by CMP-NeuNAc synthetase (EC 2.7.7.43) to form CMP-NeuNAc using CTP (Zapata *et al*., 1989).
After phosphorylation of glucose to Glc-6-P, Glc-6-P can either be isomerized to Fru-6-P (which can then be routed into glycolysis or HBP) or it can be converted to glucose-1-P (Glc-1-P) by phosphoglucomutase (EC 5.4.2.2). Glc-1-P then reacts with UTP to form uridine diphosphate-glucose (UDP-Glc), an important precursor for glycogen. Uridine diphosphate-glucuronic acid (UDP-GlcUA) is formed by oxidation of the hydroxyl group at C6 of UDP-Glc by UDP-glucose 6-dehydrogenase (EC 1.1.1.22) using nicotinamide adenine dinucleotide (NAD^+) as the oxidant (Kalckar *et al*., 1956).

Uridine diphosphate galactose (UDP-Gal) can be formed by epimerization of UDP-Glc by UDP-glucose 4-epimerase, the same enzyme that is responsible for epimerization of UDP-GlcNAc to UDP-GalNAc (Wilson & Hogness, 1964). However, galactose can also be directly activated. Galactose is first phosphorylated to galactose-1-phosphate (Gal-1-P) by galactokinase (GALK; EC 2.7.1.6) and then reacts with UTP to give UDP-Gal. Alternatively, Gal-1-P can react with UDP-Glc to form Glc-1-P and UDP-Gal, a reaction carried out by galactose-1-phosphate uridylyltransferase (GALT; EC 2.7.7.12) (Holden *et al*., 2003).

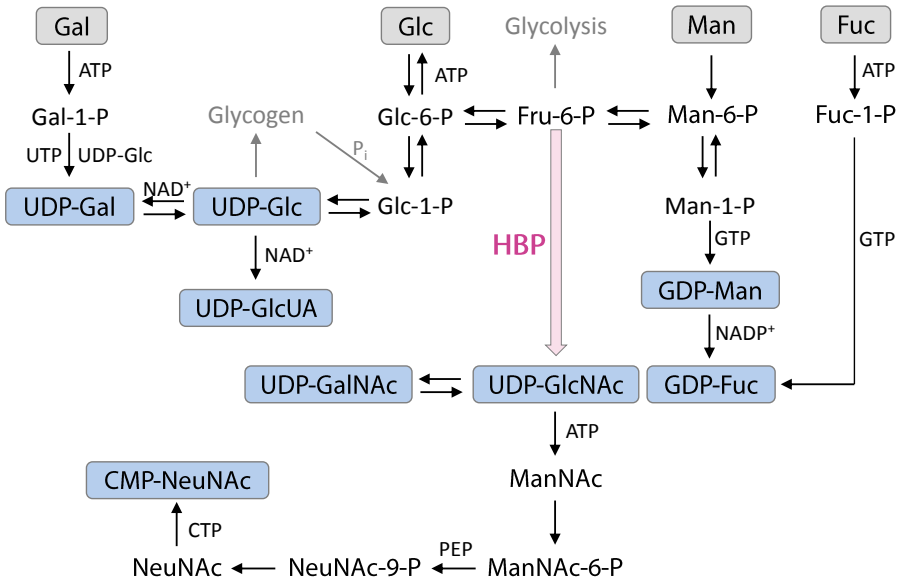

Figure 5. Major pathways for the biosynthesis and interconversion of activated sugar nucleotides. Monosaccharides are shown in grey rectangles; activated sugar nucleotides are shown in blue rectangles. For a better overview only the substrates of the reactions are displayed next to the reaction arrows. Adapted from (Varki *et al*., 1999). ATP, adenosine triphosphate; CTP, cytidine triphosphate; CMP-NeuNAc, cytidine monophosphate-*N*-acetylneuraminic acid; Fru-6-P, fructose-6-phosphate; Fuc, fucose; Fuc-1-P, fucose-1-phosphate; Gal, galactose; Gal-1-P, galactose-1-phosphate; GDP-Fuc, guanosine diphosphate-fucose; GDP-Man, guanosine diphosphate-mannose; Glc, glucose; Glc-1-P, glucose-1-phosphate; Glc-6-P, glucose-6-phosphate; GTP, guanosine triphosphate; HBP, hexosamine biosynthetic pathway; Man, mannose; Man-1-P, mannose-1-phosphate; Man-6-P, mannose-6-phosphate; ManNAc, *N*-acetylmannosamine; ManNAc-6-P, *N*-acetylmannosamine-6-phosphate; NAD(P), nicotinamide adenine dinucleotide (phosphate); NeuNAc, *N*-acetylneuraminic acid; NeuNAc-9-P, *N*-acetylneuraminic acid-9-phosphate; P_i, inorganic phosphate; PEP, phosphoenol pyruvate; UDP-Gal, uridine diphosphate galactose; UDP-GalNAc, uridine diphosphate-*N*-acetylgalactosamine; UDP-Glc, uridine diphosphate-glucose; UDP-GlcNAc, uridine diphosphate-*N*-acetylglucosamine; UDP-GlcUA, uridine diphosphate-glucuronic acid; UTP, uridine triphosphate.

The synthesis of guanosine diphosphate-mannose (GDP-Man) involves the synthesis of mannose-6-phosphate (Man-6-P) as an intermediate. Man-6-P can either be formed directly by phosphorylation of mannose via hexokinase (possibly even by a specific mannokinase; EC 2.7.1.7 (Abraham *et al*., 1961)) or by conversion of Fru-6-P to Man-6-P catalyzed by the enzyme phosphomannose isomerase (EC 5.3.1.8) (Gracy & Noltmann, 1968). In mammalian cells, GDP-Man is almost exclusively synthesized from Fru-6-P that originates from glucose. Only in fibroblasts direct phosphorylation of mannose was found to be a significant source for

GDP-Man synthesis (Panneerselvam & Freeze, 1996; Panneerselvam *et al*., 1997). Man-6-P is then converted to mannose-1-phosphate (Man-1-P) by phosphomannomutase (EC 5.4.2.8) (Hansen *et al*., 1997). As a last step Man-1-P is activated to GDP-Man with GTP catalyzed by GDP-mannose pyrophosphorylase (EC 2.7.7.13) (Munch-Petersen, 1956).

Guanosine diphosphate-fucose (GDP-Fuc) can be biosynthesized by conversion of GDP-Man (Ginsburg, 1960; Ginsburg, 1961) in three sequential steps catalyzed by two enzymes. In the first step, the hydroxyl group at C4 of the mannose residue of GDP-Man is oxidized to a keto group. This oxidation is followed by a concerted reduction of the CH_2OH group at the C6 of mannose to a methyl group, yielding GDP-4-keto-6-deoxymannose. This reaction is carried out by GDP-mannose 4,6-dehydratase (EC 4.2.1.47) (Sullivan *et al*., 1998) with nicotinamide adenine dinucleotide phosphate ($NADP^+$) as a cofactor which mediates the transfer of a hydride from C4 to C6 (Oths *et al*., 1990). The next two steps are carried out by one enzyme that has both epimerase and reductase activity, the GDP-keto-6-deoxymannose 3,5-epimerase/4-reductase (also known as the FX protein or GDP-fucose synthetase; EC 1.1.1.271) (Chang *et al*., 1988; Tonetti *et al*., 1996). In the first reaction, GDP-4-keto-6-deoxymannose is epimerized at C3 and C5 of the mannose residue to yield GDP-4-keto-6-deoxyglucose. This intermediate is finally reduced to GDP-Fuc in an NADPH dependent reaction (Menon *et al*., 1999). GDP-Fuc is a competitive feedback inhibitor of GDP-mannose 4,6-dehydratase that catalyzes the first reaction in GDP-Fuc synthesis from GDP-Man (Kornfeld & Ginsburg, 1966; Sullivan *et al*., 1998).

GDP-Fuc can also be synthesized from free fucose via fucose-1-phosphate (Fuc-1-P) as an intermediate. Free fucose can derive from extracellular sources or by lysosomal degradation of glycoproteins and glycolipids by fucosidases (Michalski & Klein, 1999). In the first step fucose is phosphorylated to Fuc-1-P by fucose kinase (EC 2.7.1.52) under the expense of ATP (Ishihara *et al*., 1968a). The final formation of GDP-Fuc by condensation of Fuc-1-P with GTP is then catalyzed by GDP-fucose pyrophosphorylase (EC 2.7.7.30) (Ishihara *et al*., 1968b).

Quantitative studies in HeLa cells showed that the primary biosynthetic route of GDP-Fuc synthesis is from GDP-Man (Yurchenco & Atkinson, 1977).

1.5 Glycosylation

Activated sugar nucleotides are donor substrates for posttranslational glycosylation of proteins and lipids. In the glycosylation process various types of glycan chains are produced by covalently linking monosaccharides glycosidically, which are then attached to proteins or lipids. Protein glycosylation occurs in the endoplasmatic reticulum (ER) and Golgi apparatus and comprises *N*-glycans, *O*-glycans, and glycosaminoglycans (also referred to as proteoglycans) (Ohtsubo & Marth, 2006). Another type of glycosylation where single *O*-GlcNAc residues are attached to proteins proceeds in the cytosol and nucleus (Holt & Hart, 1986). This modification is described in detail in the following chapter.

N-glycosylation requires a lipid-linked dolichol-phosphate precursor for synthesis. This dolichol-phosphate precursor defines the common core region of *N*-glycans, consisting of two GlcNAc residues and three mannose residues. The monosaccharide chain of an *N*-glycan is covalently linked with a GlcNAc residue to an asparagine (Asn) residue within the consensus sequence Asn-X-serine/threonine (Asn-X-Ser/Thr) of a protein. *N*-glycans can be divided into three types: high-mannose type, complex type, and hybrid type (Ohtsubo & Marth, 2006; Stanley *et al*., 2009).

O-glycosylation is not reliant on a precursor for synthesis. *O*-glycans are linked via GalNAc to the hydroxyl groups of Ser and Thr residues of proteins. Large *O*-GalNAc glycoproteins which are heavily glycosylated are called mucins. There are also several types of other *O*-linked glycoproteins, e.g. glycans linked via *O*-mannose (Ohtsubo & Marth, 2009; Brockhausen *et al*., 2009).

Glycosaminoglycans (GAGs) are linear polysaccharide chains composed of repeating disaccharide units. The repeating units usually contain an *N*-acetylhexosamine (HexNAc; GlcNAc or GalNAc) residue alternating with a glucuronic acid (GlcUA) or iduronic acid (IdoA) residue. Hyaluronan for example is a GAG that consists of GlcNAc-GlcUA repeating units and exists as a free polysaccharide chain that is not attached to proteins. With the exception of hyaluronan, GAGs are highly sulfated and covalently attached to proteins. Proteins containing one or more glycosaminoglycan chains are called proteoglycans. Examples of proteoglycans are chondroitin or dermatan sulfate (GalNAc-GlcUA/IdoA), and heparin or heparan sulfate (GlcNAc-GlcUA/IdoA) (Kolset *et al*., 2004; Esko *et al*., 2009).

Glycophosphatidylinositol (GPI) anchors attach glycoproteins to the lipid bilayer of the plasma membrane. The C-terminus of the protein is linked via ethanolamine-phosphate to the common core of the GPI anchor consisting of three mannose residues and a GlcN residue. The GlcN residue is glycosidically bound to inositol-phosphate which is in turn linked to a lipid. Typically two acyl chains of a glycerolipid anchor the protein to the membrane (Ferguson *et al*., 2009).

Glycolipids consist of diverse glycans attached to a lipid moiety. The most common and most abundant glycolipids are glycosphingolipids that are composed of a glycan chain which is glycosidically linked via glucose or galactose to the hydroxyl residue of the lipid ceramide. A ceramide is composed of a long-chain amino alcohol (sphingosine) that is linked to a fatty acid through an amide bond. The simplest glycosphingolipid is galactosylceramide which consists of a single galactose residue attached to ceramide (Maccioni *et al*., 2002). Galactosylceramide is one of the most abundant molecules in the brain and used as a marker for myelin-forming oligodendrocytes (Raff *et al*., 1978). Another type of glycolipids are glycoglycerolipids whereby the glycan chains are attached to the hydroxyl group at C3 of a diacylglycerol lipid (Hölzl & Dörmann, 2007). Glycoglycerolipids are not common in mammalian cells, but are prevalent in chloroplasts of plants and bacteria (Hölzl & Dörmann, 2007).

As outlined above, activated sugar nucleotides are donor substrates for glycosylation processes. With the exception of CMP-NeuNAc which is synthesized in the nucleus (Coates *et al*., 1980), all other sugar nucleotides are synthesized in the cytosol. Glycosylation however, occurs in most cases in the ER and Golgi. Therefore, several non-energy requiring antiporters exist that transport the activated sugar nucleotides in exchange with a nucleotide monophosphate into the lumen of the ER and Golgi (Abeijon *et al*., 1997; Varki *et al*., 1999). The nucleotide monophosphate is derived from a nucleotide diphosphate that is produced in the glycosylation reaction with an activated sugar nucleotide. This antiporter system has the advantage that the precursor for synthesis of activated sugar nucleotides in the cytosol is resupplied for further activation of sugars (Varki *et al*., 1999). Enzymes responsible for glycosylation reactions are glycosyltransferases and glycosidases. Glycosyltransferases synthesize glycan linkages, while glycosidases hydrolyze glycan chains (Lairson *et al*., 2008).

The synthesis of glycoproteins is highly regulated. This may imply that the availability of its precursors - the activated sugar nucleotides - is also highly regulated and can influence

protein glycosylation. To date, there are comprehensive discussions on how changes in the levels of activated sugar nucleotides may influence glycosylation.

Figure 6 depicts common glycans in mammalian cells.

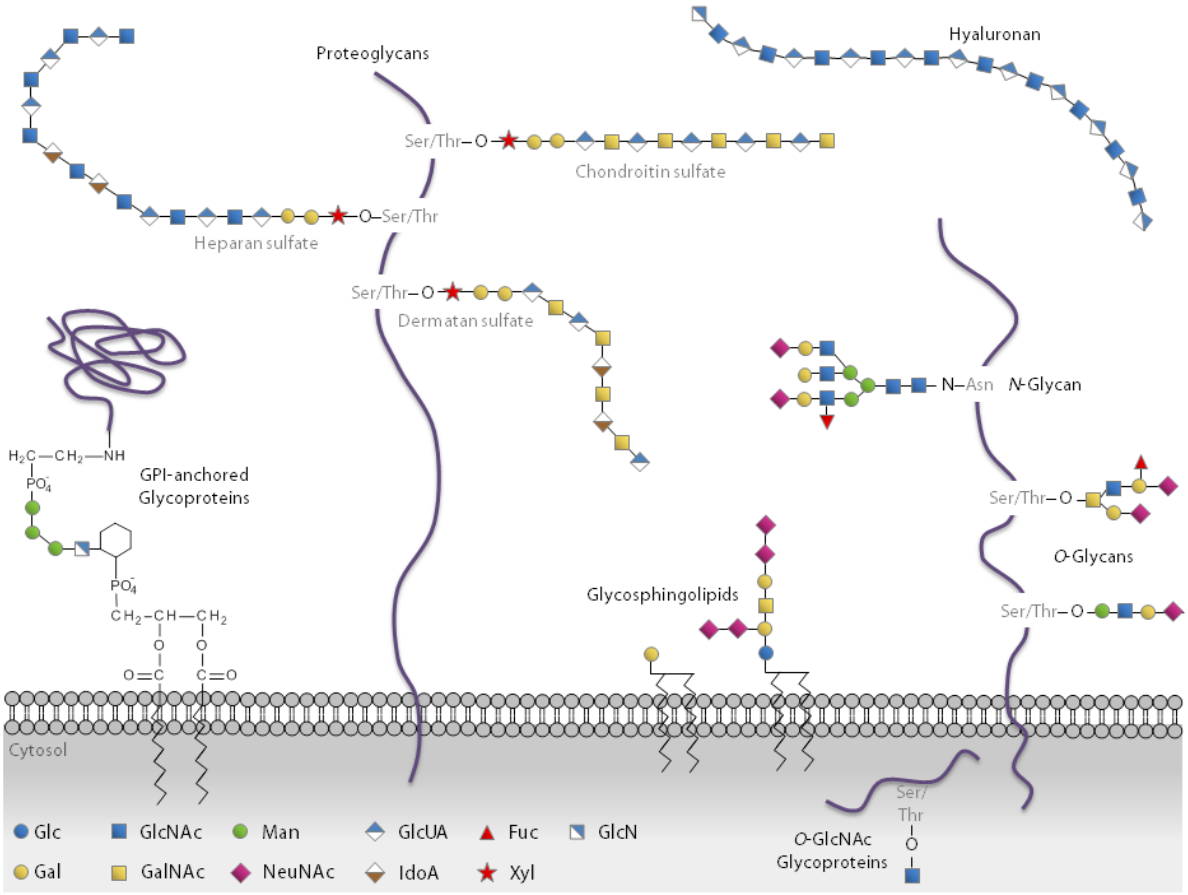

Figure 6. Common glycans in mammalian cells. *N*-Glycans are covalently attached to Asn residues of glycoproteins. *N*-Glycans contain typically two or more antennae. *O*-Glycans are covalently attached to Ser or Thr residues of glycoproteins. Glycosphingolipids are composed of glycan chains that are linked via glucose or galactose to ceramide. GPI-anchored glycoproteins are attached to the plasma membrane by a glycan covalently linked to phosphatidylinositol. Hyaluronan is a free glycosaminoglycan that is not attached to a protein. Proteoglycans (heparin sulfate, chondroitin sulfate, dermatan sulfate) are proteins containing one or more glycosaminoglycan chains. Cytoplasmic and nuclear *O*-GlcNAc glycoproteins contain a single *O*-GlcNAc residue that is not elongated. See text for detailed information (adapted from Fuster & Esko, 2005; Varki & Sharon, 2009). Asn, asparagine; Fuc, fucose; Gal, galactose; GalNAc, *N*-acetyl galactose; Glc, glucose; GlcUA, glucuronic acid; GlcN, glucosamine; GlcNAc, N-acetyl glucosamine; GPI, glycophosphatidylinositol; IdoA, iduronic acid; Man, mannose; NeuNAc, *N*-acetylneuraminic acid; Ser, serine; Thr, threonine; Xyl, xylose.

1.6 *O*-GlcNAcylation

Unlike complex *N*- and *O*-glycosylation that occurs in the secretory pathway in the ER and Golgi apparatus, a different type of glycosylation was found to post-translationally modify nuclear and cytoplasmic proteins. The covalent attachment of a single *N*-acetylglucosamine

monosaccharide to the hydroxyl group of Ser and Thr residues of proteins (*O*-GlcNAcylation) was discovered in 1984 (Torres & Hart, 1984). *O*-GlcNAcylation is a unique type of glycosylation as it is not lengthened to more complex glycan structures or further modified. Furthermore, *O*-GlcNAcylation is not static but a dynamic and inducible post-translational modification added and removed from proteins similar to phosphorylation (Slawson *et al*., 2006; Hart *et al*., 2007). Noteworthy, all *O*-GlcNAcylated proteins investigated to date are also modified by phosphorylation. *O*-GlcNAcylation sites are often the same or adjacent sites of protein phosphorylation, suggesting interplay between *O*-GlcNAc and *O*-phosphate (Slawson *et al*., 2006). Many proteins can be simultaneously *O*-GlcNAcylated and phosphorylated. However, both modifications can also be competitive when occurring at the same or adjacent sites (Kamemura *et al*., 2002; Slawson & Hart, 2003). The addition of one modification can regulate the addition of the other at the adjacent site, i.e. phosphorylation can prevent *O*-GlcNAcylation and vice versa. Thus a given protein can be phosphorylated, *O*-GlcNAcylated, modified by both *O*-phosphate and *O*-GlcNAc, or unmodified.

Several hundreds of kinases and phosphatases regulate cellular phosphorylation (Manning *et al*., 2002). Although *O*-GlcNAcylation is as abundant and as ubiquitous as phosphorylation, to date only two enzymes are known regulate the addition and removal of *O*-GlcNAc on target proteins, as shown in Figure 7.

O-GlcNAc transferase (uridine diphospho-*N*-acetylglucosamine: polypeptide ß-*N*-acetylglucosaminyltransferase; OGT; EC 2.4.1.255) attaches GlcNAc from the donor substrate UDP-GlcNAc to Ser/Thr residues of proteins. OGT is a highly conserved enzyme (Kreppel *et al*., 1997; Lubas *et al*., 1997) that has been purified, characterized and cloned (Haltiwanger *et al*., 1992; Kreppel *et al*., 1997). OGT is expressed in all tissues, but was found to be especially abundant in the brain and pancreas (Lubas *et al*., 1997). OGT is a heterotrimer consisting of two 110 kDa subunits and one 78 kDa subunit, but the 78 kDa subunit is not required for activity in most tissues (Haltiwanger *et al*., 1992). OGT is predominantly localized in the nucleus and cytoplasm, but a smaller splice variant (103 kDa) was also detected in the inner membrane of mitochondria (Love *et al*., 2003). However, only few *O*-GlcNAc modified proteins were found in this compartment (Love *et al*., 2003). In humans, the OGT gene resides on the X chromosome region Xq13, a region that is associated with neurological diseases (Shafi *et al*., 2000). OGT and *O*-GlcNAcylation are essential for cell viability, since OGT gene-knockout in mice led to embryonic lethality (Shafi *et al*., 2000).

The counterpart of OGT is *O*-GlcNAcase (ß-*N*-acetylglucosaminidase; OGA; EC 3.2.1.169) which catalyzes the removal of *O*-GlcNAc from proteins. OGA has also been purified, characterized, and cloned (Dong & Hart, 1994; Gao *et al*., 2001). OGA is located mainly in the cytosol and has unlike acidic lysosomal hexosaminidases a pH optimum near neutral (Gao *et al*., 2001). OGA is also highly conserved and ubiquitously expressed and was found to be very abundant in brain (Gao *et al*., 2001).

The OGA gene was reported to be identical to that of meningioma-expressed antigen 5 (MGEA5) which is mapped to the chromosomal region 10q24 and is associated with late-onset Alzheimer's disease (Heckel *et al*., 1998; Comtesse *et al*., 2001). Hence, like OGT, OGA may also be involved in the pathology of neurological disorders. Moreover, a single nucleotide polymorphism in MGEA5 correlates with an increased risk of type II diabetes in Mexican Americans (Lehman *et al*., 2005).

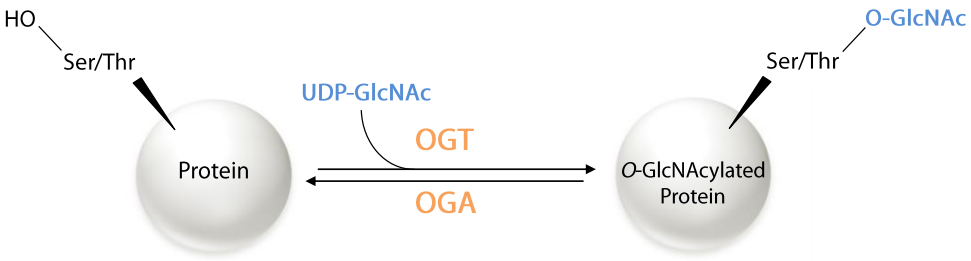

Figure 7. *O*-GlcNAc modification on Ser or Thr residues of nuclear and cytoplasmic proteins. The reaction is similar to phosphorylation and is controlled by two highly conserved enzymes, OGT and OGA. OGA, *O*-GlcNAcase; OGT, *O*-GlcNAc transferase; Ser, serine; Thr, threonine.

To date, more than 600 *O*-GlcNAc modified proteins have been identified (Copeland *et al*., 2008). *O*-GlcNAcylated proteins are well-known proteins including transcription factors (e.g. RNA polymerase II (Kelly *et al*., 1993), Sp1 (Jackson & Tjian, 1988)), cytoskeletal proteins (e.g. neurofilaments (Dong *et al*., 1996), tau (Arnold *et al*., 1996), amyloid precursor protein (APP) (Griffith *et al*., 1995)), signal transduction molecules (Wells *et al*., 2001) and many more. Several key proteins involved in glucose metabolism and insulin regulation such as enzymes of glycolysis (e.g. enolase) (Wells *et al*., 2002), glycogen synthase (Parker *et al*., 2003), glycogen synthase kinase-3 (GSK-3) (Lubas & Hanover, 2000), GLUT-1 (Buse *et al*., 2002), endothelial nitric oxide synthase (eNOS) (Federici *et al*., 2002), and insulin receptor substrate-1 (IRS-1) (Ball *et al*., 2006) are also *O*-GlcNAc modified. Accordingly, *O*-GlcNAcylation is involved in regulating transcription, cellular stability, and glucose metabolism. Moreover, further studies have shown that *O*-GlcNAc affects protein stability

(Yang *et al*., 2006), influences protein interactions (Roos *et al*., 1997), regulates protein trafficking (Zhu *et al*., 2001), and influences cell growth and proliferation (Slawson *et al*., 2005).

Not only are OGT and OGA highly expressed in brain, but also the presence of *O*-GlcNAc on proteins important for neuronal function and pathogenesis such as tau and APP indicate that *O*-GlcNAc modification is of decisive importance in brain. Furthermore, the high expression of OGT and OGA in pancreas together with the discovery of a wide range of proteins involved in glucose metabolism and insulin regulation being *O*-GlcNAcylated also suggests an important function in these metabolic pathways.

O-GlcNAcylation has been shown to participate in an early protective response to cellular stress, since *O*-GlcNAc levels on many proteins increase rapidly as a reaction to multiple forms of stress, such as osmotic, oxidative, and thermal stress (Zachara *et al*., 2004; Zachara & Hart, 2004). Increasing *O*-GlcNAc levels results in cells that are more stress tolerant, whereas decreasing *O*-GlcNAc or OGT protein levels leads to cells that are less stress tolerant (Zachara *et al*., 2004). One possible explanation how *O*-GlcNAc may mediate stress tolerance is by altering the levels of heat-shock proteins, several of which are highly *O*-GlcNAcylated (Zachara *et al*., 2004).

The regulation of OGT and OGA is yet not fully elucidated. However, it is known that OGT is highly regulated by many different mechanisms, such as post-translational modifications and nutrient availability. OGT (Kreppel *et al*., 1997), as well as OGA (Khidekel *et al*., 2007) itself, are both tyrosine phosphorylated and *O*-GlcNAc modified and thus their activity may also be regulated by post-translational modifications.

OGT activity is also dependent on its donor substrate UDP-GlcNAc since OGT is highly sensitive to varying UDP-GlcNAc concentrations (Haltiwanger *et al*., 1992; Kreppel *et al*., 1997; Kreppel & Hart, 1999). UDP-GlcNAc synthesis in turn is highly dependent on nutrients (glucose and glutamine and/or GlcN). Changes in flux through HBP either increase or decrease UDP-GlcNAc levels also affecting the extend of *O*-GlcNAcylation on many proteins (Kreppel & Hart, 1999). For this reason *O*-GlcNAcylation and the HBP are often considered as a nutrient sensor and the level of *O*-GlcNAcylation a marker of the nutritional state of the cell.

OGT activity may possibly be up-regulated by auto-*O*-GlcNAcylation, since OGT itself was found to be to be hyper-*O*-GlcNAcylated in hyperglycemic conditions (Akimoto *et al*., 2001;

Vosseller *et al*., 2002a). In this context it is interesting that in accordance with the fact that *O*-GlcNAc levels increase in response to cellular stress, glucose deprivation also leads to elevated *O*-GlcNAc levels in cells (Taylor *et al*., 2008; Talor *et al*., 2009; Cheung & Hart, 2008).

O-GlcNAc study and detection has been difficult and only moderate progress was made in the past. The *O*-GlcNAc modification is small and, unlike phosphate, uncharged. Therefore, it does not alter protein migration during gel electrophoresis even on high resolution two-dimensional gels (Copeland *et al*., 2008). Furthermore, like phosphorylation, *O*-GlcNAcylation is not stoichiometric and is rapidly removed by intracellular glycosidases when cells are damaged. On this account it is difficult to detect *O*-GlcNAc by mass spectrometry. Moreover, *O*-GlcNAc is very labile during ionization in a mass spectrometer. The lack of an apparent consensus sequence for *O*-GlcNAc further hampers its study (Copeland *et al*., 2008).
Quite recently, antibodies recognizing *O*-GlcNAc (Comer *et al*., 2001) and potent *O*-GlcNAcase inhibitors (Dorfmueller *et al*., 2006; Stubbs *et al*., 2006) have been developed that facilitate *O*-GlcNAc detection. Chemoenzymatic techniques such as BEMAD (mild ß-elimination followed Michael addition with dithiothreitol) that label *O*-GlcNAc modified proteins with dithiothreitol (Vosseller *et al*., 2005) or incorporation of sugars bearing an *N*-azido group that allows subsequent derivatization with probes or tags (Vocadlo *et al*., 2003) were developed to identify *O*-GlcNAc sites. These techniques combined with new mass-spectrometric methods such as TMS-ECD (Fourier transform mass spectrometry with electron-capture dissociation) (Vosseller *et al*., 2006) or ETD (ion-trap mass spectrometry with electron-transfer dissociation) (Mikesh *et al*., 2006) now allow *O*-GlcNAc detection and site mapping.

1.7 The Role of HBP and *O*-GlcNAc in Metabolic Diseases

O-GlcNAc not only plays an important role in many fundamental cellular processes, but also its dysregulation has been shown to be involved in the development of human diseases such as diabetes (Vosseller *et al*., 2002b), Alzheimer's disease (Dias & Hart, 2007), and cancer (Slawson *et al*., 2010).

1.7.1 Type II Diabetes

Insulin resistance is the reduced ability of insulin to mediate glucose absorption from blood into skeletal muscle and fat cells, thus lowering blood glucose levels. Insulin resistance is, along with hyperglycemia, a hallmark of type II diabetes (Reaven, 1988). In normal cells, insulin induces a complex signal transduction cascade that results in translocation of the insulin responsive glucose transporter GLUT4 to the plasma membrane (Lin & Sun, 2010).

Recent evidence has shown that elevated *O*-GlcNAc levels due to increased flux through the HBP under sustained hyperglycemia causes insulin resistance (Vosseller *et al*., 2002b; McClain *et al*., 2002). In this context the HBP is proposed to function as a nutrient sensor in the development of diabetes.
Marshall *et al*. were the first who connected elevated flux through the HBP with insulin resistance (Marshall *et al*., 1991a; Marshall *et al*., 1991b; Marshall *et al*., 1991c). Their studies in primary rat adipocytes showed that glucose, glutamine and insulin are required for the induction of insulin resistance (Traxinger & Marshall, 1991). The requirement for glutamine indicated the participation of the HBP. They confirmed this assumption by showing that insulin resistance can be reduced by inhibiting GFAT. The reduction, in turn, can be reversed by GlcN, that can enter the HBP as GlcN-6-P downstream of GFAT and therefore bypassing it, causing increased levels of UDP-GlcNAc. GlcN was even more potent than glucose in inducing insulin resistance (Marshall *et al*., 1991a; Marshall *et al*., 1991b). On the contrary, overexpression of GFAT in several tissues leads to insulin resistance in cultured adipocytes and transgenic mice (Hebert *et al*., 1996; Veerababu *et al*., 2000; Cooksey & McClain, 2002). As a side note, GFAT is most highly expressed in insulin-responsive tissues, such as fat tissue (Nerlich *et al*., 1998).
Numerous *in vitro* (Robinson *et al*., 1993; Marshall *et al*., 2004) and *in vivo* (Baron *et al*., 1995; Rossetti *et al*., 1995; McClain & Crook, 1996; Patti *et al*., 1999) studies using GlcN have now demonstrated that increased flux through the HBP may be one mechanism in the development of insulin resistance.

The use of GlcN to investigate the role of the HBP in the development of insulin resistance has been raised to question (Hresko *et al*., 1998; Virkamäki & Yki-Järvinen, 1999; Nelson *et al*., 2000; Nelson *et al*., 2002). One consequence of GlcN administration is the vast accumulation of GlcN-6-P, that leads to ATP depletion in cells (Hresko *et al*., 1998; Marshall *et al*., 2004). It was clearly shown that ATP depletion can affect insulin signaling independent

from UDP-GlcNAc formation leading to misinterpretation of the results (Hresko *et al*., 1998). Furthermore, GlcN and GlcN-6-P levels are normally very low in cells and their synthesis is limited by feedback inhibition of GFAT by UDP-GlcNAc (Kornfeld *et al*., 1964). However, low doses of GlcN were found to distinctly increase UDP-GlcNAc levels without increasing GlcN-6-P or altering ATP levels (Marshall *et al*., 2004).

A direct link between increased *O*-GlcNAc metabolism and the development of diabetes was established by studies targeting the enzymes of *O*-GlcNAc cycling. In transgenic mice even a slight overexpression of OGT in muscle and fat tissue caused insulin resistance (McClain *et al*., 2002). Furthermore, overexpression of OGT in liver also led to insulin resistance (Yang *et al*., 2008). In parallel studies it was demonstrated that elevation of *O*-GlcNAc levels by treatment of adipocytes with the OGA inhibitor *O*-(2-acetamido-2-deoxy-D-glucopyranosylidene) amino *N*-phenylcarbamate (PUGNAC) impaired insulin signaling as well (Vosseller *et al*., 2002b). In addition, increased *O*-GlcNAcylation by OGA inhibition resulted in decreased glucose-dependent insulin expression and secretion in isolated pancreatic islets (Akimoto *et al*., 2007). Besides, OGT protein levels and the extent *O*-GlcNAcylation on proteins were found to be increased in the pancreatic islets of diabetic rats (Akimoto *et al*., 2007). Hyperinsulinemia is also able to potently increase *O*-GlcNAc levels on many proteins in rat skeletal muscle (Yki-Järvinen *et al*., 1998).

The above specified studies clearly evidence that elevated flux through the HBP and increased *O*-GlcNAc levels induce insulin resistance in type II diabetes. However, what are the mechanisms? As described in the previous chapter, several key proteins involved in glucose metabolism and insulin regulation are *O*-GlcNAc modified. Hyperglycemia results in abnormal increased *O*-GlcNAcylation, which leads to an aberrant *O*-GlcNAc and *O*-phosphate balance on proteins involved in insulin signaling or proteins that control the transcription of proteins involved in insulin signaling. It is proposed that prolonged *O*-GlcNAc/*O*-phosphate imbalance induces insulin resistance in type II diabetes by disturbing the phosphorylation-dependent insulin signaling pathway (Copeland *et al*., 2008).

Under hyperglycemic conditions, the ubiquitous transcription factor Sp1 becomes hyper-*O*-GlcNAcylated (Jackson & Tijan, 1988; Walgren *et al*., 2003). Sp1 is *O*-GlcNAcylated at multiple sites (Jackson & Tijan, 1988) and its *O*-GlcNAcylation state correlates with its ability to regulate the expression of genes linked to diabetes (Du *et al*., 2000). *O*-GlcNAc enhances the DNA binding activity of Sp1, which is completely lost after *O*-GlcNAc removal

(Weigert *et al*., 2003). *O*-GlcNAcylation of Sp1 is also stimulated by insulin itself (Majumdar *et al*., 2006). This enhanced transcriptional activity may lead to insulin resistance.

NeuroD1a and pancreatic duodenal homeobox-1 (PDX-1) are key transcription factors regulating insulin synthesis in pancreatic ß-cells and both are *O*-GlcNAc modified (Gao *et al*., 2003; Andrali *et al*., 2007). It was reported that NeuroD1 is regulated by *O*-GlcNAc in MIN6 ß-cells (Andrali *et al*., 2007). Under hypoglycemic conditions, NeuroD1 is mainly located in the cytosol. However, when NeuroD1 is *O*-GlcNAcylated under hyperglycemic conditions or *O*-GlcNAc removal is inhibited by treatment with the OGA inhibitor PUGNAC, NeuroD1a is translocated into the nucleus (Andrali *et al*., 2007). Furthermore, it was demonstrated that NeuroD1 interacts with OGT at high glucose concentrations, whereas it interacts with OGA when glucose concentrations are low (Andrali *et al*., 2007).
Elevated *O*-GlcNAcylation of PDX-1 under hyperglycemic conditions increases its DNA binding activity and insulin secretion in ß-cells (Gao *et al*., 2003). Interestingly, it has been demonstrated that under high glucose PDX-1 also becomes *O*-phosphate modified, indicating that both *O*-phosphate and *O*-GlcNAc may concurrently regulate insulin secretion (Macfarlane *et al*., 1999). As with NeuroD1a, glucose stimulates the translocation of PDX-1 from the cytoplasm to the cytosol in pancreatic ß-cells (Macfarlane *et al*., 1999).
Moreover, it has been shown that *O*-GlcNAcylation of PDX-1 is increased in the pancreas of diabetic rats (Akimoto *et al*., 2007).
Taken together, high glucose flux through the HBP causes elevation of *O*-GlcNAcylation of NeuroD1a and PDX-1, which increases their transcriptional activity, leading to altered insulin synthesis.

IRS-1 plays a major role in transmitting signals from insulin to intracellular pathways such as the phosphatidylinositol-4,5-bisphosphate 3-kinase (PI3K)/Akt pathway (Guilherme & Czech, 1998). Activation of Akt leads to phosphorylation of various substrates, including AS160 which regulates GLUT4 translocation or GSK-3 which promotes glycogen formation (Lin & Sun, 2010). IRS-1 is phosphorylated and *O*-GlcNAc modified (Vosseller *et al*., 2002b; Ball *et al*., 2006). It was shown that increased flux through the HBP leads to increased *O*-GlcNAcylation of IRS-1 which appears to reduce its binding to the p85 unit of PI3K (Federici *et al*., 2002; Vosseller *et al*., 2002b; Andreozzi *et al*., 2004). The p85 subunit of PI3K itself was also found to be *O*-GlcNAc modified (Federici *et al*., 2002; Ball *et al*., 2006). Furthermore, in 3T3-L1 adipocytes where insulin resistance was induced by inhibition of *O*-GlcNAc removal by incubation with PUGNAC cells also exhibited inhibition of insulin-

stimulated Akt activation (Vosseller *et al*., 2002b). This inhibition was most probably caused by increased Akt *O*-GlcNAcylation and concomitantly decreased Akt phosphorylation (Vosseller *et al*., 2002b). Similar studies in rat primary adipocytes also revealed that increased *O*-GlcNAcylation on Akt and IRS-1 by PUGNAC treatment inhibits their phosphorylation and induces insulin resistance (Park *et al*., 2005).

Another metabolic pathway involved in insulin signaling is glycogen metabolism. Glycogen synthase, the enzyme that converts Glc-1-P into glycogen is *O*-GlcNAc modified (Parker *et al*., 2003). It has been shown that increased flux through the HBP reduces glycogen synthesis (Crook *et al*., 1995). In NIH-3T3-L1 adipocytes glucosamine or high concentrations of glucose inhibit insulin-stimulated activation of glycogen synthase and this inhibition was associated with increased *O*-GlcNAc modification of the enzyme (Parker *et al*., 2003). Furthermore, diabetic streptozotocin-treated mice exhibited reduced glycogen synthase activity and increased *O*-GlcNAcylation of glycogen synthase (Parker *et al*., 2003; Parker *et al*., 2004). GSK-3 is a key regulator of glycogen synthase. GSK-3 itself is *O*-GlcNAc modified and in the presence of PUGNAC GSK-3 phosphorylation is decreased, resulting in impaired GSK-3 signaling and reduced glucose uptake into cells (Vosseller *et al*., 2002b). This suggests that *O*-GlcNAc may inhibit glycogen synthase activity which further contributes to high intracellular glucose levels and thus increased *O*-GlcNAc modification on proteins which may exacerbate the induction of insulin resistance.

Insulin action leads to translocation of GLUT4 to the plasma membrane (Lin & Sun, 2010). *In vivo* and in *vitro* elevation of UDP-GlcNAc levels by high glucose or GlcN results in impaired GLUT4 translocation and reduced glucose uptake without changing GLUT4 expression (Heart *et al*., 2000; Park *et al*., 2005; Buse, 2006). These results were confirmed by the observation that overexpression of GFAT in transgenic mice was also accompanied by impaired GLUT4 translocation to the plasma membrane. The expression of GLUT4 and also GLUT1 was again unchanged (Cooksey *et al*., 1999). GLUT4 itself is *O*-GlcNAc modified (Park *et al*., 2005) and it is unclear whether impaired GLUT4 translocation is provoked by an increase of GLUT4 *O*-GlcNAcylation concomitant with a decrease of phosphorylation, it is caused by decreased Akt activation, or by other mechanisms (Slawson *et al*., 2006).

The HBP and *O*-GlcNAc have also been linked to the pathogenesis of complications of diabetes such as vascular diseases. Cardiomyocytes incubated with high glucose, develop impaired Ca^{2+} cycling. These cells exhibited reduced sarcoendoplasmic reticulum Ca^{2+}-

ATPase 2a (SERCA2a) mRNA and protein expression. The same results were obtained by overexpression of OGT (Clark *et al*., 2003). Overexpression of OGA, lowering *O*-GlcNAc levels, on the other hand resulted in improved Ca^{2+} cycling and restored SERCA2a protein levels in cardiomyocytes exposed to high glucose (Clark *et al*., 2003). These results suggest that *O*-GlcNAcylation is important in the development of diabetic cardiomyopathy (Clark *et al*., 2003). Furthermore, excess protein *O*-GlcNAcylation that exists in diabetic hearts of mice contributes to cardiac dysfunction. Adenovirus delivered overexpression of OGA in these diabetic hearts not only reduced overall *O*-GlcNAcylation, but also improved calcium signaling and had positive effects on diabetic cardiac function (Hu *et al*., 2005).

High glucose enhances the expression of plasminogen activator inhibitor-1 (PAI-1) which is thought to be involved in the development of nephropathy and atherosclerosis in diabetes (Eddy, 2002; Paueksakon *et al*., 2002). The expression of PAI-1 is regulated by Sp1 (Chen *et al*., 1998), a transcription factor that is *O*-GlcNAc modified (Jackson &Tjian, 1988). The *O*-GlcNAc modification of Sp1 increases under hyperglycemic conditions and by treatment with GlcN or PUGNAC (Haltiwanger *et al*., 1998; Du *et al*., 2000). The direct involvement of the HBP in PAI-1 activation has been shown by incubation with high glucose and overexpression of GFAT both of which lead to activation of the PAI-1 promoter in bovine aortic endothelial cells and mesangial cells (Du *et al*., 2000; James *et al*., 2000). In contrast, Sp1 induced activation of PAI-1 gene expression can be prevented by OGT knockdown by RNA interference (Goldberg *et al*., 2006).

Last but not least, vascular endothelial damage due to high glucose in diabetes is most probably caused by inhibition of eNOS by increased *O*-GlcNAcylation and decreased phosphorylation of the enzyme (Du *et al*., 2001). eNOS is an important vasodilator by generating the vasoprotective molecule nitric oxide (NO). NO inhibits platelet aggregation and adhesion and is an important protective molecule against vascular disease (Förstermann & Münzel, 2006). Inhibition of eNOS by *O*-GlcNAc therefore potentially contributes to endothelial dysfunction leading to increased risk of vascular damage, heart attack and stroke in diabetes. Besides, under normal conditions, eNOS activity is regulated by insulin via the insulin receptor/IRS-1/PI3K pathway (Zeng *et al*., 2000) which is impaired due to increased flux through the HBP in hyperglycemia (Federici *et al*., 2002).

There are also a few clinical studies that established a connection between insulin resistance and the HBP. GFAT activity was distinctly increased in skeletal muscle biopsies obtained from patients with type II diabetes (Yki-Järvinen *et al*., 1996). In human skeletal muscle cultures from diabetic patients glucose uptake is reversely regulated with GFAT activity and

GFAT activity is significantly stimulated by high glucose, insulin, and their combination (Daniels *et al*., 1996). Increased GFAT activity also correlates with body mass index in control patients, but not in patients with diabetes (Daniels *et al*., 1996). In accordance with the studies in muscle, GFAT activity was also shown to correlate with obesity and levels of the satiety hormone leptin in human adipose tissue (Considine *et al*., 2000). Furthermore, in healthy humans acute GlcN infusion appears to trigger some metabolic features of diabetes (Monauni *et al*., 2000).

Although numerous studies show that there is clear evidence that elevated flux through the HBP and increased *O*-GlcNAcylation are involved in the development of insulin resistance in type II diabetes (Copeland *et al*., 2008), the precise mechanisms are still not fully understood and further research remains necessary. The current opinion is that *O*-GlcNAc can induce insulin resistance; however, many other unknown factors are involved in this event (Buse, 2006; Robinson *et al*., 2007). Elucidation of the molecular events that contribute to the development of type 2 diabetes will lead to novel approaches for diagnosis and therapy.

1.7.2 Alzheimer's Disease

Alzheimer's disease is a chronic neurodegenerative disorder with various aetiologies leading to synaptic loss and dementia (Perry *et al*., 2003). Alzheimer's disease is the most common neurodegenerative disease and accounts for up to two thirds of all dementia cases and belongs to one of the leading causes of death amongst the elderly (Nussbaum & Ellis, 2003). Although the characteristic lesions of the disease were already described by Alois Alzheimer in 1906 the molecular mechanisms causing these lesions are still not fully elucidated (Möller & Graber, 1998). The major risk factor for Alzheimer's disease is aging, followed by genetic factors that also play a decisive role in the onset of the disease. Moreover, environmental factors are also discussed to increase the risk of developing Alzheimer's disease (Munoz & Feldman, 2000).

One mechanism related to aging that might play an important role in the development of Alzheimer's disease is oxidative damage evoked by reactive oxygen species such as free radicals produced during cellular respiration (Markesbery, 1997). Free radicals lead to oxidative damage of proteins, lipids, and DNA. These oxidation products are found to be increased in brains of patients with Alzheimer's disease (Markesbery, 1997).

The human brain is dependent on continuous glucose supply since the capacity of the brain to store energy is very limited (Peters *et al*., 2004). Normal aging is associated with a decline in brain glucose consumption at different regions of the brain (Kuhl *et al*., 1982; Moeller *et al*., 1996). Patients with Alzheimer's disease have a significantly marked decline in glucose uptake and metabolism compared to brains of age-matched healthy patients, as revealed by the use of fluorodeoxyglucose and positron emission tomography (FDG-PET) (Mielke *et al*., 1992; Mosconi *et al*., 2008). This impairment of glucose consumption precedes the appearance of clinical symptoms (Mosconi *et al*., 2008), leading to the assumption that it is rather a cause than a consequence of Alzheimer's disease. It has been shown that the decline in glucose metabolism in patients with Alzheimer's disease is a sensitive marker for disease progression (Alexander *et al*., 2002). However, the role of glucose metabolism in Alzheimer's disease is controversially discussed and the molecular mechanisms how impaired glucose uptake leads to, or how this impairment contributes to the disease is not fully understood. Reduced cerebral blood flow (De la Torre, 2004), impaired brain insulin signaling (Salkovic-Petrisic & Hoyer, 2007), oxidative stress (Schubert, 2005), and decreased brain glucose transporters (Simpson *et al*., 1994) are contemplable possibilities discussed in literature.
Glucose is transported from the bloodstream into the brain mainly by the major neuronal glucose transporters GLUT3 and GLUT1. Both glucose transporters were found to be decreased in Alzheimer's disease brain (Kalaria & Harik, 1989 Simpson *et al*., 1994; Harr *et al*., 1995; Mooradian *et al*., 1997; Liu *et al*., 2008; Liu *et al*., 2009a).

As already described in the previous chapters, UDP-GlcNAc synthesis is dependent of intracellular glucose concentration. Impaired glucose uptake observed in Alzheimer's disease will lead to decreased UDP-GlcNAc levels, which will in turn affect the *O*-GlcNAcylation of many proteins present in the brain since OGT is highly sensitive to varying glucose concentrations (Haltiwanger *et al*., 1992; Kreppel *et al*., 1997; Kreppel & Hart, 1999).
There are several lines of evidence that *O*-GlcNAcylation plays an important role in the brain. First, a majority of *O*-GlcNAc modified protein were isolated from brain. Many of the *O*-GlcNAc modified proteins in the brain are cytoskeletal proteins critical for neuronal function, such as neurofilaments (Dong *et al*., 1996), the microtubule-associated protein tau (Arnold *et al*., 1996), clathrin assembly protein-3 (AP-3) (Yao & Coleman 1998), and APP (Griffith *et al*., 1995). Second, as already stated, OGT and OGA are most abundant in brain (Lubas *et al*., 1997; Gao *et al*., 2001), especially in the hippocampus a brain region that is severely affected in Alzheimer's disease and which is relevant for learning and memory (Liu *et al*., 2004a). Last, the genes encoding for both OGT and OGA map regions associated with Alzheimer's

disease and other neurodegenerative diseases (Shafi *et al*., 2000; Bertram *et al*., 2000; Heckel *et al*., 1998; Comtesse *et al*., 2001).
Another evidence of importance of *O*-GlcNAc in neurons is the fact that it is involved in the regulation of axon branching and thus neuronal development (Francisco *et al*., 2009), synaptic transmission (Vosseller *et al*., 2006), and synaptic plasticity (Tallent *et al*., 2009). Synaptic plasticity is central to learning and memory and is also impaired in Alzheimer's disease (Shankar *et al*., 2008).

As indicated by the fact that glucose uptake is reduced in Alzheimer's disease brains, there are several studies that have revealed that *O*-GlcNAcylation is reduced in Alzheimer's disease brain compared to that of controls (Liu *et al*., 2004b; Liu *et al*., 2009b). Thus, the brain is likely to be sensitive to lowered glucose metabolism which affects its *O*-GlcNAcylation processes.
The above mentioned *O*-GlcNAcylated proteins, tau, APP, AP-3, and neurofilaments, are thought to be implicated in the aetiology of Alzheimer's disease with tau and APP being the most prominent proteins. The two major hallmarks of Alzheimer's disease are neurofibrillary tangles (NFTs) aggregated from hyperphosphorylated tau (Grundke-Iqbal *et al*., 1986a; Grundke-Iqbal *et al*., 1986b) and amyloid-ß (Aß) - a fragment of the APP protein - containing senile plaques (LaFerla *et al*., 2007).

Tau (tubulin associated unit) is a microtubule-associated low molecular weight protein existing in different isoforms. Tau proteins are mainly expressed in neurons (Brandt *et al*., 2005) and are required for microtubule assembly, polymerization, and stability in the cytoskeleton (Avila *et al*., 2004). Tau was originally considered to be exclusively expressed in neurons (Binder *et al*., 1985). However, recent studies indicate that tau is also present in glial cells and astrocytes (Papasozomenos & Binder, 1987; Shin *et al*., 1991; Lin *et al*., 2003).
Tau is a phosphoprotein with a molecular weight between 45 to 70 kDa, depending on the isoform and phosphorylation status (Delacourte & Buée, 2000; Lefebvre *et al*., 2003). Tau *O*-GlcNAcylation was initially shown on bovine tau (Arnold *et al*., 1996). Initial site mapping data indicated that one major site for *O*-GlcNAc modification is located to the microtubule-binding domain on bovine tau (Arnold *et al*., 1996). Subsequent investigations showed that tau is also extensively *O*-GlcNAc modified in healthy human brain (Liu *et al*., 2004b).
In Alzheimer's disease tau becomes hyperphosphorylated and forms insoluble paired helical filaments, which accumulate in the cytoplasm of neurons (Grundke-Iqbal *et al*., 1986b). As a result, tau is not able to bind to microtubules anymore, which destabilizes microtubules and

leads to failure of the neuron to maintain its cytoskeleton und ultimately to neuronal death (Ballatore *et al*., 2007). The development of NFTs is a major and possibly the main mechanism of neuronal loss in Alzheimer's disease (Ballatore *et al*., 2007). A correlation between the numbers of NFTs in brains of Alzheimer's disease patients and the severity of dementia symptoms has been shown (Arriagada *et al*., 1992).

Hyperphosphorylated tau in Alzheimer's disease brains contains less *O*-GlcNAc than normal tau (Liu *et al*., 2009b). As observed in several other *O*-GlcNAc modified proteins, *O*-GlcNAcylation and phosphorylation of tau are regulated reciprocally in cultured cells, rat brain slices, mouse brains, and human Alzheimer's disease brains (Liu *et al*., 2004b; Liu *et al*., 2009b). Furthermore, is has been shown that reduced *O*-GlcNAcylation induces hyperphosphorylation of tau (Liu *et al*., 2004b).

Lowering *O*-GlcNAcylation of tau by OGT knockdown with short hairpin RNA leads to increased phosphorylation in HEK293 cells (Liu *et al*., 2009b). Targeted deletion of OGT in mouse neurons results in neuronal dysfunction, increased levels of the tau protein, and hyperphosphorylation of tau (O'Donnell *et al*., 2004). By contrast, OGT overexpression increases *O*-GlcNAcylation and decreases phosphorylation of tau (Robertson *et al*., 2004). Similarly, inhibition of the HBP in mammalian brain decreases *O*-GlcNAcylation and induces phosphorylation of tau (Liu *et al*., 2009b). These studies indicate that *O*-GlcNAc sites negatively regulate *O*-phosphate sites and vice versa by proximal or same site occupancy (Dias & Hart, 2007). Since *O*-GlcNAcylation is regulated by intracellular glucose supply via decreased glucose flux (Kreppel & Hart, 1999) these investigations further support the hypothesis that reduced glucose metabolism in Alzheimer's disease brain decreases *O*-GlcNAcylation of tau, thus leading to hyperphosphorylation with all its detrimental effects (Dias & Hart, 2007). In this regard, an important finding was that the decrease in GLUT1 and GLUT3 is correlated to the decrease in *O*-GlcNAcylation, to the hyperphosphorylation of tau, and to the number of NFTs in human brains (Liu *et al*., 2008).

Starved mice are commonly used as an animal model to mimic lowered brain glucose metabolism (Li *et al*., 2006). Fasting causes decreased *O*-GlcNAcylation and induces hyperphosphorylation of tau, but also of neurofilaments in mouse brain (Liu *et al*., 2004b; Li *et al*., 2006; Liu *et al*., 2009b), except that the hyperphosphorylation stimulated by fasting was reversible after re-feeding, implicating that abnormal hyperphosphorylation of tau might be reversed at early stages of the disease (Li *et al*., 2006).

Phosphatases are enzymes that remove phosphate groups from its substrate. Inhibition of phosphatases may be another possibility to trigger hyperphosphorylation of tau. Protein

phosphatase 2A (PP2A) is the major phosphatase that regulates tau phosphorylation in human brain (Goedert *et al*., 1995; Liu *et al*., 2005). PP2A activity and mRNA expression were both found to be decreased in Alzheimer's disease brain (Gong *et al*., 1995; Vogelsberg-Ragaglia *et al*., 2001; Liu *et al*., 2005). These findings suggest that PP2A might, along with impaired glucose metabolism, be responsible for abnormal hyperphosphorylation of tau in Alzheimer's disease. Furthermore, fasted mice which showed decreased *O*-GlcNAcylation of tau also exhibited decreased PP2A activity (Planel *et al*., 2004).

In conclusion, impaired brain glucose metabolism in Alzheimer's disease, is at least partly caused by decreased GLUT1 and GLUT3 levels, which leads to decreased flux through the HBP. This in turn causes decreased UDP-GlcNAc levels and thus reduced *O*-GlcNAcylation of tau. Decreased *O*-GlcNAcylation again causes, in interaction with PP2A inhibition, abnormal hyperphosphorylation of tau, and ultimately, formation of NFTs leading to neurodegeneration (Liu *et al*., 2009b). Restoration of normal brain glucose metabolism, and in consequence *O*-GlcNAcylation of tau, may therefore be a promising target for treating Alzheimer's disease.

Another hallmark of Alzheimer's disease is the formation of senile plaques composed of Aß (LaFerla *et al*., 2007). Aß is derived from the intracellular cleavage of APP by ß- and γ-secretases, producing mainly $Aß_{1-40}$ and $Aß_{1-42}$ peptides with a length of 40 and 42 amino acids, respectively (Wolfe, 2002; Haass & Selkoe, 2007). APP is a single (type-I) transmembrane protein with a large extracellular domain that is ubiquitously expressed (Wilquet & De Strooper, 2004). Generation of Aß by cleavage of APP occurs via the above described amyloidogenic pathway by ß- and γ-secretases. However, the main proteolytic processing pathway of APP is the nonamyloidogenic pathway by α- and γ-secretases, generating a truncated Aß fragment, because α-secretase cleaves in the Aß sequence itself (Wilquet & De Strooper, 2004). Thus, the nonamyloidogenic pathway precludes the formation of Aß.

Aß forms multiple types of aggregates, such as monomers, oligomers, protofibrils, fibrils, and plaques (Snyder *et al*., 1994; Dahlgren *et al*., 2002). $Aß_{1-42}$ peptides are more prone to form aggregates than $Aß_{1-40}$ (Dahlgren *et al*., 2002). $Aß_{1-40}$ remains mainly as a monomer and was shown to exert less detrimental effects on neuronal viability than does $Aß_{1-42}$ (Dahlgren *et al*., 2002). Furthermore, $Aß_{1-42}$ is the predominant form found in Aß containing senile plaques (Younkin, 1998). Most familiar cases of Alzheimer's disease exhibit mutations in APP or presenilins - subunits of γ-secretase responsible for APP cleavage - leading to an increased $Aß_{1-42}$: $Aß_{1-40}$ ratio found in patients with Alzheimer's disease (Borchelt *et al*., 1996). Recent

studies have indicated that not only fibrillar Aß, but also soluble oligomers of Aß cause neurotoxicity (Klein *et al*., 2001). However, the exact role of fibrillar and oligomeric Aß in Alzheimer's disease is not yet known. At first it was thought that accumulation of insoluble fibrillar Aß occurs exclusively extracellularly. This hypothesis was modified when the pathogenic character of soluble Aß was discovered. There is now sufficient evidence that Aß accumulation occurs extracellularly, as well as inside neurons (Mohamed & Posse de Chaves, 2011). Intraneuronal Aß is derived from intracellular cleavage of APP and from internalization from the extracellular space (Mohamed & Posse de Chaves, 2011).

APP is the first plasma membrane protein reported to be *O*-GlcNAc modified (Griffith *et al*., 1995). *O*-GlcNAcylation of APP has an effect on its processing. Increasing *O*-GlcNAcylation of APP by inhibition of OGA by PUGNAC results in increased secretion of sAPPα and decreased Aß formation (Jacobsen & Iverfeldt, 2011). sAPPα is an APP fragment generated together with truncated Aß by nonamyloidogenic α-secretase processing of APP. sAPPα has been shown to have neuroprotective effects (Goodman & Mattson, 1994). Thus, stimulation of APP *O*-GlcNAcylation enhances APP processing via the nonamyloidogenic pathway, making it a promising therapeutic target (Jacobsen & Iverfeldt, 2011).

The toxic effects of Aß are mediated, at least in part, by being a potent inducer of oxidative stress through the generation of free radicals that lead to inhibition of the mitochondrial respiratory chain (Behl *et al*., 1994; Miranda *et al*., 2000; Canevari *et al*., 2004). There is strong evidence that at least one cause of tau hyperphosphorylation in neurons is mitochondrial dysfunction induced by Aß (Melov *et al*., 2007; Su *et al*., 2010; Garwood *et al*., 2011), indicating that Aß precedes hyperphosphorylation of tau (LaFerla *et al*., 2007).

The hypothesis that Aß is a causative agent in Alzheimer's disease is further corroborated by the fact that Aß can cause deficient glucose uptake and metabolism (Prapong *et al*., 2002; Niwa *et al*., 2002). However, it was shown that decreased glucose uptake by Aß occurred despite a significant increase in GLUT3 translocation and mRNA transcription, possibly by inhibiting fusion of GLUT3-containing vesicles with the plasma membrane (Prapong *et al*., 2002).

NFTs composed of hyperphosphorylated tau and Aß containing senile plaques are the major hallmarks of Alzheimer's disease. The underlying mechanisms between NFTs and senile plaques have not yet been resolved, although there is evidence that oxidative stress induced by Aß may be related to tau hyperphosphorylation and both characteristics are linked to impaired glucose uptake and metabolism.

AP-3 is *O*-GlcNAc modified (Yao & Coleman, 1998) and its *O*-GlcNAcylation was shown to be decreased in autopsied human brains with Alzheimer's disease compared to age-matched controls (Yao & Coleman, 1998). Furthermore, a negative correlation between *O*-GlcNAcylated AP-3 and the density of NFTs has been detected (Yao & Coleman, 1998). AP-3 is a synapse specific protein that is involved in vesicle assembly through a clathrin-dependent mechanism. Aberrant *O*-GlcNAcylation may therefore result in impaired synaptic vesicle recycling (Yao & Coleman, 1998).

Synapsin I is a neuron-specific phosphoprotein that anchors synaptic vesicles to the cytoskeleton and is involved in the regulation of neurotransmitter release (Ferreira & Rapoport, 2002). Synapsins are also suggested to play an important role during neuronal development (Ferreira & Rapoport, 2002). Anchoring of synaptic vesicles to the cytoskeleton proceeds in a phosphorylation-dependent manner (Yamamoto *et al*., 2003). Synapsin I is also *O*-GlcNAc modified and the *O*-GlcNAcylation sites are in close vicinity to the phosphorylation sites, suggesting interplay between both modifications (Cole & Hart, 1999). Therefore, *O*-GlcNAcylation may affect the interaction of synapsin I with the cytoskeleton.

Neurofilaments are the most abundant cytoskeletal elements in neurons (Lee *et al*., 1993). They play an important role in the growth and are responsible for the maintenance of myelinated axons (Lee *et al*., 1993; Al-Chalabi & Miller, 2003). Neurofilament mutations have been associated witch several human neurodegenerative diseases such as Parkinson's disease and amyotrophic lateral sclerosis (Al-Chalabi & Miller, 2003). The low (NF-L), medium (NF-M), and high (NF-H) molecular weight subunits of neurofilaments were shown to be *O*-GlcNAc modified (Dong *et al*., 1993; Dong *et al*., 1996). Increasing evidence indicates that phosphorylation of neurofilaments is a mechanism for regulating their transport properties (Miller *et al*., 2000). The *O*-GlcNAc levels of neurofilaments in human neurons and in spinal cord tissue of rat model of amyotrophic lateral sclerosis was found to be decreased (Lüdemann *et al*., 2005).

A relation has been established between diabetic neuropathy and phosphorylation of neurofilaments. Changes in the phosphorylation status of neurofilaments could lead to severe impairments in axon structure and function. In animal models of type I diabetes an increase in neurofilament phosphorylation has been observed. This abnormal phosphorylation may contribute to the neuropathy observed in diabetes (Fernyhough *et al*., 1999; Fernyhough *et al*., 2002). Until now, there are no studies that revealed a connection between *O*-GlcNAcylation of neurofilaments and its function or role in diseases.

In this context, it is worth mentioning that decreased *O*-GlcNAcylation of tau concomitant with hyperphosphorylation, as observed in Alzheimer's disease, was also detected in brain tissue of type II diabetes patients (Liu *et al*., 2009a). Furthermore, type II diabetes, which is also characterized by deficient glucose uptake and aberrant *O*-GlcNAcylation, is known to increase the risk for Alzheimer's disease (Xu *et al*., 2009). On this account, Alzheimer's disease is sometimes referred to as "diabetes type 3" (De la Monte *et al*., 2006).

To conclude, several important proteins in Alzheimer's disease and other neurological disorders are *O*-GlcNAc modified. The most important example in this respect is the decreased *O*-GlcNAcylation and abnormal hyperphosphorylation of tau, resulting in formation of NFTs. Although hyperphosphorylation of tau might directly result from decreased flux through the HBP due to impaired glucose metabolism in Alzheimer's disease, the exact causes leading to hyperphosphorylation of tau remain unresolved. As a candidate cause, mitochondrial oxidative stress induced by Aß toxicity is discussed. However, more studies are needed to elucidate the relationship between tau and Aß in Alzheimer's disease.

1.7.4 Cancer

There is growing evidence that glycans play a role in cancer since they are aberrantly expressed in cancer cells (Fuster & Esko, 2005). Glycans control different aspects of malignant cells such as proliferation, invasion, and metastasis (Fuster & Esko, 2005). For example, cancer cells produce lager *N*-glycans with increased branching compared to nonmalignant cells, which implies higher need for UDP-GlcNAc, the donor molecule for *N*-glycans (Yousefi *et al*., 1991). Apart from glycosylation emerging studies indicate that *O*-GlcNAc signaling is altered in cancer as well (Slawson *et al*., 2010).

A hallmark of cancer cells is the production of energy by a high rate of glycolysis instead of oxidative phosphorylation - the so called Warburg effect (Vander Heiden *et al*., 2009). Aerobic glycolysis is less efficient to produce ATP than oxidative phosphorylation; however, it provides highly proliferating cancer cells with biosynthetic molecules such as nucleotides, amino acids, and lipids required to produce new cells (Vander Heiden *et al*., 2009). Cancer cells have to metabolize carbon and nitrogen rich nutrients to sustain the metabolic demands needed for proliferation.
In addition to having high glycolytic rates, cancer cells exhibit an increased rate of glutamine consumption (Deberardinis *et al*., 2008). In many tumors glutamine is the main energy source

by being introduced as an anaplerotic substrate into the TCA cycle and by being metabolized into lactate (glutaminolysis) (Deberardinis *et al*., 2008). The HBP is highly dependent on both glucose and glutamine to produce UDP-GlcNAc.

A first relation between activated sugar nucleotides and cancer was established after UDP-sugar levels were found to be increased in ^{31}P-NMR spectra of perfused human breast cancer cells (Cohen *et al*., 1986) and human melanoma tumors (Corbett *et al*., 1987). These observations were further corroborated in ^{1}H-NMR spectra of breast tumor tissues where increased levels of UDP-GlcNAc and UDP-GalNAc were detected compared to non-involved breast tissue (Gribbestad *et al*., 1994). Elevated UDP-GlcNAc and UDP-GalNAc levels were also detected in breast and pancreatic cancer cell lines (Nakajima *et al*., 2010). In the same study higher levels of GDP-Fuc were found in both cancer cell lines compared to a noncancerous cell line (Nakajima *et al*., 2010). In colon cancer cells the intracellular accumulation of UDP-GlcNAc and UDP-GalNAc is associated with the inability of these cells to differentiate (Wice *et al*., 1985). Elevation of activated sugar nucleotides by GlcN induced growth inhibitory effects on colon carcinoma cells (Krug *et al*., 1984). These studies have demonstrated that UDP-GlcNAc and UDP-GalNAc are of significance in cancer cells and tumors, but the specific functions for these compounds were unclear.

In a recent study, elevated UDP-GlcNAc and UDP-GalNAc levels were detected as markers of cisplatin treatment response in brain tumor cells using ^{1}H-NMR spectroscopy (Pan *et al*., 2011). This study has linked UDP-GlcNAc and UDP-GalNAc to cancer cell death in response to chemotherapy (Pan *et al*., 2011). If the increase in UDP-GlcNAc and UDP-GalNAc following cisplatin treatment was due to a decrease in utilization of both activated sugar nucleotides or due to an increase in production remained unclear (Pan *et al*., 2011).

A few studies have investigated the role of *O*-GlcNAcylation in cancer progression. The *O*-GlcNAcylation level in breast cancer tissue was found to be significantly elevated as compared with noninvolved adjacent tissue (Gu *et al*., 2010). Furthermore, *O*-GlcNAcylation was also enhanced in metastatic lymph nodes (Gu *et al*., 2010). Moreover, in the same study it was shown that *O*-GlcNAcylation enhances migration and invasion of breast cancer cells (Gu *et al*., 2010).

Further studies in different cancers corroborated the finding that flux through the HBP and *O*-GlcNAcylation were upregulated in tumor tissues (Caldwell *et al*., 2010; Slawson & Hart, 2011; Lynch *et al*., 2012). Elevated expression of OGT was detected in breast cancer cells and reduction of OGT expression by RNA interference, as well as pharmacological inhibition of OGT, resulted in inhibition of cell growth in *vitro* and *in vivo* (Caldwell *et al*., 2010). The

reduced proliferation was associated with decreased cell-cycle progression and correlated with increased expression of the cell-cycle inhibitor protein p27 (Caldwell *et al*., 2010). In addition, OGT knockdown and inhibition also decreased breast cancer cell invasion (Caldwell *et al*., 2010). OGT protein levels were also found to be increased in prostate carcinoma cells and inhibition of *O*-GlcNAcylation led to inhibition of invasion (Lynch *et al*., 2012). Regulation of invasion by OGT correlated with protein degradation of the oncogenic transcription factor FoxM1, a key regulator of invasion (Lynch *et al*., 2012).
Despite few studies that reported decreased *O*-GlcNAcylation (Slawson *et al*., 2001) and increased OGA activity (Slawson *et al*., 2001; Krzeslak *et al*., 2010) in tumors, increased *O*-GlcNAcylation seems to be a common characteristic of cancer cells.

In addition, *O*-GlcNAc elevation has been shown to regulate cancer cell growth and metabolism by inhibiting phosphofructokinase 1 activity (PFK1) (Yi *et al*., 2012), a key enzyme that controls flux through glycolysis (Sola-Penna *et al*., 2010). PFK1 *O*-GlcNAcylation was shown in various different cancer cell lines, such as breast, prostate, liver, colon, and cervical cells (Yi *et al*., 2012). PFK1 *O*-GlcNAcylation is more elevated in malignant than in nonmalignant breast and prostate cancer cells and correlates with the cancer stage in lung adenocarcinoma tumors (Yi *et al*., 2012). PFK1 is *O*-GlcNAc modified at a highly conserved site important for allosteric regulation of PFK1 by fructose-2,6-bisphosphate (Fru-2,6-BP), an activator of PFK1 at high ATP concentrations usually found in cancer cells (Ferreras *et al*., 2009; Yi *et al*., 2012). This implies that *O*-GlcNAcylation of PFK1 inhibits the allosteric activation of PFK1 by Fruc-2,6-BP (Yi *et al*., 2012). It was shown that elevation of *O*-GlcNAc suppresses flux through glycolysis and redirects glucose into the PPP, supplying cells with pentose sugars for nucleotide biosynthesis required for rapid cell growth, as well as NADPH needed for biosynthesis of the cells most important antioxidant glutathione (GSH) to combat oxidative cell death (Yi *et al*., 2012). Inhibition of *O*-GlcNAc on PFK1 on the other hand was shown to decrease cancer cell proliferation and to impair tumor formation (Yi *et al*., 2012). Thus, increased flux through the PPP induced by *O*-GlcNAcylation of PFK1 might help promote proliferation and cancer cell survival (Yi *et al*., 2012).

Certain transcription factors involved in tumorigenesis are also directly *O*-GlcNAcylated by OGT (Slawson & Hart, 2011). Myc is a transcription factor that is involved in cell proliferation and is deregulated in cancers (Dang, 2010). Myc regulates genes involved in glucose metabolism, purine and pyrimidine biosynthesis, and lipid metabolism. Moreover,

myc stimulates glutamine catabolism, mitochondria biogenesis (Dang, 2010), and regulates HBP genes (Morrish *et al*., 2009). *O*-GlcNAcylation of myc at its phosphorylation site would inhibit phosphorylation and might possibly stabilize the protein leading to unregulated expression of various genes and uncontrolled cell division (Slawson *et al*., 2010).

The interplay between *O*-GlcNAc and *O*-phosphate also occurs at the tumor suppressor protein p53 (Yang *et al*., 2006). *O*-GlcNAcylation of p53 is associated with decreased phosphorylation of the protein resulting in stabilization and increased activity of p53 (Yang *et al*., 2006). Since p53 is a tumor suppressor, stabilization of the protein would prevent cancer. However, the effects of p53 *O*-GlcNAcylation are not yet understood.

It is apparent that regulation of cell cycle by *O*-GlcNAcylation is of major importance in nonmalignant, as well as cancer cells. In cervical carcinoma HeLa cells overexpression of either OGT or OGA causes defects in mitotic progression (Slawson *et al*., 2005). A characteristic of cancer is abnormal number of chromosomes (aneuploidy), which promotes tumor cell growth (Bannon & Mc Gee, 2009). Overexpression of OGT causes aneuploidy through defective mitosis (Slawson *et al*., 2005). OGT localizes to the mitotic spindle and *O*-GlcNAcylates various mitotic spindle and midbody proteins (Slawson *et al*., 2005; Wang *et al*., 2010). This leads to the conclusion that *O*-GlcNAcylation is involved in the regulation of mitotic progression and that its disruption is associated with tumorigenesis (Slawson *et al*., 2010).

To conclude, diseases such as diabetes, Alzheimer's disease, and cancer are increasingly becoming major health risks to industrialized countries. All three diseases are characterized by alterations in glucose metabolism and flux through the HBP, leading to disrupted *O*-GlcNAc signaling. These alterations disturb cellular signaling cascades involved in the pathology of the diseases. Diabetes is a risk factor for Alzheimer's disease (Xu *et al*., 2009) and cancer (Barone *et al*., 2008), and the underlying mechanisms are only gradually being understood. Elucidating the molecular mechanisms of these three diseases will provide new markers of malignancy and targets for therapeutic treatment.

1.8 Brain Energy Metabolism

1.8.1 Introduction

Since some parts of this work deal exclusively with the energy metabolism of brain cells (neurons and astrocytes) their metabolism is discussed in more detail in this chapter.

Although the weight of the human brain is only 2 % - 3 % of the total body weight, it consumes up to 50 % of the body glucose (Sokoloff, 1983-1984; Fehm *et al*., 2006). Glucose is the main energy substrate for the brain. Oxygen is utilized in the brain almost entirely for the oxidation of glucose to CO_2 and H_2O in the TCA cycle (Sokoloff, 1977; Sokoloff, 1992; Gjedde & Marrett, 2001). On this account normal brain function relies on the supply of both glucose and oxygen by the blood.

The brain consists predominantly of two cell types that differ in morphology and function: neurons and glia cells. Neurons mainly process and transmit information through electrical and chemical signals. Glial cells are sub-divided into astrocytes, oligodendrocytes (oligodendroglia), microglia, satellite sells, and Schwann cells. There are ten times more glial cells than neurons in the brain. The role of glial cells has only recently begun to be understood. In the past glial cells were only thought to structurally support neurons and serve as a kind of glue holding them together (glia: Greek from glue).
The star-shaped astrocytes are the most abundant and largest cells among the glia cells. To date, it is known that astrocytes play an important role for brain function and neuronal activity, such as the supply of neurons with energy substrates and neurotransmitter precursors (Vesce *et al*., 2001). One example is the so called “glutamine-glutamate cycle” between astrocytes and neurons (see Figure 8). Glutamate released from neurons into the synaptic cleft has to be removed quickly to guarantee normal brain function. This task is carried out by uptake of the neurotransmitter glutamate through astrocytic glutamate transporters (Rothstein *et al*., 1996). After uptake of glutamate into astrocytes, glutamate is amidated to glutamine by the glia-specific enzyme glutamine synthetase (GS) (Martinez-Hernandez *et al*., 1977; Tansey *et al*., 1991). To close the cycle glutamine is transferred back to the neuron where is it converted to glutamate by the phosphate-activated glutaminase (PAG). Since glucose is converted to glutamate by the TCA cycle the “glutamine-glutamate cycle” is coupled to glucose metabolism.

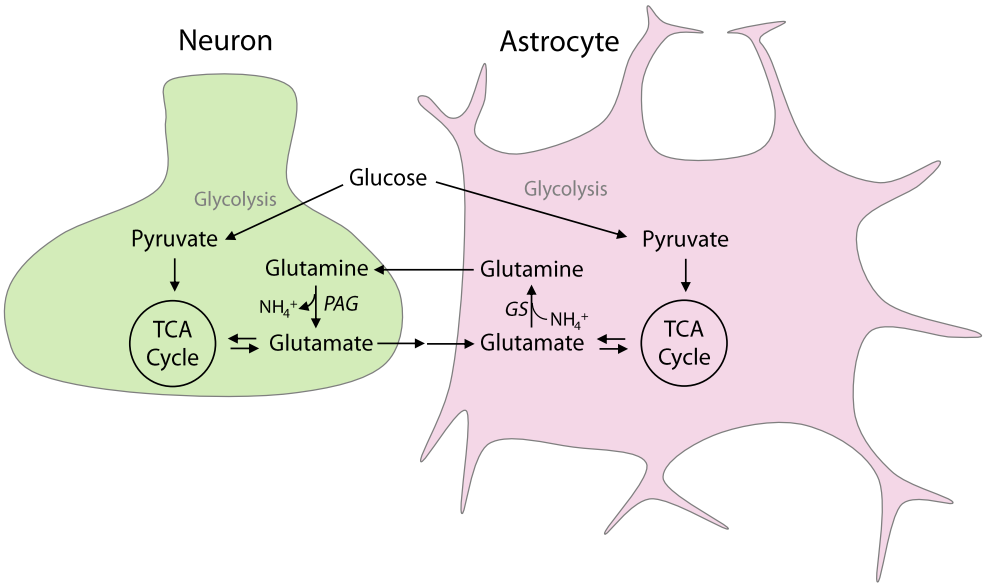

Figure 8. The "glutamine-glutamate" cycle between astrocytes and neurons. In glycolysis glucose is converted to pyruvate, which enters the TCA cycle to synthesize glutamate in both astrocytes and neurons. Neurons release glutamate as a neurotransmitter. The extracellular glutamate is now taken up into astrocytes by astrocytic glutamate transporters, where it is amidated by GS to glutamine. Glutamine is then transported back to the neurons and is converted to glutamate by PAG. GS, glutamine synthetase; PAG, phosphate-activated glutaminase; TCA cycle, tricarboxylic acid cycle.

1.8.2 Astrocytic and Neuronal Glucose Metabolism

Brain energy metabolism is often attributed exclusively to neuronal energy metabolism and glucose has been thought to be mainly metabolized by neurons, since neurons have a predominant oxidative metabolism. However, this does not necessarily mean that the majority of glucose is taken up and metabolized by neurons. Indeed, there is evidence that astrocytes are the primary site of glucose uptake during neuronal activity (Tsacopoulos & Magistretti, 1996). Glucose uptake in cultured astrocytes was measured with the 2-deoxyglucose method and revealed that glucose uptake into astrocytes (100 – 250 nmol/h/mg protein) was twice as much as into neurons (Peng *et al*., 1994). Further evidence that astrocytes display high glycolytic activity is the fact that glycogen - the storage form of glucose - is almost exclusively localized in astrocytes (Cataldo & Broadwell, 1986; Magistretti *et al*., 1993). Glycogenolysis in astrocytes is controlled by specific neurotransmitters that can be mobilized during neuronal activity (Magistretti *et al*., 1993). The anatomical localization of astrocytes also indicates a high glucose metabolism. The end-feet of astrocytes enwrap virtually all blood vessels in the brain. For this reason glucose largely passes through astrocytes (Tsacopoulos & Magistretti, 1996).

In 1994 Pellerin and Magistretti proposed the astrocyte–neuron lactate shuttle hypothesis (ANLSH) whereby lactate is produced via glycolysis in astrocytes and supplied to the neurons

as an energy substrate (Magistretti & Pellerin, 1994; Tsacopoulos & Magistretti, 1996; Magistretti *et al*., 1999; Magistretti & Pellerin, 1999; Pellerin & Magistretti, 2003; Pellerin *et al*., 2007; Pellerin & Magistretti, 2012). The mechanism is triggered by glutamate released from neurons under neuronal activity. To remove glutamate from the synaptic cleft it is taken up by astrocytes via Na^+-dependent cotransport (Kimelberg *et al*., 1989), leading to intracellular increase of Na^+ concentration. This increase activates ATP fueled Na^+/K^+-ATPase (Vizi, 1972; Silver & Erecinska, 1997) which in turn stimulates glycolysis and hence lactate production. The ANLSH is described in more detail in Figure 9. In agreement with the ANLSH, it was found that astrocytes have the capacity to release larger amounts of lactate than neurons (Walz & Mukerji, 1988).

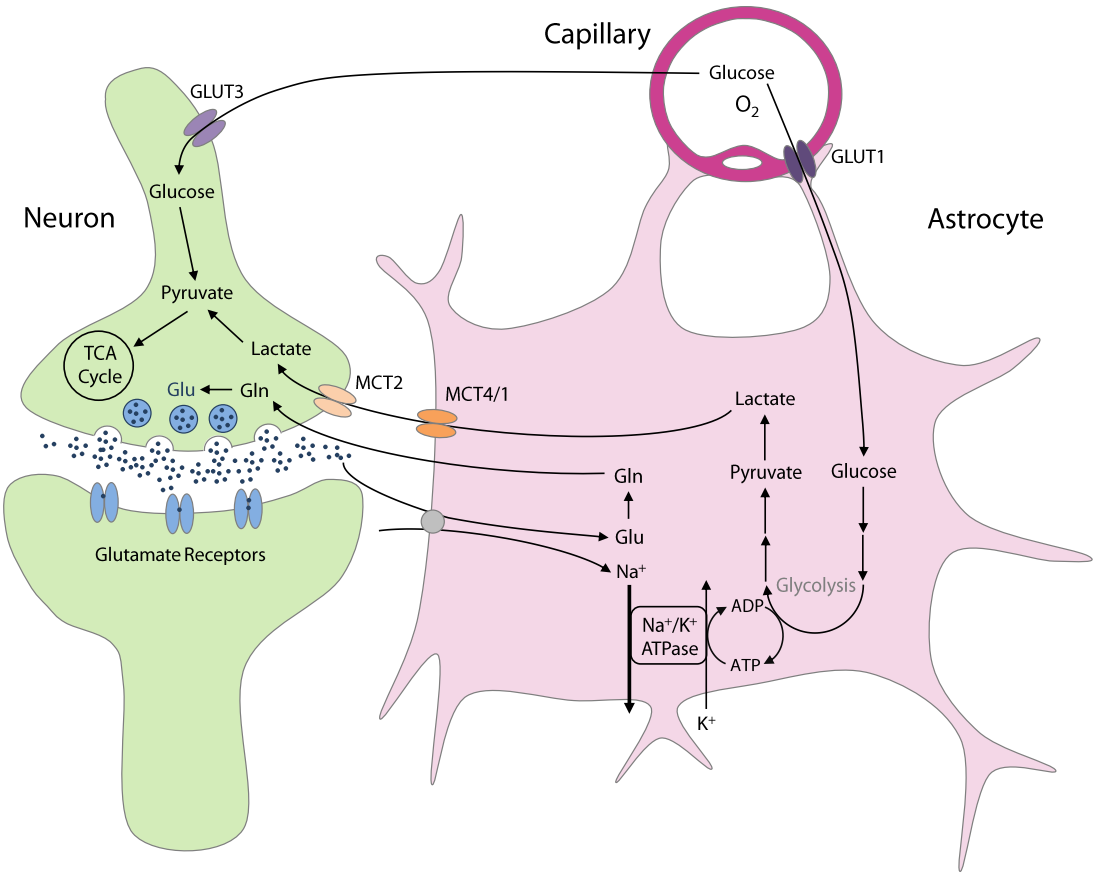

Figure 9. Schematic overview of the glucose metabolism during neuronal activity in neurons and astrocytes, according to the astrocyte–neuron lactate shuttle hypothesis (ANLSH) proposed by Pellerin & Magistretti, 1994. Glucose is directly taken up into astrocytes and neurons by GLUT1 and GLUT3 and is metabolized via mitochondrial oxidative phosphorylation. Note that astrocytes have their own TCA cycle, which is omitted for graphic clarity here. During neuronal activity glutamatergic neurons release glutamate. To remove glutamate from the synaptic cleft it is taken up by neurons and astrocytes in a Na^+-dependent cotransport. The increasing intracellular Na^+ concentration activates the Na^+/K^+-ATPase, which in turn stimulates astrocytic glycolysis and hence lactate formation. Lactate is then released to the extracellular space and can be taken up by neurons to fuel neuronal energy metabolism. ADP, adenosine diphosphate; ATP, adenosine triphosphates; Gln, glutamine; Glu, glutamate; GLUT, glucose transporter; MCT, monocarboxylate transporter; TCA cycle, tricarboxylic acid cycle.

To date, the hypothesis is controversially discussed and ambiguity still exists to which extent glucose is metabolized by neurons and astrocytes (Magistretti & Pellerin, 1999; Dienel & Hertz, 2001). However, it is important to keep in mind that this hypothesis does not exclude glucose as an energy substrate for neurons. Glucose transporters are present on both astrocytes and neurons and both cell types are able to oxidize glucose completely to CO_2 and H_2O in glycolysis and TCA cycle (Vannucci *et al*., 1997). Lactate has to be considered as an additional energy supply during neuronal activity. In recent years, several *in vitro* studies using different approaches have confirmed that lactate is an efficient energy substrate for neurons (Pellerin *et al*., 1998; Waagepetersen *et al*., 1998; Bouzier *et al*., 2000; Kitano *et al*., 2002). Aside from that, prevalent expression of genes encoding glycolytic enzymes was discovered by transcriptomic analysis of acutely isolated astrocytes compared to neurons (Lovatt *et al*., 2007; Cahoy *et al*., 2008). Moreover, *in vivo* results indicate that astrocytes respond to neuronal activity by an accelerated glucose uptake, whereas neuronal uptake remains nearly unchanged (Chuquet *et al*., 2010).

1.9 The Role of Nitric Oxide in Astrocytes

1.9.1 Hypoxia and HIF

The transcription factor hypoxia-inducible factor 1 (HIF-1) is a heterodimeric complex consisting of the subunits HIF-1α and HIF-1ß (Wang *et al*., 1995). Ubiquitously expressed HIF-1 controls the transcription of more than 100 genes that regulate cellular adaption to hypoxia (Maxwell, 2005). HIF-1 controls the transcription of genes involved in crucial cellular functions such as erythropoietin, vascular endothelial growth factor, glucose transporters and glycolytic enzymes (Maxwell, 2005). Aberrant regulation of HIF-1 is found in human diseases such as cancer (Semenza, 2000). Under normoxic conditions, two proline residues of HIF-1α (Pro-402 and Pro-564) are hydroxylated by specific HIF-1α prolyl hydroxylases (PHDs). Hydroxylation requires 2-oxoglutarate, O_2, Fe^{2+}, and ascorbate (Schofield & Zhang, 1999). In turn, von Hippel-Lindau protein binds to hydroxylated proline residues of HIF-1α leading to ubiquitin-dependent proteasomal degradation (Kamura *et al*., 2000; Ivan *et al*., 2001, Jaakkola *et al*., 2001). Under hypoxic conditions, however, PHDs are inactivated and HIF-1α is stabilized and accumulates. HIF-1α migrates to the nucleus where it dimerizes with HIF-1ß and binds to hypoxia response elements (HREs) contained in the promoter of target genes, allowing transcriptional activation (Huang *et al*., 1998; Semenza,

1999; Kallio *et al.*, 1999). The transport of HIF-1α from cytoplasm into nucleus is a complex process involving several members of the importin transporter family (Chachami *et al.*, 2009). A schematic overview of HIF-1α regulation is shown in Figure 10.

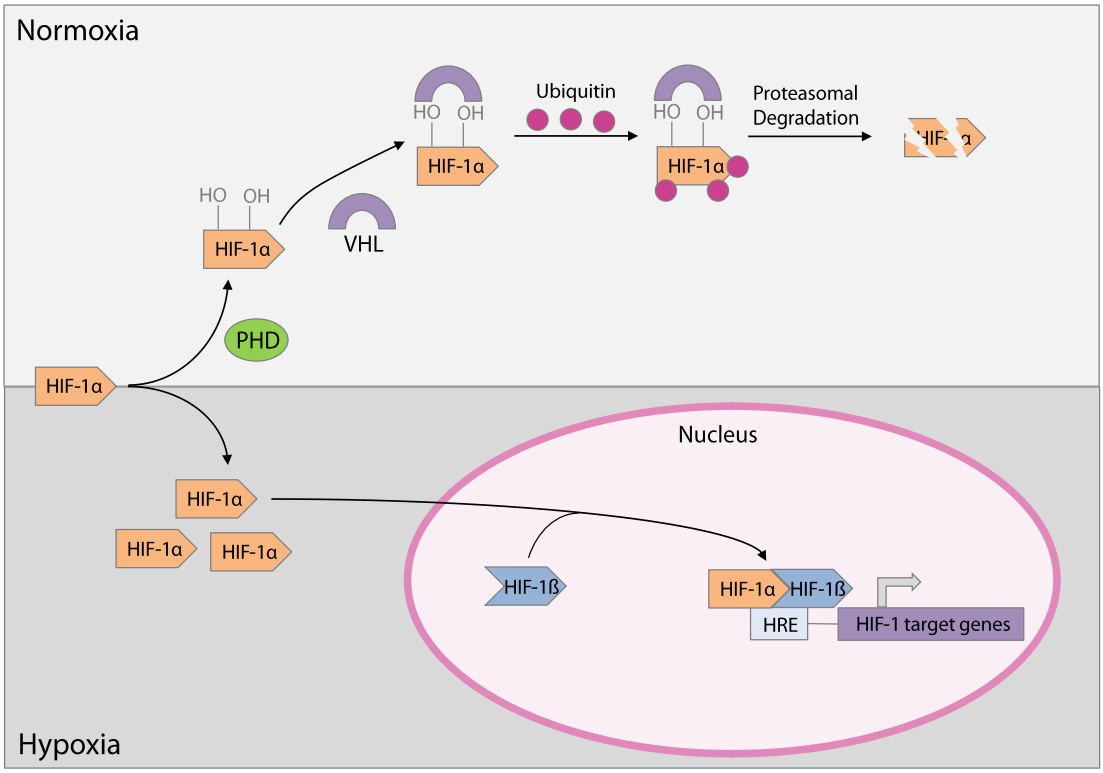

Figure 10. Simplified overview of HIF-1α regulation. In normoxia HIF-1 is hydroxylated by PHDs. Hydroxylated HIF-1α is recognized by the VHL protein. This interaction leads to ubiquitinylation and subsequent degradation of HIF-1α by the proteasome. In a hypoxic environment proline hydroxylation by PHDs is inhibited and VHL binding and proteasomal degradation does not take place. This leads to HIF-1α stabilization and translocation to the nucleus, where HIF-1α dimerizes with HIF-1ß. The complex binds to HREs within the promoters of target genes enabling transcriptional regulation. HIF, hypoxia-inducible factor; HRE, hypoxia-response element; PHD, prolyl hydroxylase; VHL, von Hippel-Lindau.

1.9.2 Nitric Oxide (NO)

HIF-1α is not only stabilized under hypoxic conditions, but also independent from O_2 tension by certain compounds. Deferoxamine, for example, induces HIF-1α stabilization by chelating iron and thus inhibiting PHDs (Wang & Semenza, 1993). Physiological substances are known to stabilize HIF-1α in normoxia, too. Amongst others, these substances comprise TNF-α, interleukin-1α, and interleukin-18 (Van Uden *et al.*, 2008; Hellwig-Bürgel *et al.*, 1999; Kim *et al.*, 2008). Other small molecules with physiological significance having impact on stabilizing HIF-1α under normoxic conditions are carbon monoxide (CO) (Choi *et al.*, 2010) and NO (Sandau *et al.*, 2001; Kasuno *et al.*, 2004; Park *et al.*, 2008). Both appear to inhibit PHDs via the PI3K/AKT/mTOR pathway (Sandau *et al.*, 2000, Choi *et al.*, 2010). In hypoxia,

however, these substances exhibit destabilizing effects on HIF-1α (Sogawa *et al*., 1998; Huang *et al*., 1999). The reason for this is that NO is also an inhibitor of mitochondrial respiration (see Chapter 1.9.3). This inhibition leads to redistribution of O_2 away from the mitochondria toward other oxygen-dependent targets, e.g. PHDs. PHDs are no longer able to sense hypoxia and HIF-1α remains destabilized (Hagen *et al*., 2003).

In mammals, NO synthases (NOS) form NO catalytically from the terminal guanidine nitrogen of L-arginine as substrate, producing L-citrulline (Figure 11) (Palmer *et al*., 1987; Knowles & Moncada, 1994). NO is an important intercellular messenger in the central nervous system (CNS) and can be produced by all brain cells, including astrocytes, neurons, and endothelial cells (Garthwaite & Boulton, 1995; Murphy & Grzybicki, 1996). NO is a gaseous radical with a physiological concentration range between 100 pM (or below) up to 5 nM (Hall & Garthwaite, 2009) that can simply and widely (≈ 400 µm) diffuse through membranes (Ledo *et al*., 2005).

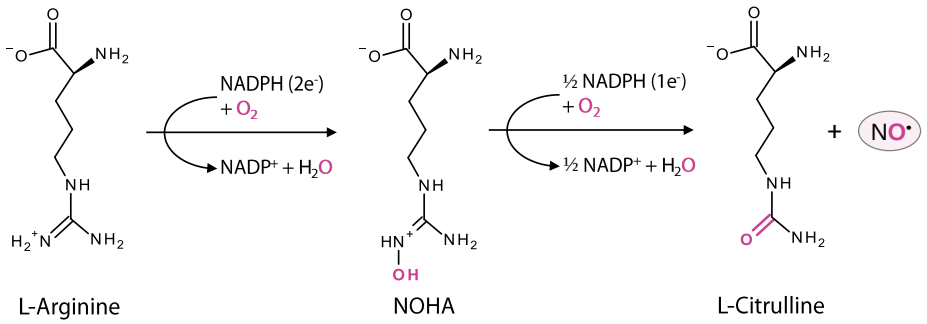

Figure 11. Catalytic steps of NO synthase: Hydroxylation of the guanidino nitrogen of L-arginine leads to the formation of NOHA. One molecule of oxygen and one equivalent of NADPH are required for this reaction. For the oxidation of NOHA a second molecule of oxygen and a single electron is needed (½ NADPH). L-Citrulline, the NO radical, and two molecules of water are formed (adapted from Santolini, 2011). NADP, nicotinamide adenine dinucleotide phosphate; NO, nitric oxide; NOHA, N^{ω}-hydroxyl-arginine.

NO synthesis is catalyzed by three different isoenzymes: The calcium/calmodulin dependent endothelial NOS (eNOS or NOS3) and neuronal NOS (nNOS or NOS1), and the inducible isoform (iNOS or NOS2), which is calcium independent and regulated by induction of transcription in glial cells, for example (Förstermann *et al*., 1991; Seidel *et al*., 1997; Stanarius *et al*., 1997; Kleinert *et al*., 2004; Zhou & Zhu, 2009). Other than calmodulin, NOS require flavin adenine dinucleotide (FAD), flavin mononucleotide (FMN), NADPH, and tetrahydrobiopterin (BH_4) as enzymatic cofactors (Knowles & Moncada, 1994). The endothelial isoform plays an important role in the regulation of the vascular tone, i.e.

vasodilation and regional blood flow, leukocyte–endothelial interactions, platelet adhesion and aggregation, and vascular smooth muscle cell proliferation (Atochin & Huang, 2010).
There is also evidence that in addition to the three known isoforms of NOS (eNOS, nNOS, iNOS), there exists a mitochondrial isoform (mtNOS). mtNOS was described in a variety of tissues, including skeletal muscle, heart, liver, and kidney (Kobzik *et al*., 1995; Bates *et al*., 1995; Bates *et al*., 1996). mtNOS, it was also found in brain (Bates *et al*., 1995; Riobó *et al*., 2002). Differences between mtNOs and the other NOS isoforms were reported by now. The mtNOS displays an amino acid sequence similar to iNOS (Tatoyan & Giulivi, 1998; Lopez *et al*., 2000), but its activity consistently depends, in contrast to iNOS, on Ca^{2+} and calmodulin (Ghafourifar & Richter, 1997; Dedkova & Blatter, 2005).

In several processes, the target of NO is soluble guanylate cyclase (sGC), a mammalian NO sensor (Poulos, 2010). When NO binds to the heme moiety of sGC, its activity increases, resulting in cyclic guanosine monophosphate (cGMP) production. cGMP is a second messenger that regulates several cell signaling functions. Amongst others cGMP mediates vascular smooth muscle relaxation (Atochin *et al*., 2003; Mergia *et al*., 2006) and effects platelet aggregation (Freedman *et al*., 1999). NO can also interact with superoxide, a toxin that belongs to the so called reactive oxygen species (ROS) to form the peroxynitrite anion.

1.9.3 NO Enhances Glycolysis in Astrocytes

As described in Chapter 1.8.2 astrocytes display high glycolytic activity. However, whether this metabolic profile is influenced by intercellular signals was unknown until recently. Brix *et al.* have shown that primary cultures of mouse cortical astrocytes treated with NO induce an enhancement in the expression of genes encoding various glycolytic enzymes as well as transporters for glucose and lactate via HIF-1α activation (Brix *et al*., 2012). This NO-mediated HIF-1α stabilization was detected in astrocytes, but not in neurons. The findings were in agreement with a previous study, where NO was found to inhibit oxidative metabolism and enhance glycolysis in astrocytes but not in neurons (Almeida *et al*., 2001a). Recently, it has been shown that NO induces the expression of MCT4 in astrocytes, leading to a persisting enhancement in lactate production and release in astrocytes (Marcillac *et al*., 2011). These findings suggest that NO plays an important role in brain energy metabolism by stabilizing HIF-1α leading to regulation of glycolysis and lactate production in astrocytes and subsequent lactate release to fuel neuronal energy needs. Previous studies also attributed enhanced lactate production and release in astrocytes to NO. NO is also a known inhibitor of

cytochrome c oxidase, the complex IV of the respiratory chain (Bolaños *et al*., 1994; Cleeter *et al*., 1994). It was shown that inhibition of cytochrome c oxidase by NO led to upregulation of glycolysis to maintain energy production in astrocytes. This response was not observed in neurons (Almeida *et al*., 2004) and inhibition of the respiratory chain by NO caused an increase in the activity of PFK1, a key regulator of glycolysis, as well as an increase in the concentration of Fru-2,6-BP, an allosteric activator of PFK1. In neurons, in turn, NO failed to alter PFK1 activity and Fru-2,6-PB concentration (Almeida *et al*., 2004). Both results (increase in PFK1 activity and Fru-2,6-BP concentration) are consistent with the results obtained by Brix *et al*., i.e. an increase of PFK1 mRNA levels and 6-phosphofructo-2-kinase/fructose-2,6-bisphosphatase 3 (PFKFB3) mRNA levels, the enzyme responsible for Fru-2,6-BP production (Brix *et al*., 2012). In addition, Brix *et al*. observed that NO treatment enhanced expression of pyruvate dehydrogenase kinase 1 (PDK1) in astrocytes but not in neurons (Brix *et al*., 2012). PDK1 is responsible for the regulation of pyruvate dehydrogenase (PDH) activity, the first enzyme of the PDC that transforms pyruvate into acetyl-CoA, which in turn enters the TCA cycle to carry out oxidative respiration. Phosphorylation of PDH by PDK1 causes its inactivation and thus reduction of mitochondrial respiration while favoring glycolysis.

As described in Chapter 1.9.2 several brain cell types are possible NO sources. Brix *et al.* found that endothelial cells that express eNOS produced the largest amount of NO in cell culture (Brix *et al*., 2012). Since the end-feet of astrocytes are localized on virtually all blood vessels in the brain, NO synthesized in endothelial cells may be the source to stabilize HIF-1α in astrocytes. Indeed, stabilization of HIF-1α and enhancement of MCT4 expression, as well as increased lactate production in astrocytes cocultured with primary cultures of brain vascular endothelial cells has been observed. This latter effect was suppressed when cells were treated with the NOS inhibitor N_{ω}-nitro-L-arginine methyl ester (L-NAME) and was absent when astrocytes were cocultured with neurons. In total, the findings of Brix *et al.* suggest that endothelial cell-derived NO leads to a high glycolytic activity in astrocytes via astrocytic HIF-1α activation (Brix *et al*., 2012). A graphical description of the stimulated lactate production in astrocytes induced by NO derived from endothelial cells is given in Figure 12.

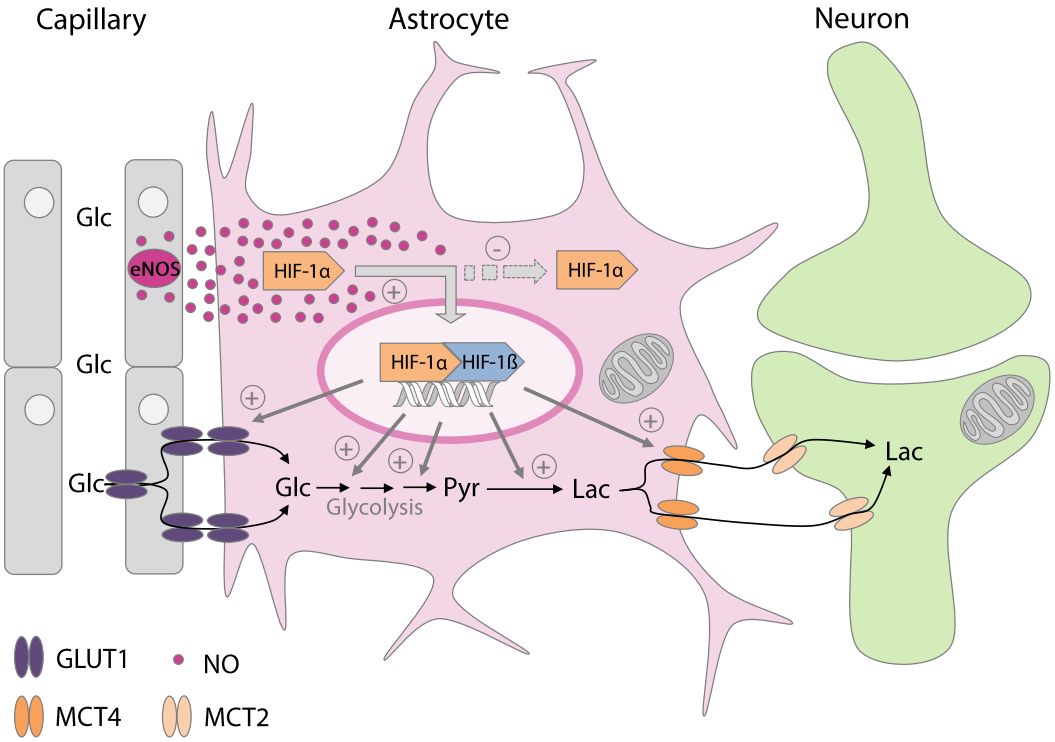

Figure 12. Model of HIF-1α regulated glycolysis and lactate production in astrocytes published by Brix *et al.*, 2012. In endothelial cells generated NO leads to local vasodilation of the capillary, and thus enhanced glucose supply. Simultaneously, HIF-1α is stabilized by NO which causes increased transcription of GLUT1 followed by an enhanced glucose uptake into astrocytes. In addition, HIF-1α stabilization leads to increased transcription of several enzymes of glycolysis (e.g. HK2, PGK1, and ENO1). Increased lactate production and release is effected by overexpression of LDHA and the transporters MCT2 and MCT4. TCA cycle and oxidative phosphorylation are inhibited by enhanced expression of PDK1. Lactate released can be taken up by neurons to fuel their energy metabolism (adapted from Brix *et al*., 2012). ENO1, enolase 1; eNOS, endothelial nitric oxide synthase; Glc, glucose; GLUT, glucose transporter; HIF, hypoxia-inducible factor; HK2, hexokinase 2; Lac, lactate; LDHA, lactate dehydrogenase A; MCT, monocarboxylate transporter; NO, nitric oxide; PGK1, phosphoglycerate kinase 1; Pyr, pyruvate.

2 Objectives

UDP-GlcNAc is the major end product of the HBP and the donor molecule for *O*-GlcNAcylation of many proteins. UDP-GlcNAc is an ideal metabolic marker since several different metabolic pathways are involved in its synthesis. Aberrant *O*-GlcNAcylation has been associated with the development of diseases such as diabetes, Alzheimer's disease, and cancer.

Pathological changes in a cell are first reflected by changes in metabolism. Analysis of metabolites can therefore provide valuable information about the role of metabolites in pathological conditions before the onset of a disease. Since *O*-GlcNAcylation of proteins is highly dependent on UDP-GlcNAc concentrations it is likely that changes in *O*-GlcNAc levels of proteins will be first manifested by changes in UDP-GlcNAc concentrations.

For the investigation of metabolite profiles *in vitro* as well as *in vivo* NMR spectroscopy has become well established because it allows simultaneous nonselective metabolite detection and quantification through various metabolic pathways. Metabolites of cell and tissue extracts, body fluids, or intact cells and tissues can be directly detected and quantified in one single experiment. A further advantage is that NMR spectroscopy allows structure determination of unknown metabolites.

A central point of this thesis is the identification of an efficient cell extraction method that allows the quantitative recovery of UDP-GlcNAc and other activated sugar nucleotides with good reproducibility and low variability that is suitable for NMR spectroscopy as analytical method.

Furthermore, the levels of UDP-GlcNAc and other activated sugar nucleotides will be determined in several different cell lines and primary cortical astrocytes using ^{1}H-NMR spectroscopy. To obtain more information about the regulation of UDP-GlcNAc levels in different cell types, changes in their synthesis will be investigated by influencing nutrient flux through the HBP by addition or withdrawal of precursor molecules.

Another aim of the present thesis is to investigate NO-induced alterations on cellular energy metabolism of astrocytes, as well as on UDP-GlcNAc concentrations. To investigate metabolic changes stimulated by NO, primary cultures of cortical astrocytes were incubated with [1-^{13}C]glucose as labeled substrate in the presence and absence of DETA-NONOate as NO-donor. Cell extracts and culture medium were analyzed by 1D and 2D ^{1}H,^{13}C-HSQC NMR spectroscopy in order to detect ^{13}C-labeled metabolites deriving from [1-^{13}C]glucose, e.g. *de novo* synthesized metabolites deriving from glycolysis and TCA cycle.

Since aberrant *O*-GlcNAcylation is associated with Alzheimer's disease, another aim of this thesis was to investigate the effect of Aß - the main component of senile plaques present in Alzheimer's disease brain - on UDP-GlcNAc synthesis in neuronal HT-22 cells and primary astrocytes. Moreover, the effect of Aß on glucose uptake and lactate release was also investigated.

In addition to determination of UDP-GlcNAc metabolite levels by NMR spectroscopy, changes in the mRNA expression of HBP enzymes induced by glucose deprivation, NO-, and Aß treatment will be investigated using quantitative real-time polymerase chain reaction (qRT-PCR).

The ultimate purpose of these metabolic analyses is to provide insights into disease mechanisms and to prove the suitability of UDP-GlcNAc and other activated sugar nucleotides as biomarkers in the development of diseases such as Alzheimer's disease as well as in response to therapy.

3 Results

3.1 Stability of Activated Sugar Nucleotides against Acid Hydrolysis

3.1.1 Comparison of M/C and PCA Cell Extracts

In the M/C procedure only the water-soluble phase with the cellular metabolites obtained from neuronal HT-22 cells was used. The metabolites were quantitatively recovered and compared with the PCA extraction method. In addition, I compared the M/C extracts with a so called PCA extraction under mild conditions, where I worked on ice and used 0,5 M PCA instead of 0,9 M PCA. Figure 13 shows typical ^{1}H-NMR spectra of the anomeric protons (H1) of activated sugar nucleotides.

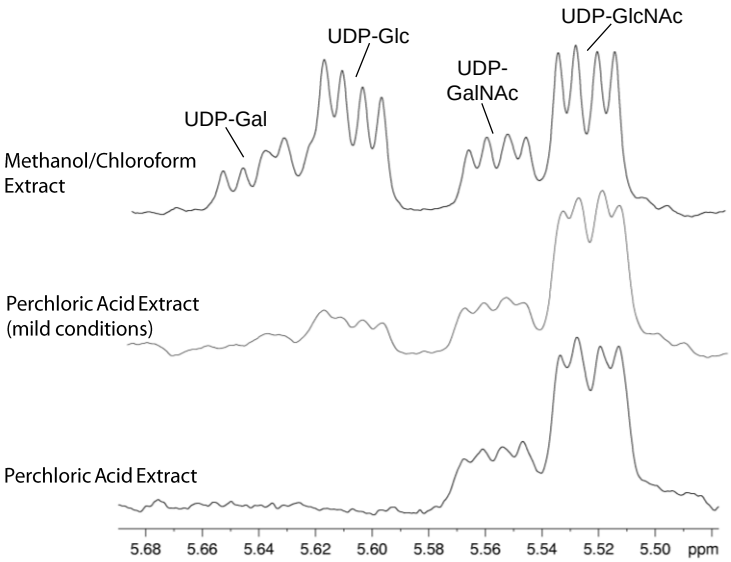

Figure 13. ^{1}H-NMR spectra from methanol/chloroform (M/C), perchloric acid (PCA), and PCA under mild conditions extracts of HT-22 cells. The expanded regions of the spectra show the anomeric protons (H1) of UDP-GlcNAc (δ = 5,52 ppm), UDP-GalNAc (δ = 5,56 ppm), UDP-Glc (δ = 5,61 ppm) and UDP-Gal (δ = 5,65 ppm). Under the signals of UDP-Glc and UDP-Gal lies the signal of the H1 of UDP-GlcUA (δ = 5,63 ppm).

In the spectra of M/C extracts 5 different activated sugar nucleotides were consistently identified: UDP-GlcNAc (δ = 5,52 ppm), UDP-GalNAc (δ = 5,56 ppm), UDP-Glc (δ = 5,61 ppm), and UDP-Gal (δ = 5,65 ppm). Under the signals of UDP-Glc and UDP-Gal lies the signal of the H1 of UDP-GlcUA (δ = 5,63 ppm). The characteristic doublet of doublets pattern of the anomeric proton in activated sugar nucleotides results from a vicinal coupling to H2 of the pyranose ring (^{3}J(H1,H2)) and to ^{31}P (^{3}J(H1,^{31}P)). In spectra of PCA

extracts only UDP-GlcNAc and UDP-GalNAc could be identified. In PCA extracts under mild conditions UDP-Glc and UDP-Gal could be identified as well, but the signal intensity was much lower compared to the M/C extracts. Since the anomeric protons of activated sugars resonate in a non-crowed region, they are amenable to quantification. For quantification I determined the signal integrals and normalized to cell number. In the case of UDP-GlcNAc and UDP-GalNAc, signal integration was done over the entire doublet of doublets. Since the H1 of UDP-GlcUA resonates in between the signals of the H1 of UDP-Glc and UDP-Gal, partially overlapping them, signal integration over the entire doublet of doublets of UDP-Glc and UDP-Gal would not reveal the actual concentration of both metabolites. Therefore only the outer doublets of the signals were integrated and the concentration thus obtained was doubled afterwards, giving maximum accuracy for determination of the concentration in this particular case. The concentration of UDP-GlcUA was calculated by the difference of UDP-Hex(NAc) and the sum of UDP-GlcNAc, UDP-GalNAc, UDP-Glc, and UDP-Gal. UDP-Hex(NAc) stands for the sum of all activated sugar nucleotides as determined by signal integration over the whole range of signals from anomeric protons of activated sugar nucleotides resonating in this area. Metabolite quantification showed no significant differences for the amount of UDP-GlcNAc in M/C and PCA extracts, even though the level of UDP-GlcNAc was slightly higher in M/C extracts. The metabolite yield of UDP-GalNAc, however, was significantly greater in M/C extracts than in PCA extracts. The amount of UDP-Glc and UDP-Gal, as well as the sum of all activated sugar nucleotides (UDP-Hex(NAc)) is, as expected, significantly higher in M/C extracts (Figure 14A).

To test, whether the PCA extraction under mild conditions is suitable for quantification of activated sugar nucleotides I calculated the UDP-Hex/UDP-HexNAc ratio for both M/C and PCA extraction under mild conditions. UDP-Hex denotes the sum of UDP-Glc and UDP-Gal, whereas UDP-HexNAc denotes the sum of the two stable *N*-acetylated sugar nucleotides UDP-GlcNAc and UDP-GalNAc. UDP-Hex/UDP-HexNAc signal integral ratio was significantly lower in PCA extracts under mild conditions than in M/C extracts (Figure 14B). These results clearly show that PCA extraction is not suitable for quantification of activated sugar nucleotides, as both UDP-Glc and UDP-Gal seem to be acid labile. The decomposition of the two metabolites can be decelerated by using a less concentrated PCA and working on ice, however the actual concentration cannot be quantified under these conditions. UDP-GalNAc is most likely not acid labile, but nevertheless recovery of this metabolite is unsatisfactory using PCA extraction.

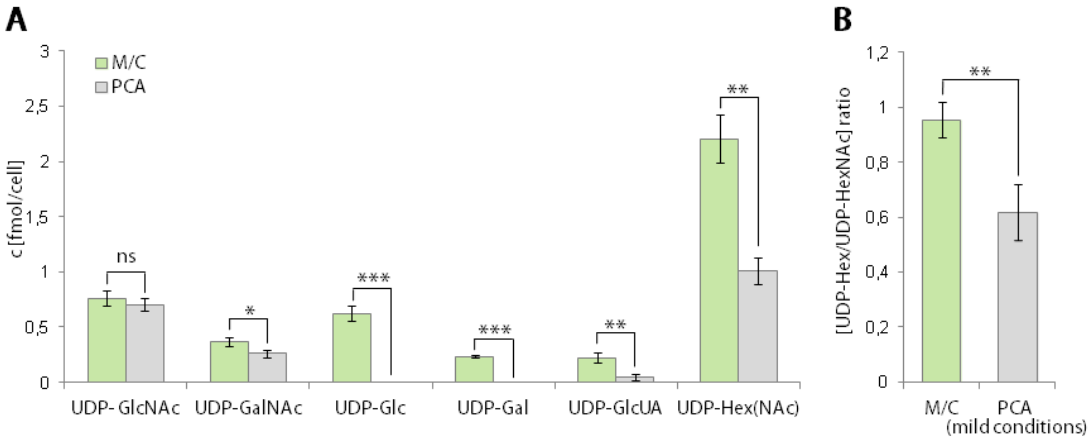

Figure 14. (A) UDP-GlcNAc, UDP-GalNAc, UDP-Glc, UDP-Gal, and UDP-GlcUA levels quantified from M/C extracts (green bars) and PCA extracts (grey bars) of HT-22 cells (n = 3). (B) [UDP-Hex]/[UDP-HexNAc] ratios of HT-22 cells extracted with M/C (green bars) and PCA (mild conditions) (grey bars) (n = 3). UDP-Hex(NAc) means sum of c(UDP-GlcNAc), c(UDP-GalNAc), c(UDP-Glc), c(UDP-Gal), c(UDP-GlcUA); UDP-Hex means sum of c(UDP-Glc), c(UDP-Gal), and c(UDP-GlcUA); UDP-HexNAc means sum of c(UDP-GlcNAc), c(UPD-GalNAc). Values are mean ± standard deviation. *P* values of $P < 0.05$ were considered to be significant. *Represents $P < 0.05$; **represents $P < 0.01$; ***represents $P < 0.001$; ns, not significant.

3.1.2 Effect of PCA on Pure Compound Activated Sugar Nucleotides

To directly test the effect of PCA on the activated sugars identified in HT-22 cell extracts and as well as on other activated sugar nucleotides, I used the pure compounds of UDP-GlcNAc, UDP-GalNAc, UDP-Glc, UDP-Gal, UDP-GlcUA, CMP-NeuNAc, GDP-Man, and GDP-Fuc. I treated the pure compounds (1 mM solutions in H_2O) with PCA and M/C in the exact way as I prepared the cell extracts and compared the ^{1}H-NMR spectra of the treated compounds with reference spectra of each sugar nucleotide.

In consistency with the results obtained from cell extracts, UDP-GlcNAc and UDP-GalNAc are not being decomposed by PCA treatment. UDP-Glc and UDP-Gal, however, are completely decomposed after PCA treatment, as shown in Figure 15. UDP-Glc is readily decomposed to glucose-1,2-cyclo-phosphate (Glc-1,2-cyclo-P), glucose-2-phosphate (Glc-2-P), Glc-1-P, uridine monophosphate (UMP), and minor amounts of glucose and UDP. UDP-Gal is decomposed similarly into the corresponding galactose metabolites. UDP-GlcUA decomposes akin to UDP-Glc and UDP-Gal to glucuronic acid-1,2-cyclo-phosphate (GlcUA-1,2-cyclo-P), glucuronic acid-1-phosphate (GlcUA-1-P), glucuronic acid-2-phosphate (GlcUA-2-P), and UMP. The decomposition was on the contrary to UDP-Glc and UDP-Gal not complete (60 % decomposition). CMP-NeuNAc decomposed completely to NeuNAc, cytidine monophosphate (CMP), and minor amounts of cytidine. GDP-Fuc decomposed completely to Fucose and GDP. GDP-Man was stable against PCA treatment (see Appendix 7.3 for spectra of UDP-GlcUA, CMP-NeuNAc, GDP-Fuc, and GDP-Man). All activated

sugar nucleotides are stable against M/C treatment. Results from the analysis off the effect of PCA on all activated sugar nucleotides tested are summarized in Table 2.

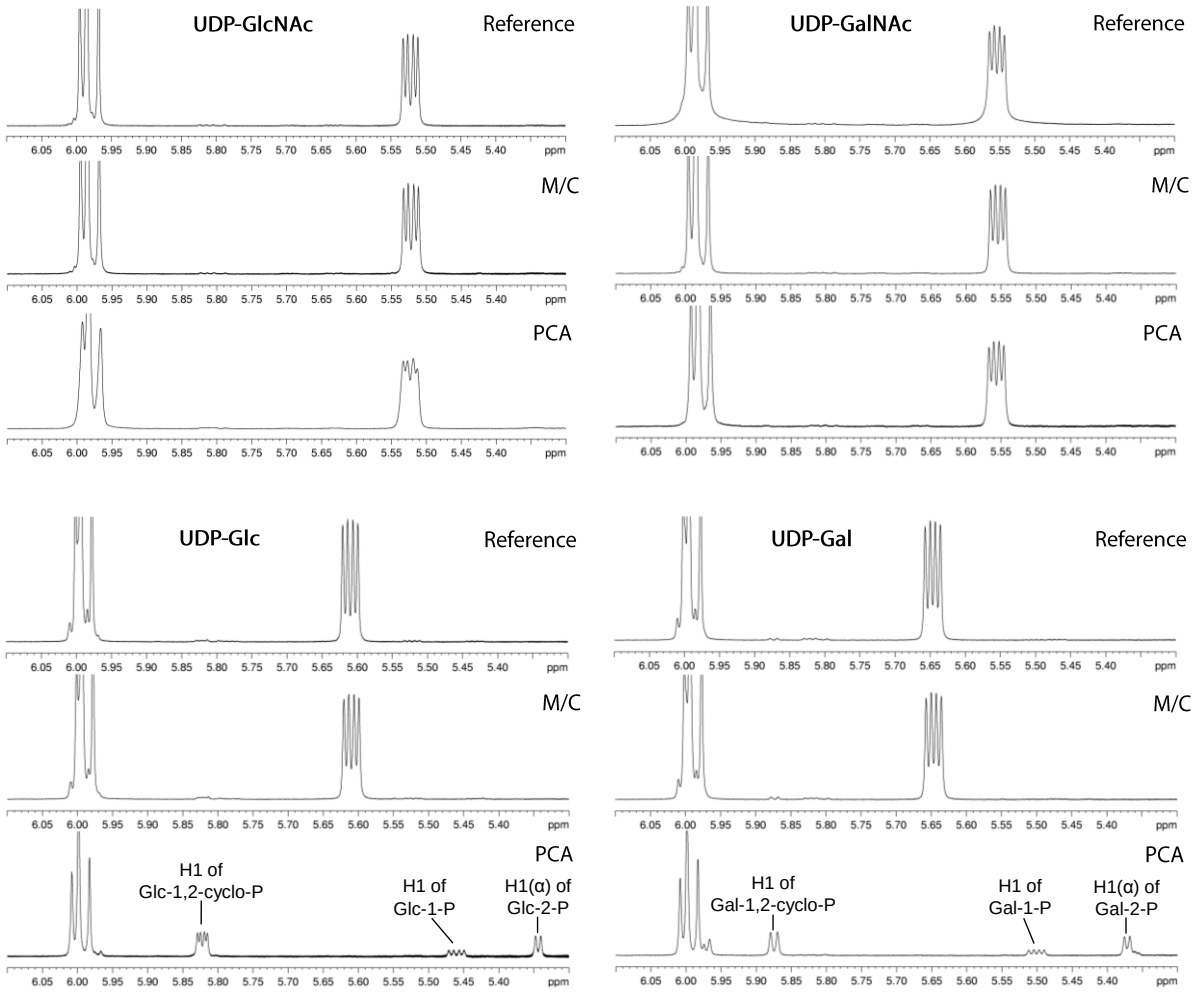

Figure 15. ^{1}H-NMR spectra of the pure compounds UDP-GlcNAc, UDP-GalNAc, UDP-Glc, and UDP-Gal. The expanded regions of the spectra show the signals of the anomeric protons (H1) in reference spectra and after treatment with M/C or PCA. The signals of the decomposition products of UDP-Glc after PCA treatment shown are: glucose-1,2-cyclo-phosphate (Glc-1,2-cyclo-P), glucose-1-phosphate (Glc-1-P), and glucose-2-phosphate (Glc-2-P). The signals of the decomposition products of UDP-Gal are the corresponding galactose metabolites.

Table 2. Comparison of the decomposition and stability of activated sugar nucleotides after PCA treatment as evaluated by ^{1}H-NMR.

Sugar nucleotide	Decomposition Product	Decomposition grade
UDP-GlcNAc	-	-
UDP-GalNAc	-	-
UDP-Glc	Glc-1-P Glc-2-P Glc-1,2-cyclo-P UMP minor amounts of Glc, UDP	complete decomposition
UDP-Gal	Gal-1-P Gal-2-P	complete decomposition

Sugar nucleotide	Decomposition Product	Decomposition grade
	Gal-1,2-cyclo-P UMP minor amounts of Gal, UDP	
UDP-GlcUA	GlcUA-1-P GlcUA-2-P GlcUA-1,2-cyclo-P UMP	incomplete decomposition
CMP-NeuNAc	NeuNAc CMP minor amounts of cytidine	complete decomposition
GDP-Man	-	-
GDP-Fuc	Fuc GDP	complete decomposition

Peak assignment of the decomposition products, despite the 1,2-cyclo-phosphates and 2-phosphates, was done by comparison with spectra of authentic compounds or using data from the human metabolome database (http://www.hmdb.ca; Wishart *et al*., 2009). The formation of 1,2-cyclo-phosphates and 2-phosphates originating from UDP-glucose and UDP-galactose has been reported before (Paladini & Leloir, 1952; Piras, 1963; Nunez & Barker, 1976; Kokesh *et al*., 1978; Spik *et al*., 1979; O'Connor *et al*., 1979). Since there were no authentic compounds commercially available, I treated UDP-glucose and UDP-galactose with $ZnCl_2$ (1 mM UDP-Glc + 2,5 mM $ZnCl_2$ in H_2O for 24 h, RT) (Nunez & Barker, 1976) to yield the 1,2-cyclo-phosphates. The arising doublet of doublet at 5,82 ppm in the ^{1}H-NMR spectrum of $ZnCl_2$ treated UDP-glucose (see Figure 18) derives from the H1 of glucose-1,2-cyclo-phosphate. The doublet at 5,87 ppm in the spectrum of $ZnCl_2$ treated UDP-galactose can be assigned to the H1 of galactose-1,2-cyclo-phosphate (Figure 16 and Figure 18, respectively). Both signals were identical with the signals in PCA treated UDP-glucose and UDP-galactose. Note that the signal of galactose-1,2-cyclo-phosphate is a doublet and not a doublet of doublets as expected. The conformation of the pyranose ring is slightly affected by the formation of the cyclo-phosphate causing the H1-^{31}P coupling constant in the galactose-1,2-cyclo-phosphate to be 0 Hz as previously described (O'Connor *et al*., 1979). For this reason no coupling to ^{31}P can be observed resulting in a single doublet in the corresponding spectrum. The ^{1}H chemical shifts of the 2-phosphates are not known to date. To confirm that the signals in the spectra of PCA treated UDP-Glc and UDP-Gal, can actually be assigned to Glc-2-P and Gal-2-P, the 2-phosphates were obtained by treatment of the 1,2-cyclo-phosphates with acid (0,1 M HCl, 5 min, 100 °C). This acid hydrolysis to yield the 2-phosphates from their corresponding cyclo-phosphates has been described before (Paladini &

Leloir, 1952; Nunez & Barker, 1976). The resonance at 5,34 ppm could be assigned to the H1(α) of glucose-2-phosphate and the resonance at 5,37 ppm to the H1(α) galactose-2-phosphate (both doublets; see Figure 16). The signals were identical to the peaks of the PCA treated compounds.

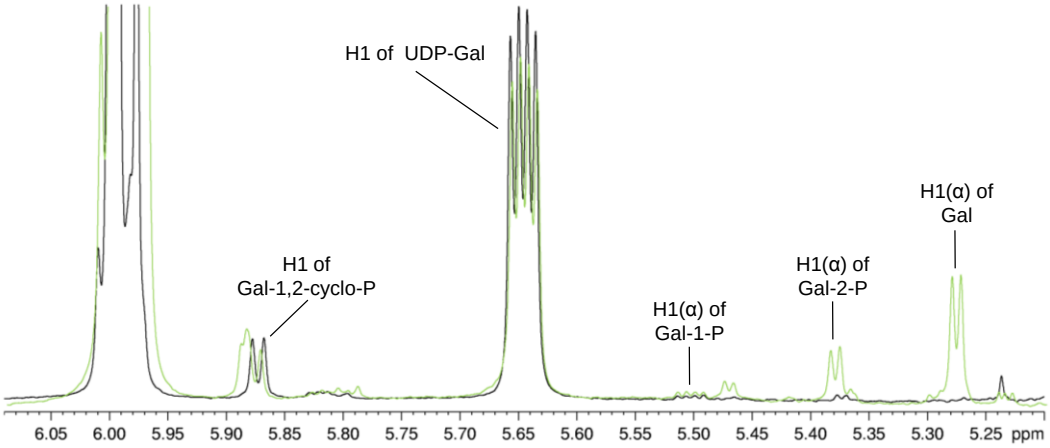

Figure 16. ^{1}H-NMR spectrum of UDP-Gal (1 mM) treated with 2,5 mM $ZnCl_2$ for 24 h at RT to form Gal-1,2-cyclo-P (black spectrum). The spectrum shows the anomeric proton (H1) of Gal-1,2-cyclo-P (δ_{H1} = 5,87 ppm) and the signal of the H1 of non converted UDP-Gal (δ_{H1} = 5,65 ppm). Treatment of the same sample with 0,1 M HCl for 5 min at 100 °C gives rise to Gal-2-P ($\delta_{H1(\alpha)}$ = 5,37 ppm) due to cleavage of the cyclo-phosphate (green spectrum). Cleavage of the cyclo-phosphate also leads to formation of Gal ($\delta_{H1(\alpha)}$ = 5,28 ppm) because apart from Gal-2-P, also Gal-1-P is formed. Gal-1-P is hydrolysed immediately to Gal and mainly Gal-2-P remains (Paladini & Leloir, 1952). A small signal of Gal-1-P is still detectable in the spectra. Note: The H1(α) of Gal usually resonates at 5,27 ppm when measured in D_2O (pH 7) using TSP as reference. It is highly probable that this signal belongs to Gal and the slight chance in chemical shift is due to changes in pH because of the treatment with HCl and subsequent neutralization with NaOH. Treatment of UDP-Glc with $ZnCl_2$ results analogously in formation of Glc-1,2-cyclo-P (δ_{H1} = 5,82 ppm) and cleavage with HCl leads to formation of Glc-2-P ($\delta_{H1(\alpha)}$ = 5,34 ppm), but with a lower signal intensity. The signals of the cyclo-phosphates and 2-phosphates obtained from UDP-Glc and UDP-Gal, respectively were identical to the peaks of the PCA treated compounds. Gal, galactose; Gal-1,2-cyclo-P, galactose-1,2-cyclo-phoshate; Gal-1-P, galactose-1-phosphate; Gal-2-P, galactose-2-phosphate; Glc-1,2-cyclo-P, glucose-1,2-cyclo-phoshate; Glc-2-P, glucose-2-phoshate; UDP-Gal, uridine diphosphate-galactose; UDP-Glc, uridine diphosphate-glucose.

To further verify that the signals actually belong to the 2-phosphates I took advantage of the vicinal coupling of H2 to ^{31}P (^{3}J(H2,^{31}P)). The H2 of α-D-galactose and ß-D-galactose resonate at 3,60 ppm and 3,28 ppm, respectively. The H2 of Gal-2-P is expected to be shifted downfield due to the binding of the phosphate group. I recorded 2 different ^{1}H-NMR spectra of Gal-2-P obtained by formation of Gal-1,2-cyclo-P by treatment of UDP-Gal with $ZnCl_2$ and subsequent hydrolysis with HCl. The first spectrum recorded was a ^{1}H-NMR spectrum where coupling of ^{1}H to ^{31}P is visible, resulting in an additional splitting of the signal of H2 of Gal-2-P compared to galactose. A second ^{1}H-NMR spectrum was recorded where phosphorus decoupling was applied. If Gal-2-P is present in the sample, the multiplicity of a signal downfield of 3,60 ppm should diminish. Indeed, in the second spectrum, where ^{31}P-decoupling was applied, a signal at 4,20 ppm exhibited a change in the splitting pattern as

shown in Figure 17. Although part of this signal is overlapping with other signals in this region, it may be assumed that this signal changes from a doublet of doublets in the spectrum where ^{31}P-coupling is visible into a doublet in the ^{31}P-decoupled spectrum. The signal of the H2 of galactose is a doublet of doublets due to a vicinal the coupling to the anomeric proton (H1) (^{3}J(H2,H1)) and to H3 (^{3}J(H2,H3)). The multiplicity of the H2 of Gal-2-P is therefore expected to be a doublet of doublet of doublets (ddd) caused by an additional vicinal coupling to ^{31}P (^{3}J(H1,^{31}P)). The multiplicity of the signal at 4,20 ppm is most likely a dd and not a ddd. However, the spectrum is recorded on a 250 MHz spectrometer and it is possible that one of the couplings of H2 to H1 or H3 is influenced due to bonding of the phosphate group and the resolution is too low.

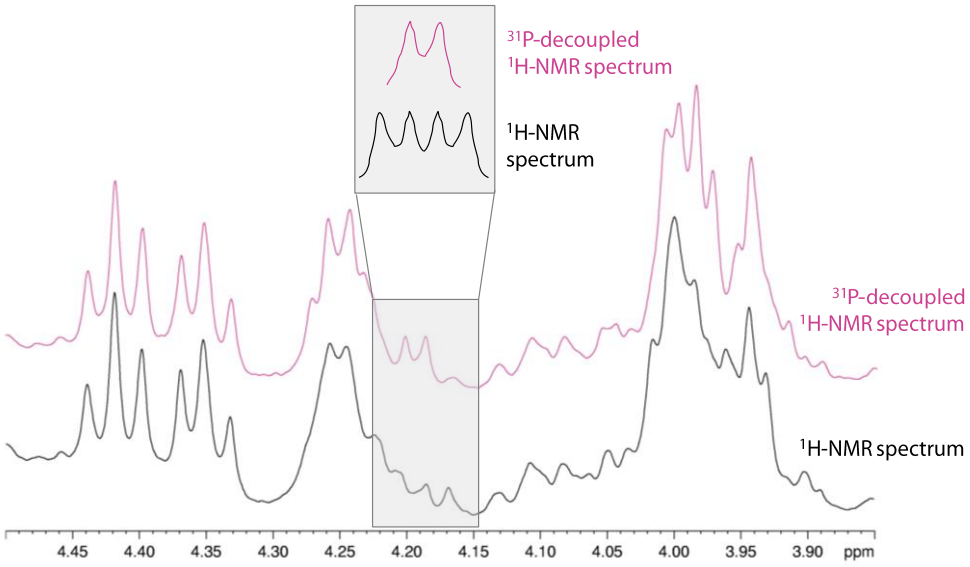

Figure 17. ^{1}H-NMR spectra of Gal-2-P obtained by formation of Gal-1,2-cyclo-P by treatment of UDP-Gal with $ZnCl_2$ and subsequent hydrolysis with HCl. In the lower grey box a signal at 4,20 ppm is displayed whose splitting pattern is changed when a ^{31}P-decoupled ^{1}H-NMR spectrum of the same sample is recorded (pink spectrum). For simplicity, the upper grey box depicts a graphical illustration of the change in the splitting pattern of the signal when decoupling of ^{1}H to ^{31}P is applied. This signal may therefore belong to the H2 of Gal-2-P, further indicating that Gal-2-P is formed when UDP-Gal is treated with PCA. Gal-2-P, galactose-2-phosphate; Gal-1,2-cyclo-P, galactose-1,2-cyclo-phoshate; PCA, perchloric acid; UDP-Gal, uridine diphosphate-galactose.

Gal-1,2-cyclo-P is also present in this sample. It has to be excluded that this signal actually belongs to the H2 of Gal-2-P and not to the H2 of Gal-1,2-cyclo-P. The multiplicity of the H2 of Gal-1,2-cyclo-P is also expected to be an ddd and not a dd. The ^{1}H-NMR chemical shift of H2 of Gal-1,2-cyclo-P was reported to be 4,39 ppm referenced to 3-trimethylsilylpropanesulfonate sodium (TPS) at pH 8 (O'Connor *et al.*, 1979). The pH of a sample has an effect on chemical shift of a substance. This chemical shift was determined at a slightly higher pH, compared to my measurements at pH 7,5. However, a change from low to

higher pH even leads to a shift to lower ppm. For that reason, the signal at 4,2 ppm can be assigned to the H2 of Gal-2-P, because the H2 of Gal-1,2-cyclo-P is expected to resonate downfield. It may be concluded that this signal belongs to the H2 of Gal-2-P, further corroborating that Gal-2-P is formed when UDP-Gal is treated with PCA.

Last but not least it was examined if the cyclo-phosphates are also present in cell extracts in NMR-detectable levels. For this reason PCA extracts of HT-22 cells were compared with extracts obtained by the M/C procedure and the anomeric region was compared with the signals in the extracts with ^{1}H-NMR spectra of Gal-1,2-cyclo-P and Glc-1,2-cyclo-P obtained by treatment of UDP-Gal and UDP-Glc, respectively with $ZnCl_2$.

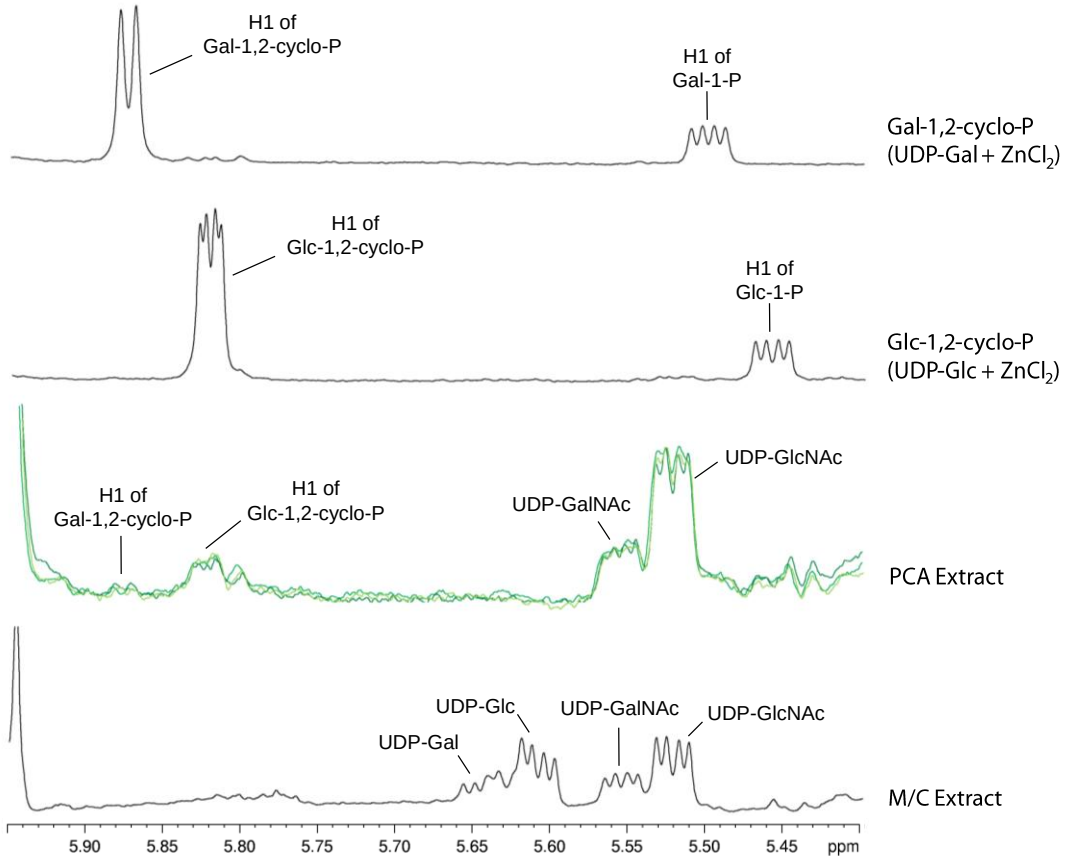

Figure 18. Representative sections of ^{1}H-NMR spectra of the anomeric region of a HT-22 PCA and M/C extract, as well as, the signals of Gal-1,2-cyclo-P and Glc-1,2-cyclo-P obtained by treatment of UDP-Gal and UDP-Glc, respectively with $ZnCl_2$. In the M/C cell extract of HT-22 cells, the signals of UDP-GlcNAc, UDP-GalNAc, UDP-Glc, and UDP-Gal can be detected. In the PCA extract of HT-22 cells, the signals of the acid stable activated sugar nucleotides, UDP-GlcNAc and UDP-GalNAc can be detected. In consistency with PCA treatment of pure compounds, also the signals of Gal-1,2-cyclo-P (δ_{H1} = 5,87 ppm) and Glc-1,2-cyclo-P (δ_{H1} = 5,82 ppm) can be detected in PCA extracts (n = 3), which are absent in M/C extracts. Gal-1-P, galactose-1-phosphate; Gal-1,2-cyclo-P, galactose-1,2-cyclo-phoshate; Glc-1-P, glucose-1-phosphate; Glc-1,2-cyclo-P, glucose-1,2-cyclo-phoshate; M/C, methanol/chloroform; PCA, perchloric acid; UDP-Gal, uridine diphosphate-galactose; UDP-GalNAc, uridine diphosphate-*N*-acetyl-galactosamine; UDP-Glc, uridine diphosphate-glucose; UDP-GlcNAc, uridine diphosphate-*N*-acetyl-glucosamine.

In consistency with PCA treatment of pure compounds, the signals of Gal-1,2-cyclo-P (δ_{H1} = 5,87 ppm) and Glc-1,2-cyclo-P (δ_{H1} = 5,82 ppm) are consistently present in PCA extracts (n = 3), as shown in Figure 18. These signals are absent in M/C extracts (n = 3). The signal intensity of the cyclo-phosphates may seem low in the PCA extracts, however, it has to be regarded that a considerable small cell mass was used (cells from one 10 cm diameter petri dish; approximately $1 \cdot 10^7$ cells per extract) in these experiments. Using more cells for extraction the signals will become more prominent in the spectra.

3.1.3 Quantification of Activated Sugar Nucleotide Levels in Different Cell Lines and Primary Astrocytes

Now being capable of quantitatively analyzing activated sugar nucleotides, I determined their intracellular concentration in 4 different cell lines: immortalized clonal mouse hippocampal neuronal cell line (HT-22), human embryonic kidney cells (HEK293), Madin-Darby bovine kidney cells (MDBK), and Chinese hamster ovarian cells (CHO), as well as primary cortical astrocyte-enriched cultures from mice (astrocytes). All cell lines were seeded for 72 h in the same density in their standard growth medium containing 25 mM glucose, despite CHO cells which were cultured in medium containing 12,5 mM glucose. Murine primary cortical astrocytes were used after 21 days in culture. Medium was exchanged and cells were incubated for 72 h with fresh standard growth medium containing 25 mM glucose. Approximately 10^7 cells per extract were harvested and M/C extraction was performed. For HT-22 cells four separate preparations and for primary astrocytes five separate preparations were analyzed. For HEK293, MDBK, and CHO cells three separate preparations were analyzed. The concentrations of the four activated sugar nucleotides UDP-GlcNAc, UDP-GalNAc, UDP-Glc, and UDP-Gal were determined by quantification from fully relaxed ^{1}H-NMR spectra. The concentration of UDP-GlcUA was again calculated by the difference of UDP-Hex(NAc) and the sum of UDP-GlcNAc, UDP-GalNAc, UDP-Glc, and UDP-Gal. UDP-Hex(NAc) stands for the sum of all activated sugar nucleotides as determined by signal integration over the whole range of signals from anomeric protons of activated sugar nucleotides resonating in this area. The absolute concentrations of those activated sugar nucleotides in [fmol/cell] are presented in Table 3. For easier comparability, Figure 19A shows the levels of activated sugar nucleotides in different cell lines and primary astrocytes expressed as % of UDP-GlcNAc (HT-22) with the level of UDP-GlcNAc in HT-22 cells set as 100 %. UDP-GlcNAc had the highest intracellular level of all activated sugar nucleotides in all cell lines tested, followed by UDP-Glucose, UDP-GalNAc, and UDP-Gal. The highest

level of UDP-GlcNAc, the key metabolite for *O*-GlcNAcylation, exhibited primary astrocytes (170 % ± 17 %). HT-22 (100 % ± 7 %), HEK293 (93 % ± 17 %), and MDBK cells (102 % ± 9 %) comprised approximately equal amounts of UDP-GlcNAc. In CHO cells the level of UDP-GlcNAc (48 % ± 9 %) was only half as high as compared to HT-22, HEK293, and MDBK cells. However, it has to be considered that CHO cells were cultured in medium containing 12,5 mM glucose compared to the other cells lines, which were cultured in medium containing 25 mM glucose. It is interesting to note that UDP-GlcUA is almost absent in HEK293 cells.

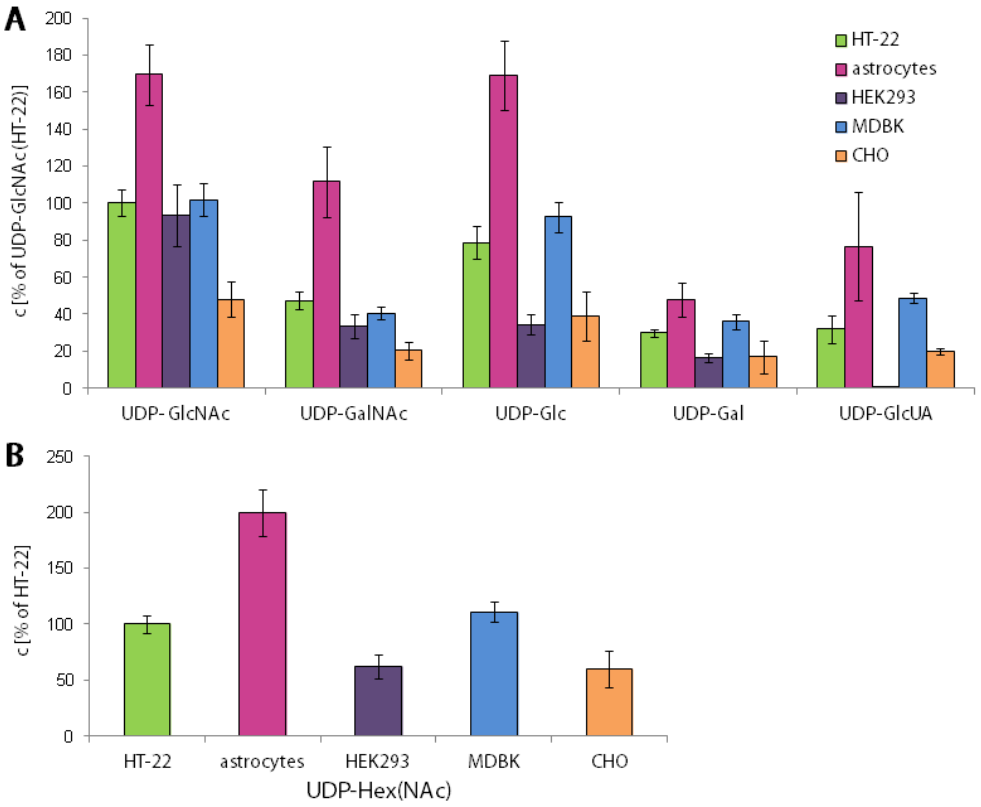

Figure 19. Levels of activated sugar nucleotides in different cell lines and primary astrocytes quantified from fully-relaxed ^{1}H-NMR spectra of water-soluble cell extracts. (A) Concentrations of UDP-GlcNAc, UDP-GalNAc, UDP-Glc, UDP-Gal, and UDP-GlcUA expressed in % of UDP-GlcNAc (HT-22). All cells were cultured in medium containing 25 mM glucose, despite CHO cells which were cultured in medium containing 12,5 mM glucose. HT-22 (n = 4), astrocytes (n = 5), HEK293, MDBK, and CHO (all n = 3). (B) Total levels of activated sugar nucleotides (UDP-Hex(NAc)) in the cells tested expressed in % of HT-22. UDP-Hex(NAc) means sum of c(UDP-GlcNAc), c(UDP-GalNAc), c(UDP-Glc), c(UDP-Gal), and c(UDP-GlcUA).

The total amount of activated sugar nucleotides (UDP-Hex(NAc)) in the different cell lines and primary astrocytes quantified from ^{1}H-NMR spectra is shown in Figure19B. Concentrations are expressed as % of UDP-Hex(NAc) (HT-22) with the level of UDP-Hex(NAc) in HT-22 cells set as 100 %. By comparison of the UDP-Hex(NAc) levels three groups with a high, medium and low level can be separated: Primary astrocytes exhibit by far

the highest amount of UDP-Hex(NAc) (200 % ± 21 %). HT-22 cells (100 % ± 8 %; half as much compared to primary astrocytes) and MDBK cells (111 % ± 9 %) form the second group with medium UDP-Hex(NAc) levels. HEK293 (62 % ± 11 %; one third compared to primary astrocytes) and CHO (60 % ± 16 %) cells represent the third group with the lowest UDP-Hex(NAc) levels of all cells tested.

Table 3. Levels of activated sugar nucleotides in HT-22, HEK293, MDBK, and CHO cell lines and primary astrocytes quantified from fully-relaxed ^{1}H-NMR spectra of water-soluble cell extracts. HT-22 (n = 4), astrocytes (n = 5), HEK293, MDBK, and CHO (all n = 3). Values are mean ± standard deviation.

	Activated sugar nucleotides [fmol/cell]				
	HT-22	astrocytes	HEK293	MDBK	CHO
UDP- GlcNAc	0,76 ± 0,05	1,30 ± 0,13	0,72 ± 0,13	0,78 ± 0,07	0,37 ± 0,07
UDP-GalNAc	0,36 ± 0,04	0,85 ± 0,14	0,26 ± 0,05	0,31 ± 0,02	0,16 ± 0,04
UDP-Glc	0,60 ± 0,07	1,29 ± 0,14	0,26 ± 0,04	0,71 ± 0,06	0,30 ± 0,10
UDP-Gal	0,23 ± 0,02	0,37 ± 0,07	0,13 ± 0,02	0,28 ± 0,03	0,13 ± 0,07
UDP-GlcUA	0,24 ± 0,06	0,59 ± 0,23	0,01 ± 0,00	0,37 ± 0,02	0,15 ± 0,01
UDP-Hex(NAc)	2,20 ± 0,18	4,39 ± 0,47	1,37 ± 0,24	2,45 ± 0,19	1,32 ± 0,36

3.2 Hexosamine Induced Changes in Activated Sugar Nucleotide Levels in HT-22 and CHO Cells

To determine the effect of different hexosamines (HexN) on the levels of activated sugar nucleotides and to examine if these effects are NMR-detectable, I incubated HT-22 and CHO cells with 100 µM GlcN, galactosamine (GalN), and mannosamine (ManN) for 24 h. A concentration of 100 µM was used, because at this concentration significant changes in the intracellular levels of activated sugar nucleotides were detected without affecting cell viability or leading to enhanced cell detachment in GlcN, GalN, or ManN treated HT-22 and CHO cell cultures. The concentration of activated sugar nucleotides was obtained from fully relaxed ^{1}H-NMR spectra of M/C cell extracts. The spectra acquired from these experiments are shown in Figure 20 and Figure 21. The levels of UDP-sugars quantified from these spectra are depicted in Figure 22. A significant change in the total level of activated sugar nucleotides (UDP-Hex(NAc)) was only achieved in GlcN treated cells, in both HT-22 and CHO cells. This significant increase is caused by the marked increase in UDP-GlcNAc induced by GlcN in both cell lines. In HT-22 cells, the amount of UDP-GlcNAc was triplicated after incubation

with 100 µM GlcN for 24 h. The concentration of controls was 0,95 ± 0,10 fmol/cell and increased to 3,04 ± 0,31 fmol/cell in GlcN treated cells. In CHO cells the concentration increased from 0,55 ± 0,05 fmol/cell to 2,02 ± 0,62 fmol/cell after incubation with GlcN. Therefore, the concentration of UDP-GlcNAc was even four times higher compared to controls in CHO cells. However, this value has a quite large error bar and is therefore not as significant as the increase in HT-22 cells. GlcN treatment also led to a significant increase in UDP-GalNAc, which can be formed by epimerization of UDP-GlcNAc. Similar to the increase in UDP-GlcNAc, the UDP-GalNAc level was triplicated after GlcN treatment in HT-22 cells. The concentration increased from 0,41 ± 0,11 fmol/cell to 1,22 ± 0,06 fmol/cell when GlcN treated. In CHO cells there was again an almost fourfold increase compared to untreated cells. The UDP-GalNAc concentration of controls was 0,22 ± 0,01 fmol/cell and in GlcN incubated cells 0,80 ± 0,26 fmol/cell.

GalN treatment caused a small, but significant increase in the UDP-GalNAc level in CHO cells. The concentration increased from 0,22 ± 0,01 fmol/cell in untreated cells to 0,27 ± 0,02 fmol/cell in GalN treated cells. In HT-22 cells no increase was observed in the UDP-GalNAc level after incubation with GalN. In the spectra of GalN treated HT-22 and CHO cells a novel resonance at 5,69 ppm arose, as shown in Figure 20 and Figure21. This signal was assigned to the anomeric proton (H1(α)) of galactosamine-1-phosphate (GalN-1-P) by comparison with spectra of the authentic compound. The GalN-1-P concentration determined was higher in HT-22 cells (1,58 ± 0,36 fmol/cell) compared to CHO cells (0,43 ± 0,14 fmol/cell).

ManN administration resulted in significantly elevated UDP-GlcNAc and UDP-GalNAc levels in HT-22 cells. The UDP-GlcNAc level increased from 0,95 ± 0,10 fmol/cell to 1,47 ± 0,12 fmol/cell. The UDP-GalNAc level increased from 0,41 ± 0,11 fmol/cell to 0,62 ± 0,03 fmol/cell in ManN treated HT-22 cells. Both levels are 1,5 times higher compared to controls. Hence, the increase is not as pronounced as in GlcN and GalN treated cells. ManN did not change any level of activated sugar nucleotides in CHO cells.
No significant changes in the levels of UDP-Glc and UDP-Gal were observed in GlcN, GalN, or ManN treated cells. There may be a trend towards decreased UDP-Glc and UDP-Gal levels in GlcN treated HT-22 and CHO cells, however this decrease is not significant. UDP-GlcUA levels are omitted, because no significant changes were observed, as already deduced from the fact that no significant changes were detected in UDP-Glc levels.

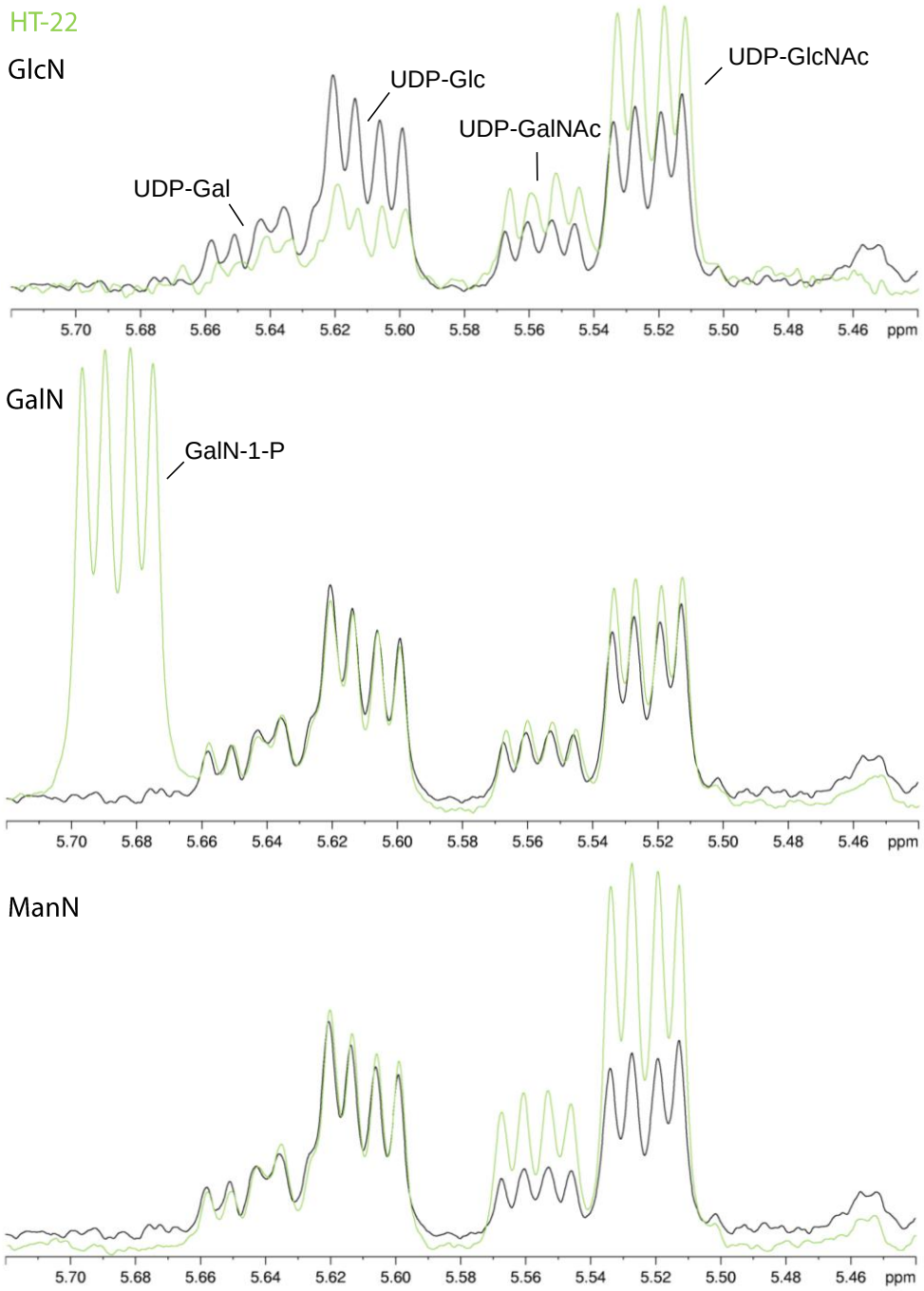

Figure 20. Effect of hexosamines on activated sugar nucleotide levels in HT-22 cells: Sections of ^{1}H-NMR spectra of M/C extracts of neuronal HT-22 cells after 24 h incubation with 100 µM HexN (GlcN, GalN, ManN; green) compared to controls (black) are shown. The expanded regions of the spectra show the anomeric protons (H1) of UDP-GlcNAc, UDP-GalNAc, UDP-Glc, and UDP-Gal. In the spectrum of GalN treated cells, a novel resonance emerges, belonging to the H1 of GalN-1-P. GalN, galactosamine; GalN-1-P, galactosamine-1-phosphate; GlcN, glucosamine; HexN, hexosamine; ManN, mannosamine; M/C, methanol/chloroform; UDP-Gal, uridine diphosphate-galactose; UDP-GalNAc, uridine diphosphate-*N*-acetyl-galactosamine; UDP-Glc, uridine diphosphate-glucose; UDP-GlcNAc, uridine diphosphate-*N*-acetyl-glucosamine.

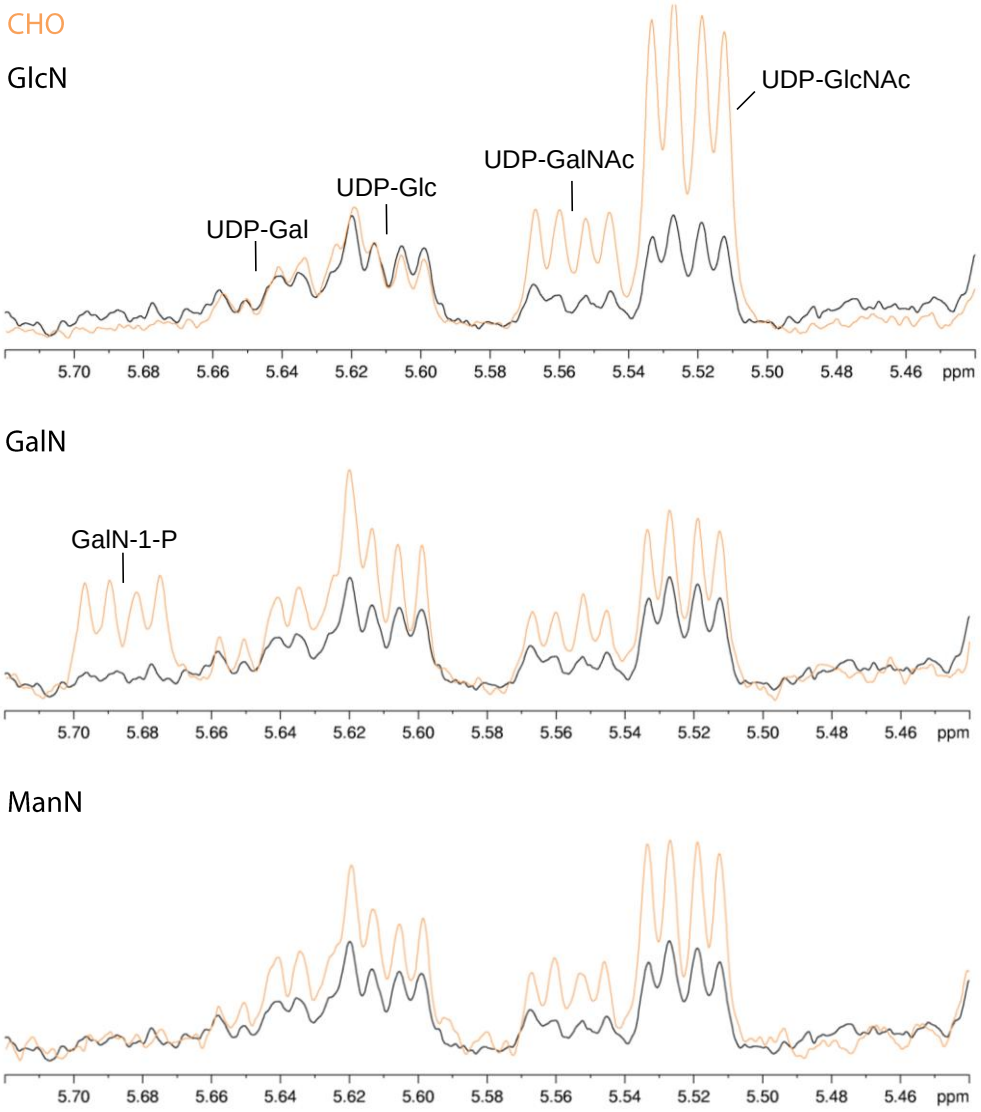

Figure 21. Effect of hexosamines on activated sugar nucleotide levels in CHO cells: Sections of ^{1}H-NMR spectra of M/C extracts of CHO cells after 24 h incubation with 100 µM HexN (GlcN, GalN, ManN; orange) compared to controls (black) are shown. The expanded regions of the spectra show the anomeric protons (H1) of UDP-GlcNAc, UDP-GalNAc, UDP-Glc, and UDP-Gal. In the spectrum of GalN treated cells, a novel resonance emerges, belonging to the H1 of GalN-1-P. CHO, Chinese hamster ovarian; GalN, galactosamine; GalN-1-P, galactosamine-1-phosphate; GlcN, glucosamine; HexN, hexosamine; ManN, mannosamine; M/C, methanol/chloroform; UDP-Gal, uridine diphosphate-galactose; UDP-GalNAc, uridine diphosphate-*N*-acetyl-galactosamine; UDP-Glc, uridine diphosphate-glucose; UDP-GlcNAc, uridine diphosphate-*N*-acetyl-glucosamine.

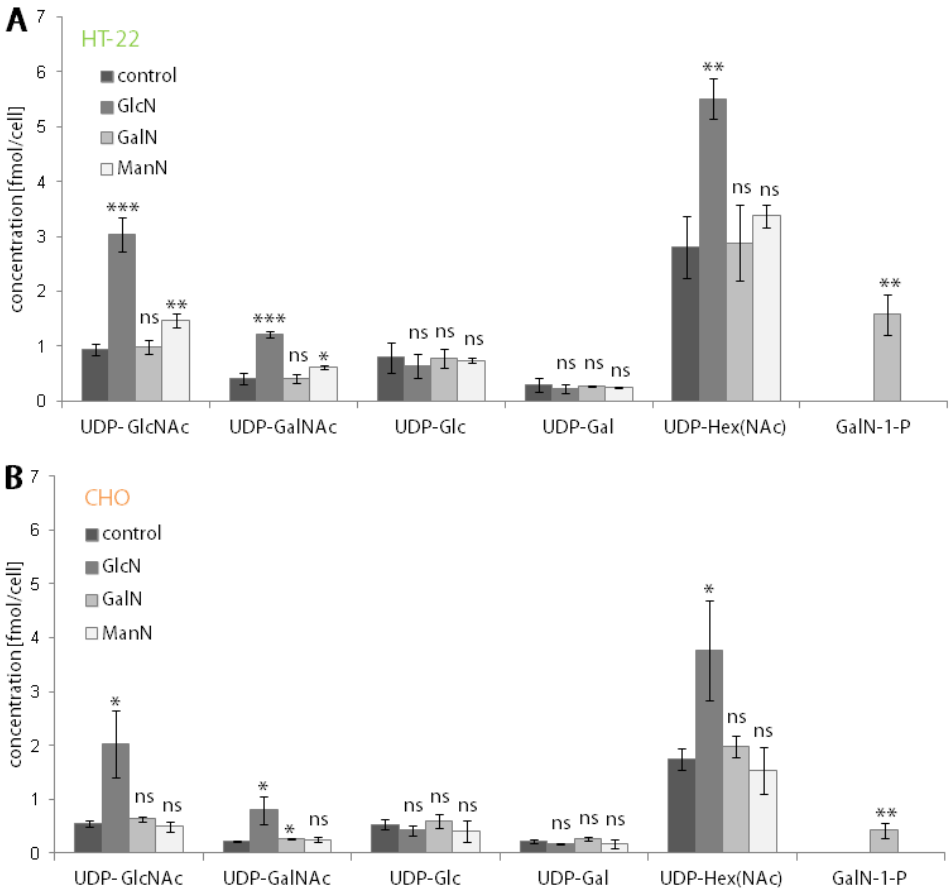

Figure 22. Effect of hexosamines on activated sugar nucleotide levels in HT-22 and CHO cells: Quantification of activated sugar nucleotide concentrations after incubation with 100 µM HexN (GlcN, GalN, ManN) for 24 h from fully relaxed ^{1}H-NMR spectra of HT-22 (A) and CHO (B) M/C cell extracts (n = 3). Values are mean ± standard deviation. *P* values of $P < 0.05$ were considered to be significant. *Represents $P < 0.05$; **represents $P < 0.01$; ***represents $P < 0.001$; ns, not significant. CHO, Chinese hamster ovarian; GalN, galactosamine; GalN-1-P, galactosamine-1-phosphate; GlcN, glucosamine; HexN, hexosamine; ManN, mannosamine; M/C, methanol/chloroform; UDP-Gal, uridine diphosphate-galactose; UDP-GalNAc, uridine diphosphate-*N*-acetyl-galactosamine; UDP-Glc, uridine diphosphate-glucose; UDP-GlcNAc, uridine diphosphate-*N*-acetyl-glucosamine; UDP-Hex(NAc); uridine diphosphate-(*N*-acetyl-)hexoses.

3.3 Galactose as Precursor for Synthesis of Activated Sugar Nucleotides in HT-22 and CHO cells

Glucose is the primary energy substrate of the brain (Fehm *et al*., 2006) and the precursor for the synthesis of activated sugar nucleotides. Here I have tested galactose as a potential substrate for formation of these metabolites. In this study, neuronal HT-22 cell and CHO cells were incubated with either 10 mM glucose, 5 mM glucose + 5 mM galactose, 5 mM galactose, or 10 mM galactose. In conditions with 5 mM galactose and 10 mM galactose, no glucose was present as energy source. The incubation time was 24 h for all conditions. Spectra acquired from HT-22 and CHO M/C extracts of cells incubated with 10 mM glucose

and 10 mM galactose are shown in Figure 23. In the spectrum of HT-22 cells incubated with 10 mM galactose, as well as in the spectrum of CHO cells a novel resonance at 5,50 ppm of a highly accumulated metabolite arose. This signal belongs to the anomeric proton (H1) of Gal-1-P. At first sight there is a decrease in the signal intensities of UDP-GlcNAc and UDP-GalNAc in both HT-22 and CHO cells when incubated with 10 mM galactose compared to incubation with 10 mM glucose. Since the signal of Gal-1-P heavily overlaps with the signal of UDP-GlcNAc, only the inner doublet of the doublet of doublets of the UDP-GlcNAc signal was used for quantification and the concentration calculated was subsequently doubled.

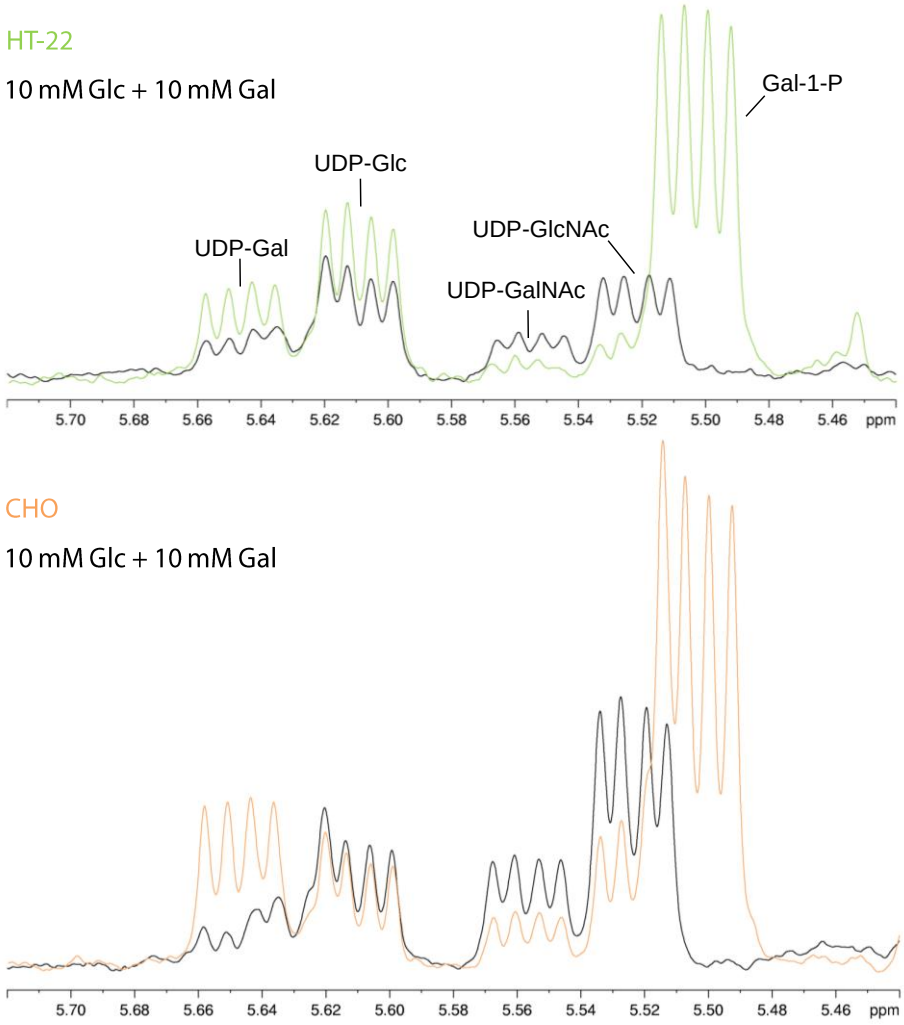

Figure 23 Galactose as Precursor for Synthesis of Activated Sugar Nucleotides in HT-22 and CHO cells: Sections of ^{1}H-NMR spectra of M/C extracts of neuronal HT-22 cells incubated with 10 mM Gal (green) and CHO cells incubated with 10 mM Gal (orange) for 24 h compared to respective cells treated with 10 mM Glc (control; black). The expanded regions of the spectra show the anomeric protons (H1) of UDP-GlcNAc, UDP-GalNAc, UDP-Glc, and UDP-Gal. In the spectrum of Gal treated cells, a novel resonance emerges, belonging to the H1 of Gal-1-P. Gal, galactose; Gal-1-P, galactose-1-phosphate; Glc, glucose; M/C, methanol/chloroform; UDP-Gal, uridine diphosphate-galactose; UDP-GalNAc, uridine diphosphate-*N*-acetyl-galactosamine; UDP-Glc, uridine diphosphate-glucose; UDP-GlcNAc, uridine diphosphate-*N*-acetyl-glucosamine.

In contrast to UDP-GlcNAc and UDP-GalNAc, the signal intensities of UDP-Glc and UDP-Gal were higher in HT-22 cells incubated with 10 mM galactose compared to incubation with 10 mM glucose. In the spectrum of CHO cells treated with 10 mM galactose only UDP-Gal, but not UDP-Glc exhibits higher signal intensity.

Figure 24 shows the levels of activated sugar nucleotides calculated from these fully relaxed ^{1}H-NMR spectra. In HT-22 cells cultured with 10 mM glucose, the UDP-GlcNAc concentration was 0,81 ± 0,04 fmol/cell. No significant changes in the UDP-GlcNAc concentration (0,74 ± 0,12 fmol/cell) were observed when the incubations medium contained 5 mM glucose + 5 mM galactose. However, when cells were incubated without glucose the UDP-GlcNAc levels decreased significantly. The UDP-GlcNAc concentration decreased to 0,44 ± 0,11 fmol/cell in HT-22 cells incubated with 5 mM galactose and to 0,37 ± 0,06 fmol/cell in cell incubated with 10 mM galactose. There were no significant changes in the UDP-GlcNAc levels between HT-22 cells incubated with 5 mM galactose and 10 mM galactose. In CHO cells, no significant changes in the UDP-GlcNAc concentration were detected in all conditions.

The same pattern was observed for UDP-GalNAc. In HT-22 cells no significant change in the UDP-GalNAc concentration was observed when the incubation medium was switched from 10 mM glucose (0,36 ± 0,02 fmol/cell) to 5 mM glucose + 5 mM galactose (0,36 ± 0,04 fmol/cell). However, when no glucose was present the UDP-GalNAc level decreased significantly. The UDP-GalNAc concentration was 0,18 ± 0,08 fmol/cell in HT-22 cells incubated with 5 mM galactose and 0,18 ± 0,04 fmol/cell in cells incubated with 10 mM galactose. It is obvious, that there are no significant changes between HT-22 cells incubated with 5 mM galactose compared to cells incubated with 10 mM galactose. Again, no significant changes were detected in the UDP-GalNAc levels in CHO cells under all conditions.

There were also no significant changes in the UDP-Glc levels in CHO cells. In HT-22 cells, on the contrary, the UDP-Glc level significantly increased from 0,80 ± 0,13 fmol/cell (10 mM glucose) to 1,15 ± 0,13 fmol/cell in HT-22 cell incubated with 10 mM galactose. There was also an increase to 1,33 ± 0,41 fmol/cell in the UDP-Glc level in cells exposed to 5 mM galactose alone. Nevertheless, this increase is not significant due to the large error bar.

The UDP-Gal levels were increased in both neuronal HT-22 and CHO under all conditions where galactose was present in the culture medium. In HT-22 cells the UDP-Gal concentration was 0,31 ± 0,02 fmol/cell in cells incubated with 10 mM glucose. This concentration increased to 0,64 ± 0,11 fmol/cell when incubated with 5 mM glucose + 5 mM galactose, to 0,66 ± 0,08 fmol/cell in cells incubated with 5 mM galactose, and to

0,70 ± 0,07 fmol/cell in cells incubated with 10 mM galactose. There are no significant changes between the conditions where galactose was present. In CHO cells the UDP-Gal concentration significantly increased from 0,28 ± 0,13 fmol/cell in (10 mM glucose) to 1,18 ± 0,46 fmol/cell (5 mM glucose + 5 mM galactose), to 0,89 ± 0,15 fmol/cell (5 mM galactose), and to 0,84 ± 0,14 fmol/cell (10 mM galactose).

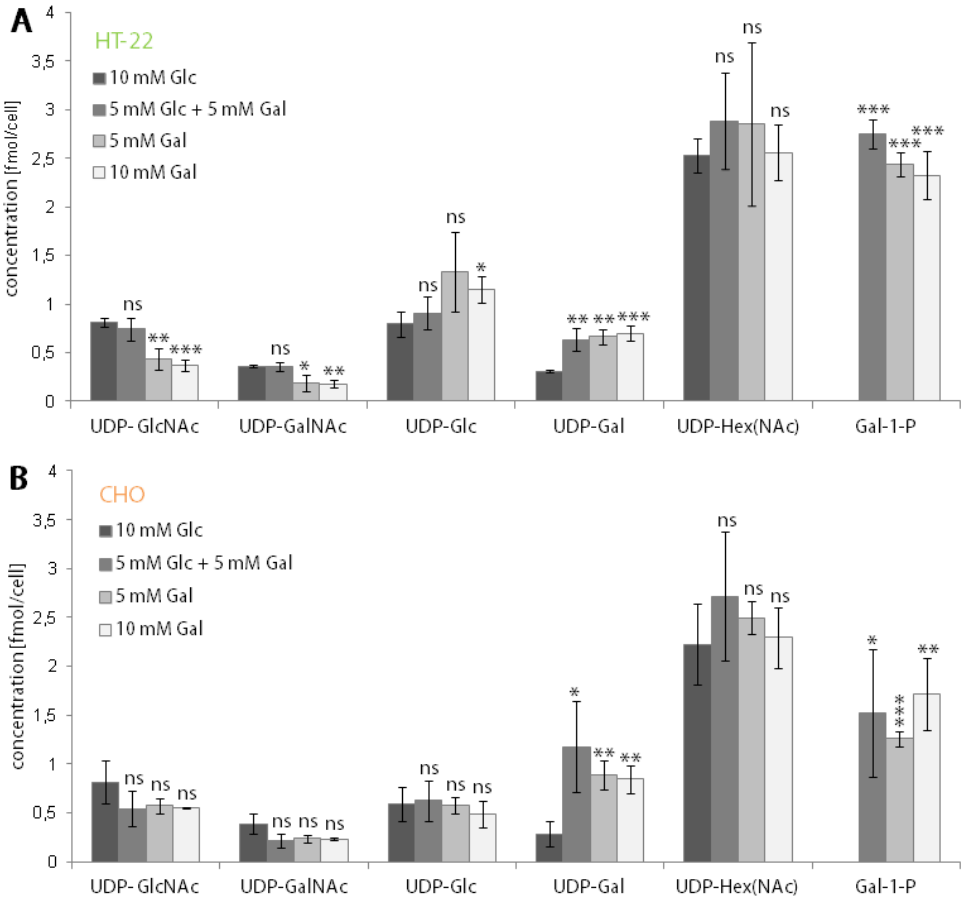

Figure 24. Galactose as precursor for synthesis of activated sugar nucleotides in HT-22 and CHO cells: Quantification of activated sugar nucleotide concentrations after incubation with 10 mM Glc, 5 mM Glc + 5 mM Gal, 5 mM Gal, or 10 mM Gal for 24 h from fully relaxed ^{1}H-NMR spectra of HT-22 (A) and CHO (B) M/C cell extracts (n = 3). Values are mean ± standard deviation. *P* values of $P < 0.05$ were considered to be significant. *Represents $P < 0.05$; **represents $P < 0.01$; ***represents $P < 0.001$; ns, not significant. CHO, Chinese hamster ovarian; Gal, galactose; Gal-1-P, galactose-1-phosphate; Glc, glucose; GlcN, glucosamine; M/C, methanol/chloroform; UDP-Gal, uridine diphosphate-galactose; UDP-GalNAc, uridine diphosphate-*N*-acetyl-galactosamine; UDP-Glc, uridine diphosphate-glucose; UDP-GlcNAc, uridine diphosphate-*N*-acetyl-glucosamine; UDP-Hex(NAc); uridine diphosphate-(*N*-acetyl-)hexoses.

No significant changes were detected in the overall concentration of activated sugar nucleotides detected (UDP-Hex(NAc)) in HT-22 and CHO cells. UDP-GlcUA concentrations are omitted for clarity, but no significant changes were detected for all conditions in both cell lines.

In HT-22 and CHO cells, Gal-1-P significantly accumulated when galactose was present in the culture medium. The accumulation of Gal-1-P was more pronounced in HT-22 cells with concentrations of 2,44 ± 0,12 fmol/cell and 2,33 ± 0,25 fmol/cell in cells treated with 5 mM galactose and 10 mM galactose, respectively. In HT-22 cell incubated with 5 mM glucose and 5 mM galactose, the concentration of Gal-1-P was with 2,75 ± 0,15 fmol/cell even slightly higher. In CHO cells the Gal-1-P levels were lower and ranged between 1,5 and 1,7 fmol/cell.

3.4 Effect of Limited Glucose Availability and Glucose-Deprivation on Brain Cells

3.4.1 Influence of Glucose Concentrations on Activated Sugar Nucleotide Levels in HT-22 Cells

One of the characteristics in AD and type II diabetes brains is impaired glucose utilization and subsequent down-regulation of *O*-GlcNAcylation along with hyperphosphorylation of tau (Liu *et al*., 2009a). In this chapter I investigated the effect of different glucose concentration on the formation of activated sugar nucleotides in neuronal HT-22 cells. HT-22 cells were directly seeded for 72 h into medium containing 25 mM, 18 mM, 12 mM, and 6 mM glucose. The concentrations of activated sugar nucleotides were obtained from fully relaxed ^{1}H-NMR spectra of M/C cell extracts. The levels of UDP-sugars quantified from these spectra are shown in Figure 25. The levels of all activated sugar nucleotides detected (UDP-GlcNAc, UDP-GalNAc, UDP-Glc, UDP-Gal, and UDP-GlcUA) remained almost constant when the glucose concentration was reduced from 25 mM glucose to 18 mM glucose. No significant changes were detected. When the glucose level was further reduced to 12 mM glucose, however, there was a sharp and significant decline in all activated sugar nucleotide levels detected. Another reduction of the glucose concentration from 12 mM to 6 mM, again, did not significantly decrease activated sugar nucleotide levels. To clarify this with UDP-GlcNAc as an example: HT-22 cells cultured in medium containing 25 mM glucose exhibited a UDP-GlcNAc level of 0,83 ± 0,06 fmol/cell. When the glucose concentration was reduced to 18 mM glucose, the UDP-GlcNAc concentration remained constant (0,85 ± 0,07 fmol/cell). A further reduction of the glucose level to 12 mM, however, leads to a significant decrease in the UDP-GlcNAc level to 0,22 ± 0,03 fmol/cell. This is a reduction of 73 % compared to the UDP-GlcNAc levels in HT-22 cells cultured with 25 mM glucose or 18 mM glucose. When the glucose concentration was again lowered to 6 mM the UDP-GlcNAc concentration

slightly decreases to 0,16 ± 0,05 fmol/cells. This decrease is not significant compared to the levels obtained from cells seeded in 12 mM glucose. This implies that although the glucose concentration was gradually lowered, the decrease in UDP-GlcNAc concentration is non-linear with a sharp decline between a glucose concentration of 18 mM and 12 mM. This sharp decline was not only observed for activated sugar nucleotides produced in the HBP (UDP-GlcNAc and UDP-GalNAc), but also for all other activated sugar nucleotides detected.

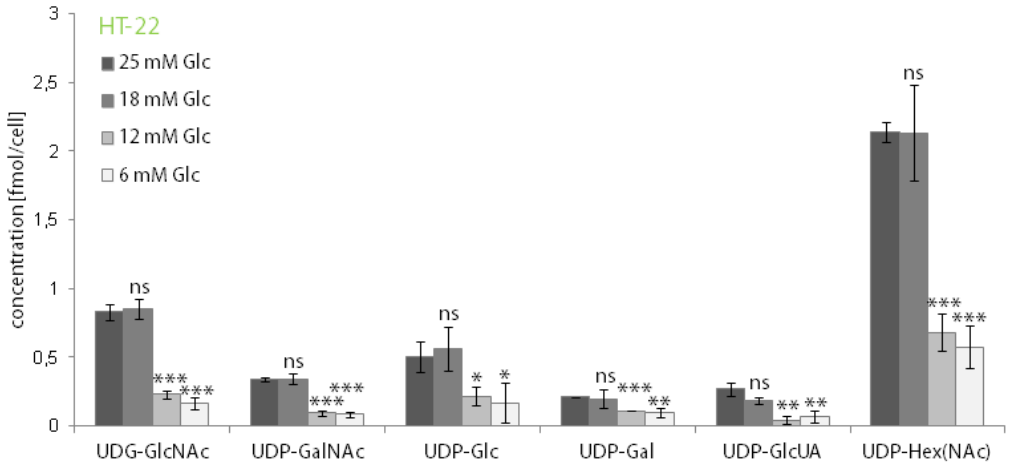

Figure 25. Effect of limited glucose availability on synthesis of activated sugar nucleotides in HT-22 cells: Quantification of activated sugar nucleotide levels in HT-22 cells directly seeded in medium containing different glucose concentrations for 72 h from fully relaxed ^{1}H-NMR spectra of M/C cell extracts (n = 3). Values are mean ± standard deviation. *P* values of $P < 0.05$ were considered to be significant. *Represents $P < 0.05$; **represents $P < 0.01$; ***represents $P < 0.001$; ns, not significant. Glc, glucose; M/C, methanol/chloroform; UDP-Gal, uridine diphosphate-galactose; UDP-GalNAc, uridine diphosphate-*N*-acetyl-galactosamine; UDP-Glc, uridine diphosphate-glucose; UDP-GlcNAc, uridine diphosphate-*N*-acetyl-glucosamine; UDP-GlcUA, uridine diphosphate-glucuronic acid, UDP-Hex(NAc); uridine diphosphate-(*N*-acetyl-)hexoses.

3.4.2 mRNA Expression of HBP Enzymes Influenced by Glucose Availability

The mRNA expression of the HBP enzymes GFAT, GlcN-6-P *N*-acetyltransferase, and UDP-GlcNAc pyrophosphorylase was tested using qRT-PCR in HT-22 cells. Furthermore, their mRNA levels in HT-22 cells cultured for 72 h in medium containing 25 mM glucose were quantified compared to cells cultured in 12 mM glucose. GFAT, the rate-limiting enzyme of the HBP, exists in three isoforms, GFAT1 (McKnight *et al*., 1992), GFAT2 (Oki *et al*., 1999) and GFAT1L (Niimi *et al*., 2001). GFAT1 plays a role in diabetes and obesity and has the highest expression in tissues involved with this disease, e.g. fat tissue (Nerlich *et al*., 1998). GFAT1L is a splice variant of GFAT1, and is primarily expressed in muscle (DeHaven *et al*., 2001). GFAT2, on the other hand, seems to be highly expressed in brain (Oki *et al*., 1999). In this study, the expression of GFAT1 and GFAT2 isoforms were investigated.

I found that both GFAT1 and GFAT2 are expressed in neuronal HT-22 cells (Figure 26). However, GFAT1 is more highly expressed than GFAT2. The mRNA expression of GlcN-6-P *N*-acetyltransferase is slightly higher compared to GFAT1. UDP-GlcNAc pyrophosphorylase comprises the highest mRNA level of all enzymes of the HBP investigated in HT-22 cells. There were no significant changes in the mRNA expression of GFAT1 and GFAT2 when cells were incubated for 72 h in medium containing only 12 mM glucose instead of 25 mM glucose. However, the mRNA levels of GlcN-6-P *N*-acetyltransferase and UDP-GlcNAc pyrophosphorylase decreased significantly when HT-22 cells were cultured in medium containing 12 mM glucose compared to cells grown in medium containing 25 mM glucose, as shown in Figure 26.

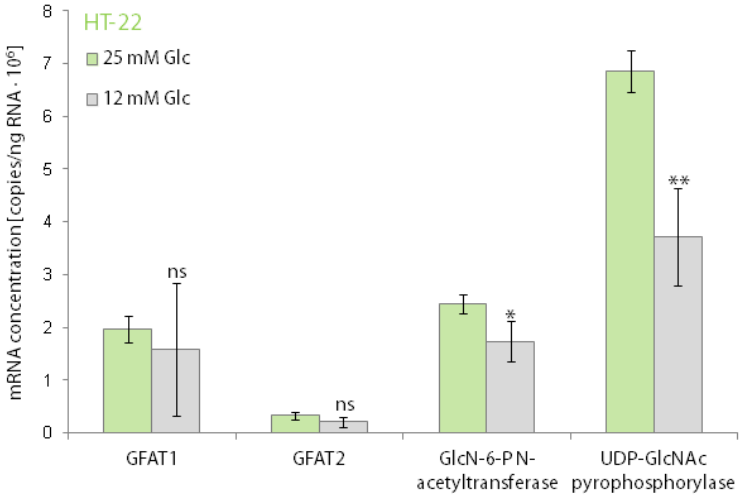

Figure 26. Quantitative RT-PCR for mRNA expression of enzymes of the HBP obtained from HT-22 cells seeded for 72 h in medium containing 25 mM Glc (green bars) or medium containing 12 mM Glc (gray bars; n = 3). Values are mean ± standard deviation. *P* values of $P < 0.05$ were considered to be significant. *Represents $P < 0.05$; **represents $P < 0.01$; ***represents $P < 0.001$; ns, not significant. GFAT, *Glutamine-fructose-6-P aminotransferase*; Glc, glucose; GlcN, glucosamine; GlcNAc, uridine diphosphate-*N*-acetylglucosamine.

3.4.3 UDP-GlcNAc Levels in Glucose-Deprived Neuronal Cells and Astrocytes

In contrast to neurons, astrocytes can store glucose as glycogen (Cataldo & Broadwell, 1986; Magistretti *et al.*, 1993). For this reason it is of interest to study the differences of the maintenance of UDP-GlcNAc levels in glucose-deprived astrocytes compared to neurons. I compared UDP-GlcNAc levels in neuronal HT-22 cells and primary astrocytes glucose-deprived for 12 h and 18 h compared to controls that were cultured in medium containing 25 mM glucose for the same time span. UDP-GlcNAc levels were quantified from fully relaxed ^{1}H-NMR spectra of M/C cell extracts. The levels of UDP-GalNAc, UDP-Glc, UDP-

Gal, and UDP-GlcUA were not quantified, because the concentrations of these sugars were too low when glucose deprived and uncertainties in these values became too big. In HT-22 cells the UDP-GlcNAc level decreased significantly from 0,76 ± 0,05 fmol/cell (control) to 0,13 ± 0,05 fmol/cell in cells glucose-deprived for 12 h as shown in Figure 27. UDP-GlcNAc levels remained constant (0,22 ± 0,04 fmol/cell) when glucose deprivation was prolonged to 18 h compared to levels obtained after 12 h glucose deprivation. No significant changes were detected. In astrocytes, the UDP-GlcNAc concentration under control conditions was 1,30 ± 0,13 fmol/cell. This concentration decreased significantly to 0,70 ± 0,10 fmol/cell in astrocytes glucose-deprived for 12 h. As in the case of HT-22 cells, glucose deprivation in astrocytes for 18 h did not significantly further reduce UDP-GlcNAc levels (0,68 ± 0,27 fmol/cell) compared to 12 h glucose deprivation.

In HT-22 12 h glucose deprivation led to an 83 % decrease in the UDP-GlcNAc levels compared to controls. In primary astrocytes the decrease was with 46 % less marked than in HT-22 cells. Consequently, the decrease in HT-22 cells ($P < 0{,}0001$) was more significant than in astrocytes ($P = 0{,}024$).

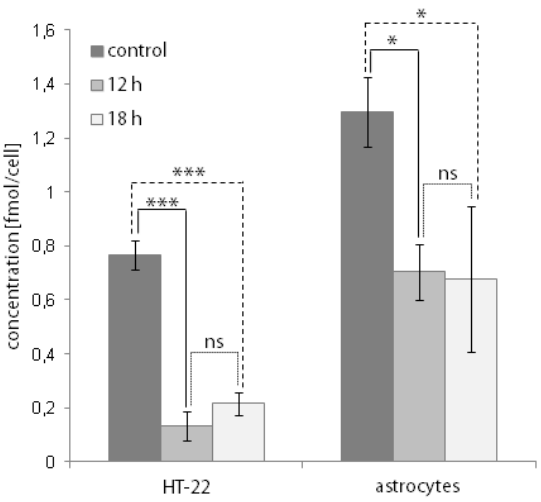

Figure 27. Comparison of UDP-GlcNAc levels in glucose deprived neuronal HT-22 cells and primary astrocytes: UDP-GlcNAc levels in neuronal HT-22 cells and primary astrocytes glucose-deprived for 12 h and 18 h compared to controls quantified from fully relaxed ^{1}H-NMR spectra of M/C cell extracts (n = 4 for HT-22 controls, n = 5 for astrocytic controls, n = 3 for Glc deprived cells). Values are mean ± standard deviation. *P* values of $P < 0.05$ were considered to be significant. *Represents $P < 0.05$; **represents $P < 0.01$; ***represents $P < 0.001$; ns, not significant. Glc, glucose; M/C, methanol/chloroform; UDP-GlcNAc, uridine diphosphate-*N*-acetyl-glucosamine.

3.5 NO-Induced Metabolic Changes in Astrocytes

Previous studies have shown that treatment of astrocytes with NO switches astrocytes into a glycolytic state, while TCA cycle and thus mitochondrial respiration are inhibited. These studies mainly focused on mRNA levels of glycolytic enzymes, as well as of glucose and lactate transporters, or the studies focused on particular metabolites of specific enzymatic pathways, such as glucose, lactate, or Fru-2,6-BP (Bolaños *et al*., 1994; Almeida *et al*., 2001; Almeida *et al*., 2004; Marcillac *et al*., 2011; Brix *et al*., 2012). NMR spectroscopy is an important analytical tool for detection and quantification of metabolites and has already been proven to be useful in studying astrocytic and neuronal metabolism (e.g. Brand *et al*., 1993; Zwingmann & Leibfritz, 2003).

The aim of the present study was to investigate the changes of metabolite concentrations induced by NO in astrocytes. Furthermore, the effect of NO on the concentration of UDP-GlcNAc was investigated since a prior NMR study in our lab had shown that UDP-GlcNAc concentrations were sensitive to varying acetyl-CoA levels in neuronal HT-22 cells (Gallinger *et al*., 2011).

To investigate metabolic changes stimulated by NO, primary cultures of cortical astrocytes were preincubated with 22 mM [1-^{13}C]glucose for 12 h, and then for additional 12 h with 0,8 mM DETA-NONOate as NO-donor. For a control, cells were incubated only with [1-^{13}C]glucose, or with 0,8 mM Sulfo-NONOate, a NO-donor that does not produce NO at physiological pH. Unless otherwise indicated, these same experimental conditions were used for all NO experiments in this chapter. M/C extracts of cells, as well as lyophilized and redissolved culture medium were analyzed by NMR spectroscopy in order to detect ^{13}C-labeled metabolites deriving from [1-^{13}C]glucose. Spectra of astrocytes incubated with [^{12}C]glucose instead of [1-^{13}C]glucose were analyzed additionally.

3.5.1 Changes in Glucose Uptake and Lactate Release Caused by NO

The glycolytic flux can be determined by the rate of glucose consumption and lactate formation. However, this does not exactly reflect the total glycolytic activity of a cell. Pyruvate and lactate can also be produced from other precursors such fatty acids, ketone bodies, or amino acids, which are present in culture media or generated by degradation of cellular proteins. *De novo* lactate synthesis exclusively from glucose can be determined using ^{13}C-labeled glucose and subsequent analysis by NMR spectroscopy. ^{13}C-labeled lactate originating from ^{13}C-labeled glucose exhibits an additional ^{1}H-^{13}C coupling (J = 128 Hz).

These peaks can be distinguished from the peaks of unlabeled ^{12}C-lactate synthesized from unlabeled pyruvate originating from substances other than ^{13}C-labeled glucose.

Segments of ^{1}H-NMR spectra of lyophilized cell culture media after incubation of astrocytes either with [1-^{13}C]glucose alone or with the NO-donor DETA-NONOate are shown in Figure 28A.

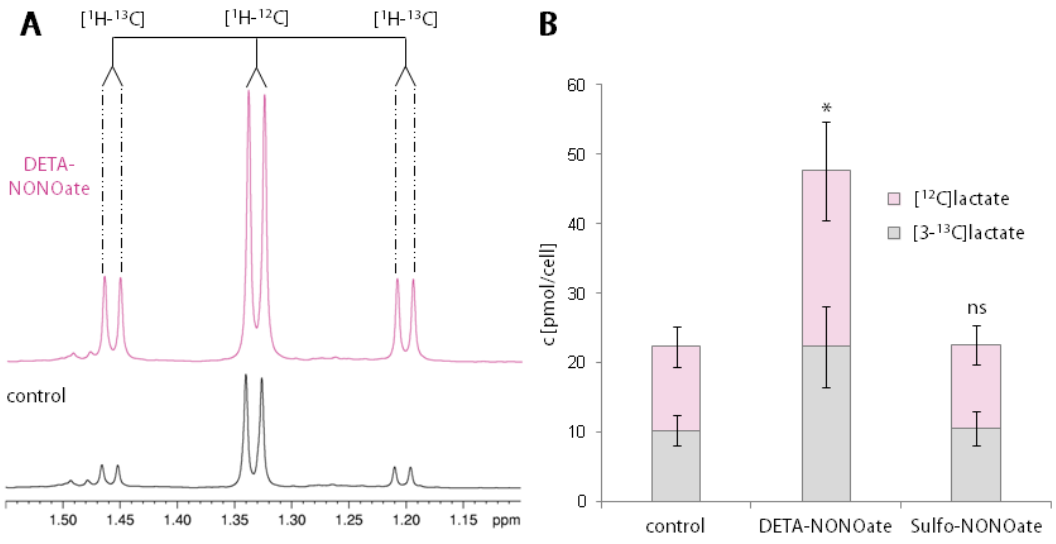

Figure 28. ^{13}C-incorporation into extracellular lactate: (A) Sections of ^{1}H-NMR spectra of lyophilized culture medium obtained from astrocytes after 24 h incubation with 22 mM [1-^{13}C]glucose (control) and after incubation with 22 mM [1-^{13}C]glucose for 24 h and 0,8 mM DETA-NONOate for 12 h (DETA-NONOate). The signal of the methyl protons of unlabeled lactate ([^{1}H-^{12}C]) at 1,33 ppm can be distinguished from the satellites arising from ^{1}H-^{13}C-coupling ($J_{1H\text{-}13C}$ = 128 Hz) of the ^{13}C-labeled isotopomer ([^{1}H-^{13}C]). (B) Quantification of the [^{12}C]lactate and [3-^{13}C]lactate concentrations from these fully relaxed ^{1}H-NMR spectra (n = 4 for controls and DETA-NONOate treated cells, n = 3 for Sulfo-NONOate treated cells). Values are mean ± standard deviation. *P* values of $P < 0.05$ were considered to be significant. *Represents $P < 0.05$; ns, not significant. *P* values were calculated from the sum of [^{12}C]lactate and [3-^{13}C]lactate.

In glycolysis [1-^{13}C]glucose is degraded to [3-^{13}C]pyruvate, which is further converted to [3-^{13}C]lactate. The spectra show an additional doublet splitting from the ^{1}H-^{13}C coupling ([^{1}H-^{13}C]) as described above. The signal of unlabeled ^{12}C-lactate ([^{1}H-^{12}C]) is also present in the spectra, not only because of ^{12}C-lactate deriving from other substances than the administered [1-^{13}C]glucose, but mainly because only half of the lactate derived from [1-^{13}C]glucose is ^{13}C-labeled. In glycolysis one molecule [3-^{13}C]lactate and one molecule unlabeled lactate are produced. The lactate signal intensities of NO treated astrocytes are much higher than in control cells. To confirm this observation, lactate release and glucose consumption were quantified from ^{1}H-NMR spectra by calculating the difference of their concentration before (t = 0) and after incubation (t = 24 h), as depicted in Figure 28B. Treatment of astrocytes with DETA-NONOate significantly increased the release of *de novo* synthesized [3-^{13}C]lactate from 10,22 ± 2,23 pmol/cell for control and 10,52 ± 2,38 pmol/cell for Sulfo-NONOate

treated cells, respectively to 22,33 ± 5,85 pmol/cell. This means that lactate release in astrocytes increased more than 2-fold after exposure to NO.

Similar to lactate release, glucose consumption in astrocytes increased significantly when cells were treated with DETA-NONOate (Figure 29). Under normal conditions, glucose consumption in astrocytes was 13,67 ± 2,17 pmol/cell and 18,00 ± 5,49 pmol/cell when cells were treated with Sulfo-NONOate, respectively. Glucose consumption in astrocytes treated with NO, however, was 26,35 ± 4,23 pmol/cell. This is again twice as much as, compared to control conditions.

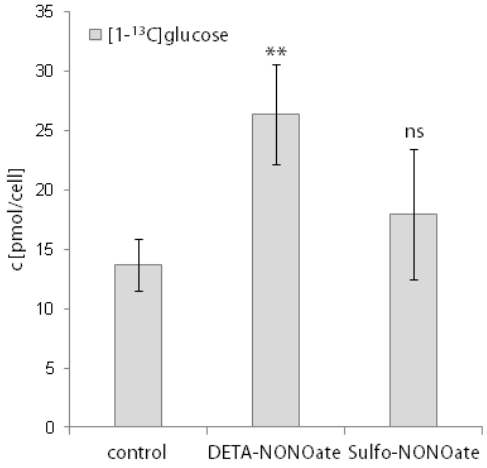

Figure 29. Effect of NO on glucose consumption in astrocytes. The uptake of [1-^{13}C]glucose was quantified by integration of ^{13}C-satellite signals of the H1 proton of the α anomer at 5,41 ppm and 5,07 ppm from fully relaxed ^{1}H-NMR spectra und subsequent extrapolation to total glucose (α anomer plus ß anomer). Spectra of lyophilized culture medium obtained from astrocytes after 24 h incubation with 22 mM [1-^{13}C]glucose (control, n = 4) or after incubation with 22 mM [1-^{13}C]glucose for 24 h plus 0,8 mM DETA-NONOate (n = 4) or Sulfo-NONOate (n = 3) for 12 h were analyzed. Values are mean ± standard deviation. *P* values of $P < 0.05$ were considered to be significant. *Represents $P < 0.05$; **represents $P < 0.01$; ***represents $P < 0.001$; ns, not significant.

In addition to quantification of absolute lactate release in astrocytes treated with NO, the fractional ^{13}C-enrichment of extracellular lactate was also calculated. ^{13}C-enrichment can give information about the contribution of lactate derived from flux of [1-^{13}C]glucose through glycolysis as compared to pyruvate or lactate produced from unlabeled precursors such as fatty acids, amino acids present in the culture medium, products of the pentose phosphate pathway, or formation of lactate from TCA cycle intermediates. In astrocytes, glycogenolysis may also contribute to a decrease of ^{13}C-enrichment in lactate. However, it has to be kept in

mind, that glycogen itself incorporates ^{13}C from [1-^{13}C]glucose. Enhanced glycogenolysis can only party be responsible for a decrease of ^{13}C-enrichment if and only if a negligible part of glycogen is ^{13}C-labeled. In this case a decrease of ^{13}C-enrichment provides an estimate of lactate derived from glucose versus lactate derived from glycogen. Fractional ^{13}C-enrichment was determined by referencing the concentration of ^{13}C-labeled lactate ([^{1}H-^{13}C]) to the sum of unlabeled lactate plus ^{13}C-labeled lactate ([^{1}H-^{12}C] + [^{1}H-^{13}C]) and subsequent correction for 1,1 % natural abundance. But, in contrast to an absolute increase in synthesis of [3-^{13}C]lactate from [1-^{13}C]glucose no significant alterations of ^{13}C-enrichment in extracellular lactate of astrocytes treated with DETA-NONOate compared to controls were observed (Figure 30).

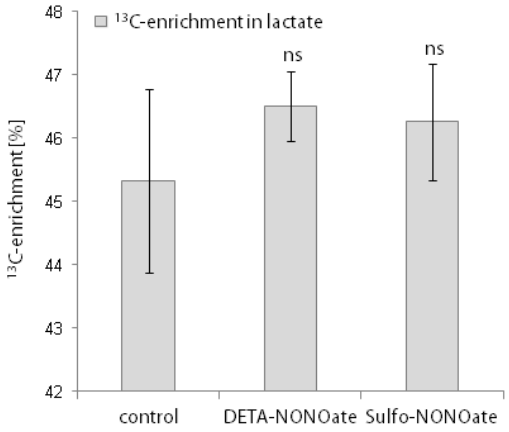

Figure 30. Influence of NO on the percentage of ^{13}C-enrichment in extracellular lactate. Fractional ^{13}C-enrichment was calculated by referencing the concentration of ^{13}C-labeled lactate ([^{1}H-^{13}C]) to the sum of unlabeled lactate plus ^{13}C-labeled lactate ([^{1}H-^{12}C] + [^{1}H-^{13}C]) and subsequent correction for natural abundant ^{13}C. ^{1}H-NMR spectra were obtained from lyophilized culture medium of astrocytes incubated with 22 mM [1-^{13}C]glucose (control, n = 4) for 24 h or with 22 mM [1-^{13}C]glucose for 24 h and 0,8 mM DETA-NONOate (n = 4) or Sulfo-NONOate (n = 3) for 12 h. Values are mean ± standard deviation. *P* values of $P < 0.05$ were considered to be significant. *Represents $P < 0.05$; **represents $P < 0.01$; ***represents $P < 0.001$; ns, not significant.

3.5.2 Impact of NO on Astrocytic Cell Viability

Besides being an important physiological messenger in the brain, excessive NO is toxic and may lead to neurotoxicity. To analyze changes in cell viability resulting from NO treatment, cells were counted after trypsinization in a hemocytometer using trypan blue exclusion. Figure 31B shows the number of counted viable cells after incubation with 22 mM glucose

alone, or after pretreatment with 22 mM glucose for 12 h and subsequent incubation with either 0,8 mM DETA-NONOate or Sulfo-NONOate. No significant changes in cell viability were detected in treated cells compared to control cells. It has to be noted that only viable cells were counted, but not the blue-stained dead cells, because those were rapidly degraded and difficult to count correctly. However, monitoring primary astrocytes treated with Sulfo-NONOate or DETA-NONOate by taking photomicrographs depicted no increased detachment or changes in the shape of cells (Figure 31A).

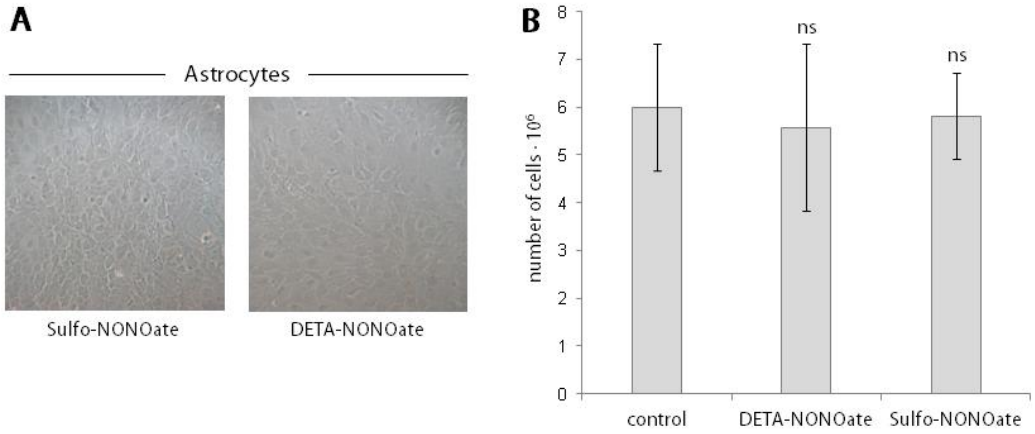

Figure 31. (A) Bright-field photomicrographs of primary cortical astrocytes pretreated with 22 mM glucose for 12 h and subsequent incubation with 0,8 mM DETA-NONOate or Sulfo-NONOate for 12 h. All images were acquired using a 10x lens. (B) Number of viable cells after incubation with 22 mM glucose (control; n = 8) for 24 h or after preincubation with 22 mM glucose for 24 h and following incubation with either 0,8 mM DETA-NONOate (n = 6) or Sulfo-NONOate (n = 6) for 12 h. Cells were counted after trypsinization using trypan blue exclusion. *P* values of $P < 0.05$ were considered to be significant. *Represents $P < 0.05$; **represents $P < 0.01$; ***represents $P < 0.001$; ns, not significant.

3.5.3 Correlation between Enhanced Glycolysis and TCA Cycle Intermediates Induced by NO

To detect metabolic changes caused by NO in astrocytes, $^{1}H,^{13}C$-HSQC spectra of M/C cell extracts and lyophilized cell culture media were analyzed. Two different incubation conditions each with [1-^{13}C]glucose alone, [1-^{13}C]glucose plus DETA-NONOate, or [1-^{13}C]glucose plus Sulfo-NONOate were used. Under condition 1 cells were preincubated with 22 mM [1-^{13}C]glucose. After 12 h 0,8 mM DETA-NONOate or 0,8 mM Sulfo-NONOate were added for further 12 h. For control experiments, cells were incubated for 24 h with 22 mM [1-^{13}C]glucose. Under condition 2 [1-^{13}C]glucose and DETA-NONOate, or Sulfo-NONOate were added at once to the incubation medium. Incubation time was 12 h. For controls, cells were incubated with [1-^{13}C]glucose alone for 12 h. Condition 2 was chosen, to exclude that preincubation with [1-^{13}C]glucose leads to less distinct differences in the metabolic profiles, since [1-^{13}C]glucose is incorporated into the metabolites before NO is

added. However, to anticipate the results, there were no differences in the $^{1}H,^{13}C$-HSQC spectra for both conditions. Figure 32 shows representative regions of $^{1}H,^{13}C$-HSQC spectra from M/C cell extracts and media of astrocytes incubated as described for condition 2. Control spectra of astrocytes treated with [1-^{13}C]glucose alone are shown in black and spectra from DETA-NONOate treated astrocytes are shown in pink. Spectra of Sulfo-NONOate treated cells are omitted for graphical clarity, but they show the same peak pattern as controls. Incubation of astrocytes with DETA-NONOate leads to an altered labeling pattern of two metabolites in the M/C cell extracts, namely citrate and glutamate (encircled). The resonances of citrate are not visible in spectra of M/C cell extracts of untreated astrocytes. However, in DETA-NONOate treated astrocytes, citrate accumulates significantly. The direct opposite is observed for glutamate. The intensity of the glutamate peak diminishes in the spectra of astrocytic M/C cell extracts after incubation with DETA-NONOate. The signal intensities of citrate peaks from citrate released into the cell culture medium by astrocytes, however, do not vary between treated and untreated astrocytes. Glutamate was not released by astrocytes and therefore not detectable in cell culture medium held in contact with astrocytes.

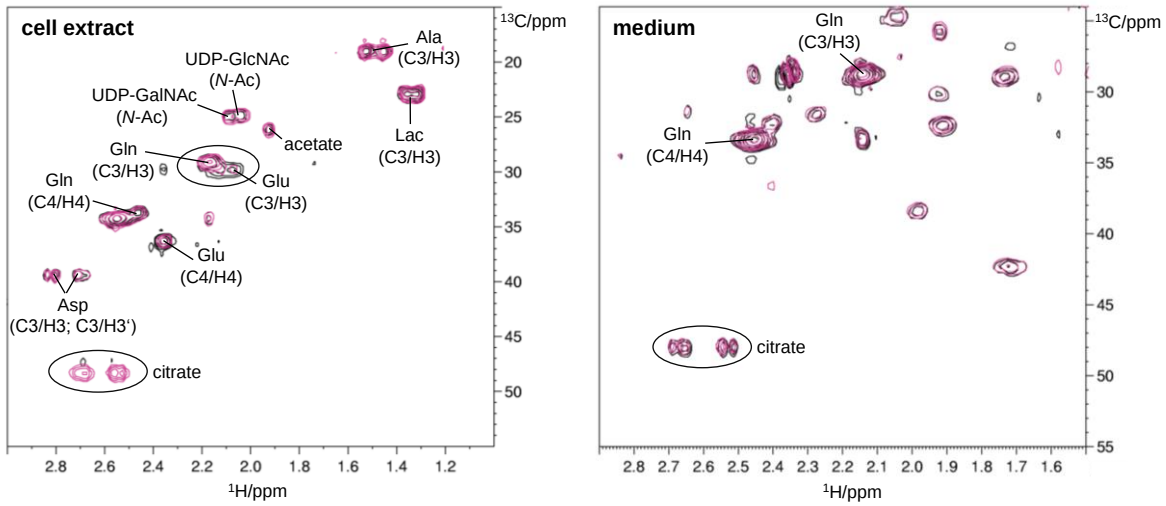

Figure 32. Representative sections of $^{1}H,^{13}C$-HSQC spectra obtained from M/C cell extracts and medium after incubation with 22 mM [1-^{13}C]glucose alone (control; black) or with [1-^{13}C]glucose and 0,8 mM DETA-NONOate (DETA-NONOate; pink) for 12 h. Spectra of cells treated with Sulfo-NONOate are omitted for graphical clarity. Encircled are the signals of citrate and glutamine/glutamate (Gln/Glu). Citrate signals merely appear in DETA-NONOate treated cells in the M/C cell extract. In the incubation medium, citrate signals are present in both untreated und treated conditions. Ala, alanine; Asp, aspartate; Gln, glutamine; Glu, glutamate; Lac, lactate; UDP-GalNAc, uridine diphosphate-*N*-acetylgalactosamine; UDP-GlcNAc, uridine diphosphate-*N*-acetylglucosamine.

To confirm these findings the level of glutamate was quantified from ^{1}H-NMR spectra in M/C cell extracts of astrocytes treated as described for condition 1 but with [^{12}C]glucose instead of [1-^{13}C]glucose. The resonances of citrate are not well suited for quantification because they overlap with other signals in ^{1}H-NMR spectra. The expanded region of a ^{1}H-NMR spectrum

showing the ethyl resonances of protons at C4 of unlabeled glutamate already indicate that the concentration of glutamate is reduced in astrocytes treated with DETA-NONOate (Figure 33A). Quantification finally confirms this observation. Glutamate levels are significantly reduced in astrocytes treated with DETA-NONOate (6,41 ± 0,41 fmol/cell) compared to controls (11,26 ± 2,44 fmol/cell) and astrocytes incubated with Sulfo-NONOate (13,97 ± 1,04 fmol/cell) (Figure 33B).

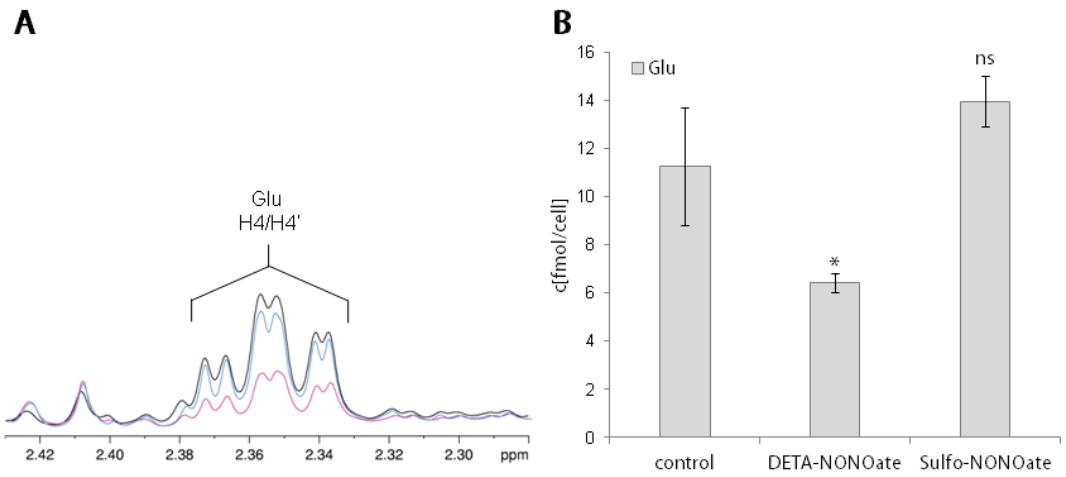

Figure 33. Effect of NO on intracellular glutamate: (A) Expanded region of a ^{1}H-NMR spectra showing the ethyl resonances of the protons at C4 of unlabeled glutamate (Glu) in M/C cell extracts obtained from astrocytes. Black: astrocytes incubated for 24 h with 22 mM [^{12}C]glucose. Blue: astrocytes incubated for 24 h with 22 mM [^{12}C]glucose and 0,8 mM Sulfo-NONOate for 12 h. Pink: astrocytes incubated for 24 h with 22 mM [^{12}C]glucose and 0,8 mM DETA-NONOate for 12 h. (B) Quantification of the intracellular glutamate level from these fully relaxed ^{1}H-NMR spectra (n = 7 for control, n = 3 for DETA-NONOate and Sulfo-NONOate). Values are mean ± standard deviation. *P* values of $P < 0.05$ were considered to be significant. *Represents $P < 0.05$; **represents $P < 0.01$; ***represents $P < 0.001$; ns, not significant.

3.5.4 Effect of NO on UDP-GlcNAc

It was shown that NO has strong influence on astrocytic glucose metabolism. Since the HBP is a minor branch of glycolysis, and since UDP-GlcNAc - the major product of the HBP - is sensitive to varying glucose concentrations, the effect of NO on UDP-GlcNAc and other activated sugar nucleotides was investigated. First, the levels of UDP-GlcNAc, UDP-GalNAc, UDP-Glc, UDP-Gal and UDP-Hex(NAc) were quantified. UDP-Hex(NAc) is the concentration calculated from the integral of the signals over all activated sugar nucleotides in that region. That includes UDP-GlcUA, since the anomeric signal of UDP-GlcUA strongly overlaps with the signals of the other sugars. Figure 34 shows the levels of these activated sugar nucleotides quantified from fully-relaxed ^{1}H-NMR spectra of M/C extracts from astrocytes treated either with 22 mM [^{12}C]glucose alone (control), with 22 mM [^{12}C]glucose + 0,8 mM DETA-NONOate (DETA-NONOate), or with 22 mM [^{12}C]glucose + 0,8 mM Sulfo-

NONOate (Sulfo-NONOate). Incubation times were as follows: 24 h for control and 12 h preincubation with glucose plus additional 12 h after administration of DETA- or Sulfo-NONOate. No significant changes between control and DETA-NONOate treated astrocytes and between Sulfo-NONOate and DETA-NONOate treated astrocytes were observed. However, there were significant changes between control and Sulfo-NONOate in the case of UDP-GlcNAc, UDP-GalNAc, and UDP-HexNAc ($P < 0{,}05$ for all). Since the results of control conditions and Sulfo-NONOate treated astrocytes did not reveal any differences so far, it can be assumed that these significant changes may be due to associated uncertainties of the experimental setup in the three independent experiments for this group.

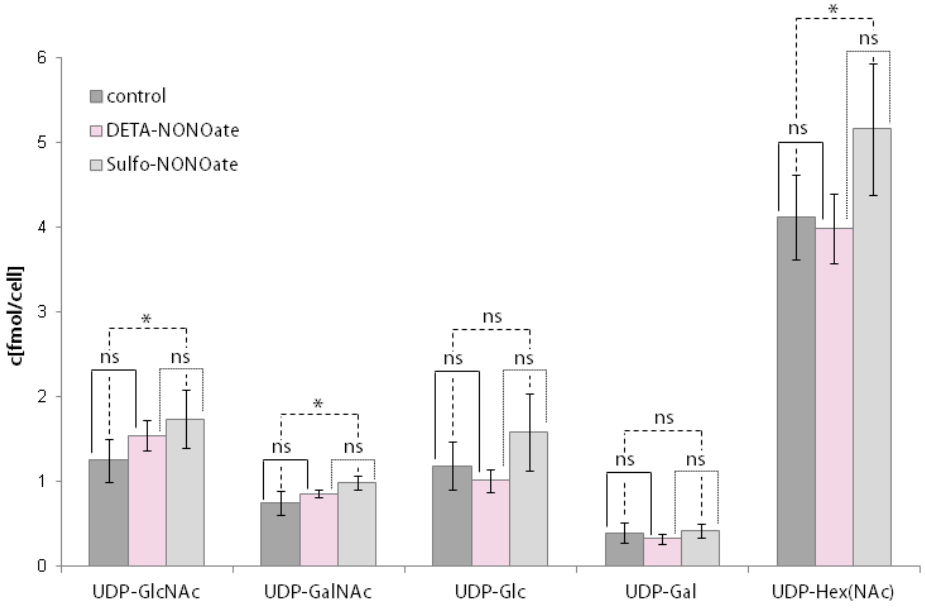

Figure 34. Levels of activated sugar nucleotides in astrocytes incubated with 22 mM [^{12}C]glucose alone (n = 7) for 24 h or with 22 mM [^{12}C]glucose for 24 h plus 0,8 mM DETA-NONOate or Sulfo-NONOate (both n = 3) for 12 h. Concentrations were determined from fully-relaxed ^{1}H-NMR spectra of M/C cell extracts. Values are mean ± standard deviation. *P* values of $P < 0.05$ were considered to be significant. *Represents $P < 0.05$; **represents $P < 0.01$; ***represents $P < 0.001$; ns, not significant.

Quantification of UDP-GlcNAc, or other activated sugar nucleotides do not reflect exactly the aberrant glucose metabolism caused by NO, since the glucose moiety and the *N*-acetyl group of UDP-GlcNAc can be produced from other precursors than glucose. These sources comprise, e.g. glycogen, fatty acids, and TCA cycle intermediates. [1-^{13}C]glucose as a source of glucose allows identification of peaks of unlabeled UDP-GlcNAc synthesized from unlabeled precursors originating from substances other than [1-^{13}C]-labeled glucose. A previous study in our lab utilizing [1-^{13}C]glucose as the sole source of glucose has shown that the ^{1}H-NMR signal of the *N*-acetyl group of UDP-GlcNAc can serve as a marker for decreased mitochondrial respiration and hence decreased acetyl-CoA synthesis in neuronal

cells (Gallinger *et al*., 2011). Briefly, neuronal HT-22 cells showed a decrease in labeling of the *N*-acetyl group of UDP-GlcNAc when incubated with [1-^{13}C]glucose and sodium azide, an inhibitor of complex IV of the respiratory chain, compared to untreated cells. As a consequence of this inhibition NAD^+ production by complex I of the respiratory chain is disrupted and NADH accumulates. NAD^+ in turn is an essential cofactor of the pyruvate dehydrogenase complex (PDC) that transforms pyruvate into acetyl-CoA. Therefore, acetyl-CoA production decreases when NAD^+ is no longer available. UDP-GlcNAc synthesis in the HBP occurs in the cytosol, while acetyl-CoA synthesis by PDC takes place in the mitochondrion. Since acetyl-CoA cannot pass the mitochondrial membrane, it cannot be directly incorporated into the *N*-acetyl group of UDP-GlcNAc. To reach the cytosol, mitochondrial acetyl-CoA is introduced into the TCA cycle where it is transformed to citrate. Citrate is then transported into the cytosol, where it is cleaved by ATP-citrate-lyase to yield cytosolic acetyl-CoA. Since the production of cytosolic ^{13}C-labeled acetyl-CoA depends on formation of mitochondrial ^{13}C-labeled acetyl-CoA by PDC, which in turn is relies on NAD^+ supply from mitochondrial respiration, the incorporation of the ^{13}C-label from cytosolic acetyl-CoA into the *N*-acetyl group of UDP-GlcNAc reflects mitochondrial respiration and flux through the TCA cycle.

The direct identification of ^{13}C-labeled acetyl-CoA in ^{1}H,^{13}C-HSQC spectra of cell extracts is not unambiguously possible due to severe overlap with signals of other metabolites e.g. succinyl-CoA. The ^{13}C-label of [1-^{13}C]glucose can be incorporated at 5 positions in UDP-GlcNAc of which 4 can be detected in ^{1}H,^{13}C-HSQC spectra of astrocytic cell extracts. The C1 of the GlcNAc residue is directly labeled from [1-^{13}C]glucose. The ^{13}C-label in the C1 of the ribose moiety is incorporated via PPP and pyrimidine biosynthesis and the C6 of uracil derives its label from aspartate formed in the TCA cycle used in *de novo* pyrimidine synthesis. The *N*-acetyl group receives its label from ^{13}C-labeled cytosolic acetyl-CoA (see Figure 50 in the discussion part).

Figure 35 shows these signals detected in ^{1}H,^{13}C-HSQC spectra obtained from M/C cell extracts after incubation with 22 mM [1-^{13}C]glucose alone or with [1-^{13}C]glucose and 0,8 mM DETA-NONOate for 12 h. The labeling pattern does not differ from astrocytes preincubated with [1-^{13}C]glucose for 12 h. Spectra of cells incubated with Sulfo-NONOate (not shown for graphical clarity) have the same labeling pattern as spectra of controls, incubated with [1-^{13}C]glucose alone. The signals of ^{13}C-labeled UDP-GalNAc at the C1 position and *N*-acetyl group are also detected. They partially overlap with the corresponding signals of UDP-GlcNAc, but both can be assigned unambiguously and it should be possible to detect changes in their concentrations independently. However, no differences in the signal intensity of the

N-acetyl group in UDP-GlcNAc (Figure 35A) and the signal intensity of the C1 of UDP-GlcNAc (Figure 35B) were observed. The signals of ribose and uracil moiety of UDP-GlcNAc were not used for detection of concentration changes, since these signals overlap with correspondent signals of other activated sugar nucleotides.

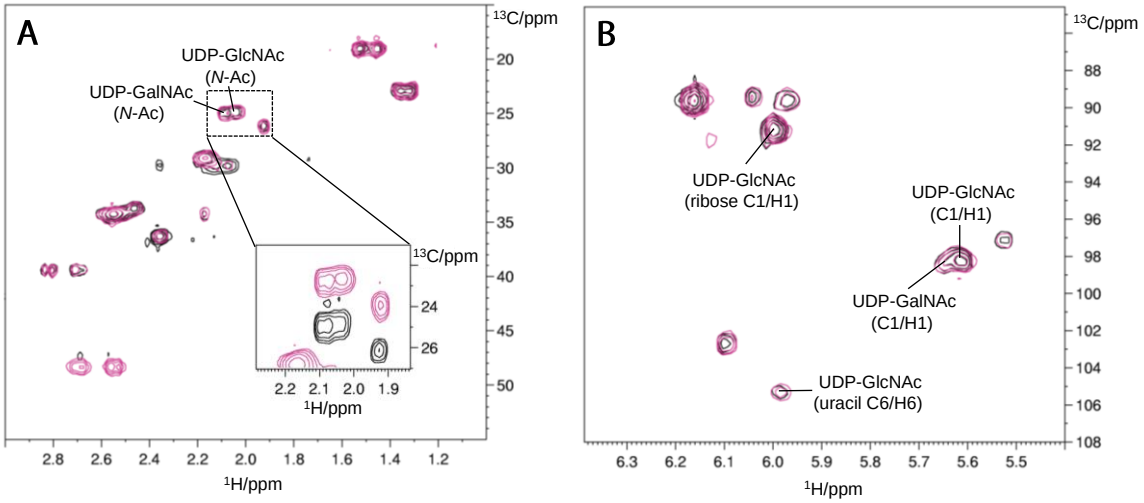

Figure 35. Expanded regions of representative $^{1}H,^{13}C$-HSQC spectra obtained from M/C cell extracts after incubation with 22 mM [1-^{13}C]glucose alone (control; black) or with [1-^{13}C]glucose and 0,8 mM DETA-NONOate (DETA-NONOate; pink) for 12 h. Spectra of cells treated with Sulfo-NONOate are omitted for graphical clarity. (A) Enlarged region focusing on the *N*-acetyl groups of UDP-GlcNAc (δ(*N*-Ac C/H) = 25,21/2,08 ppm) and UDP-GalNAc (δ(*N*-Ac C/H) = 25,22/2,09 ppm). The pink spectrum is shifted by 2 ppm in direction of the carbon axis. (B) Overview of the anomeric region. The signals of the carbon/anomeric proton (C1/H1) of UDP-GlcNAc and UDP-GalNAc, as well as of the ribose (C1/H1) and uracil (C6/H6) of UDP-GlcNAc are shown. UDP-GlcNAc: δ(anomeric C1/H1) = 97,61/5,52 ppm; δ(ribose C1/H1) = 91,27/5,99 ppm; δ(uracil C6/H6) = 105,35/5,98 ppm. UDP-GalNAc: δ(anomeric C1/H1) = 97,73/5,56 ppm. The signals of ribose and uracil are not well suited for studying UDP-GlcNAc, since the signals overlap with correspondent signals of other activated sugar nucleotides. *N*-Ac, *N*-acetyl; UDP-GalNAc, uridine diphosphate-*N*-acetylgalactosamine; UDP-GlcNAc, uridine diphosphate-*N*-acetylglucosamine.

To corroborate these findings one-dimensional (1D) $^{1}H,^{13}C$-HSQC spectra were recorded. Figure 36 and Figure 37 display spectra from cell extracts of astrocytes treated with [1-^{13}C]glucose for 24 h (control) or with [1-^{13}C]glucose for 24 h plus DETA-NONOate for 12 h (DETA-NONOate). Figure 36 focusses on the signal of the anomeric proton attached to C1 of the GlcNAc moiety of UDP-GlcNAc, whereas Figure 37 shows the signal of the *N*-acetyl group of UDP-GlcNAc. The ^{1}H-NMR spectra at the bottom show the signals of the anomeric proton attached to ^{12}C1 of UDP-GlcNAc (Figure 36) and the signal of the methyl protons of the *N*-acetyl group attached to ^{12}C of UDP-GlcNAc (Figure 37), respectively (signals in grey box). The 1D $^{1}H,^{13}C$-HSQC spectra (middle and top) show the doublets of the anomeric protons attached to ^{13}C1 of UDP-GlcNAc (Figure 36) and the doublets of the methyl protons of the *N*-acetyl group attached to ^{13}C1 of UDP-GlcNAc (Figure 37) (signals in grey boxes). Neither the signal of the anomeric proton/carbon nor the *N*-acetyl group of UDP-GlcNAc reveal changes in the signal intensity between control and DETA-NONOate treated cells.

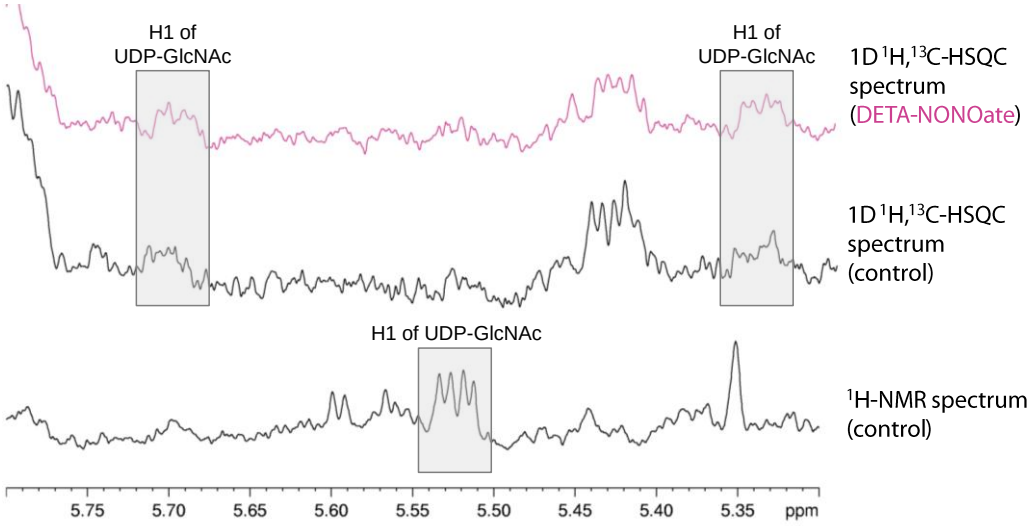

Figure 36. Representative expanded regions of ^{1}H-NMR spectrum (bottom) and 1D ^{1}H,^{13}C-HSQC spectra (middle and top) from cell extracts of astrocytes treated with [1-^{13}C]glucose for 24 h (control) or with [1-^{13}C]glucose for 24 plus DETA-NONOate for 12 h (DETA-NONOate). The ^{1}H-NMR spectrum (bottom) shows the peak of the anomeric proton attached to ^{12}C1 of UDP-GlcNAc (grey box). The ^{13}C-sattelite signals are not detectable in this spectrum. The 1D ^{1}H,^{13}C-HSQC spectra (middle and top) show the doublets of the anomeric protons attached to ^{13}C1 of UDP-GlcNAc (grey boxes). Note that in contrast to the 2D ^{1}H,^{13}C-HSQC spectra no ^{1}H decoupling has been applied. UDP-GlcNAc, uridine diphosphate-*N*-acetylglucosamine.

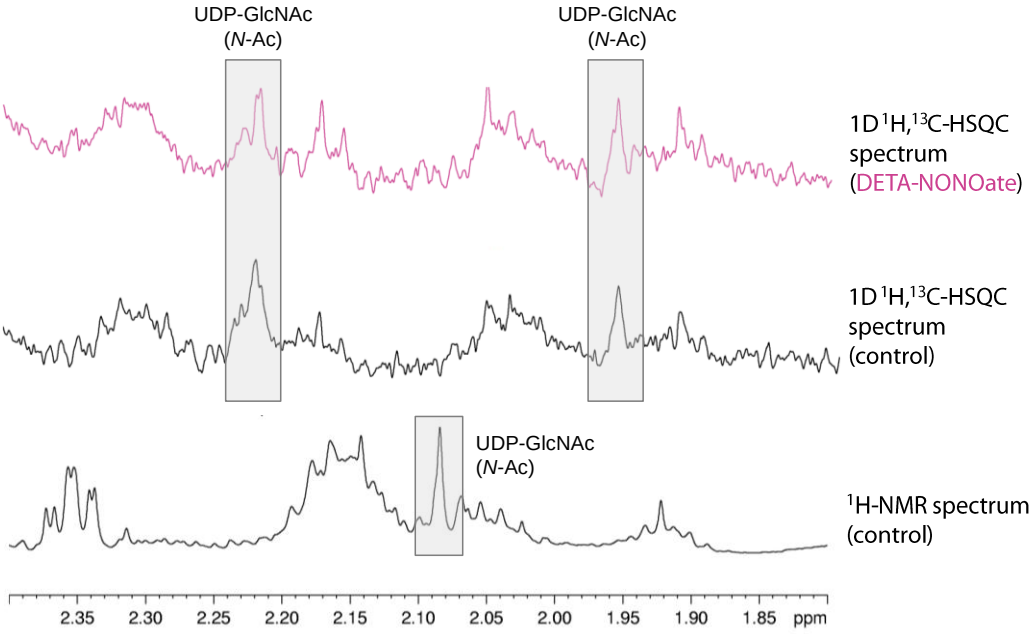

Figure 37. Representative expanded regions of ^{1}H-NMR spectrum (bottom) and 1D ^{1}H,^{13}C-HSQC spectra (middle and top) from cell extracts of astrocytes treated with [1-^{13}C]glucose for 24 h (control) or with [1-^{13}C]glucose for 24 plus DETA-NONOate for 12 h (DETA-NONOate). The ^{1}H-NMR spectrum (bottom) shows the peak of the methyl protons of the *N*-acetyl group attached to ^{12}C of UDP-GlcNAc (grey box). The ^{13}C-sattelite signals are not detectable in this spectrum. The 1D ^{1}H,^{13}C-HSQC spectra (middle and top) show the doublets of the methyl protons of the *N*-acetyl group attached to ^{13}C1 of UDP-GlcNAc (grey boxes). Note that in contrast to the 2D ^{1}H,^{13}C-HSQC spectra no ^{1}H decoupling has been applied. UDP-GlcNAc, uridine diphosphate-*N*-acetylglucosamine.

3.6 Metabolic Effects of Amyloid-ß on Neuronal HT-22 Cells and Primary Astrocytes

The two major hallmarks in the development of AD are Aß containing senile plaques (LaFerla *et al*., 2007) and NFTs aggregated from hyperphosphorylated tau protein (Grundke-Iqbal *et al*., 1986a; Grundke-Iqbal *et al*., 1986b). There is strong evidence that Aß and tau pathologies are mechanistically linked. Since hyperphosphorylation of tau involves reduced *O*-GlcNAcylation of the protein (Liu *et al*., 2004b), I tested the effect of Aß on the donor substrate of *O*-GlcNAcylation, UDP-GlcNAc, in neuronal HT-22 cells and primary astrocytes. Moreover, the effect of Aß on glucose uptake and lactate release was also investigated.

For this study, I used the $Aß_{25-35}$ fragment, which is known to exhibit the same toxic effects as the naturally occurring $Aß_{1-42}$ fragment (Yankner *et al*., 1990; Pike *et al*., 1995; Frozza *et al*., 2009). This being the case, $Aß_{25-35}$ is a suitable tool for investigating the toxic mechanisms exerted by this peptide in brain cells on the metabolic level. Furthermore, $Aß_{25-35}$ was also detected *in vivo* in senile plaques in AD brains (Kubo *et al*., 2002; Kubo *et al*., 2003).

Neurons (Ida *et al*., 1996; Saavedra *et al*., 2007; Yu *et al*., 2010) as well as astrocytes (Nagele *et al*., 2003; Pihlaja *et al*., 2008) can internalize the Aß peptide and intraneuronal Aß was found in brain of AD patients and is thought to be an important early step in the pathogenesis of the disease (Gouras *et al*., 2000; D'Andrea *et al*., 2001). The $Aß_{25-35}$ fragment, in particular, was also found to be able to bind and internalize into neuronal cells (Boland *et al*., 1995; Beffert *et al*., 1998) and astrocytes (Allaman *et al*., 2010). Aß internalization in neurons and astrocytes is mediated via endocytosis and several cells surface receptors are discussed to be involved in this process (Mohamed & Posse de Chaves, 2011). The precise mechanisms, however, remain unclear and seem to be different in neurons and astrocytes (Mohamed & Posse de Chaves, 2011).

To investigate metabolic changes stimulated by $Aß_{25-35}$, neuronal HT-22 cells and primary cultures of cortical astrocytes were incubated for 24 h with 25 µM $Aß_{25-35}$ peptide supplemented to the standard culture medium. These experimental conditions were used, because a recent study has shown that a concentration of 25 µM altered glucose utilization with a maximum effect at this concentration in primary astrocytes (Allaman *et al*., 2010). In addition, it was shown that $Aß_{25-35}$ was not degraded for up to 48 h (Allaman *et al*., 2010).

3.6.1 Influence of Aß on Glucose Uptake and Lactate Release in Neuronal HT-22 Cells and Astrocytes

To explore the glycolytic flux in neuronal HT-22 cells and primary astrocytes under influence of $Aß_{25-35}$, I determined glucose uptake and lactate release in these cells. Lactate release and glucose uptake were quantified from ^{1}H-NMR spectra of lyophilized cell culture media by calculating the difference of their concentration before (t = 0) and after incubation (t = 24 h) with 25 µM $Aß_{25-35}$ compared to respective controls. The concentration was normalized to number of cells. The quantified concentrations given in pmol/cell from these experiments are shown in Figure 38.

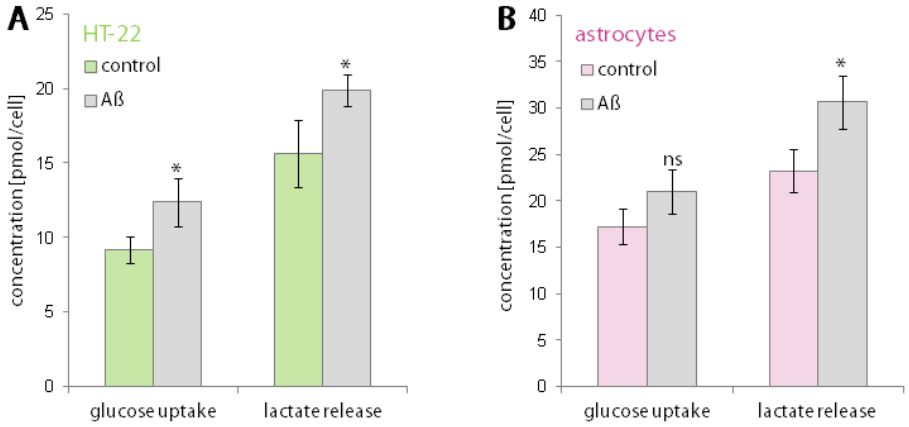

Figure 38. Effect of Aß on glucose consumption and lactate release in HT-22 cells and primary astrocytes: The uptake of glucose was quantified by integration of the H1 proton of the α anomer at 5,24 ppm from fully relaxed ^{1}H-NMR spectra and subsequent extrapolation for total glucose (α anomer plus ß anomer). Spectra of lyophilized cell culture medium obtained from HT-22 cells (A) and primary astrocytes (B) after incubation with 25 µM $Aß_{25-35}$ peptide for 24 h (gray bars; n = 3 each) and respective controls (green bars for HT-22; pink bars for astrocytes; n = 3 each) were analyzed. Values are mean ± standard deviation. *P* values of $P < 0.05$ were considered to be significant. *Represents $P < 0.05$; ns, not significant. Aß, amyloid-ß.

Treatment of HT-22 cells with 25 µM $Aß_{25-35}$ significantly elevated the release of lactate into the cell culture medium. The lactate concentration increased from 15,67 ± 2,25 pmol/cell for control to 19,87 ± 1,06 pmol/cell in $Aß_{25-35}$ treated HT-22 cells. Similar to lactate release, glucose consumption in HT-22 cells increased significantly when cells were treated with $Aß_{25-35}$. Under control conditions, glucose consumption in HT-22 cells was 9,15 ± 0,88 pmol/cell. Glucose consumption increased to 12,36 ± 1,63 pmol/cell when HT-22 cells were exposed to $Aß_{25-35}$. In primary astrocytes, treatment with $Aß_{25-35}$ also led to a significant increase in lactate release. Lactate release was 23,21 ± 2,33 pmol/cell in control cells and increased to 30,63 ± 2,89 pmol/cell in $Aß_{25-35}$ treated cells. No significant increase in glucose uptake in primary astrocytes treated with $Aß_{25-35}$ was detected. However, there was a trend

toward increased glucose uptake in astrocytes. The glucose consumption increased from 17,21 ± 1,94 pmol/cell to 21,02 ± 2,37 pmol/cell in $Aß_{25-35}$ treated astrocytes compared to controls. These results show increased glycolysis in $Aß_{25-35}$ treated HT-22 cells and indicate increased glycolysis in primary astrocytes. In the previous chapter it was described that the increase in total glycolytic activity can only be determined exactly by quantifying the *de novo* lactate synthesis deriving from ^{13}C-labeled glucose. Experiments using unlabeled glucose still give information about increased glycolysis in cells, although other precursors than glucose can contribute to enhanced lactate synthesis.

3.6.2 Aß Induced Changes in Activated Sugar Nucleotide Levels in Neuronal HT-22 Cells and Astrocytes

The levels of activated sugar nucleotides, whereas UDP-GlcNAc was of peculiar interest, were quantified from fully-relaxed ^{1}H-NMR spectra of M/C extracts from HT-22 cells or astrocytes treated either with 25 µM $Aß_{25-35}$ supplemented to the standard culture medium or incubated with standard culture medium alone (controls). In neuronal HT-22 cells no significant changes in the concentrations of activated sugar nucleotides were observed in $Aß_{25-35}$ treated cells compared to controls, as shown in Figure 39.

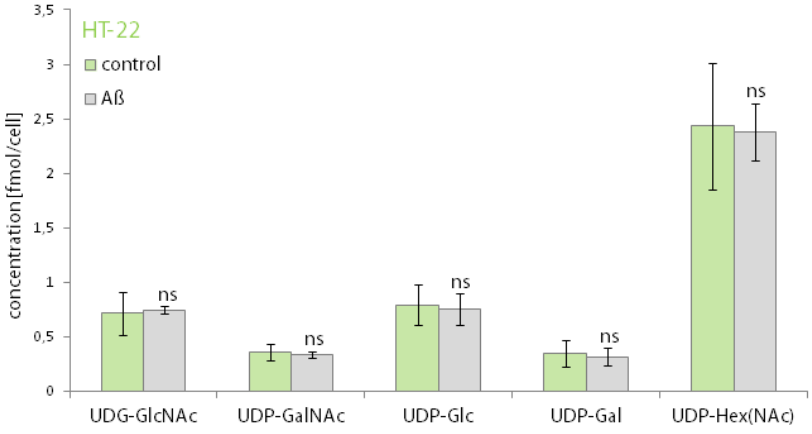

Figure 39. Effect of Aß on activated sugar nucleotides levels in HT-22 cells: Concentration of activated sugar nucleotide levels in HT-22 cells treated with 25 µM $Aß_{25-35}$ peptide for 24 h (gray bars; n = 3) and respective controls (green bars; n = 3) quantified from fully relaxed ^{1}H-NMR spectra of M/C cell extracts. Values are mean ± standard deviation. *P* values of $P < 0.05$ were considered to be significant. ns, not significant. Aß, amyloid-ß; M/C, methanol/chloroform; UDP-Gal, uridine diphosphate-galactose; UDP-GalNAc, uridine diphosphate-*N*-acetyl-galactosamine; UDP-Glc, uridine diphosphate-glucose; UDP-GlcNAc, uridine diphosphate-*N*-acetyl-glucosamine; UDP-Hex(NAc); uridine diphosphate-(*N*-acetyl-)hexoses.

In primary astrocytes, on the contrary, I detected a significant decrease in UDP-GlcNAc as well as UDP-GalNAc levels in $Aß_{25-35}$ cells (Figure 40). The UDP-GlcNAc level decreased

from 1,41 ± 0,13 fmol/cell in controls to 1,02 ± 0,14 fmol/cell in Aß$_{25-35}$ treated astrocytes. The UDP-GalNAc level in controls was 0,71 ± 0,04 fmol/cell and was found to be reduced to 0,54 ± 0,07 fmol/cell in Aß treated astrocytes.

There were no significant changes in the levels of UDP-Glc, UDP-Gal, UDP-GlcUA (not shown) and UDP-Hex(NAc) in neither HT-22 cells, nor primary astrocytes.

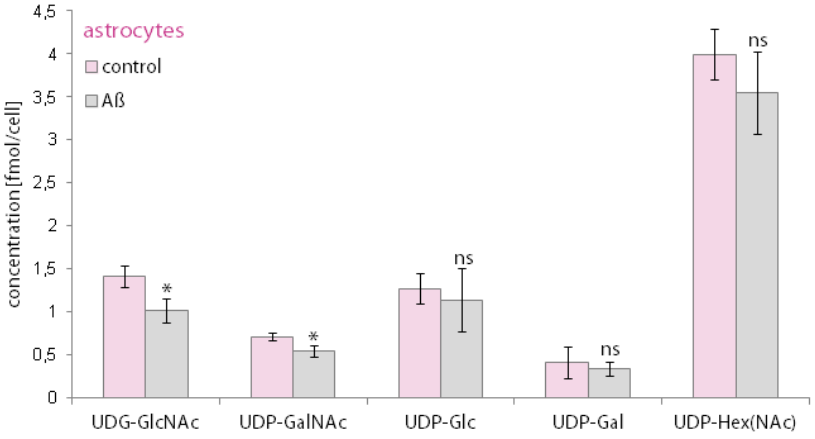

Figure 40. Effect of Aß on activated sugar nucleotides levels in primary astrocytes: Concentration of activated sugar nucleotide levels in primary astrocytes treated with 25 µM Aß25-35 peptide for 24 h (gray bars; n = 3) and respective controls (pink bars; n = 3) quantified from fully relaxed ^{1}H-NMR spectra of M/C cell extracts. Values are mean ± standard deviation. *P* values of $P < 0.05$ were considered to be significant. *Represents $P < 0.05$; ns, not significant. Aß, amyloid-ß; M/C, methanol/chloroform; UDP-Gal, uridine diphosphate-galactose; UDP-GalNAc, uridine diphosphate-*N*-acetyl-galactosamine; UDP-Glc, uridine diphosphate-glucose; UDP-GlcNAc, uridine diphosphate-*N*-acetyl-glucosamine; UDP-Hex(NAc); uridine diphosphate-(*N*-acetyl-)hexoses.

3.6.3 mRNA Expression of HBP Enzymes Influenced by Aß

To evaluate, whether Aß$_{25-35}$ affects mRNA expression of HBP enzymes, the mRNA levels of GFAT1, GFAT2, GlcN-6-P *N*-acetyltransferase, and UDP-GlcNAc pyrophosphorylase were quantified in HT-22 cells and primary astrocytes treated with 25 µM Aß$_{25-35}$ for 24 h compared to untreated controls using qRT-PCR. I have not detected any changes in the UDP-GlcNAc level and UDP-GalNAc level in Aß$_{25-35}$ treated HT-22 cells. Therefore, it was not surprising, that I did not detect any changes in the mRNA levels of HBP enzymes in these cells after incubation with Aß$_{25-35}$, as shown in Figure 41. In primary astrocytes, however, I detected a decrease in the UDP-GlcNAc levels as well as UDP-GalNAc levels when cells were exposed to Aß$_{25-35}$. Indeed, Aß$_{25-35}$ not only affects UDP-GlcNAc levels, but also GFAT1 expression in primary astrocytes. A small but significant increase of 23 % compared to controls in GFAT1 mRNA expression was detected in Aß$_{25-35}$ treated astrocytes (Figure 42). There was also a slight trend towards increased GFAT2, GlcN-6-P *N*-acetyltransferase,

and UDP-GlcNAc pyrophosphorylase mRNA levels. However, these increases were not significant.

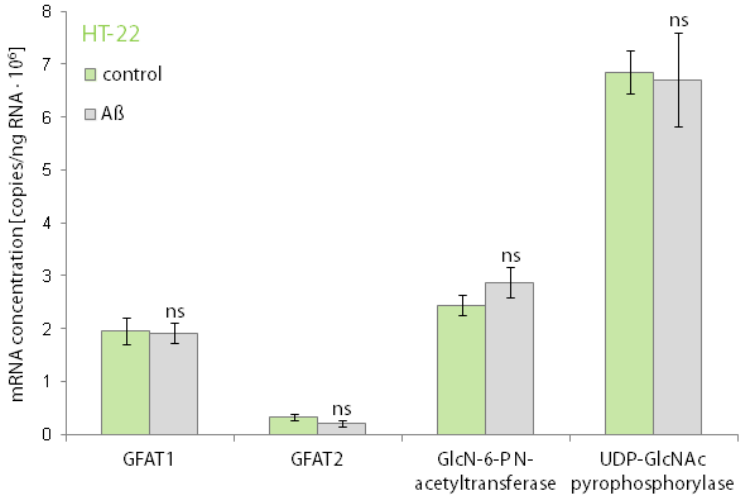

Figure 41. Quantitative RT-PCR for mRNA expression of enzymes of the HBP obtained from HT-22 cells incubated with 25 µM $Aß_{25-35}$ peptide for 24 h (green bars) compared to respective controls (gray bars; n = 3). Values are mean ± standard deviation. *P* values of $P < 0.05$ were considered to be significant. ns, not significant. Aß, amyloid-ß; GFAT, *Glutamine-fructose-6-P aminotransferase*; GlcN, glucosamine; GlcNAc, uridine diphosphate-*N*-acetylglucosamine.

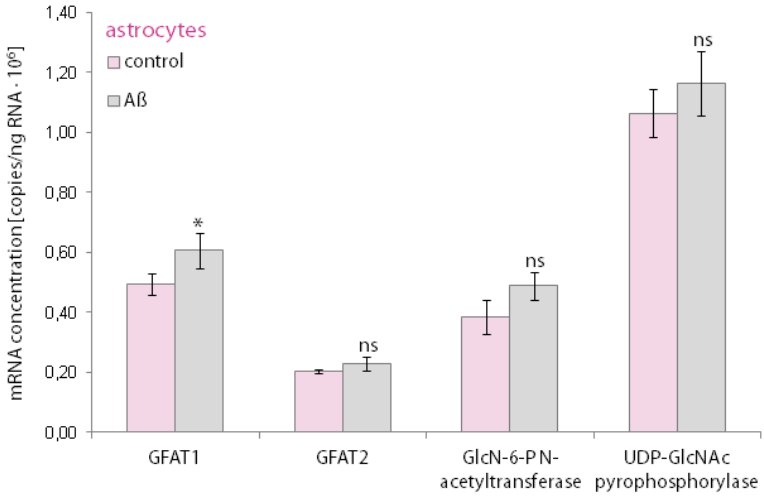

Figure 42. Quantitative RT-PCR for mRNA expression of enzymes of the HBP obtained from primary astrocytes incubated with 25 µM $Aß_{25-35}$ peptide for 24 h (green bars) compared to respective controls (gray bars; n = 3). Values are mean ± standard deviation. *P* values of $P < 0.05$ were considered to be significant. *Represents $P < 0.05$; ns, not significant. Aß, amyloid-ß; GFAT, *Glutamine-fructose-6-P aminotransferase*; GlcN, glucosamine; GlcNAc, uridine diphosphate-*N*-acetylglucosamine.

As in the case of HT-22 cells, the expression of the GFAT1 isoform in primary astrocytes is much higher compared to the expression of GFAT2. Furthermore, primary astrocytes

comprise much lower mRNA levels of enzymes of the HBP compared to the neuronal HT-22 cell line.

3.6.4 Elevated Glucose-1-P Levels in Aß Treated Astrocytes

In primary astrocytes, a signal at 5,46 ppm, arose when cells were exposed to $Aß_{25-35}$. This signal belongs to the anomeric proton (H1 α) of Glc-1-P. In untreated astrocytes, this signal is almost undetectable. The signal is absent in spectra of both $Aß_{25-35}$ treated and untreated HT-22 M/C cell extracts. Figure 43 shows the concentration of Glc-1-P quantified from fully-relaxed ^{1}H-NMR spectra of M/C extracts from astrocytes incubated with 25 µM $Aß_{25-35}$ compared to the respective controls. A significant increase in the Glc-1-P levels in astrocytes treated with $Aß_{25-35}$ was found. The concentration increased from 0,20 ± 0,07 fmol/cell in untreated astrocytes to 0,40 ± 0,08fmol/cell in $Aß_{25-35}$ treated astrocytes. Although the concentration is low compared to other metabolites, this is a 2-fold increase in the concentration of this intermediate.

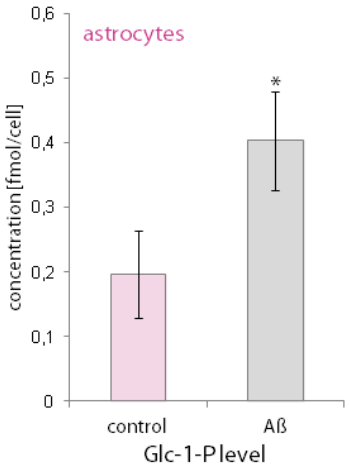

Figure 43. Effect of Aß on the Glc-1-P level in primary astrocytes: Concentration of Glc-1-P level in primary astrocytes treated with 25 µM Aß25-35 peptide for 24 h (gray bar; n = 3) and respective controls (pink bar; n = 3) quantified from fully relaxed ^{1}H-NMR spectra of M/C cell extracts. Values are mean ± standard deviation. *P* values of $P < 0.05$ were considered to be significant. *Represents $P < 0.05$. Aß, amyloid-ß; Glc-1-P, glucose-1-phosphate; M/C, methanol/chloroform; UDP-Gal, uridine diphosphate-galactose; UDP-GalNAc, uridine diphosphate-*N*-acetyl-galactosamine; UDP-Glc, uridine diphosphate-glucose; UDP-GlcNAc, uridine diphosphate-*N*-acetyl-glucosamine; UDP-Hex(NAc); uridine diphosphate-(*N*-acetyl-)hexoses.

3.6.5 Impact of Aß on Cell Viability in HT-22 Cells and Astrocytes

The Aß peptide is a toxic agent that leads to neuronal death and is strongly associated with the development of AD (Klein *et al*., 2001). To analyze changes in cell viability resulting from $Aß_{25-35}$ treatment, cells were counted after trypsinization in a haemocytometer using trypan blue exclusion. Figure 44C and D shows the number of counted viable cells after incubation with standard culture medium alone compared to the number of viable cells after treatment with 25 µM $Aß_{25-35}$ for 24 h in HT-22 cells and primary astrocytes. Although there was a trend towards decreased cell viability of primary astrocytes treated with $Aß_{25-35}$, the peptide

did not significantly alter cell viability in both HT-22 cells and primary astrocytes. It has to be noted that only viable cells were counted, but not the blue-stained dead cells, because those were rapidly degraded and difficult to count correctly. However, monitoring primary astrocytes treated with 25 µM $Aß_{25-35}$ by taking photomicrographs depicted no increased detachment or changes in the shape of cells (Figure 44A and B).

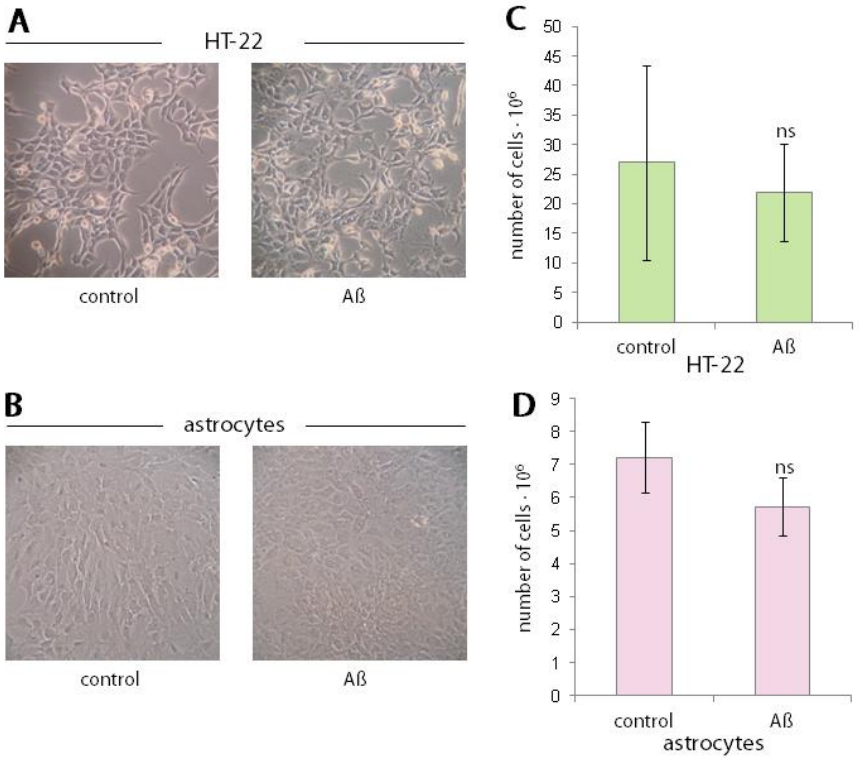

Figure 44. Bright-field photomicrographs of HT-22 cells (A) and primary cortical astrocytes (B) treated with 25 µM $Aß_{25-35}$ peptide for 24 h and respective controls. All images were acquired using a 10x lens. Number of viable HT-22 cells (C, n = 3) and astrocytes (D, n = 3) after incubation with $Aß_{25-35}$ peptide for 24 h compare to controls (n = 3 each). Cells were counted after trypsinization using trypan blue exclusion. *P* values of $P < 0.05$ were considered to be significant. *Represents $P < 0.05$; **represents $P < 0.01$; ***represents $P < 0.001$; Aß, amyloid-ß; ns, not significant.

4 Discussion

4.1 Stability of Activated Sugar Nucleotides against Acid Hydrolysis

4.1.1 Effect of M/C and PCA Extraction on Cell Extracts and Pure Compounds

Here I have shown that PCA is not suitable for the detection of activated sugar nucleotides, since most of these sugars are being decomposed. In PCA extracts of neuronal HT-22 cells only the two *N*-acetylated sugar nucleotides UDP-GlcNAc and UDP-GalNAc could be identified. In M/C extracts, however, I was able to consistently and simultaneously detect five activated sugar nucleotides, namely UDP-GlcNAc, UDP-GalNAc, UDP-Glucose, UDP-Galactose, and UDP-GlcUA. UDP-Glc and UDP-Gal, as well as UDP-GlcUA, are acid labile. Since the anomeric protons of activated sugar nucleotides resonate in a non-crowded region of the ^{1}H-NMR spectrum they are easy to quantify, except for UDP-GlcUA which resonates between UDP-Glc and UDP-Gal, overlapping with these two metabolites. However, UDP-GlcUA levels can be calculated by the difference of UDP-Hex(NAc) and the sum of UDP-GlcNAc, UDP-GalNAc, UDP-Glc, and UDP-Gal. The methyl protons of the *N*-acetyl groups of UDP-GlcNAc and UDP-GalNAc can also be detected in ^{1}H-NMR spectra of cell extracts. The signals resonate as singlets with slightly different chemical shifts (UDP-GlcNAc: δ(*N*-Ac) = 2,08 ppm; UDP-GlcNAc: δ(*N*-Ac) = 2,09 ppm). However, since these signals resonate within signals from Glu and Gln, they are not suitable for quantification. Although UDP-GlcNAc and UDP-GalNAc are not acid labile, the metabolite yield was lower in PCA extracts. This reduction was even significant for UDP-GalNAc. Contrary to my results, Kochanowski *et al*. reported that PCA does not have degradative effects on activated sugar nucleotides and they suggested that the material loss during the extraction may be caused by coprecipitation with $KClO_4$ when the PCA extract is neutralized with KOH (Kochanowski *et al*., 2005). These authors used a less concentrated PCA and worked on ice during the extraction procedure. To examine the effect under these mild conditions on activated sugar nucleotides, I extracted HT-22 cells in almost the same manner as did Kochanowski *et al*. and analyzed the activated nucleotide sugar levels using ^{1}H-NMR spectroscopy. I observed that the decomposition of the metabolites can be decelerated by using a less concentrated PCA and working on ice, however, the actual concentration cannot be determined under these conditions since UDP-Glc, UDP-Gal, and UDP-GlcUA are still degraded. Seeing that UDP-GlcNAc and UDP-GalNAc are stable against PCA treatment, the ratio of UDP-Glc + UDP-

Gal : UDP-GlcNAc + UDP-GalNAc is a good measure for comparison of the stability of UDP-hexoses in a cell extract. This ratio, however, also depends on the cell type and culturing method. *Kochanowski* et al. investigated the levels of activated sugar nucleotides in CHO cells cultivated in a bioreactor batch (Kochanowski *et al*., 2005). The ratio of UDP-Glc + UDP-Gal : UDP-GlcNAc + UDP-GalNAc calculated from their results using ion-pair reverse-phase high-performance liquid chromatography (HPLC) as analytical method was 0,66. The ratio I obtained from M/C extracted adherent growing CHO cultures was 0,81. The higher ratio indicates that UDP-Glc and UDP-Gal levels are higher referred to the stable *N*-acetylated sugar nucleotides in the M/C procedure, compared to the PCA extraction used by Kochanowski *et al*. and thus these sugars seem to be degraded. However, is has to be noted that cultivation of the cells differed, which may also have an influence on the level. Tomiya *et al*. investigated the level of activated sugar nucleotides in adherent growing CHO cultures with high-performance anion-exchange chromatography, using solely 75 % ethanol and filtration for extraction (Tomiya *et al*., 2001). The ratio calculated from their results (1,01) was even higher, suggesting that this is also a good extraction method in terms of UDP-hexose recovery.

Although PCA is widely used for extraction of water-soluble metabolites, the type of extraction method to be selected depends greatly on the metabolites investigated. It is essential to use extraction procedures that quantitatively recover the metabolites of interest. Therefore great care should be taken during extraction to minimize decomposition of labile metabolites. Moreover the M/C extraction has some advantages compared to the PCA extraction: The solid residue of the entire water-soluble phase after lyophilization is extremely small and can be solubilized in a small, concentrated volume for further NMR analysis. The pH of the extract remains near the physiological range during the whole procedure. Furthermore, a huge precipitate of $KClO_4$ is formed, when the PCA extract is neutralized with KOH. Several centrifugation steps are needed to get rid of the precipitate which leads to a loss of sample. This may be the reason for the lower UDP-GlcNAc and significantly lower UDP-GalNAc levels detected in PCA extracts compared to M/C extracts. Besides, not all $KClO_4$ is precipitable. For this reason PCA extracts contain high salt concentrations which may interfere with NMR measurements (Tyagi *et al*., 1996; Le Belle *et al*., 2002).

To verify the results obtained from the extracts of the neuronal HT-22 cells and to test the stability of other activated sugar nucleotides against PCA, I treated the pure compounds of 8 activated sugar nucleotides (UDP-GlcNAc, UDP-GalNAc, UDP-Glc, UDP-Gal, UDP-GlcUA, CMP-NeuNAc, GDP-Man, and GPD-Fuc) with PCA and M/C in the exact way as I

prepared the cell extracts. I found that UDP-GlcNAc, UDP-GalNAc, and GDP-Man are stable against acid hydrolysis. UDP-Glc, UDP-Gal, CMP-NeuNAc, and GDP-Fuc are completely decomposed when treated with PCA. UDP-GlcUA is also not stable against PCA, however, it is more stable than the other activated sugar nucleotides and only 60 % decomposition occurred under these conditions. All 8 activated sugar nucleotides, were stable against M/C treatment. Whereas CMP-NeuNAc and GDP-Fuc decomposed to NeuNAc + CMP and Fuc + GDP, respectively, in the case of UDP-Glc, UDP-Gal, and UDP-GlcUA formation of the 1,2-cyclo-phosphates and 2-phosphates was observed. The formation of 1,2-cyclo-phosphates and 2-phosphates originating from UDP-glucose and UDP-galactose has been reported before (Paladini & Leloir, 1952; Nunez & Barker, 1976; Kokesh *et al*., 1978; Spik *et al*., 1979; O'Connor *et al*., 1979), as well as the formation of GlcUA-1,2-cyclo-P from UDP-GlcUA (Spik *et al*., 1979; Cummings & Roth,1982).

Paladini *et al*. observed that glucose-1,2-cyclo-P is formed from UDP-Glc in a mild alkaline environment. Under more drastic alkaline conditions, however, glucose-1,2-cyclo-P is cleaved to Glc-2-P (75 %) and Glc-1-P (25 %) (Paladini & Leloir, 1952). Treatment with acid also leads to cleavage of the cyclo-phosphate to Glc-2-P and Glc-1-P, but the latter is hydrolyzed immediately to free glucose and only Glc-2-P remains (Paladini & Leloir, 1952). Direct treatment of UDP-Glc with acid, on the other hand, gives rise to UDP, UMP, and glucose (Paladini & Leloir, 1952). Divalent metal ion catalyzed formation of 1,2-cyclo-phosphates from activated sugar nucleotides was studied by Nunez *et al*. (Nunez & Barker, 1976). They observed that UDP-Glc and UDP-Gal decomposed to the respective 1,2-cyclo-phosphates and UMP in the presence of Mn^{2+}. Furthermore, they found that UDP-Gal forms the 1,2-cyclo-phosphate 2 - 3 times more rapidly than does UDP-Glc. The pathway for formation of the cyclo- and 2-phosphates originating from activated sugar nucleotides is illustrated in Figure 45. GDP-Fuc does not form the cyclo-phosphate and is decomposed to free fucose in the presence of divalent metal ions. UDP-GlcNAc and GDP-Man do not form the cyclo-phosphate and are stable. The reaction rate accelerates with increasing hydroxide ion concentration from pH 6,5 to 7,9 and with increasing metal ion concentrations from 10 to 200 mM (Nunez & Barker, 1976). These authors also observed that treatment of the 1,2-cyclo-phosphate with alkali (1,0 M NH_4OH, 1 h, 25 °C) or with acid (0,1 M HCl, 5 min, 100 °C) yields the 2-phosphate and the 2-phosphate and free sugar, respectively (Nunez & Barker, 1976). In a subsequent study, CMP-NeuNAc was also found to not form the 1,2-cyclo-phosphate and is decomposed to the free sugar and CMP in presence of divalent cations (Spik *et al*., 1979) and acid (Comb *et al*., 1966).

Formation of the cyclo- and 2-phosphates by PCA has not been shown before, but all these results are in complete accordance with the results I obtained from treatment of activated sugar nucleotides with PCA and subsequent neutralization with KOH. I found that UDP-GlcNAc and UDP-GalNAc, as well as GDP-Man are stable against PCA treatment and do not form the 1,2-cyclo-phosphate. In the spectra of UDP-Gal, UDP-Glc, and UDP-GlcUA I detected the signals of the 1,2-cyclo-phosphates, as well as the ^{1}H-NMR resonances of the anomeric protons (H1) of the 2-phosphates (Glc-2-P, δ_{H1} = 5,34 ppm; Gal-2-P, δ_{H1} = 5,37 ppm; GlcUA-2-P, δ_{H1} = 5,36 ppm). Assignments of the ^{1}H resonances of the latter sugars have not been previously reported. In contrast to Spik *et al.*, who found that UDP-GlcUA is the most easily hydrolyzed of the activated sugar nucleotides (Spik *et al.*, 1979), I found that UDP-GlcUA is more stable against decomposition by PCA compared to the other sugars tested. I observed that GDP-Fuc and CMP-NeuNAc do not form the 1,2-cyclo-phosphates and are decomposed to Fuc and GDP and NeuNAc and CMP, respectively.

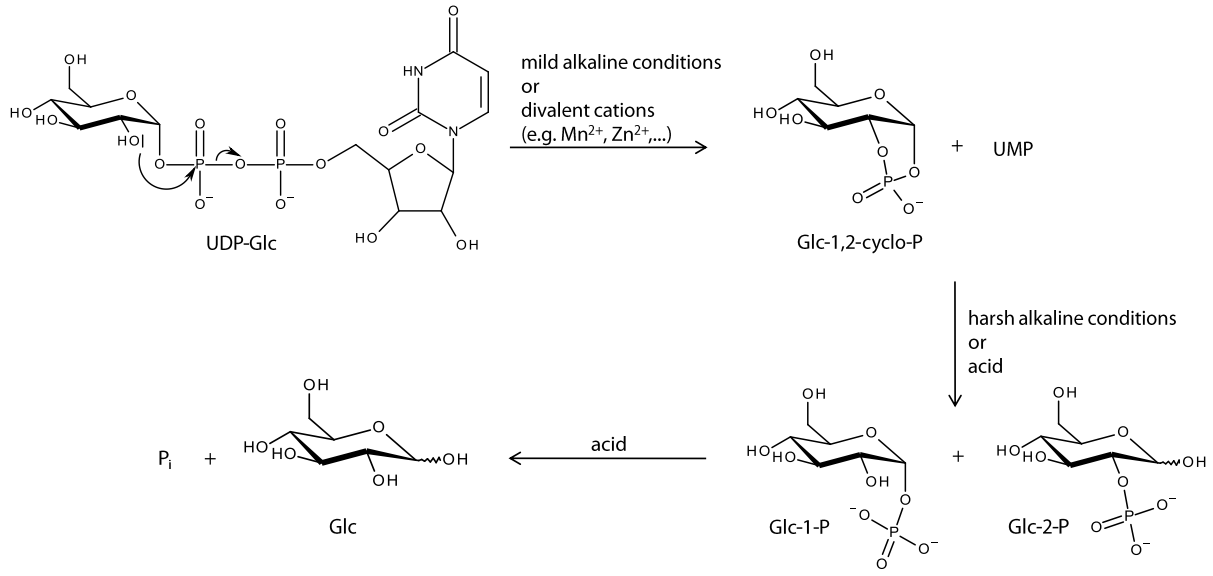

Figure 45. Formation and cleavage of 1,2-cyclo-phosphates from UDP-sugars (UDP-Glc, UDP-Gal, and UDP-GlcUA) using the example of UDP-Glc. Glc-1,2-P can be obtained by mild alkaline treatment of UDP-Glc (Paladini & Leloir, 1952) or by divalent metal ion catalyzed decomposition at neutral pH (Nunez & Barker, 1976). Alkaline hydrolysis (1,0 M NH_4OH, 1 h, 25 °C) of Glc-1,2-P yields Glc-1-P and Glc-2-P (Paladini & Leloir, 1952), whereas acid hydrolysis (0,1 M HCl, 100 °C, 5 min / 0,05 M H_2SO_4, 100 °C) yields free glucose and Glc-2-P (Paladini & Leloir, 1952; Nunez & Barker, 1976). Acid hydrolysis of Glc-1,2-P initially gives rise to both Glc-1-P and Glc-2-P, but Glc-1-P is not stable and further hydrolyzes to free glucose and P_i. Glc, glucose; Glc-1-P, glucose-1-phosphate; Glc-1,2-cyclo-P, glucose-1,2-cyclo-phosphate; Glc-2-P, glucose-2-phosphate; P_i, inorganic phosphate; UDP-Gal, uridine diphosphate-galactose; UDP-Glc, uridine diphosphate-glucose; UDP-GlcUA, uridine diphosphate-glucuronic acid; UDP-sugars, uridine diphosphate-sugars; UMP, uridine monophosphate.

Although the 1,2-cyclo-phosphates are already present in the commercially available pure compounds, as observed in minimal amounts in the reference spectra of UDP-Glc and UDP-Gal (also observed by Spik *et al.*, 1997), but not in the spectrum of UDP-GlcUA, all activated sugar nucleotides are stable in water or a mixture of MeOH/$CHCl_3$/water (1:1:1) at neutral

pH, as used for M/C extraction. In mild alkaline conditions or in the presence of divalent metal ions 1,2-cyclo phosphate esters are produced by attack of the C2 hydroxyl group of the pyranose sugar moiety on the ß-phosphate group of UDP (Nunez & Barker, 1976), as shown in Figure 45. The existence and the position of the C2 hydroxyl group influence if the reaction can occur (Nunez & Barker, 1976).

In UDP-Glc, UDP-Gal, and UDP-GlcUA the C2 hydroxyl group is equatorial to the pyranose moiety and thus in close spacial proximity to the ß-phosphate group of UDP, which exhibits α-configuration in these activated sugar nucleotides. The pyranosyl ring can be bent to enable the formation of the five-membered ring of the 1,2-cyclo-phosphate (Nunez & Barker, 1976). The formation of the cyclo-ester ring has only minor effects on the conformation of the pyranosyl ring in the case of α-anomers, as UDP-Glc and UDP-Gal exist (O'Connor *et al*., 1979). The structure of the five-membered cyclo-phosphate diester ring is that of an envelope with O(C2) above the plane of the ring (O'Connor *et al*., 1979).

In GDP-Man, the C2 hydroxyl group is axial and therefore the formation of α-Man-1,2-cyclo-P is hindered and thus not expected (Khorana *et al*., 1957; Nunez & Barker, 1976). 1,2-cyclo-phosphates can also arise from the 1-phosphates of the respective hexoses by treatment with N,N'-dicyclohexylcarbodiimide (DCC) (Piras, 1963; Piras & Cabib, 1963). Starting from Man-1-P the ß-anomer is able to form the 1,2-cyclo-phosphate because in the ß-anomer the equatorial C2 hydroxyl group is close to the ß-phosphate group of the nucleotide, therefore enabling the attack of the C2 hydroxyl group (O'Connor *et al*., 1979).

It was shown that treatment of Fuc-1-P with DCC leads to formation of the 1,2-cyclo-phosphate (Khorana *et al*., 1957; Prihar & Behrman, 1973; O'Connor *et al*., 1979). However, metal ion catalyzed formation of the 1,2-cyclo-phosphate starting from GDP-Fuc was not observed (Nunez & Barker, 1976; Spik *et al*., 1979). Nunez & Barker discussed that GDP-Fuc either does not form a complex with Mn^{2+} or that formation of the 1,2-cyclo-phosphate is sterically hindered (Nunez & Barker, 1976). L-fucose exists in the $^1C_4$ conformation, while D-glucose und D-galactose are in the $^4C_1$ conformation. This difference may have an effect on the formation of the cyclo-phosphate, but because in GDP-Fuc ß-L-fucose is linked to GDP, the ß-phosphate group of UDP, as well as the C2 hydroxyl group are both in equatorial position and therefore in special proximity. I did not observe formation of the 1,2-cyclo-phosphate from GDP-Fuc in the presence of PCA and subsequent neutralization with KOH as well, although no divalent cations were present in the reaction batch. My results therefore corroborate the assumption that sterical effects may be responsible for the absence of the cyclo-phosphate. As free fucose is formed in PCA treated GDP-Fuc, cleavage of the phosphate bond takes places in any case. However, because I did not observe the formation of

the 2-phosphate from fucose, it is unlikely that formation of free fucose comprises the formation of the cyclo-phosphates as an intermediate that is further cleaved to Fuc-2-P and Fuc-1-P, which finally yields free fucose due to hydrolysis of Fuc-1-P. For this reason, it is more likely that free fucose is directly formed. This observation is again in consistency with the results obtained by Nunez & Barker, 1976.

In the case of UDP-GlcNAc and UDP-GalNAc it is clear that those substances cannot form a 1,2-cyclic phosphate, because the C2 hydroxyl group is substituted by an *N*-acetyl group that cannot attack the pyranose sugar moiety on the ß-phosphate group of UDP. CMP-NeuNAc cannot form the 1,2-cyclo-phosphate under any circumstances, because it does not possess a hydroxyl group at the respective C-atom of the pyranose ring to form the phosphate diester ring. The chemical structures of all activated sugar nucleotides are shown in Appendix 7.1.

Formation of the 1,2-cyclo-phosphates from UDP-hexoses has been reported under mild alkaline conditions (Paladini & Leloir, 1952) or catalyzed by divalent metal ions at neutral pH (Nunez & Barker, 1976). Furthermore, 1,2-cyclo-phosphates are also obtained in the presence of DCC starting from the 1-phosphates as the base molecule (Khorana *et al*., 1957; Piras, 1963; Piras & Cabib, 1963; Prihar & Behrman, 1973). I have now observed that the cyclo-phosphates of UDP-Glc, UDP-Gal, and UDP-GlcUA are formed when treated like a PCA extract that means treatment with 0,9 M PCA and subsequent neutralization with 2,7 M KOH. PCA ($HClO_4^-$) is an inorganic acid and a potent oxidizer. Acid treatment of the UDP-hexoses, however, was shown not to yield the 1,2-cyclo-phosphates. One might assume that PCA treatment may lead to cleavage of the UDP-hexoses to UMP and the hexose-1-phosphates which might form the 1,2-cyclo-phosphates during the following neutralization with KOH. It has to be said that during neutralization of the PCA extracts, independently if cells are extracted or the reaction batch of pure compounds is neutralized, the pH sometimes fluctuates so that the solution may have an alkaline pH during the procedure. However, if this mechanism proceeds, one might also expect the formation of Fuc-1,2-cyclo-P from Fuc-1-P, because formation of the cyclo-phosphate from the 1-phosphate was at least reported in presence of DCC (Khorana *et al*., 1957; Prihar & Behrman, 1973). Besides, acid hydrolysis of the UDP-sugars is normally known to give the free sugars and UDP. Only minor amounts of free Glc and Gal, as wells as of UDP and no free GlcUA, but distinct signals of UMP were detected in the spectra. For this reason, one can exclude that PCA has the same effect on UDP-hexoses than HCl as previously reported (Paladini & Leloir, 1952). Furthermore, if the neutralization with KOH would trigger the formation of the cyclo-phosphates it would be unlikely that these intermediates will be steadily found the spectra of PCA treated UDP-

hexoses, because fluctuations in pH do not occur equally and in every sample. It seems most likely that PCA itself triggers the formation of the cyclo-phosphates. To test this assumption, I treated UDP-Glc with PCA without subsequent neutralization with KOH. However, this experiment failed due to the inability of PCA to be lyophilized. The sample changed its color from clear to a brown/black residue. Dilution of the sample prior to lyophilization did also not facilitate lyophilization. The spectrum of this sample was unusable. To manage this problem, I prepared a sample of UDP-Glc in water and added the PCA directly before NMR measurements without lyophilization or neutralization with KOH. The aim of this experiment was to directly follow the changes of UDP-Glc when treated with PCA in the spectrometer by recording several successive spectra. Unfortunately this experiment was also not successful because, although water-suppression was applied, the signals of interest were too close to the water signal and therefore not visible. However, from this experiment it can be at least concluded that PCA has an effect of the UDP-sugars, because signals changed. To conclude, although the direct evidence that PCA itself is responsible for the decomposition of UDP-hexoses with formation of the 1,2-cyclo-phosphates in PCA extraction, it is anyhow more than likely that this is the case. PCA has definitely an effect on the stability of UDP-hexoses and this effect differs from the one reported for HCl on these activated sugar nucleotides. For this reason there seems no other possibility than the direct formation of the 1,2-cyclo-phosphates by PCA.

Detection and quantification of hexose-1,2-cyclo-phosphates does so far not play a decisive role in mammalian cells. However, Sijens *et al*. detected Glc-1,2-cyclo-phosphate in ^{31}P-NMR spectra of PCA extracts of rhabdomyosarcoma tumor cells (Sijens *et al*., 1989). Cheng *et al*. detected Gal-1,2-cyclo-phosphate in ^{31}P-NMR spectra of PCA extracted lenses of galactose fed rats (Cheng *et al*., 1990). The signal was not observed in controls. However, galactose administration can lead to elevated UDP-Gal levels (see Chapter 4.3) that can be degraded to Gal-1,2-cyclo-phosphate when PCA treated. This may explain why the signals are not observed in lenses of normal fed rats. Since PCA was used in both studies, it cannot be excluded that the signals of the hexose-1,2-cyclo-phosphates arise from PCA treatment and are not of natural occurrence through metabolism. The results should therefore be regarded with suspicion. On basis of the new knowledge, it will be necessary to reassess the conclusions based on data where hexose-1,2-cyclo-phosphates are detected in PCA extracts.
Nevertheless, the cyclo-phosphates may have biological significance. Tagliabracci *et al*. discussed that formation of Glc-1,2-cyclo-P may possibly play a role in the introduction of phosphate into glycogen by glycogen synthase. Hyperphosphorylation of glycogen is a

hallmark of Lafora disease, a fatal genetic disorder causing epilepsy (Tagliabracci *et al*., 2011). With respect to future studies, where the cyclo-phosphates become important it is essential to know that Glc-1,2-cyclo-P and Gal-1,2-cyclo-P were generated in NMR-detectable amounts in HT-22 cells extracted with PCA, whereas in M/C extracts the signals of these compounds were absent. The signal intensity of the cyclo-phosphates was relatively low, however, it has to be regarded that a considerable small cell mass was used (cells from one 10 cm diameter petri dish; approximately $1 \cdot 10^7$ cells per extract) in my experiments. Using more cells, the signals will become more prominent in the spectra. PCA extraction is on this account not only inapplicable for detection and quantification of activated sugar nucleotides, but also for hexose-1,2-cyclo-phosphates.

4.1.2 Quantification of Activated Sugar Nucleotides in Different Cell Lines and Primary Astrocytes

Glycosylation is a post-translational modification whereby saccharides are covalently attached to proteins and lipids. Proteins can be glycosylated in the secretory pathway leading to *N*- or *O*-linked glycans (Ohtsubo & Marth, 2006). *O*-GlcNAcylation, the modification where a single GlcNAc residue is transferred to proteins, however, occurs in the cytosol (Hart *et al*., 2007). In addition to glycosyltransferases and glycosidases, as well as other mechanisms, the synthesis and availability of activated sugar nucleotides - the donor substrates of glycosyltransferases - can regulate glycan formation. Inhibition of the synthesis of activated sugar nucleotides can impede glycosylation of proteins (Smith *et al*., 2002; Schwarzkopf *et al*., 2002). An increase in UDP-GlcNAc/UDP-GalNAc levels evoked by GlcN administration, on the contrary, leads to an increase in the complexity of *N*-linked glycans in mammalian cells (Gawlitzek *et al*., 1998).

Previous studies were mainly concentrated on the expression of the enzymes involved in glycosylation (Lowe & Marth, 2003; Ohtsubo & Marth, 2006; Taniguchi *et al*., 2006), but to date only little is known about the intracellular levels of activated sugar nucleotides in mammalian cells. Studying the intracellular concentrations of activated sugar nucleotides could yield valuable information for the understanding of glycosylation processes in cells.

Aberrant glycosylation occurs in several human genetic diseases (Ohtsubo & Marth, 2006). Congenital disorders of glycosylation for example are a consequence of defective formation of the glycan moiety of glycoproteins (Freeze, 2006). Some of these disorders are caused by impaired formation of activated sugar nucleotides and can be treated by ingestion of the substances (Niehues *et al*., 1998).

Furthermore, aberrant glycosylation is associated with a wide range of human cancers (Dennis *et al*., 1999; Hakomori, 2002; Lau & Dennis, 2008). Elevated UDP-GlcNAc and UDP-GalNAc levels were detected in different cancer cell lines (Wice *et al*., 1985; Nakajima *et al*., 2010), as well as in breast tumor tissue compared to adjacent non-involved breast tissue (Gribbestad *et al*., 1994). Only recently, Pan *et al*. linked increased UDP-GlcNAc and UDP-GalNAc levels to cancer cell death following chemotherapeutic treatment (Pan *et al*., 2011).

Changes in *O*-GlcNAcylation pattern, plays an important role in Alzheimer's disease (Arnold *et al*., 1996; Liu *et al*., 2004b; Lefebvre *et al*., 2005; Gong *et al*., 2006; Dias & Hart, 2007) and type II diabetes (Marshall *et al*., 1991a ; Hawkins *et al*., 1997; McClain *et al*., 2002; Buse, 2006; Dias & Hart, 2007).

OGT, the enzyme that transfers the GlcNAc residues to proteins from the donor substrate UDP-GlcNAc is highly sensitive to varying UDP-GlcNAc concentrations (Haltiwanger *et al*., 1992; Kreppel *et al*., 1997; Kreppel & Hart, 1999).

In Alzheimer's disease, glucose uptake and metabolism are impaired (Casadesus *et al*., 2007). Restrictions in glucose availability also affect UDP-GlcNAc levels through its biosynthesis from glucose in the HBP. The tau protein, which is involved in the development of Alzheimer's disease exhibits reduced *O*-GlcNAcylation and hyperphosphorylation (Arnold *et al*., 1996; Liu *et al*., 2004b; Lefebvre *et al*., 2005; Gong *et al*., 2006; Dias & Hart, 2007).

Type II diabetes on the other hand is associated with increased *O*-GlcNAcylation. Hyperglycemia and insulin resistance are the most important hallmarks of type II diabetes. High glucose leads to an increased flux through the HBP which results in increased UDP-GlcNAc levels and increased *O*-GlcNAcylation (Marshall *et al*., 1991a; Hawkins *et al*., 1997; McClain *et al*., 2002; Buse, 2006; Dias & Hart, 2007). Recently, decreased *O*-GlcNAcylation of tau concomitant with hyperphosphorylation, as observed in Alzheimer's disease, was also detected in brain tissue of type II diabetes patients (Liu *et al*., 2009a). Type II diabetes is known to increase the risk for Alzheimer's disease (Xu *et al*., 2009) and the reduced *O*-GlcNAcylation and hyperphosphorylation of tau may be one mechanism how these diseases are connected (Liu *et al*., 2009a). For more details on *O*-GlcNAcylation in diabetes and Alzheimer's disease see Chapter 1.7.1 and Chapter 1.7.2, respectively. In terms of the above mentioned diseases, investigations of the intracellular levels of activated sugar nucleotides could not only provide information about glycosylation processes in cells, but also for the understanding of disease mechanisms occurring in cancer, Alzheimer's disease, and diabetes.

NMR spectroscopy has been used before to detect activated sugar nucleotides, in particular UDP-GlcNAc and UDP-GalNAc. To the best of my knowledge, this is the first study where

five activated sugar nucleotides (UDP-GlcNAc, UDP-GalNAc, UDP-Glc, UDP-Gal, and UDP-GlcUA) were simultaneously detected and quantified in absolute concentration (fmol/cell) in four different cell lines (HT-22, CHO, HEK293, and MDBK) and primary astrocytes using ^{1}H-NMR spectroscopy. Gribbestad *et al*. were the first who detected elevated UDP-GlcNAc and UDP-GalNAc levels in PCA extracts from breast tumor tissue using high-resolution ^{1}H-NMR spectra (Gribbestad *et al*., 1994). Since the PCA procedure was used for extraction, UDP-hexoses were not detectable in their spectra. Mosely *et al*. identified four activated sugar nucleotides (UDP-GlcNAc, UDP-GalNAc, UDP-Glc, and UDP-Gal) in a prostate cancer cell line (Moseley *et al*., 2011). Quantification of these UDP-sugars, however, was not part of their study. Grande *et al*. quantified the level of UDP-GlcNAc/UDP-GalNAc in intact carcinoma cell lines using the signal of the proton at C6 in the uracil ring of UDP in UDP-GlcNAc/UDP-GalNAc (Grande *et al*., 2011). Due to the lower resolution of intact cell NMR, the signals of UDP-GlcNAc and UDP-GalNAc were not separated. Pan *et al*. detected UDP-GlcNAc and UDP-GalNAc in ^{1}H-NMR and high-resolution magic angle spinning ^{1}H-NMR (HR-MAS) of four different brain cancer cell lines and were able to observe changes in signal intensity induced by cisplatin treatment (Pan *et al*., 2011).

Quantification of activated sugar nucleotides in four different cell lines and primary astrocytes revealed that the intracellular concentration is a cell specific feature. Primary astrocytes revealed the highest amount of the total content of activated sugar nucleotides, as well as the highest amount of every single UDP-hexose.

Astrocytes are known to be glycolytic cells with high glucose turnover. It is suggested that astrocytes are the primary site of glucose uptake during neuronal activity (Tsacopoulos & Magistretti, 1996). Glucose uptake into cultured astrocytes was found to be twice as much as into neurons (Peng *et al*., 1994). Moreover, glycogen is almost exclusively localized in astrocytes (Cataldo & Broadwell, 1986; Magistretti *et al*., 1993). Furthermore, almost all blood vessels in the brain are enwrapped with astrocytic end-feet permitting that glucose can largely pass through astrocytes (Tsacopoulos & Magistretti, 1996). This high glucose uptake may be responsible for the high levels of activated sugar nucleotides in astrocytes and seems to be still reflected in primary cultures of cortical astrocytes. High intracellular glucose levels lead to an enhanced flux through the HBP and thus enhanced UDP-GlcNAc levels, as well as UDP-GalNAc levels which can be formed by epimerization of UDP-GlcNAc. The synthesis of the other activated sugar nucleotides, which are not generated in the HBP can also be influenced by high glucose levels, since glucose is the precursor of all *de novo* synthesized activated sugar nucleotides.

The high abundance of UDP-GlcNAc in astrocytes might stimulate OGT activity and brain cells are known to have a high *O*-GlcNAc metabolism. OGT mRNA expression was found to be especially abundant in brain and pancreas (Lubas *et al*., 1997). Even though *O*-GlcNAcase is less expressed than OGT, it is most abundant in brain (Gao *et al*., 2001). The highest concentrations of both OGT and *O*-GlcNAcase mRNA were detected in hippocampal neurons and cerebellar Purkinje cells (Akimoto *et al*., 2003; Liu *et al*., 2004a). Taken together, the high level of UDP-GlcNAc detected in primary astrocytes by ^{1}H-NMR spectroscopy may give information about the importance and degree of *O*-GlcNAcylation in these cells.
The neuronal HT-22 cell line exhibited together with MDBK cells the second high level in the total content of activated sugar nucleotides. However, the UDP-GlcNAc level of HT-22 cells was quite similar with the levels detected HEK293 and MDBK cells (approximately 50 % compared to primary astrocytes). Only CHO cells showed a lower UDP-GlcNAc level in the cell lines tested, but these cells were cultured in medium containing only 12,5 mM glucose compared to the other cells lines, which were cultured in medium containing 25 mM glucose. The lower UDP-GlcNAc level (≈ 50 % compared to HT-22, HEK293, and MDBK) in CHO cells therefore possibly reflects the lower glucose concentration. For a better comparison of the UDP-GlcNAc level in astrocytes and neurons, the experiments should also be performed with primary neurons. Cell lines sometimes show specific characteristics that may differ from the corresponding primary cultures. The neuronal marker *N*-acetyl aspartate, for example, is not detectable in ^{1}H-NMR spectra of HT-22 cells, although the methyl protons appear as a prominent singlet resonating at 2,01 ppm normally detectable in ^{1}H-NMR spectra of cell extracts and *in vivo* ^{1}H-NMR spectra (Govindaraju *et al*., 2000). However, we can not exclude that the signal is superposed by other metabolites resonating in this region.

GLUT2, which is exclusively located in astrocytes (Leloup *et al*., 1994; Dwyer *et al*., 2002) and is together with GLUT1 (Pardridge,1991; Vannucci *et al*., 1997) responsible for glucose uptake into astrocytes, was found to be considerably elevated in Alzheimer's disease brain (Liu *et al*., 2008; Liu *et al*., 2009a). GLUT3, the major neuronal GLUT, and GLUT1, on the other hand, were found to be decreased in Alzheimer's disease brain (Kalaria & Harik, 1989; Simpson *et al*., 1994; Harr *et al*., 1995; Mooradian *et al*., 1997; Liu *et al*., 2008; Liu *et al*., 2009a). Moreover, in type II diabetes brain GLUT3 levels were also found to be decreased, whereas GLUT1 and GLUT2 levels were not affected (Liu *et al*., 2009a). This impaired glucose uptake caused by decreased GLUT1 and GLUT3 in Alzheimer's disease, as well as, GLUT3 in diabetes type II leads to decreased flux through the HBP and thus leading to reduced *O*-GlcNAcylation and concomitant hyperphosphorylation of tau, which is crucial for

the development of Alzheimer's disease. The increase in GLUT2 expression in Alzheimer's disease, however, should lead to the converse phenomenon: increased flux through HBP and increased *O*-GlcNAcylation of proteins. Liu *et al*. observed that astrocytes in Alzheimer's disease brain were activated to a similar extent as the GLUT2 elevation (Liu *et al*., 2008). Astrocyte activation is a well known occurrence in Alzheimer's disease brain (Akiyama *et al*., 2000). On this account the authors concluded that the increase in the GLUT2 level in Alzheimer's disease is most probably just due to astrocyte overactivation and increased glucose uptake into astrocytes is not expected, because GLUT1 is decreased (Liu *et al*., 2008; Liu *et al*., 2009a). GLUT1 is needed to transport glucose from the blood stream through the endothelial cells into the extracellular space where it can be taken up into astrocytes by GLUT2 (Dwyer *et al*., 2002). The uptake of glucose by astrocytes (and neurons) under these disease mechanisms, as well as the levels of UDP-GlcNAc and other activated sugars can now be simultaneously detected by ^{1}H-NMR spectroscopy bringing new facts of disease mechanisms where *O*-GlcNAcylation is involved to light.

In all cell lines investigated, the most abundant activated sugar nucleotide was UDP-GlcNAc. The second most abundant UDP-sugar was UDP-Glc, followed by UDP-GalNAc. In HEK293 cells, UDP-Glc and UDP-GalNAc exhibited the same concentration. In HT-22 cells, primary astrocytes, and CHO cells, the lowest levels revealed UDP-GlcUA, followed by UDP-Gal. UDP-GlcUA was found to be almost absent in HEK293 cells. MDBK cells exhibited a distinct pattern. UDP-GlcNAc and UDP-Glc were the most abundant and second most abundant activated sugar nucleotides, respectively, as observed in the other cells. The levels of the other UDP-sugars were in descending order: UDP-GlcUA, UDP-GalNAc, and UDP-Gal. In consistency with my results, Kochanowski *et al*. and Tomiya *et al*. detected UDP-GlcNAc as the most abundant sugar nucleotide in CHO cells (Kochanowski *et al*., 2006; Tomiya *et al*., 2001). Nakajima *et al*. on the contrary reported that UDP-Glc has the highest level in CHO cells. UDP-GlcNAc was found to be the second abundant activated sugar nucleotide in their study (Nakajima *et al*., 2010). In both, MCF7 breast cancer cells and KLM1 pancreatic cancer cells, the authors detected UDP-GlcNAc as the most abundant UDP-sugar (Nakajima *et al*., 2010). Mosely *et al*. identified in LN3 prostate cancer cells UDP-GlcNAc as the activated sugar nucleotide with the highest level, but indicated that in other cancer or normal cells UDP-Glc was the most abundant sugar (Moseley *et al*., 2011).

The UDP-GlcNAc : UDP-GalNAc ratio calculated from the quantified levels of CHO cells was 2,3 in my experiments. This value is in good agreement with the ratio calculated from the levels in CHO cells determined by Nakajima *et al*., which was 2,2 (Nakajima *et al*., 2010).

The ratio calculated from the results of Kochanoswki *et al.* was with 3,5 quite higher (Kochanowski *et al*., 2006). The ratios for the other cell lines, except for primary astrocytes, are all between 2,1 and 2,8. These ratios are in accordance with those calculated from previous publications in different cells (Sweeney *et al*., 1993; Nakajima *et al*., 2010). The only cells with a vastly diverging UDP-GlcNAc : UDP-GalNAc ratio in my experiments were primary astrocytes. Their ratio was calculated to be 1,5. Interestingly, Pan *et al*. estimated their UDP-GlcNAc : UDP-GalNAc ratio in glioblastoma, medulloblastoma, and supraentorial primitive neuroectodermal tumor cell lines also to be 1,5 (Pan *et al*., 2011). Although their cells were cancer cell lines, they all derive from brain and astrocytes belong to glial cells. Furthermore, the UDP-GlcNAc : UDP-GalNAc ratio is independent from the elevated levels of UDP-GlcNAc and UDP-GalNAc detected in cancer cell lines. It has to be borne in mind, that this ratio can of course be influenced in cancer. However, the ratio of MCF-7 breast cancer cells was with 2,5 (calculated from the results of Nakajima *et al*., 2010) in the range detected in most cells, including non-malignant cells. I concluded that primary astrocytes exhibit such high levels of activated sugar nucleotides through their high glycolytic activity. The comparatively lower UDP-GlcNAc : UDP-GalNAc ratio means that under high glycolytic activity the increase of UDP-GalNAc is even more pronounced in relation to UDP-GlcNAc, in these cells. This increase in UDP-GalNAc in the UDP-GlcNAc/UDP-GalNAc balance could be caused by an increase in UDP-GlcNAc utilization. Since OGT is highly sensitive to varying UDP-GlcNAc concentrations (Haltiwanger *et al*., 1992; Kreppel *et al*., 1997; Kreppel & Hart, 1999), the activity of OGT in these cells induced by high UDP-GlcNAc levels may be higher than in other cells with lower UDP-GlcNAc levels, whereas UDP-GalNAc utilization is not increased, thus leading to a lower UDP-GlcNAc : UDP-GalNAc ratio. Another possibility could be a shift in the epimerization equilibrium of UDP-GlcNAc to UDP-GalNAc, by increased UDP-glucose 4-epimerase activity or expression. UDP-GalNAc is used for example as the first building block of mucin-type *O*-glycoprotein biosynthesis and mucins are also involved in the development of cancer and influence cellular growth (Hollingsworth & Swanson, 2004; Dube & Bertozzi, 2005). The actual reason for the lower UDP-GlcNAc : UDP-GalNAc ratio in primary astrocytes compared to the other cell lines investigated here cannot be revealed at this point. However, it indicates that UDP-GlcNAc and UDP-GalNAc, and maybe *O*-GlcNAcylation play a special role in these cells.

A comparison of the absolute concentration of activated sugar nucleotides in my experiments with those obtained from others proves to be difficult. Apart from the fact that in some publications, the concentration is normalized to total protein content (Tomiya *et al*., 2001; Nakajima *et al*., 2010), the culture conditions vary greatly between publications. In particular,

the glucose concentration in the culture medium has great impact on the formation of the activated sugar nucleotides and sometimes even differs between the different cell lines compared in the same study (Grande *et al*., 2011). Besides, in some studies the concentration was determined in cancer cells (Kochanowski *et al*., 2005; Grande *et al*., 2011), which are known to have elevated UDP-GlcNAc and UDP-GalNAc levels. However, to compare the intracellular concentrations of activated sugar nucleotides, neuronal HT-22 cells and CHO cells are used in the following as an example. HT-22 cell were cultured in medium containing 25 mM glucose, whereas CHO cells were cultured in medium containing 12,5 mM glucose. Both cell lines were seeded in the same concentration and were let to grow for 72 h before M/C extraction. The concentrations determined from ^{1}H-NMR spectra were as follows: HT-22 (UDP-GlcNAc 0,76 ± 0,05 fmol/cell, UDP-GalNAc 0,36 ± 0,04 fmol/cell, UDP-Glc 0,60 ± 0,07 fmol/cell, UDP-Gal 0,23 ± 0,02 fmol/cell, and UDP-GlcUA 0,24 ± 0,06 fmol/cell), CHO (UDP-GlcNAc 0,37 ± 0,07 fmol/cell, UDP-GalNAc 0,16 ± 0,04 fmol/cell, UDP-Glc 0,30 ± 0,10 fmol/cell, UDP-Gal 0,13 ± 0,07 fmol/cell, and UDP-GlcUA 0,15 ± 0,01 fmol/cell). Kochanowski *et al*. detected sharply higher concentrations in CHO bioreactor batch cultures with medium containing probably 5,56 mM glucose. Their levels were given as the maximal concentrations detected over a time course. The maximal concentrations of UDP-GlcNAc and UDP-GalNAc were 8,8 ± 1 fmol/cell and 2,5 ± 0,3 fmol/cell, respectively (both after 40 h of culture). The concentration of UDP-Glc was 6,2 ± 0,6 fmol/cell after 40 h of cultivation and the concentration of UDP-Gal 1,25 ± 0,1 after 80 h of cultivation (Kochanowski *et al*., 2005). The CHO cells in this study were cultured in bioreactor batch cultures, which could definitely have an effect on UDP-sugar production in cells. However, it is surprising that the levels are greatly higher, since the glucose concentration was 5-times lower compared to my experiments. Sweeney *et al*. detected concentrations of 2,9 fmol/cell for UDP-GlcNAc, 1,2 fmol/cell for UDP-GalNAc, 2,5 fmol/cell for UDP-Glc + UDP-Gal, and 0,6 fmol/cell for UDP-GlcUA in freshly isolated chondrocytes (Sweeney *et al*., 1993). These levels were lower than those obtained by Kochanowski *et al*., but are still higher than those obtained by us. However, since the level of activated sugar nucleotides is a cell specific feature, comparison of different cell lines is not significant. For the sake of completeness, the levels obtained for the sum of UDP-GlcNAc and UDP-GalNAc by Grande *et al*. (Grande *et al*., 2011) in different cancer cells lie between 5 and 27 fmol/cell, and are therefore also greatly higher than those obtained in my study. It is unlikely that this difference is entirely due to the increase in the levels of UDP-GlcNAc and UDP-GalNAc observed in cancer cells. Due to the above mentioned differences in cultivation and the fact that different cell lines are compared it is difficult to evaluate the causes for the differences in the levels of activated

sugar nucleotides. For most studies, HPLC or related methods were used for quantification of UDP-sugars. Only Grande *et al*. used ^{1}H-NMR spectroscopy as analytical method (Grande *et al*., 2011). However, they used the signal of the proton at C6 in the uracil ring of UDP in UDP-GlcNAc/UDP-GalNAc for integration, not being able to determine the level of UDP-GlcNAc and UDP-GalNAc separately. I integrated the signals of the anomeric protons of UDP-GlcNAc and UDP-GalNAc, being able to determine their levels separately. These differences may also have an effect on the concentration of activated sugar nucleotides determined.

In other studies using high-performance anion-exchange chromatography or ion-pair reversed phase HPLC CMP-NeuNAc, GDP-Man, and GDP-Fuc were also found in CHO and MCF-7 cell extracts (Tomiya *et al*., 2001; Kochanowski *et al*., 2006; Nakajima *et al*., 2010). I was not able to detect GDP-Man, GDP-Fuc, and CMP-NeuNAc in the M/C cell extracts. The signal of the H1 of GDP-Man is buried under signal of UDP-GlcNAc. For this reason I cannot be certain whether GDP-Man is present in my cell extracts. If GDP-Man is present in the cell extracts, the quantified level of UDP-GlcNAc is actually the sum of UDP-GlcNAc and GDP-Man. For quantification of these metabolites, ^{1}H-NMR spectroscopy is not suitable. However, I was still able to detect 5 activated sugar nucleotides involved in glycosylation and *O*-GlcNAcylation processes. Using NMR spectroscopy has the advantage to simultaneously detect and quantify various metabolites from other metabolic pathways using one sample.

4.1.3 Conclusions and Perspectives

In summary, in this chapter I have shown that PCA extraction is not suitable for the detection of activated sugar nucleotides, because most of these sugars are being degraded.

I tested 8 activated sugar nucleotides for their stability against PCA and found that UDP-GlcNAc, UDP-GalNAc, and GDP-Man are stable against acid hydrolysis. UDP-Glc, UDP-Gal, UDP-GlcUA, CMP-NeuNAc, and GDP-Fuc are completely decomposed when treated with PCA. In the case of UDP-Glc, UDP-Gal, and UDP-GlcUA formation of the 1,2-cyclo-phosphates and 2-phosphates was observed when PCA treated. Assignments of the ^{1}H resonances of the latter sugars have not been previously reported. Using M/C extraction, however, I was able to consistently and simultaneously detect five activated sugar nucleotides, namely UDP-GlcNAc, UDP-GalNAc, UDP-Glucose, UDP-Galactose, and UDP-GlcUA in cells extracts of HT-22, CHO, MDBK, HEK293 cell lines and primary astrocytes. Some studies have used PCA extraction for determination of activated sugar nucleotides in

cell extracts. It will be necessary to reassess the conclusions based on data supposing that UDP-Glc and UDP-Gal were stable.

Since the anomeric protons of activated sugar nucleotides resonate in a non-crowded region of the ^{1}H-NMR spectrum they are easy to quantify. To the best of my knowledge, this is the first study where five activated sugar nucleotides were simultaneously detected and quantified in absolute concentration using ^{1}H-NMR spectroscopy.

Activated sugar nucleotides are the donor substrate of glycosyltransferases and can regulate glycan formation. However, little is known about the intracellular levels of activated sugar nucleotides in mammalian cells. Studying the intracellular concentrations of activated sugar nucleotides could yield valuable information for the understanding of glycosylation processes in cells. Quantification of activated sugar nucleotides in four different cell lines and primary astrocytes revealed that the intracellular concentration is a cell specific feature. Primary astrocytes revealed the highest amount of the total content of activated sugar nucleotides, as well as the highest amount of every single UDP-hexose. I concluded that these high levels of activated sugar nucleotides are due to the fact that astrocytes are known to be glycolytic cells with high glucose turnover. OGT mRNA expression is especially abundant in brain and high UDP-GlcNAc levels can stimulate OGT activity, leading to the assumption that astrocytes exhibit high *O*-GlcNAc metabolism. The UDP-GlcNAc concentration in the neuronal HT-22 cell line was not as high as expected, however for a better comparison with primary astrocytes, these experiments should also be carried out with primary neurons. Furthermore, in all cell lines investigated, the most abundant activated sugar nucleotide was UDP-GlcNAc and the second most abundant UDP-sugar was UDP-Glc. The abundance of the other activated sugar nucleotides varied in between different cell lines. Besides being the cells with the highest levels of activated sugar nucleotides, astrocytes also exhibited another characteristic. Whereas the UDP-GlcNAc : UDP-GalNAc ratio was between 2,1 and 2,8, the ratio calculated in astrocytes was 1,5. This increase in UDP-GalNAc in relation to UDP-GlcNAc may be caused by an increase in UDP-GlcNAc utilization due to high OGT activity or by increased UDP-glucose 4-epimerase activity or expression. In either case, this aberrant ratio indicates a special role of glycosylation or *O*-GlcNAcylation in these cells.

Although ^{1}H-NMR spectroscopy has the disadvantage that detection of GDP-Man, GDP-Fuc, and CMP-NeuNAc is not possible in cell extracts due to their low abundance and overlap with other signals, ^{1}H-NMR spectroscopy has been proven useful for detection and quantification of activated sugar nucleotides. NMR spectroscopy has the advantage that in addition to activated sugar nucleotides, a large number of metabolites from other metabolic pathways can be simultaneously and nonselectivel detected and quantified. NMR

spectroscopy can detect unexpected aberrant metabolic profiles that may not be observed using other methods that concentrate on a particular metabolite or enzymatic pathway. Another major advantage of NMR is that metabolic markers that were identified *in vitro* can often be transferred into *in vivo* applications using localized magnetic resonance spectroscopy or even to whole body magnets for human spectroscopy in a clinical setting, if the resolution is sufficient.

4.2 Hexosamine Induced Changes in Activated Sugar Nucleotide Levels in HT-22 and CHO Cells

Here, the effect of GlcN, GalN, and ManN on the levels of activated sugar nucleotides was determined in neuronal HT-22 cells and CHO cells. It was found that HexN induced changes in these sugars are NMR-detectable.

Increased flux through the HBP due to hyperglycemia leads to insulin resistance, a major hallmark of type II diabetes. Marshall *et al.* were the first who connected elevated flux through the HBP with insulin resistance in isolated rat adipocytes (Marshall *et al.*, 1991a). These authors also found that GlcN is at least 40 times more potent than glucose in mediating desensitization (Marshall *et al.*, 1991a). GlcN can enter the HBP as GlcN-6-P after phosphorylation by glucosamine kinase or hexokinase. GlcN therefore bypasses the rate-limiting step of the pathway, the conversion of Fru-6-P to GlcN-6-P catalyzed by GFAT.

Numerous *in vitro* (Robinson *et al.*, 1993; Marshall *et al.*, 2004) and *in vivo* (Baron *et al.*, 1995; Rossetti *et al.*, 1995; McClain & Crook, 1996; Patti *et al.*, 1999) studies using GlcN have now demonstrated that increased flux through the HBP may be one mechanism in the development of insulin resistance. It is not surprising that GlcN treatment leads to elevated *O*-GlcNAcylation of many proteins, also regulating a variety of signaling pathways that are involved in the development of insulin resistance (Singh & Crook, 2000; Vosseller *et al.*, 2002b; Buse, 2006; Dias & Hart, 2007). Although there is clear evidence that elevated flux through the HBP and increased *O*-GlcNAcylation are involved in the development of insulin resistance in type II diabetes, the precise mechanisms are still not fully understood and further research remains necessary.

All these studies were undertaken in insulin responsive-tissues like adipocytes or skeletal muscle. The effect of GlcN on insulin non-responsive tissue, such as brain cells, however, is not well investigated. Matthews *et al.*, for example observed an increase in Akt phosphorylation in GlcN treated astrocytes that was most likely a result of increased

endoplasmatic reticulum stress (Matthews *et al*., 2007). However, it is crucial to investigate the effect of hyperglycemia and increased hexosamine flux in brain cells, since it is known that insulin signaling regulates brain glucose metabolism (Clodfelder-Miller *et al*., 2005; Gerozissis, 2008). That means the brain is affected by insulin resistance and diabetes. Moreover, *O*-GlcNAcylation seems to play an important role in brain cells, as high levels of OGT mRNA and *O*-GlcNAcase are found in brain (Lubas *et al*., 1997; Gao *et al*., 2001), especially in hippocampal neurons and cerebellar Purkinje cells (Akimoto *et al*., 2003; Liu *et al*., 2004a). Furthermore, the highest levels of UDP-GlcNAc was detected in primary astrocytes, followed by neuronal HT-22 cells.

Using NMR-spectroscopy, I was able to investigate the early events in triggering insulin-resistance, i.e. the formation of UDP-GlcNAc through the HBP. For my study I used the neuronal HT-22 cell line and CHO cells for comparison. Cells were incubated with 100 µM of GlcN (or other HexN in subsequent experiments) additional to the physiological glucose concentration, which is 25 mM for HT-22 cells and 12,5 mM for CHO cells. The use of GlcN in investigations of the role of the HBP in the development of insulin resistance has been raised to question (Hresko *et al*., 1998; Virkamäki & Yki-Järvinen, 1999; Nelson *et al*., 2000; Nelson *et al*., 2002). One consequence of GlcN administration is the vast accumulation of GlcN-6-P, that leads to ATP depletion in cells (Hresko *et al*., 1998; Marshall *et al*., 2004). This ATP loss is possibly caused by phosphate consumption (for the formation of GlcN-6-P) or energy consumption needed for the phosphorylation step (Marshall *et al*., 2004). The ATP depletion, in turn, can also affect insulin signaling independent from UDP-GlcNAc formation leading to misinterpretation of the results (Hresko *et al*., 1998). However, low doses of GlcN (< 250 µM) were found to distinctly increase UDP-GlcNAc levels without increasing GlcN-6-P levels or without altering ATP levels (Marshall *et al*., 2004). On this account I used such a low concentration of GlcN in my study to not exceed the capacity of the HBP.

As expected, both HT-22 and CHO cells actively converted GlcN into UDP-GlcNAc, as determined by a significant increase in this metabolite in M/C cell extracts. In HT-22 cells the UDP-GlcNAc levels increased threefold when GlcN treated compared to controls. In CHO cells, the increase was even fourfold, with the limitation that the error bar was quite large for the experiments with CHO cells. These values are in good agreement with the results obtained by Marshall *et al*., who detected increased UDP-GlcNAc levels in isolated adipocytes by 4 - 5-fold incubating with low doses of GlcN (< 500 µM) for 4 h (Marshall *et al*., 2004). Krug *et al*. observed a more than sixfold increase in the UDP-HexNAc pool (mixture of UDP-GlcNAc and UDP-GalNAc) in colon carcinoma cells after treatment with 2,5 mM GlcN for 4 h (Krug

et al., 1984). In both studies PCA extraction was used and UDP-GlcNAc/UDP-HexNAc levels were measured by HPLC. Independently, from the type of cell, incubation time, and particularly GlcN concentrations, combining these studies, it seems that the capacity of the HBP for GlcN is almost the same. The massive accumulation of UDP-GlcNAc using such low concentrations of GlcN is even more astonishing considering the fact that it has to compete with glucose for uptake into the cell, having a higher affinity for these transporters (Marshall *et al*., 2004). The high accumulation of UDP-GlcNAc therefore indicates that GlcN must be almost exclusively routed into the HBP.

In contrast to my results, Krug *et al*. also observed a decrease in UDP-Glc, UDP-Gal, and UDP-GlcUA in GalN treated colon carcinoma cells (Krug *et al*., 1984). Concomitant, with the decrease in these metabolites, they also detected a decrease in UTP and CTP (Krug *et al*., 1984). I did not detect any significant changes in UDP-Glc, UDP-Gal, and UDP-GlcUA, although there may be a trend towards decreased UDP-Glc and UDP-Gal levels in GlcN treated HT-22, as well as CHO cells. The authors concluded that the decrease in UDP-Glc and UDP-Gal was due to UTP depletion, because UTP was consumed in the excess formation of UDP-GlcNAc and UDP-GalNAc from GlcN. Krug *et al*. used GlcN concentrations of 2,5 mM, 5 mM, and 10 mM (Krug *et al*., 1984). Therefore, their concentrations were 25 – 100 times higher than the concentration I used in my experiments. Still, the increase in UDP-GlcNAc and UDP-GalNAc in my study was comparable to the increase those authors detected. If the decrease in UDP-Glc and UDP-Gal had only been exclusively attributable to the consumption of UTP for UDP-GlcNAc and UDP-GalNAc synthesis, a significant decrease in UDP-Glc and UDP-Gal should have been observed. As mentioned above, high GlcN concentrations are correlated with ATP depletion. UDP-Glc is formed by phosphorylation of glucose to Glc-6-P. Glc-6-P is then converted to Glc-1-P. Glc-1-P is finally activated with UTP to yield UDP-Glc. UDP-Gal is directly phosphorylated to Glc-1-P, which is then reacts with UTP to give UDP-Gal. The initial phosphorylation step of both pathways consumes ATP. On this account ATP deficiency, together with UTP depletion, leads to decreased formation of UDP-Glc and UDP-Gal. Monitoring UDP-Glc and UDP-Gal can therefore be used as an indirect detection of ATP deprivation in a cell. The fact that I did not detect significant decreases in the UDP-Glc and UDP-Gal levels indicates that a GlcN concentration of 100 µM does not lead to ATP depletion in HT-22 and CHO cells. Furthermore, it proofs that UTP is also still available in sufficient amounts.

GlcN treatment also led to a significant increase in UDP-GalNAc, which can be formed by epimerization of UDP-GlcNAc, thus being also an end-product of the HBP. Similar to the increase in UDP-GlcNAc, the UDP-GalNAc level increased threefold after GlcN treatment in

HT-22 cells and 4-fold in CHO cells. Since the UDP-GalNAc levels increase as much as UDP-GlcNAc does using only a concentration of 100 µM, GlcN treatment can not only influence *O*-GlcNAcylation of proteins, but also severely affect glycosylation of proteins and lipids. This side effect, in contrast to ATP or UTP depletion, will therefore also occur using low doses of GlcN. GlcN-induced increases in UDP-GlcNAc/UDP-GalNAc levels, for example, were shown to increase the complexity of *N*-linked glycans in mammalian cells (Gawlitzek *et al*., 1998).

I also investigated the impact of other low concentrated hexosamines, on the formation of UDP-HexNAcs and UDP-hexoses. Incubation of neuronal HT-22 cells and CHO cells with 100 µM GalN resulted in unexpected findings. GalN is a well-investigated hepatotoxin that is usually used in studies on liver damage (Keppler *et al*., 1968; Coen *et al*., 2007). GalN is first phosphorylated by galactokinase, yielding GalN-1-P (Ballard, 1966; Walker & Khan, 1968). GalN-1-P then reacts with UDP-Glc, leading to the formation of UDP-GalN and Glc-1-P. The reaction is catalyzed by the enzyme galactose-1-phosphate uridylyltransferase (GALT; EC 2.7.7.12) (Maley, 1970; Keppler & Decker, 1969). GALT, as well as the other enzymes participating in GalN metabolism, are not specific for GalN and also catalyze galactose metabolism. The involvement of galactose in the biosynthesis of activated sugar nucleotides is discussed in the next chapter. UDP-GalN is then epimerized to UDP-GlcN by UDP-galactose-4-epimerase (GALE; EC 5.1.3.2) (Maley & Maley, 1959). UDP-hexosamines (UDP-GlcN & UDP-GalN) are normally no naturally occurring intermediates in cell metabolism (Keppler *et al*., 1970). UDP-GlcN and UDP-GalN can exclusively be formed after GalN (Maley *et al*., 1968; Keppler, 1977; Krug *et al*., 1984), but not after GlcN administration, which passes a through a distinct metabolic route (Decker & Keppler, 1974). The further pathway leading to UDP-GlcNAc and UDP-GalNAc has not been fully elucidated until now. UDP-GlcN and UDP-GalN may possibly be directly *N*-acetylated to yield the respective UDP-HexNAc. However, since no evidence of this direct acetylation has been found in mammalian cells (Maley *et al*., 1968), another mechanism is more likely. In this pathway, proposed by Weckbecker & Keppler, 1982, UDP-GlcN is converted to GlcN-1-P. This enzymatic step is again catalyzed by GALT, meaning that this enzyme accomplishes a dual role in GalN metabolism. GALT catalyzes the activation of GalN-1-P to UDP-GalN and after epimerization to UDP-GlcN, it catalyzes the conversion to GlcN-1-P (Weckbecker & Keppler, 1982). GlcN-1-P is subsequently epimerized to the HBP intermediate GlcN-6-P by phosphoglucomutase (Brown, 1953). GlcN-6-P can then be routed into the HBP to finally give UDP-GlcNAc and UDP-GalNAc. The metabolism of GalN is summarized in Figure 46.

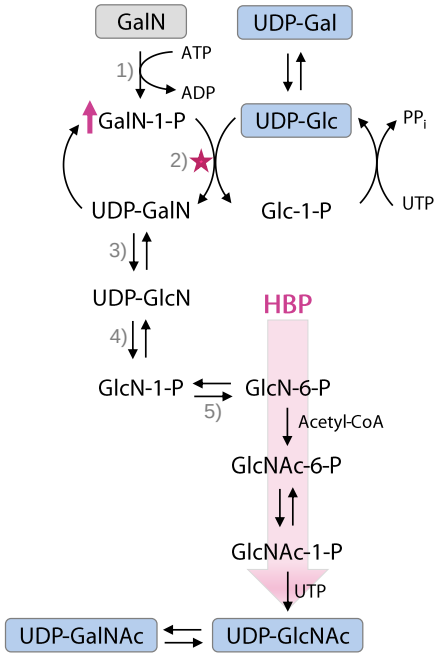

Figure 46. GalN metabolism: 1) GalN is phosphorylated to GalN-1-P by galactokinase. 2) GalN-1-P then reacts with UDP-Glc, leading to the formation of UDP-GalN and Glc-1-P. The reaction is catalyzed by the enzyme galactose-1-phosphate uridylyltransferase (GALT; EC 2.7.7.12). 3) UDP-GalN is then epimerized to UDP-GlcN by UDP-galactose-4-epimerase (GALE; EC 5.1.3.2). 4) UDP-GlcN is converted to GlcN-1-P. This enzymatic step is again catalyzed by GALT. 5) GlcN-1-P is subsequently epimerized to GlcN-6-P by phosphoglucomutase and can be routed into the HBP to synthesize UDP-GlcNAc and UDP-GalNAc. GalN-1-P heavily accumulated in HT-22 and CHO cells incubated with low doses of GalN, due to the low affinity of GALT for GalN-1-P (pink asterisk). ADP, adenosine diphosphate; ATP, adenosine triphosphates; HBP, hexosamine biosynthesis pathway; GalN, galactosamine; GalN-1-P, galactosamine-1-phosphate; GlcN-1-P, glucosamine-1-phosphate; GlcN-6-P, glucosamine-6-phosphate; GlcNAc-1-P, *N*-acetylglucosamine-1-phosphate; GlcNAc-6-P, *N*-acetylglucosamine-6-phosphate; PP_i, pyrophosphate; UDP-GalN, uridine diphosphate-galactosamine; UDP-GalNAc, uridine diphosphate-*N*-acetylgalactosamine; UDP-GlcN, uridine diphosphate-glucosamine; UDP-GlcNAc, uridine diphosphate-*N*-acetylglucosamine; UTP, uridine triphosphate.

It was surprising that I did not detect an increase in the UDP-GlcNAc levels in neither HT-22 nor CHO cells. Only in CHO cells, a small, but significant increase in the UDP-GalNAc level was observed. This fact, that I observed an elevated UDP-GalNAc level, without an increase in the UDP-GlcNAc level in GalN treated CHO cells, may indicate a direct acetylation of UDP-GalN. The metabolism of GalN through the pathway depicted in Figure 46 would rather lead to elevated UDP-GlcNAc levels or UDP-GlcNAc and UDP-GalNAc levels. However, my results may only be an indication of the direct acetylation and further investigation is needed. Nevertheless, the fail of increasing UDP-GlcNAc and UDP-GalNAc levels in HT-22 and UDP-GlcNAc levels in CHO cells was unexpected. An increase in the UDP-HexNAc level has been previously detected in GalN treated liver tissue (Keppler *et al*., 1969; Keppler *et al*., 1974; Pels Rijcken *et al*., 1995; Coen *et al*., 2007) and in intact rats by localized in vivo ^{31}P magnetic resonance spectroscopy (Weisdorf *et al*., 1991). Similar to GlcN metabolism, a concomitant drastic decrease in UDP-Glc, UDP-Gal, UDP-GlcUA, as well as UTP and other nucleotides has been observed (Keppler *et al*., 1969; Keppler *et al*., 1970; Keppler *et al*., 1974; Pels Rijcken *et al*., 1995; Coen *et al*., 2007). This decrease has been attributed to be a consequence of the rapid production of UDP-GlcNAc, UDP-GalNAc, UDP-GlcN, and UDP-GalN in these studies. It has also been shown that the toxicity of GalN can be diminished by uridine, glycine (Stachlewitz *et al*., 1999; Coen *et al*., 2007), or orotate (Keppler *et al*., 1970; Scharnbeck *et al*., 1972). All three metabolites are precursors for UMP and thus UTP. It seems obvious that these substances reduce GalN toxicity by preventing UTP depletion. Indeed Coen *et al*. detected a marked increase in uridine, UDP-Glc, and UDP-Gal levels in

liver samples treated with GalN and glycine compared to samples treated with GalN alone (Coen *et al*., 2007). Since I have not observed an increase in the UDP-HexNAc levels, apart from the small but significant increase of UDP-GalNAc, in CHO cells, it is not surprising that no decrease in either UDP-Glc, UDP-Gal, or UDP-GlcUA was detected in GalN treated cells.

In the spectra of GalN treated HT-22 and CHO cells a novel resonance at 5,69 ppm arose. This signal was assigned to the anomeric proton (H1(α)) of galactosamine-1-phosphate (GalN-1-P) by comparison with spectra of the authentic compound. The GalN-1-P accumulation was almost four times higher in HT-22 compared to CHO cells. The increase of GalN-1-P can be attributed to the low affinity of GALT for GalN-1-P (Keppler & Decker, 1969). An increase in this compound was also detected previously in GalN treated intact rats in *in vivo* ^{31}P NMR spectra (Weisdorf *et al*., 1991). The fact that the accumulation of GalN-1-P in CHO cell was less pronounced compared to HT-22 cells, may explain why I detected a small but significant increase in the UDP-GalNAc level in CHO cells. My results may indicate that in those cells, the turnover of GalN-1-P by GALT is higher than in HT-22 cells, thus leading to further metabolism of GalN right up to the formation of UDP-GalNAc. Keppler and Decker revealed that the low affinity of GALT for GalN-1-P accounts only in part for the high levels of this metabolite in the liver of GalN treated rats (Keppler & Decker, 1969). GalN-1-P inhibits the enzyme UDP-glucose-pyrophosphorylase (EC 2.7.7.9), which catalyzes the reaction of Glc-1-P and UTP to UDP-Glc and inorganic pyrophosphate (PP_i). The inhibition is competitive with Glc-1-P and therefore dependent on the GalN concentrations administered. UDP-Glc, however, is needed for the conversion of GalN-1-P to UDP-GalN. By the inhibition of UDP-glucose-pyrophosphorylase, GalN-1-P impedes its own conversion to UDP-GalN and enhances the accumulation of GalN-1-P (Keppler & Decker, 1969). The fact that I did not detect a decrease in the UDP-Glc level in GalN treated HT-22 and CHO cells, indicates that the accumulation of GalN-1-P was exclusively due to the low affinity of GALT for GalN-1-P and inhibition of UDP-glucose-pyrophosphorylase was probably not involved. These differences may be in the first place due to the different cell types used in my studies, but also due to the low doses of GalN used in my experiments. In the studies mentioned above, GalN was injected into rats and liver tissue was investigated afterwards. Therefore, a comparison of the GalN concentrations used compared to my study is difficult. However, it can be assumed that the concentration of 100 µM GalN, I used in my study was much lower. Since such low concentrations of GalN already led to massive accumulation of GalN-1-P it is doubtful that higher concentrations would lead to elevated UDP-GlcNAc and UDP-GalNAc levels in neuronal HT-22 or CHO cells. It is rather expected that higher GalN concentrations would lead to ATP depletion is these cells, because

phosphorylation of GalN to GalN-1-P consumes ATP. Depleted adenosine levels, which are equivalent to depleted ATP levels, were indeed found in liver tissue of GalN treated rats (Coen *et al*., 2007).

To sum up, it is theoretically possible to increase the UDP-GlcNAc and UDP-GalNAc levels by GalN in mammalian cells. Like GlcN, GalN also bypasses GFAT, the rate-limiting enzyme of the HBP. An increase of UDP-GlcNAc and UDP-GalNAc has been observed in liver tissue of GalN treated rats. In HT-22 cells and in CHO cells, with the exception of UDP-GalNAc in CHO cells, it is in contrast to GlcN, not possible to elevate UDP-HexNAc levels using small doses of GalN. This difference is most likely attributable to the fact that GalN is metabolized by enzymes of the galactose pathway, having low-specificity for GalN. GlcN, on the other hand, is metabolized by specific enzymes.

In contrast to GlcN and GalN, the metabolism of ManN in mammalian cells is not extensively studied. This is highly probable due to the limited metabolism of this metabolite. In 1970 Raisys & Winzler studied the metabolism of exogenous ManN in Sarcoma 180 cells and intact rats (Raisys & Winzler, 1970). They observed that ManN is rapidly taken up into the cells and then phosphorylated to ManN-6-P. However, no other metabolites deriving from ManN were detected and ManN as well as ManN-6-P accumulated in cells (Raisys & Winzler, 1970). Furthermore, most of the ManN injected intraperitoneally to rats was excreted unaltered in the urine. A substantial amount of free ManN was detected in the liver and kidney of the rats, and only less than 1 % ManN-6-P was detected in these organs (Raisys & Winzler, 1970).

The fact that I found significantly elevated UDP-GlcNAc and UDP-GalNAc levels in HT-22 cells proves that ManN has to be further metabolized in these cells. There are theoretically at least three metabolic routes how ManN can be converted to UDP-GlcNAc. Two of the routes require the ability of the cells to acetylate ManN. Although Raisys & Winzler did not detect any acetylated ManN metabolites deriving from ManN in their study, these metabolites were detected in bovine thyroid gland slices (Gan, 1975). ManNAc, ManN-6-P, ManNAc-6-P, and CMP-NeuNAc were identified as intermediates after incubation with radioactive labeled ManN (Gan, 1975). On this account it may be possible that ManN is also acetylated in HT-22 cells. ManNAc is the precursor for synthesis of CMP-NeuNAc, the donor substrate for sialic acids. Terminal sialic acids are found in a variety of cell surface glycoconjugates and are involved in cell recognition processes like cell-cell adhesion or cell migration (Varki, 1997; Traving & Schauer, 1998). Sialoglycoproteins also play an important role in malignant transformation of cells (Yogeeswaran & Salk, 1981) and virus infection (Karlsson, 1995;

Vimr & Lichtensteiger, 2002). In mammalian cells, ManNAc is formed from UDP-GlcNAc by the enzyme UDP-*N*-acetyl-D-glucosamine 2-epimerase (UDP-GlcNAc 2-epimerase; E.C. 5.1.3.14) (Van Rinsum *et al*., 1983). CMP-NeuNAc is then generated by the following consecutive reactions: ManNAc → ManNAc-6-P → NeuNAc-9-P → NeuNAc → CMP-NeuNAc (Angata & Varki, 2002). To elevate the UDP-GlcNAc levels in HT-22 cells after ManN administration, the epimerization of UDP-GlcNAc to ManNAc by UDP-GlcNAc 2-epimerase has to be reversible. However, this is not the case in mammalian cells. Merely in bacteria, the non-hydrolyzing UDP-GlcNAc 2-epimerases catalyzes the reversible conversion of UDP-GlcNAc into ManNAc (Kawamura *et al*., 1978; Kawamura *et al*., 1979; Sala *et al*., 1996; Morgan *et al*., 1997). The corresponding hydrolyzing enzyme in mammalian cells, however, catalyzes the irreversible conversion of UDP-GlcNAc to ManNAc (Hinderlich *et al*., 1997; Tanner, 2005). Not being reversible, the elevated UDP-GlcNAc concentration cannot be generated by this metabolic route. In several publications it was reported, that ManN is converted at a high rate into GlcN in *Plasmodium falciparum* (Azzouz *et al*., 2005), *Leishmania Mexicana* (Field *et al*., 1993), and *Trypanosoma brucei* (Ralton *et al*., 1993). As described above, GlcN is easily converted to UDP-GlcNAc, thus leading to elevated UDP-GlcNAc and UDP-GalNAc levels. However, it is highly questionable, that the ManN to GlcN conversion detected in parasites also occurs in mammalian cells especially considering that no publications exist reporting this metabolic step in mammalians.

Another enzyme participating in ManNAc metabolism is the *N*-acetyl-D-glucosamine 2-epimerase (GlcNAc 2-epimerase, E.C. 5.1.3.8) that catalyzes the reversible conversion of GlcNAc and ManNAc (Datta, 1970; Maru *et al*., 1996). GlcNAc 2-epimerase was found in different mammalian tissues (Van Rinsum *et al*., 1983; Takahashi *et al*., 1983), as well as in human cells (Luchansky *et al*., 2003). GlcNAc 2-epimerase was found to play a catabolic role in sialic acid metabolism, by favoring the conversion of ManNAc to GlcNAc (Luchansky *et al*., 2003), making it an ideal enzyme for the formation of UDP-GlcNAc from ManN administered to HT-22 cells. GlcNAc can then be introduced into the HBP as GlcNAc-6-P after phosphorylation by GlcNAc kinase (Hinderlich *et al*., 1998).

I therefore suggest the following metabolic pathway for ManN leading to significantly elevated UDP-GlcNAc and UDP-GalNAc levels in neuronal HT-22 cells: After entering the cell ManN is acetylated by a specific hitherto not known acetylase to ManNAc. ManNAc is then epimerized to GlcNAc by GlcNAc 2-epimerase. After that GlcNAc is phosphorylated by GlcNAc kinase to GlcNAc-6-P which can enter the HBP to finally yield UDP-GlcNAc and UDP-GalNAc, as shown in Figure 47.

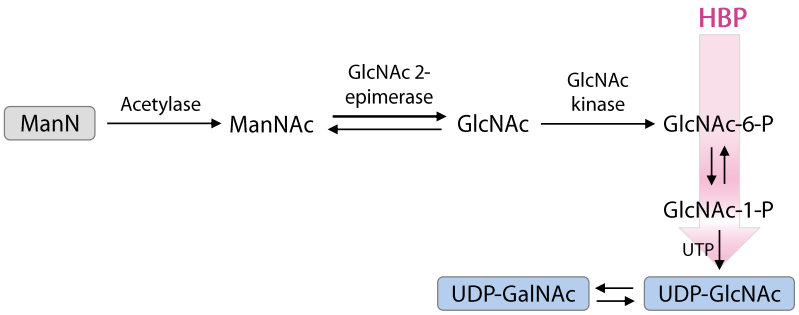

Figure 47. Possible metabolic pathway for the synthesis of UDP-GlcNAc and UDP-GalNAc from ManN: After entering the cell ManN is acetylated in the cytosol by a specific hitherto not known acetylase to ManNAc. ManNAc is then epimerized to GlcNAc by GlcNAc 2-epimerase. GlcNAc is subsequently phosphorylated by GlcNAc kinase to GlcNAc-6-P which can enter the HBP to finally yield UDP-GlcNAc and UDP-GalNAc. HBP, hexosamine biosynthesis pathway; GlcNAc, *N*-acetylglucosamine; GlcNAc-1-P, *N*-acetylglucosamine-1-phosphate; GlcNAc-6-P, *N*-acetylglucosamine-6-phosphate; GlcNAc kinase, *N*-acetylglucosamine kinase; GlcNAc 2-epimerase, *N*-acetylglucosamine 2-epimerase; ManN, mannosamine; ManNAc, *N*-acetylmannosamine; UDP-GalNAc, uridine diphosphate-*N*-acetylgalactosamine; UDP-GlcNAc, uridine diphosphate-*N*-acetylglucosamine; UTP, uridine triphosphate.

In CHO cells no changes in the UDP-GlcNAc and UDP-GalNAc levels after incubation with ManN were observed. This difference may probably be caused by cell-specific differences in the expression or activity of GlcNAc 2-epimerase or the ability of CHO cells to acetylate ManN. It is rather unlikely that the non-occurrence of elevated UDP-GlcNAc and UDP-GalNAc levels in ManN treated cells is due to differences in cellular uptake of ManN, because ManN is known to be taken up by cells (Raisys & Winzler, 1970; Gan, 1975; Oetke *et al*., 2001).

4.2.1 Conclusions

To conclude, I have shown that low concentrations of GlcN are sufficient to massively accumulate UDP-GlcNAc and UDP-GalNAc in neuronal HT-22 and CHO cells and that these changes are easily detectable using ^{1}H-NMR spectroscopy. The high accumulation of these two compounds also indicates that GlcN must be almost exclusively routed into the HBP. Furthermore, UDP-Glc and UDP-Gal levels were not significantly altered in GlcN treated cells. Since the formation of both metabolites depends on UTP as well as ATP availability, I have indirectly shown that UTP and ATP levels, respectively, are not depleted in my experiments. ATP depletion may lead to undesirable side effects that can impede the elucidation of the development of insulin resistance.

In contrast to GlcN, it is not possible to elevate UDP-GlcNAc and UDP-GalNAc levels in HT-22 and UDP-GlcNAc levels in CHO cells using small doses of GalN. This difference may

be due to the fact that GalN is metabolized by enzymes of the galactose pathway, showing low-specificity for GalN. In GalN treated HT-22 and CHO cells, I detected a massive accumulation of GalN-1-P. This accumulation was almost four times higher in HT-22 cells compared to CHO cells and may explain that at least UDP-GalNAc was found to be significantly higher in GalN treated CHO cells. It can be assumed that the turnover of GalN-1-P by GALT is higher in these cells, thus leading to further metabolism of GalN right up to the formation of UDP-GalNAc.

I have shown for the first time that ManN can be used as a precursor for the synthesis of UDP-GlcNAc and UDP-GalNAc. This ability is a cell-specific feature and was observed in neuronal HT-22 cells, whereas in CHO cells no changes in the UDP-GlcNAc/UDP-GalNAc levels were observed when ManN treated. Formation of UDP-GlcNAc may most likely proceed by acetylation of ManN, by a hitherto unknown acetylase, and subsequent epimerization of ManNAc to GlcNAc by GlcNAc 2-epimerase. GlcNAc can then be phosphorylated by GlcNAc kinase to yield GlcNAc-6-P, which then enters the HBP to generate UDP-GlcNAc. Furthermore, I concluded that the non-occurrence of elevated UDP-GlcNAc/UDP-GalNAc levels in CHO cells may be restricted by the ability of cells to acetylate ManN or to epimerize ManNAc by GlcNAc 2-epimerase.

4.3 Galactose as Precursor for Synthesis of Activated Sugar Nucleotides in HT-22 and CHO cells

Glucose is the primary energy substrate of the brain (Fehm *et al*. 2006) and the precursor for the synthesis of activated sugar nucleotides. Galactose is a non-essential nutrient that can contribute to the energy supply in a cell since it can be routed into glycolysis. However, in the brain galactose is insufficiently metabolized and induces neurotoxicity (Haworth *et al*., 1970; Kozak & Wells, 1971; Knull *et al*., 1973). Galactose can theoretically be the precursor for UDP-Glc, UDP-Gal, UDP-GlcNAc, and UDP-GalNAc whereas the latter two occur late in the metabolic pathway as depicted in Figure 48. In this chapter I have evaluated the effect of galactose on the formation of these activated sugar nucleotides in neuronal HT-22 cells. The results were compared to those obtained from the same experiments carried out in CHO cells, to serve as an example of a non-brain cell line. HT-22 and CHO cells were treated for 24 h with 10 mM glucose, 5 mM glucose + 5 mM galactose, 5 mM galactose, or 10 mM galactose. In conditions with 5 mM galactose and 10 mM galactose, no glucose was present as an energy source.

Galactose metabolism is carried out by three subsequent enzymatic steps catalyzed by galactokinase (GALK; EC 2.7.1.6), GALT and GALE (Holden *et al*., 2003). GALT and GALE are the same enzymes that catalyze the conversion of GalN that has been described in the previous chapter. In the first reaction galactose is phosphorylated to Gal-1-P by GALK. In the second step Gal-1-P reacts with UDP-Glc to form Glc-1-P and UDP-Gal. Glc-1-P can enter glycolysis or react with UTP to regenerate UDP-Glc (Duggleby *et al*., 1996). The third enzyme GALE catalyzes the epimerization of UDP-Gal to UDP-Glc with NAD^+ as cofactor. Deficiency of each of the three enzymes of galactose metabolism results in inborn human diseases commonly referred to as galactosemia, whereby GALT deficiency is the most common and best-studied form (Petry & Reichardt, 1998; Novelli & Reichardt, 2000).

UDP-Gal levels were significantly increased in both neuronal HT-22 and CHO cells under all conditions when galactose was present in the cell culture medium. However, there were no differences in the UDP-Gal levels between cells incubated with 5 mM galactose or 10 mM galactose, indicating that there is a limit of GALT to catalyze the reaction of Gal-1-P with UDP-Glc to form UDP-Gal and Glc-1-P. The UDP-Gal concentration was similar in HT-22 and CHO cells in the absence of galactose. However, when cells were incubated with galactose, the increase in UDP-Gal concentration was higher in CHO cells than in HT-22 cells, indicating that HT-22 cells have a limited ability to metabolize galactose. In galactose fed chicks, the UDP-Gal level was found to be increased in the liver of these animals (Hansen *et al*., 1956). In a different study, the levels of UDP-Gal, as well as, UDP-Glc were not found to be increased in brains of galactose fed chicks (Kozak & Wells, 1971), also emphasizing the poor galactose utilization in the brain.

UDP-Gal is the only donor substrate for incorporation of galactose into glycoproteins and glycolipids. Accordingly, aberrant UDP-Gal levels might cause alterations in these carbohydrates which, in turn, may lead to non-functional proteins. Amongst other tissues, in particular the brain seems to be affected by impaired galactose metabolism. Abnormal glycosylation was detected in the brain of a galactosemic patient (Haberland *et al*., 1971). A reduction in galactose- and GalNAc-containing glycolipids and an accumulation of the precursors of these metabolites have been detected in the brain of a newborn with galactosemia (Petry *et al*., 1991).

GALT plays an important role in the development of the nervous system and is highly expressed during myelination of neurons forming neuronal tracts that compose the white matter; a process that is associated with development of the brain (Daude *et al*., 1996a; Daude *et al*., 1996b). Formation of the glycolipids galactosyl-ceramide and galactosyl-ceramide-3-

sulfate play a major role in myelination and their synthesis depends on UDP-Gal. Galactosyl-ceramides were observed to decrease in the brain of a galactosemic patient, indicating that myelination might be impaired, possibly explaining the neurologic complications of galactosemic patients (Petry *et al*., 1991; Petry & Reichardt, 1998). Increased UDP-Gal levels, as observed in neuronal HT-22 cells, may also affect the formation of galactose-containing glycoproteins and glycolipids.

Although UDP-Gal can be epimerized by GALE to UDP-Glc, UDP-Glc levels were not as affected as UDP-Gal by galactose treatment. In CHO cells, no changes were observed in the UDP-Glc levels. Neuronal HT-22 cells exhibited significantly increased UDP-Glc levels only when cells were incubated with 10 mM galactose.

Both cell lines highly accumulated Gal-1-P, but the accumulation was much higher in neuronal HT-22 cells compared to CHO cells. In the previous chapter an accumulation of GalN-1-P in GalN treated CHO and HT-22 cells was detected. I attributed this increase in GalN-1-P to the low affinity of GALT for GalN-1-P (Keppler & Decker, 1969) because GALT is an enzyme of the galactose metabolism and not specific for GalN metabolism. My results do not allow the interpretation of GALT specificity for galactose versus GalN in HT-22 and CHO cells, because the experimental set-up was different for both administered metabolites. However, it can be concluded that the galactose concentrations used in my experiments widely exceeded the capacity of GALT to metabolize the Gal-1-P levels produced from galactose by GALK. Besides, the accumulation of GalN-1-P in GalN treated HT-22 cells was also much higher in HT-22 compared to CHO cells, further emphasizing that the galactose pathway that can also be passed through by GalN is less sufficient in neuronal HT-22 cells compared to CHO cells. The high accumulation of Gal-1-P can only be caused by limited amount or activity of GALT, indicating that this enzyme is responsible for the restricted ability of CHO and especially neuronal HT-22 cells to metabolize galactose. GALT-deficiency exhibits the most severe pathological phenotype of all three types of galactosemia. Since the main difference in GALT-deficient galactosemia, compared to other the other types, is the high accumulation of Gal-1-P (Donnell *et al*., 1963; Gitzelman, 1995), the acute toxicity of GALT-deficiency is mainly attributed to this metabolite (Lai *et al*., 2003; Bhat, 2003; Slepak *et al*., 2005; Slepak *et al*., 2007). Besides, Gal-1-P most likely interferes phosphoglucomutase (Schwarz *et al*., 1956; De Jongh *et al*., 2008), the enzyme that catalyzes the conversion of Glc-1-P to Glc-6-P. Under these circumstances, galactose can no longer be introduced into glycolysis or HBP (see Figure 48). It is also possible that Gal-1-P inhibits glycogen phosphorylase (Maddaiah & Madsen, 1966) thus preventing the formation of Glc-1-P by glycogenolysis. Furthermore, Gal-1-P is known to inhibit UDP–glucose

pyrophosphorylase (Oliver, 1961; Lai *et al*., 2003), the enzyme that catalyzes the reaction of Glc-1-P with UTP to form UDP-Glc. Inhibition of UDP-glucose pyrophosphorylase by Gal-1-P was discussed to be responsible for the reduction of UDP-Glc and UDP-Gal in GALT-deficient human cell lines (Lai *et al*., 2003). Since Gal-1-P also highly accumulated in galactose treated CHO and HT-22 cells, UDP-glucose pyrophosphorylase should also be affected in these conditions. However, as mentioned above, I did not detect any changes in the UDP-Glc levels in CHO cells and only as significant increase in the UDP-Glc concentration in HT-22 cells when incubated with 10 mM galactose. Apart from the reaction of Glc-1-P with UTP, UDP-Glc can also be formed by epimerization of UDP-Gal by GALE. Therefore, an increase in UDP-Glc is even more probable in galactose treated cells than a decrease. Increased Glc-1-P levels, however, could indicate an inhibition of the enzyme. Nevertheless, there were no NMR-detectable Glc-1-P levels in galactose treated HT-22 or CHO cells in my experiments. When no glucose is present in the experiments, it is highly probable that cells route the produced Glc-1-P into glycolysis by conversion of Glc-1-P into Glc-6-P. However, as described above, phosphoglucomutase, the enzyme that catalyzes this reaction is also known to be inhibited by Gal-1-P.

In principle, galactose can be used to maintain UDP-GlcNAc and UDP-GalNAc levels in cells although these activated sugars occur late in the pathway. I therefore tested the effect of galactose on the formation of UDP-GlcNAc and UDP-GalNAc. When glucose was present in addition to galactose, no significant changes in the UDP-GlcNAc/UDP-GalNAc levels were detected in both HT-22 and CHO cells. However, when neuronal HT-22 cells were incubated with galactose alone, a significant decrease in these activated sugar nucleotides was observed. In CHO cells, in contrast, no such decrease was detected. Under these conditions not only the biosynthesis of glycoproteins and glycolipids that depend on UDP-Gal as a precursor will be affected, but also those glycoproteins and glycolipids whose precursors are UDP-GlcNAc and UDP-GalNAc might aberrate. This leads to the assumption that *O*-GlcNAcylation of proteins might as well be affected in these conditions in neuronal HT-22 cells. It can be concluded that CHO cells are able to maintain UDP-GlcNAc and UDP-GalNAc levels in conditions when galactose is present but glucose is absent, whereas neuronal HT-22 cells do not have this ability. There are several plausible reasonings for this observation. First of all CHO cells contain glycogen, but neuronal HT-22 cells not. For that reason it is possible that CHO cells preserve UDP-GlcNAc and UDP-GalNAc levels in the absence of glucose and in the presence of galactose. This does not necessarily imply that galactose is used as a precursor for UDP-GlcNAc and UDP-GalNAc in CHO cells.

Furthermore, I have discussed above that accumulated Gal-1-P might interfere with phosphoglucomutase and glycogen phosphorylase. Both enzymes are crucial for UDP-GlcNAc/UDP-GalNAc synthesis either by using galactose as a precursor or glycogenolysis. Inhibition of phosphoglucomutase would prevent the conversion of Glc-1-P to Glc-6-P with the result that galactose cannot be introduced in the HBP. Inhibition of glycogen phosphorylase on the other hand would impede the formation of Glc-1-P by glycogenolysis. Since Gal-1-P was accumulated to a lesser extend in CHO cells than in HT-22 cells it might be possible that phosphoglucomutase as well as glycogen phosphorylase are not entirely inhibited and thus permit the metabolism of galactose to UDP-GlcNAc/UDP-GalNAc. Both effects (presence of glycogen and potentially lesser inhibition of the involved enzymes) can of course concurrently contribute to the maintenance of the UDP-GlcNAc/UDP-GalNAc levels in CHO cells.

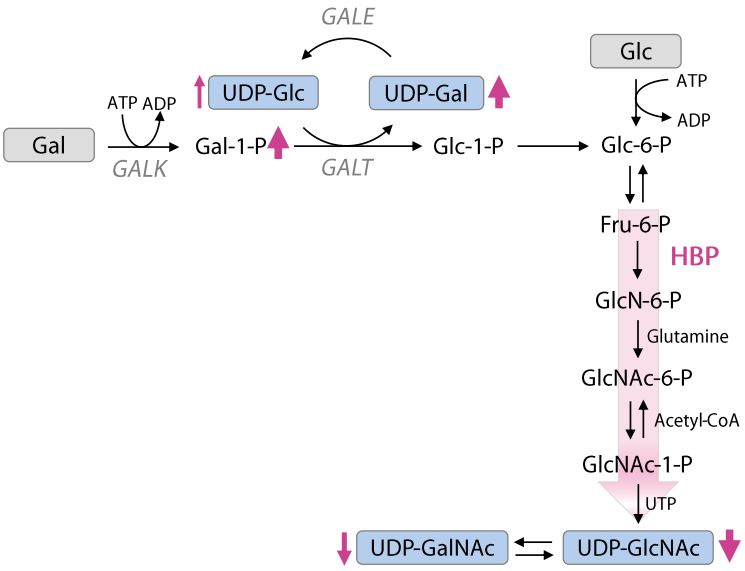

Figure 48. Influence of galactose on the formation of activated sugar nucleotides in HT-22 cells: Theoretically, galactose can be the precursor of UDP-Glc, UDP-Gal, UDP-GlcNAc, and UDP-GalNAc, whereas the latter two occur late in the metabolic pathway. Gal is phosphorylated to Gal-1-P by GALK. Gal-1-P then reacts with UDP-Glc, leading to the formation of UDP-Gal and Glc-1-P. The reaction is catalyzed by GALT. UDP-Gal is then epimerized to UDP-Glc by GALE. Glc-1-P can be epimerized to GlcN-6-P and then be routed into the HBP to synthesize UDP-GlcNAc and UDP-GalNAc. The arrows depict the changes in levels of activated sugar nucleotides in HT-22 cells after incubation with 10 mM galactose in the absence of glucose after 24 h. UDP-Gal and UDP-Glc were both found the be significantly decreased in galactose treated HT-22 cells. The increase in UDP-Gal was more pronounced than in UDP-Glc. UDP-GalNAc and UDP-GlcNAc by contrast were both decreased in galactose treated cells and the decrease was more pronounced in UDP-GlcNAc. Gal-1-P heavily accumulated in HT-22 and CHO cells incubated with galactose, showing that the galactose concentrations used in my experiments exceed the capacity of the GALT to form Glc-1-P. The thickness of the arrow represents the significance (*P* value) of the observed increase or decrease of the respective sugar. ADP, adenosine diphosphate; ATP, adenosine triphosphates; HBP, hexosamine biosynthesis pathway; Gal, galactose; Gal-1-P, galactose-1-phosphate; GALE, UDP-galactose-4-epimerase; GALK, galactokinase; GALT, galactose-1-phosphate uridylyltransferase; Glc-1-P, glucose-1-phosphate; Glc-6-P, glucose-6-phosphate; GlcNAc-1-P, *N*-acetylglucosamine-1-phosphate; GlcNAc-6-P, *N*-acetylglucosamine-6-phosphate; UDP-Gal, uridine diphosphate-galactose; UDP-GalNAc, uridine diphosphate-*N*-acetylgalactosamine; UDP-Glc, uridine diphosphate-glucose; UDP-GlcNAc, uridine diphosphate-*N*-acetylglucosamine; UTP, uridine triphosphate.

Last but not least, decreased UDP-GlcNAc/UDP-GalNAc levels were detected under conditions when glucose was absent and cells had to cope with limited energy. To maintain energy homeostasis galactose can be routed into glycolysis as long as phosphoglucomutase is not fully inhibited by Gal-1-P. The precedence of cells to route galactose into glycolysis versus HBP may also influence UDP-GlcNAc/UDP-GalNAc levels.
The galactose metabolism and the influence of galactose on the formation of activated sugar nucleotides in HT-22 cells is graphically summarized in Figure 48.

4.3.1 Conclusions and Perspectives

In summary, these data show that galactose metabolism greatly differs in neuronal HT-22 cells compared to CHO cells. UDP-Gal levels significantly increased in the presence of galactose in both HT-22 and CHO cells, whereas the increase was higher in CHO cells, indicating that HT-22 cells have a limited ability to metabolize galactose. UDP-Glc levels in contrary were hardly affected by galactose treatment. Both cell lines highly accumulated Gal-1-P, but the accumulation was much higher in neuronal HT-22 cells. It was concluded that GALT restricts the galactose metabolism in both cell lines, but particular in neuronal HT-22 cells.
Furthermore, UDP-GlcNAc and UDP-GalNAc levels were also found to be regulated differently in neuronal HT-22 cells compared to CHO cells. CHO cells are able to maintain UDP-GlcNAc/UDP-GalNAc levels in the presence of galactose and absence of glucose, whereas the levels decreased significantly in neuronal HT-22 cells. The reasons for this observation are not clear. CHO cells might maintain the levels by glycogenolysis which is not possible in neuronal cells due to the lack of glycogen as a glucose storage form. When glycogenolysis is used, the maintenance is independent from galactose metabolism. However, Gal-1-P that is less accumulated in CHO cells compared to neuronal HT-22 cells is a known inhibitor of phosphoglucomutase and glycogen phosphorylase and might also contribute to the maintenance. Furthermore, the ratio of galactose routed into glycolysis versus HBP may also influence UDP-GlcNAc/UDP-GalNAc levels. To evaluate which of the proposed mechanisms caused the maintenance of UDP-GlcNAc/UDP-GalNAc levels in CHO cells or the decrease in HT-22 cells, experiments with ^{13}C-labeled galactose and subsequent analysis with ^{1}H,^{13}C-HSQC NMR spectroscopy should be accomplished.
To date, there is only little information about the pathogenesis of galactosemia and it is still not known why certain tissues or organs are more prone to galactose toxicity. As a first step it is important to investigate the metabolite levels and metabolic pathways in different cell types

as realized in this study. Evaluation of the precise mechanisms of the harmful secondary effects resulting from the limited ability of neuronal cells to metabolize galactose will give valuable information of galactose neurotoxicity. In this regard it should be focused on the formation of activated sugar nucleotides and the biosynthesis of glycoproteins and glycolipids, including *O*-GlcNAcylated proteins.

4.4 Effect of Limited Glucose Availability and Glucose-Deprivation on Brain Cells

4.4.1 Influence of Glucose Concentrations on Activated Sugar Nucleotide Levels in HT-22 Cells

Glucose deprivation or more precisely hypoglycemia is an important factor to which cells have to adapt in several diseases, including cancer (Gatenby & Gillies, 2004), diabetes (Cryer *et al*., 2003), or neurodegenerative diseases such as AD (Mosconi *et al*., 2008). These diseases are also all associated with changes in protein *O*-GlcNAcylation (Dias & Hart, 2007; Slawson *et al*., 2010).

In accordance with previous studies (Marshall *et al*., 2004; Taylor *et al*., 2008; Taylor *et al*., 2009), I have shown that UDP-GlcNAc levels in HT-22 cells depend on changes in glucose concentration. *O*-GlcNAcylation of proteins is regulated by UDP-GlcNAc availability because OGT is highly sensitive to varying UDP-GlcNAc concentrations (Haltiwanger *et al*., 1992; Kreppel *et al*., 1997; Kreppel & Hart, 1999). Based on this, flux through the HBP and *O*-GlcNAcylation have been proposed as a nutrient sensor (Wells *et al*., 2003; Zachara & Hart, 2004; Love & Hanover, 2005). At this point I would have expected a linear decrease of UDP-GlcNAc levels with decreasing glucose concentration. However, this was not the case. I detected a sharp decline in the UDP-GlcNAc concentration in HT-22 cells when the glucose concentration in the culture medium was reduced from 18 mM to 12 mM. However, the UDP-GlcNAc levels in HT-22 cells remained constant between 25 mM and 18 mM glucose and between 12 mM and 6 mM glucose. Hence, the UDP-GlcNAc concentration in neuronal HT-22 cells does not decline linearly with decreasing glucose concentrations.

A decrease in UDP-GlcNAc can be caused by a decrease in its synthesis, by enhanced *O*-GlcNAcylation or a combination of both. Since increases in UDP-GlcNAc under hyperglycemic conditions have been shown to enhance protein *O*-GlcNAcylation, it would seem likely that hypoglycemia leads to decreased *O*-GlcNAcylation. However, exactly the

opposite is true. Enhanced *O*-GlcNAcylation was observed in glucose deprived human hepatocellular carcinoma (HepG2) (Taylor *et al*., 2008; Talor *et al*., 2009), Neuro-2a neuroblastoma (Cheung & Hart, 2008), lung carcinoma A549 (Kang *et al*., 2009) cells, primary neonatal cardiomyocytes (Zou *et al*., 2012), and various other cells (Kang *et al*., 2009; Zou *et al*., 2012). While there is great consensus that glucose deprivation enhances *O*-GlcNAcylation the mechanisms leading to this phenomenon are not yet clear and seem to be a highly cell-specific feature. In Neuro-2a neuroblastoma cells, Cheung and Hart (Cheung & Hart, 2008) detected that OGT mRNA and protein expression was increased via activation of the AMP-activated protein kinase (AMPK) pathway in glucose deprived cells. AMPK is a nutrient sensor that is activated by increases in the AMP to ATP ratio. It maintains energy homeostasis by facilitating ATP production by increasing the activity or expression of proteins involved in ATP synthesis, whereas metabolic pathways that consume ATP are downregulated (Hardie *et al*., 2012). OGT activity on the other hand was found to be regulated by the stress-activated p38 mitogen-activated protein kinase (MAPK) pathway in glucose deprived Neuro-2a cells (Cheung & Hart, 2008). Taylor *et al*. detected in glucose deprived HepG2 cells that the increase in *O*-GlcNAcylation was mediated by an increase in OGT mRNA and proteins levels, as well as a decrease in OGA protein levels (Taylor *et al*., 2008). However, the increase in *O*-GlcNAcylation was not mediated by the AMPK pathway in these cells (Taylor *et al*., 2009). Furthermore, these authors investigated that prevention of the decrease in HBP flux by low doses of GlcN reversed the effects induced by glucose deprivation on OGT expression and *O*-GlcNAcylation (Taylor *et al*., 2009). These observations lead to the assumption that decreased HBP flux mediates increased *O*-GlcNAcylation in HepG2 cells (Taylor *et al*., 2009). Kang *et al*. detected unchanged *O*-GlcNAc protein levels in glucose-deprived A549 cells, but they observed that OGT itself was less *O*-GlcNAcylated which led to increased OGT activity (Kang *et al*., 2009). Furthermore, OGA protein and activity were found to be reduced (Kang *et al*., 2009). These results are in contrast to the above mentioned studies, where OGT protein was up-regulated in response to glucose deprivation (Cheung & Hart, 2008; Taylor *et al*., 2009). Increased *O*-GlcNAcylation was also independent on activation of the AMPK pathway in A594 cells (Kang *et al*., 2009). The study by Kang *et al*. also showed that cultured cancer cells use glycogenolysis for the enhanced *O*-GlcNAcylation observed in glucose deprived cells and not for generating ATP (Kang *et al*., 2009). In line with Kang *et al*., Zou *et al*. detected decreased OGA, but not OGT protein in primary neonatal cardiomyocytes (Zou *et al*., 2012). Enzyme activities were not determined in this study. Their results indicate that increased cellular calcium and subsequent activation of calcium/calmodulin-dependent kinase (CaMKII) but not p38 MAPK are

involved in increased *O*-GlcNAc levels in glucose deprived cells (Zou *et al*., 2012). Zou *et al*. also found that the increase in *O*-GlcNAcylation could be diminished or even blocked by GlcN (Zou *et al*., 2012).

Based on these investigations one might hypothesize that the sharp decline observed between 18 mM and 12 mM glucose may be due to the onset of increased *O*-GlcNAcylation in HT-22 cells. One might assume that there is a threshold glucose concentration in HT-22 when increased *O*-GlcNAcylation starts and this threshold concentration lies between 18 mM and 12 mM glucose in HT-22 cells when cultured for 72 h. This assumption would at least explain why I did not detect a linear decrease in the UDP-GlcNAc level with decreasing glucose concentration. Taylor *et al*. observed a steady decline in UDP-GlcNAc levels as well as *O*-GlcNAcylation in the first 6 h of glucose deprivation, before induction of OGT occurred and they therefore suggested a negative feedback mechanism (Taylor *et al*., 2009). These observations, especially that *O*-GlcNAcylation is initially decreased in glucose derived cells, further indicates that the sharp decrease in UDP-GlcNAc levels I observed may be the threshold concentration where a switch from decreased *O*-GlcNAcylation to increased *O*-GlcNAcylation happens initiated by a specific response.

In this regard it is interesting to note that Zou *et al*. (Zou *et al*., 2012) observed the biggest increase in *O*-GlcNAc levels at a concentration between 3 mM and 4 mM of extracellular glucose in primary neonatal cardiomyocytes after a incubation time of 24 h. This is a concentration that should pretty much coincide with a starting concentration of 12 mM glucose but with an incubation time of 72 h.

Taylor *et al*. and Zou *et al*. assume that enhanced *O*-GlcNAcylation is at least in part triggered by a decrease in HBP flux, because the effect could be reversed by GlcN (Taylor *et al*., 2009; Zou *et al*., 2012). I did not observe a significant decrease in the UDP-GlcNAc level in HT-22 cells before the sharp decline in UDP-GlcNAc concentration occurred. This may indicate that there was no noticeable decrease in HBP flux before the hypothesized increased *O*-GlcNAcylation, reflected by the sharp and not linear decrease occurred. However, to evaluate this, the glucose concentration steps (25 mM, 18 mM, 12 mM, 6 mM) have to be minimized.

Before it was shown that glucose deprivation just like hyperglycemic conditions lead to enhanced *O*-GlcNAcylation, it was believed that *O*-GlcNAcylation was entirely regulated by substrate availability. The results may emphasize that formation of UDP-GlcNAc and in this context also *O*-GlcNAcylation may not only regulated by nutrient availability.

In addition to UDP-GlcNAc levels, I tested the mRNA expression of the HBP enzymes GFAT, GlcN-6-P *N*-acetyltransferase, and UDP-GlcNAc pyrophosphorylase using qRT-PCR

in HT-22 cells cultured for 72 h in medium containing 25 mM glucose compared to cells cultured 12 mM glucose. Both, the GFAT1 and GFAT2 isoforms were found to be expressed in neuronal HT-22 cells, whereas GFAT1 exhibited the higher mRNA level. I detected no significant changes in the expression of GFAT1 and GFAT2 mRNA in cells cultured in medium containing 25 mM glucose compared to 12 mM glucose. To the best of my knowledge there are no studies investigating the mRNA expression of GFAT in hypoglycemic conditions. Kang *et al*. on the contrary observed increased GFAT protein under glucose deprivation (Kang *et al*., 2009). However, mRNA levels and protein levels do not necessarily correlate (Gry *et al*., 2009). Furthermore, GFAT mRNA, as well as protein expression in hypoglycemia could be a cell type specific feature. Hyperglycemic conditions revealed also no effect on GFAT mRNA expression in human myotubes (Weigert *et al*., 2003), MDA468 breast cancer cells (Paterson & Kudlow, 1995), and muscle and liver tissue of hyperglycemia-induced diabetic rats (Robinson *et al*., 1995). Although at least the data of GFAT mRNA expression indicate that GFAT is not involved in enhanced *O*-GlcNAcylation in both hyper- and hypoglycemic conditions further studies, especially in hypoglycemic conditions, are required.

In contrast to GFAT, the mRNA levels of GlcN-6-P *N*-acetyltransferase and UDP-GlcNAc pyrophosphorylase were significantly decreased in HT-22 cells incubated with 12 mM glucose compared to 25 mM glucose. These results were quite surprising, because I would have expected an increase in the mRNA level of the enzymes of the HBP to counteract the decreased HBP flux due to limited glucose availability. Decreased mRNA levels will further contribute to decreased UDP-GlcNAc levels and it is interesting to know how cells accomplish the increase in *O*-GlcNAcylation under these circumstances.

The above mentioned results refer solely to UDP-GlcNAc and the HBP. However, the sharp decrease between a glucose concentration of 12 mM and 18 mM was not only detected in UDP-GlcNAc, but also in UDP-GalNAc, UDP-Glc, UDP-Gal, UDP-GlcUA and UDP-HexNAc. How can this be explained? UDP-GalNAc is the epimerization product of UDP-GlcNAc. Therefore, it is consequential that UDP-GalNAc levels decrease in the same manner as UDP-GlcNAc. UDP-Glc and UDP-Gal can both be converted to Glc-6-P that can fuel the HBP when glucose is limited. Since neuronal cells do not contain glycogen as glucose storage form, this pathway may be probable. UDP-GlcUA cannot be converted into an intermediate that fuels the HBP, however, since UDP-GlcUA is the oxidation product of UDP-Glc, it is expected that the level of UDP-GlcUA decrease with decreasing UDP-Glc concentrations. On

this account glucose deprivation may not only alter *O*-GlcNAcylation in cells, but may also severely affect the synthesis of many other glycans.

4.4.2 UDP-GlcNAc Levels in Glucose-Deprived Neuronal Cells and Astrocytes

In glucose-deprived cell cultures, glucose is supplied from intracellular glycogen through glycogenolysis. Thus the degree of decrease in the UDP-GlcNAc leves by glucose deprivation may depend on the ability of cells to store glucose as glycogen. Since astrocytes contain glycogen, but neuronal cells not (Cataldo & Broadwell, 1986; Magistretti *et al*., 1993), I was curious to figure out how UDP-GlcNAc levels decrease in glucose-deprived primary astrocytes compared to neuronal HT-22 cells. I compared UDP-GlcNAc levels in cells glucose-deprived for 12 h and 18 h compared to controls that were cultured in medium containing 25 mM glucose for the same time span. In both cell types UDP-GlcNAc levels decreased significantly when cells were glucose deprived for 12 h and prolonged glucose-deprivation to 18 h did not significantly further reduce UDP-GlcNAc levels compared to 12 h glucose deprivation. As a side note, in HepG2 cells induction of *O*-GlcNAcylation appeared at 12 h glucose deprivation and therefore it will be of interest to assay UDP-GlcNAc levels at this time of occurrence (Taylor *et al*., 2009). However, the degree of the decrease in UDP-GlcNAc concentration differed greatly in both cell lines. In HT-22 cells, glucose deprivation led to an 83 % decrease in the UDP-GlcNAc level, whereas in glycogen containing primary astrocytes a decrease of only 46 % was observed. These results clearly demonstrate that astrocytes are much more resistant against glucose deprivation than neuronal HT-22 cells and that most likely glycogen is used for maintaining UDP-GlcNAc synthesis in severe hypoglycemia. The observation that glycogen is used as a source for UDP-GlcNAc was also observed in cancer cells by Kang *et al*., 2009. These authors further investigated that glycogen is preferentially used for UDP-GlcNAc synthesis and not for generation of ATP because PFK1, a pivotal enzyme of glycolysis (Uyeda, 1979), was found to exhibit decreased protein expression levels in glucose deprived A549 lung carcinoma cells (Kang *et al*., 2009). In addition, increased *O*-GlcNAcylation of glycogen synthase was observed in glucose-deprived HepG2 cells which led to decreased activity of the enzyme (Taylor *et al*., 2009).

4.4.3 Conclusions

In summary, I have shown that UDP-GlcNAc levels do not decrease linearly with decreasing glucose concentration in HT-22 cells. Between a concentration of 18 mM and 12 mM glucose

there seems to be a threshold value which may reflect the induction of increased *O*-GlcNAcylation commonly observed in glucose-deprived cells. This characteristic was not only observed in UDP-GlcNAc levels, but also in levels of UDP-GalNAc, UDP-Glc, UDP-Gal, and UDP-GlcUA. My data reveal the changes of UDP-GlcNAc and other activated sugar nucleotides in response to physiological conditions occurring in diseases such as diabetes, cancer, or AD that are associated with aberrant *O*-GlcNAcylation.

For future studies, it would be interesting to carry out this experiment in other cell types, e.g. astrocytes and to investigate whether the decrease in UDP-GlcNAc levels is also non-linear with a certain threshold concentration where the UDP-GlcNAc concentration declines sharply and if so, it would be of interest to investigate whether these threshold concentrations vary in different cell types. Moreover, OGT and OGA mRNA and protein levels, as well as, activity or *O*-GlcNAc levels could be examined and investigated if these correlate with the threshold concentration. Even though it appears that enhanced *O*-GlcNAcylation is a general response to glucose deprivation in cells, it should be tested if this is the case in neuronal HT-22 cells.

Furthermore, I have shown that GFAT – the rate-limiting enzyme of the HBP – is not involved in provoking the sharp decrease in UDP-GlcNAc levels in glucose-deprived HT-22 cells because its mRNA expression was not altered. GlcN-6-P *N*-acetyltransferase and UDP-GlcNAc pyrophosphorylase mRNA levels in contrast were significantly decreased in HT-22 cells incubated with 12 mM glucose instead of 25 mM and therefore definitely contributing to the decreased UDP-GlcNAc levels detected. These results are kind of controversial to the commonly observed increase in *O*-GlcNAcylation in glucose-deprived cells. However, there is limited knowledge about mRNA expression of HBP enzymes in hypoglycemic conditions and further studies, also on the protein expression and enzyme activity of these enzymes, are needed to understand the mechanisms.

Moreover, I have shown that the decrease in UDP-GlcNAc is much more pronounced in neuronal HT-22 cells that do not have the ability to store glucose as glycogen, compared to glycogen containing astrocytes. This also implies that glycogen is used for synthesis of UDP-GlcNAc in hypoglycemia.

These results provide important information how UDP-GlcNAc synthesis and probably protein *O*-GlcNAcylation are regulated during hypoglycemia and may lead to better insights how these mechanisms contribute to several human diseases.

4.5 NO-Induced Metabolic Changes in Astrocytes

NO is an important intercellular messenger in the CNS (Garthwaite & Boulton, 1995) that either prevents or causes apoptosis of cells in different biological systems (Melino *et al*., 2000; Sastry & Rao, 2000). Previous studies have shown that treatment of astrocytes with NO switches astrocytes into a glycolytic state, while TCA cycle and thus mitochondrial respiration are inhibited. These studies mainly focused on the mRNA level of glycolytic enzymes, as well as glucose and lactate transporters or on particular metabolites of specific enzymatic pathways, such as glucose, lactate, or Fru-2,6-BP (Bolaños *et al*., 1994; Almeida *et al*.,2001; Almeida *et al*., 2004; Marcillac *et al*., 2011; Brix *et al*., 2012).

NMR spectroscopy is a practical analytical method for simultaneous and nonselective detection and quantification of small metabolites through various metabolic pathways, like glycolysis and TCA cycle. On this account NMR spectroscopy has been proven to be useful in studying astrocytic and neuronal metabolism (e.g. Brand *et al*., 1993; Zwingmann & Leibfritz, 2003).

In these experiments I used, in addition to ^{1}H-NMR spectroscopy with unlabeled substances, [1-^{13}C]glucose as a precursor for selective labeling of metabolites. ^{13}C-labeling not only reduces the amount of cell mass needed for metabolite detection, it also provides the possibility to record isotope-edited ^{1}H,^{13}C-HSQC NMR spectra, which have the advantage of reduced complexity compared to ^{1}H-NMR spectra.

4.5.1 NO Enhances Glucose Uptake and Lactate Release in Astrocytes

I have determined the glycolytic flux in astrocytes by quantifying *de novo* lactate synthesis using ^{13}C-labeled glucose and analysis by NMR spectroscopy. I have shown that treatment of primary cortical astrocytes with nitric oxide leads to increased glucose consumption and lactate release into the medium. Both, glucose uptake and lactate release are doubled after NO-treatment under these conditions. The increase in lactate detected arises solely from [1-^{13}C]glucose. This implies that glycolysis is enhanced in astrocytes treated with NO. There are mainly two reasons why cells, or in particular astrocytes, up-regulate glycolysis and hence lactate formation. First, to prevent energy (ATP) depletion when the respiratory chain is inhibited, and second, to supply neurons with lactate as an energy substrate during neuronal activation (Pellerein & Magistretti, 1994).

The first reason for enhanced glycolysis is widely discussed in the literature, since excessive NO and its byproducts are potent inhibitors of the mitochondrial respiratory chain as detected

in several systems, including astrocytes (Bolaños *et al*., 1994; Mitrovic *et al*., 1994; Heales *et al*., 1994; Brown, 1995; Barker *et al*., 1996; Almeida *et al*., 2001; Almeida *et al*., 2004) and neurons (Bolaños *et al*., 1995; Bolaños *et al*., 1996; Almeida *et al*., 2001; Almeida *et al*., 2004). The effect of NO on the respiratory chain of astrocytes will be discussed in detail later in this chapter.

It was shown that inhibition of the respiratory chain by NO (Moncada *et al*., 1991; Melino *et al*., 2000; Sastry & Rao, 2000) leads to enhanced glycolysis in astrocytes to maintain ATP-levels (Almeida *et al*., 2004). This response, however, was not observed in neurons (Almeida *et al*., 2004). Almeida *et al*. have shown that treatment with NO leads to a 25 % decrease in ATP concentration in both astrocytes and neurons, but activation of glycolysis in astrocytes prevented further ATP reduction, whereas in neurons the ATP-depletion sustains. This decrease led to enhanced apoptotic cell death in neurons, whereas in astrocytes no increased apoptosis was observed (Almeida *et al*., 2001). Indeed, I could not detect any changes in cell viability in astrocytes treated with 0,8 mM of the NO-donor DETA-NONOate for 12 h, as evaluated by trypan blue staining. Astrocytes are regarded as "glycolytic" cells because other mitochondrial inhibitors, such as antimycin, robustly stimulate glucose metabolism through glycolysis, whereas this response fails in neurons to maintain ATP production (Pauwels *et al*., 1985; Walz & Mukerji, 1988). In a subsequent study, Almeida *et al*. have shown that NO rapidly increases the activity of PFK1, a key regulator of glycolysis (Uyeda, 1979), in astrocytes (Almeida *et al*., 2004). They also observed an increase in the concentration of fructose-2,6-bisphosphate (Fru-2,6-BP), an allosteric activator of PFK1. In neurons, in turn, NO failed to alter PFK1 activity and Fru-2,6-PB concentration (Almeida *et al*., 2004). They assumed that this failure may be due to virtual absence of PFK2 (also referred to as PFKFB3), the enzyme responsible for Fru-2,6-BP production, in neurons (Almeida *et al*., 2001; Almeida *et al*., 2004). Both results (increase in PFK1 activity and Fru-2,6-BP concentration) are consistent with the results obtained by Brix *et al*.. These researchers detected an increase in PFK1 mRNA level and PFKFB3 mRNA level (Brix *et al*., 2012). This study has also shown that primary cultures of mouse cortical astrocytes treated with NO induce an enhancement in the expression of genes encoding various glycolytic enzymes as well as transporters for glucose and lactate and they found that this enhancement was due to HIF-1α stabilization (Brix *et al*., 2012). This NO-mediated HIF-1α stabilization was detected in astrocytes but not in neurons (Brix *et al*., 2012). Besides, it was recently shown that NO induces the expression of MCT4 in astrocytes, leading to a persisting enhancement in lactate production and release in astrocytes (Marcillac *et al*., 2011). Interestingly, NO synthesized in endothelial cells may be the source of NO to stabilize HIF-1α in astrocytes (Brix *et al*., 2012). Brix *et al.* found that

endothelial cells, expressing the eNOS isoform, produced the largest amount of NO in cell culture (Brix *et al*., 2012). The end-feet of astrocytes enwrap virtually all blood vessels in the brain and are therefore in close contact to endothelial cells. Accordingly, stabilization of HIF-1α and enhancement in MCT4 expression, as well as increased lactate production in astrocytes cocultured with primary cultures of brain vascular endothelial cells was observed. This effect was hindered when cells were treated with the NOS inhibitor L-NAME and was not seen when astrocytes were cocultured with neurons. The findings of Brix *et al*. suggest that endothelial cell-derived NO leads to elevated glycolytic activity in astrocytes via astrocytic HIF-1α activation (Brix *et al*., 2012). These findings support the role of NO as an important messenger molecule in the energy metabolism of the CNS by stabilizing HIF-1α, leading to regulation of glycolysis and lactate production in astrocytes, and subsequent lactate release to fuel neuronal energy needs.

Furthermore, I have shown that fractional ^{13}C-enrichment in extracellular lactate, in contrast to an absolute increase of synthesis of ^{13}C-lactate from [1-^{13}C]glucose, showed no significant alterations when astrocytes were exposed to NO. This means that the contribution of lactate derived from flux of [1-^{13}C]glucose through glycolysis or lactate produced from unlabeled precursors is the same for both conditions. The fractional ^{13}C-enrichment in lactate never reaches the maximal theoretical value due to attenuation of the label by incorporation of pyruvate and thus lactate derived from interconversion of unlabeled precursors. ^{13}C-enrichment in lactate from [1-^{13}C]glucose of the order of 40 %, as I observed in my studies, indicates a high aerobic glycolytic flux in primary astrocytes (Zwingmann & Leibfritz, 2003). As already described, unlabeled lactate can be produced from unlabeled precursors such as fatty acids, amino acids present in the culture medium, involvement of the pentose phosphate pathway (PPP), or formation of lactate from TCA cycle intermediates. Glycogenolysis in astrocytes could also contribute to a decrease in ^{13}C-enrichment in lactate. Glycogen is almost entirely localized in astrocytes and serves as an endogenous energy source. During glycogenolysis, astrocytes produce lactate, which then serves as an energy substrate for neurons (Dringen *et al*., 1993; Brown *et al*., 2004; Magistretti, 2006). For this reason, glycogenolysis is, in addition to glycolysis, required for the response of astrocytes to increasing energy demands. Hence I would have expected a decrease in ^{13}C-enrichment when astrocytes are shifted into a glycolytic state. Since I did not observe any significant changes in fractional ^{13}C-enrichment, these results may indicate that glycogenolysis is not enhanced in astrocytes treated with NO. However, it has to be kept in mind, that glycogen itself gets ^{13}C-labeled through incorporation of [1-^{13}C]glucose. Enhanced glycogenolysis can only be in part responsible for a decrease in ^{13}C-enrichment if and only if a small fraction of glycogen is ^{13}C-

labeled. Another fact to consider is that a glucose concentration of 22 mM used in my cell culture experiments exceeds the concentration of glucose in the brain by far. The normal extracellular glucose concentration in the brain ranges between 1 - 2 mM (McNay & Gold, 1999). The glucose supply in my experiments was far from being consumed and therefore there was no necessity of the astrocytes to break down their glycogen storage. If the experiments had been carried out at the edge of sufficient glucose availability, glycogenolysis would have been more likely.

To summarize, I detected elevated glycolysis in astrocytes treated with NO. This elevation is most likely a defense against inhibition of the respiratory chain. My results may also indicate that enhanced glycogenolysis, does not occur under these conditions because glucose is sufficiently available.

4.5.2 Importance of Astrocytic TCA Cycle under Nitrosative Stress

Accumulation of the TCA intermediate citrate in cell extracts of astrocytes treated with NO was observed. This intracellular accumulation of citrate is not a big surprise, since NO is known to inhibit aconitase, the enzyme that catalyzes the reversible isomerization of citrate to isocitrate (Breusch, 1937), the initiating step of the TCA cycle. Direct detection of citrate accumulation in NO-treated astrocytes, however, has not been shown before. The isomerization by aconitase is a two-step reaction, involving dehydration and hydration with the formation of the intermediate *cis*-aconitate. Two aconitase isoenzymes exist in mammalian cells, the mitochondrial aconitase and the cytosolic isoform, which also functions as iron-responsive element 1 (IRP1) having a role in the regulation of iron metabolism (Tong & Rouault, 2007). Aconitase is an iron-sulfur proteins with a labile 4Fe-4S cluster in its active site. This cluster can be readily disassembled by various oxidants to form an inactive 3Fe-4S cluster (Beinert *et al*., 1996). Nitric oxide can bind to the iron center of aconitase and thus reversibly inhibit the enzyme (Andersson *et al*., 1998; Cooper, 1999). However, this disruption occurs at very low rates, since NO is a weak oxidant (Castro *et al*., 1994). Peroxynitrite ($ONOO^-$), however, is an oxidizing and nitrating agent that is rapidly formed by a reaction between the superoxide anion ($O_2^{\bullet -}$) and NO (Beckman *et al*., 1990; Radi *et al*., 1991). Peroxynitrite can rapidly oxidize and disrupt aconitase by release of iron from the 4Fe-4S cluster (Castro *et al*., 1994; Hausladen & Fridovich, 1994; Cheung *et al*., 1998; Han *et al*., 2005). Peroxynitrite also causes irreversible nitration of tyrosine and oxidation of the thiol-groups of cysteine residues in the active center of aconitase which also leads to inactivation of the enzyme (Ischiropoulos *et al*., 1992; Stamler, 1994; Zou *et al*., 1997). Thiols, in particular

GSH, are able to protect aconitase from the harmful effect of peroxynitrite (Cheung *et al*., 1998).

Citrate is a key metabolite that interfaces TCA cycle and mitochondrial respiration to glycolysis and fatty acid synthesis in the cytosol. During energy deficiency (low ATP), citrate is metabolized through the TCA cycle to produce the reducing equivalents NADH and $FADH_2$, which are essential for ATP production in the respiratory chain. When the ATP level is high, citrate is transferred into the cytosol via a tricarboxylate transporter (Bisaccia *et al*., 1989), where it is metabolized to cytosolic acetyl-CoA by the enzyme ATP-citrate-lyase and subsequently incorporated into fatty acids for energy storage (Cheema-Dhadli & Halperin, 1976). It is assumed that constriction of the TCA cycle due to mitochondrial aconitase inhibition may lead to obesity, insulin resistance and diabetes (Belfiore & Iannello, 1998; Wlodek & Gonzales, 2003; Wolfgang & Lane, 2006). Citrate is also an allosteric inhibitor of phosphofructokinase, the rate limiting enzyme of glycolysis in the cytosol (Denton & Randle, 1966; Randle, 1998). Since citrate is shuttled into the cytosol when ATP concentrations are high, citrate efflux leads to suppression of glycolysis. Inhibition of aconitase can, for this reason, lead to a decrease in the ATP level, stimulation of lipogenesis, and to a decrease in glycolysis. However, in astrocytes treated with NO, accumulation of citrate does not lead to decreased glycolysis. Quite to the contrary, enhanced glycolysis is observed by us and others (Almeida *et al*., 2001; Almeida *et al*., 2004; Marcillac *et al*., 2011; Brix *et al*., 2012), as judged by enhanced glucose uptake and *de novo* synthesis of lactate from [1-^{13}C]glucose. The fact that citrate does not inhibit glycolysis may indicate that citrate takes over a different task in astrocytes coping with nitrous stress.

In addition to NO and peroxynitrite, aconitase was also found to be inhibited by other ROS like the superoxide anion (Gardner *et al*., 1994; Patel *et al*., 1996; Gardner *et al*., 1997) and hydrogen peroxide (H_2O_2) (Tretter & Adam-Vizi, 2000). The liberation of reactive iron, due to the disassembly of aconitase, may further enhance oxidative damage of cellular components (Lipinski *et al*., 2005). It was shown that mitochondrial aconitase is more sensitive to ROS than the cytosolic isoform (Matasova & Popova, 2008). Treatment of HeLa S3 cells with the NO-donor DEA-NONOate (Diethylammonium (Z)-1-(N,N-diethylamino)diazen-1-ium-1,2-diolate) also led to inhibition of mitochondrial aconitase, whereas treatment with H_2O_2 resulted in inhibition of cytosolic aconitase (Tong & Rouault, 2007).

In contrast to the intracellular accumulation of citrate, an increase of citrate release into the cell culture medium, however, was not detected in my experiments. Citrate release from astrocytes has been shown in *in vitro* studies. Citrate is exclusively released by astrocytes and

is the only TCA cycle intermediate that can be found in large amounts in the culture media (Sonnewald *et al*., 1991; Westergaard *et al*., 1994). Citrate efflux was found to be higher in cerebellar astrocytes than cortical astrocytes (Westergaard *et al*., 1994). Therefore it may be the most important TCA cycle intermediate that is released by astrocytes and subsequently utilized by neurons. Since citrate release remains constant, although it is highly accumulated inside the cell, the results may indicate that the accumulated intracellular citrate is used for protection of astrocytes against the deleterious effects of NO and/or peroxynitrite. In contrast to my observation, Hassel *et al.* observed that the net export of citrate into the culture medium increased, when the aconitase inhibitor fluorocitrate was used for TCA cycle inhibition in astrocytes (Hassel *et al*., 1994).

A protective effect of citrate on astrocytes has been shown before. Kelleher *et al*. demonstrated that citrate protects astrocytes, but not neurons, from hypoxia. However, if both cell types were co-cultured, citrate increased neuronal viability through its effect on astrocytes (Kelleher *et al*., 1996). Sonnewald *et al*., on the contrary, did not observe a protective effect of citrate during hypoxia, but they observed protective effects of citrate during prolonged hypoglycemia (Sonnewald *et al*., 2002).

Kelleher *et al*. proposed two possible mechanism of citrate protection in the CNS under hypoxia (Kelleher *et al*., 1996). 1) They assumed on basis of a previous publication, where was Fru-1,6-BP used instead of citrate as an inhibitor of phosphofructokinase, that protection of astrocytes is not the result of increased glycolysis (Gregory *et al*., 1990). They assumed that glucose metabolism is shifted to the PPP, because citrate is an inhibitor of glycolysis and they have demonstrated this shift to the PPP in Fru-1,6-BP treated cells (Kelleher *et al*., 1996). This shift ensures that ATP-production can be maintained. 2) Citrate can chelate divalent cations like Ca^{2+}. Mitochondria are major calcium buffers and NO is known to stimulate Ca^{2+} influx into neurons (Brorson & Zhang, 1997; Brorson *et al*., 1997; Marks *et al*., 2005) and astrocytes (Bal-Price *et al*., 2002). Therefore, citrate can protect the CNS by reducing Ca^{2+} influx into cells.

The first hypothesis for the protective effect of citrate cannot be brought in line with my findings of citrate accumulation in NO-treated astrocytes. As said, although citrate is an inhibitor of glycolysis, glycolysis was found to be enhanced in my experiments. Besides, no shift towards PPP was observed. Enhanced involvement of the PPP would also lead to a decrease in ^{13}C-enrichment of lactate in NO-treated astrocytes, which was not observed in my studies.

The second hypothesis, that citrate serves as a chelator of divalent cations, is more likely in my experiments. However, Ca^{2+} increase requires activation of the *N*-methyl-D-aspartate

(NMDA) receptor by extracellular glutamate. Since glutamate is not supplemented into the culture media and glutamate is not detected in the incubation media of astrocytes, increased Ca^{2+} influx should not be an issue, at least in the experimental conditions I used. But, citrate is also able to chelate ferrous iron ions (Fe^{2+}) (Bradbury, 1997). As already described, inhibition of aconitase by NO leads to release of Fe^{2+} from the 4Fe-4S cluster, which may enhance oxidative damage in cells (Lipinski *et al*., 2005). By chelating Fe^{2+}, citrate can potentially protect astrocytes from the harmful effects of this iron ion.

Given that 1) citrate accumulated due to inhibition of aconitase does not inhibit glycolysis in my experiments, although it is a known inhibitor of phosphofructokinase (Denton & Randle, 1966; Randle, 1998) that is known to catalyze the rate limiting stept of glycolysis, and that 2) I did not observe enhanced citrate release into the cell culture medium due to NO-treatment, and that 3) treatment of HeLa S3 cells with the NO-donor DEA-NONOate was found to inhibit mitochondrial aconitase, but not cytosolic aconitase (Tong & Rouault, 2007) it may be hypothesized that citrate is not transferred into the cytosol. Citrate it is most likely needed in the mitochondria to protect astrocytes against damage by NO and/or peroxynitrite. Staying in the mitochondrion, citrate will not be able to inhibit glycolysis in the cytosol. Another possibility may be that if citrate is transferred into the cytosol, it is rapidly converted into acetyl-CoA by cytosolic ATP-citrate-lyase and maybe used for fatty acid synthesis, which will be discussed in the next chapter.

Since citrate is produced in mitochondria, to be released into the medium it has to be transported from the mitochondria into the cytosol and from the cytosol into the medium. The transport across the inner mitochondrial membrane is mediated by the citrate carrier (CIC; also known as tricarboxylate transporter) in exchange for cytosolic malate (citrate-malate antiport) (Palmieri & Pierri, 2010; Sun *et al*., 2010). From there it can passively diffuse through an anion selective channel through the outer mitochondrial membrane to reach the cytoplasm (Sun *et al*., 2010). CIC is a nuclear-encoded protein, belonging to the mitochondrial carrier gene family SLC25 (Palmieri *et al*., 1992; Palmieri, 2004), that catalyzes the electroneutral transport of citrate (or isocitrate, and cis-aconitate) in exchange for another tricarboxylate, a dicarboxylate (like malate or succinate), or phosphoenolpyruvate (Palmieri *et al*., 1972). In the case of citrate/malate, CIC only transports single protonated H-citrate^{2-} against the unprotonated malate^{2-} (Palmieri, 2004). In the cytosol citrate is cleaved by ATP-citrate-lyase to oxaloacetate and acetyl-CoA mainly for lipid biosynthesis. Oxaloacetate can be reduced to malate, which is either converted to pyruvate by malic enzyme or it can be used as counter-substrate for further citrate export of the mitochondrion (Palmieri, 2004). To export the highly accumulated citrate observed in my experiments out of the mitochondria,

sufficient amounts of cytosolic malate are required. However, malate (as well as succinate) levels were too low to be detected by NMR spectroscopy in my experiments; supporting the hypothesis that citrate remains in the mitochondrion. Furthermore, CIC mRNA expression and protein levels are high in liver (where fatty acid synthesis takes place), pancreas, and kidney, but are low or absent in brain, heart, skeletal muscle, placenta and lung (Huizing *et al*., 1998). This means that in addition to the low malate levels, there are also probably only few CIC transporters in astrocytes to accomplish the transport. Interestingly, it was shown that GSH uptake from the cytosol into mitochondria was partially inhibited by citrate in brain mitochondria (Wadey *et al*., 2009). Hence, high cytosolic citrate levels would decrease the protecting effect of GSH against NO and/or peroxynitrite in mitochondria.

Whilst citrate transport out of the mitochondria is known, citrate transport across the plasma membrane is not well investigated. For citrate uptake into the cytosol different transporters have been identified in brain tissue. The sodium-dependent citrate transporter (NaCT) is in brain almost exclusively expressed in neurons and therefore most likely responsible for uptake of citrate into neurons (Inoue *et al*., 2002a; Inoue *et al*., 2002b; Yodoya *et al*., 2006). Uptake of citrate released from astrocytes is necessary to supply neurons with TCA cycle intermediates to replenish the TCA cycle for synthesis of the neurotransmitters glutamate and γ-aminobutyric acid (GABA) and is known to modulate neuronal excitability (Westergaard *et al*., 1994; Schousboe *et al*., 1997). The plasma membrane transporter NaDC3 was found to be mainly localized in astrocytes and mediates citrate transport inwardly (Yodoya *et al*., 2006). The transport mechanisms and transporter for citrate release by astrocytes, however, are not known yet. It is so far known that citrate synthesis, as well as release, is probably controlled by extracellular K^+ ions (Westergaard *et al*., 1994; Hassel & Sonnewald, 2002). For my assumption that citrate is not transported into the cytosol, it would be interesting to know, if citrate release from the cytosol into the medium depends on the cytosolic citrate concentration, because I have not seen an increase in citrate in the incubation medium of astrocytes treated with NO. If citrate release depends on the intracellular citrate concentration, this would substantiate my hypothesis that citrate remains in the mitochondrion. It is known that citrate release is independent of the extracellular citrate concentration (Westergaard *et al*., 1994). For this reason, the lack of enhanced citrate release in NO-treated astrocytes cannot be a result of inhibition of the export due to the normal extracellular concentration of citrate. Moreover, there is evidence that chelation of Fe^{2+} by citrate may be involved in suppression of citrate release into the culture medium. In the above mentioned study of Hassel *et al*., where export of citrate into the culture medium was observed, fluorocitrate was used as an inhibitor of aconitase (Hassel *et al*., 1994). Inhibition of aconitase by fluorocitrate, in contrast

to NO and/or peroxynitrite does not lead to liberation of iron from the 4Fe-4S cluster (Kent *et al*., 1985; Lauble *et al*., 1996).

Previous studies have attributed the failure of neurons to compensate the NO-induced impairment of the respiratory chain by enhancing glycolysis to the inability of increasing expression of PFK2, an enzyme that is almost absent in neurons. PFK 2 is responsible for Fru-2,6-BP production, a key activator of glycolysis (Almeida *et al*., 2001; Almeida *et al*., 2004). However, since I assume that citrate might play a role in protecting astrocytes from the harmful effects of NO, it is interesting to note, that exclusively astrocytes, but not neurons are able to produce citrate in large amounts (Sonnewald *et al*., 1991; Westergaard *et al*., 1994).

Concomitant with the accumulation of citrate, I observed a decrease in intracellular glutamate content in astrocytes treated with NO. Glutamate is not completely recycled in astrocytes by glutamine formation via the "glutamine-glutamate cycle". Glutamate is also used for the synthesis of other metabolites such as glutathione, cellular proteins, etc.. Moreover, glutamate is also recycled in the TCA cycles in neurons and astrocytes. To replenish the TCA cycle, glutamate is deaminated by the enzyme glutamate dehydrogenase (GDH) to form the TCA intermediate α-ketoglutarate. Since glutamine can be converted to glutamate by PAG, glutamine is also able to supply the TCA cycle. Due to the fact that the normal flux through the TCA cycle is blocked because of inhibition of aconitase, I assume that glutamate serves as an alternative substrate to fuel and thereby partially maintain a segment of the TCA cycle (Figure 49). Another advantage of glutamate entering the TCA cycle is that in the reaction of glutamate to α-ketoglutarate, as well as in two other reactions of the partially active TCA cycle, NADH is generated, which would otherwise decrease, when the whole TCA cycle is blocked. For this reason, glutamate may maintain the NADH level necessary for ATP production via the respiratory chain. In accordance with my observation of glutamate decrease and the assumption that it may be used to fuel the TCA cycle, decreased glutamate content was also observed in intact isolated nerve terminals treated with H_2O_2 (Tretter & Adam-Vizi, 2000) and also *in vivo* in heart metabolites of rats (Fréminet, 1981). The authors of both studies also suggested that glutamate may serve as a substrate to replenish the TCA cycle. In addition, Tretter *et al*. found that the NADH level was maintained in intact isolated nerve terminals when aconitase was inhibited at low H_2O_2 concentrations (≤ 50 µM), and even when aconitase was inhibited by 100 % (Tretter & Adam-Vizi, 2000). At high H_2O_2 concentrations (> 50 µM), they also found α-ketoglutarate dehydrogenase (α-KGDH), the enzyme that catalyzes the reaction of α-ketoglutarate to succinyl-CoA, to be inhibited (Tretter & Adam-Vizi, 2000). At this stage flux through the segment of the TCA cycle can no longer

be preserved and the NADH level should decrease. Indeed, they found a decrease in NADH only under conditions, where α-KGDH and aconitase were inhibited simultaneously by H_2O_2 (Tretter & Adam-Vizi, 2000). Inhibition of the α-KGDH complex and thus inactivation of the TCA cycle in microglia was also shown by NO and $ONOO^-$ after induction of iNOS with lipopolysaccharide (Park *et al.*, 1999). Given the significant decrease of intracellular glutamate and the observation that viability of astrocytes was unchanged it is unlikely that α-KGDH is inhibited by NO and/or $ONOO^-$ under my experimental conditions.

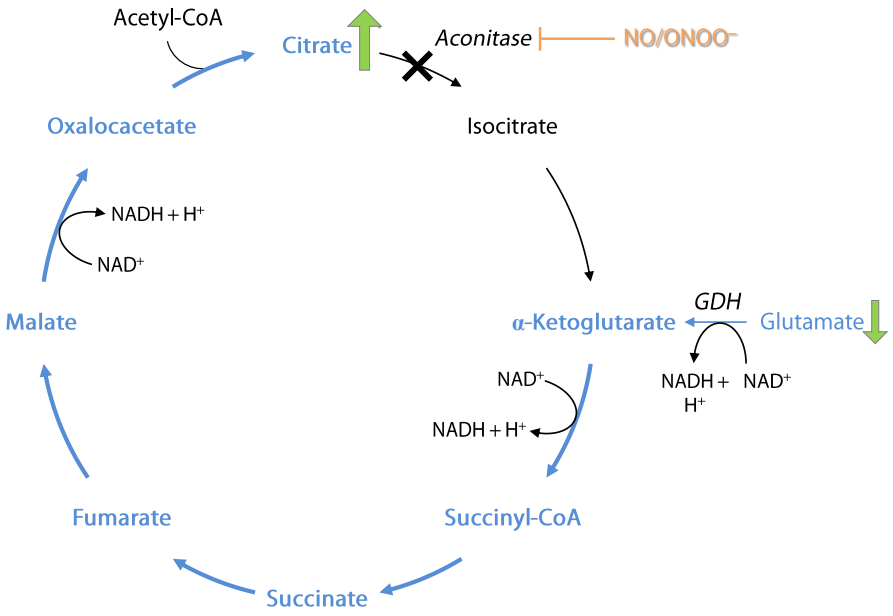

Figure 49. TCA cycle influenced by NO. In the presence of NO/$ONOO^-$ the TCA cycle enzyme aconitase is completely inhibited, leading to accumulation of citrate (green upwards pointing arrow). A concomitant decrease in intracellular glutamate leads to the assumption that glutamate becomes a key metabolite to fuel and thereby partially maintain a segment of the TCA cycle (bold blue arrows). To replenish the TCA cycle, glutamate is deaminated by GDH to form the TCA intermediate α-ketoglutarate. The reaction of glutamate to α-ketoglutarate as well as two reactions of the partially active TCA cycle generate NADH. Glutamate may maintain the NADH level necessary for ATP production via the respiratory chain. GDH, glutamate dehydrogenase; NAD, nicotinamide adenine dinucleotide; NO, nitric oxide; $ONOO^-$, peroxynitrite; TCA, tricarboxylic acid.

Another observation that supports the assumption that glutamate replenishes the TCA cycle is that GS, which is primarily located in astrocytes, was found to be inhibited in human fetal brain cell cultures after induction of NO synthesis in astrocytes by the cytokines interleukin-1 (IL-1) and tumor necrosis factor-α (TNF- α) (Chao *et al.*, 1995). Inhibition of GS was also observed in primary cultures of astrocytes treated with the NO-donor S-nitroso-*N*-acetylpenicillamine (Miñana *et al.*, 1997). GS catalyzes the formation of glutamine from glutamate, which is subsequently supplied to neurons via the "glutamine-glutamate cycle". This supply would lead to a loss of TCA cycle intermediates in astrocytes. Inhibition of GS

therefore ensures that glutamate remains in astrocytes to fuel the TCA cycle. However, intracellular as well as extracellular glutamine levels remained constant in my experiments. Hassel *et al.*, on the contrary, observed reduced glutamine formation during treatment of astrocytes with the aconitase inhibitor fluorocitrate (Hassel *et al*., 1994).

Acute glutamate release from neurons or co-cultures of neurons and astrocytes due to NO is a known feature (Bal-Price & Brown, 2001). Recently, NO-induced glutamate release was also reported in astrocytes (McNaught & Jenner, 2000; Bal-Price *et al*., 2002). High levels of glutamate are exocytoxic to neurons, and thus glutamate released from astrocytes due to NO leads to neuronal death (McNaught & Jenner, 2000; Bal-Price *et al*., 2002). Interestingly, the glutamate release from astrocytes can be prevented by calcium chelators (Bal-Price *et al*., 2002). I did not observe glutamate release from astrocytes after treatment with the NO-donor DETA-NONOate. On the one hand, this observation substantiates the assumption that the glutamate-pool in astrocytes is used to partially maintain the TCA cycle and on the other hand, the accumulation of citrate, which can chelate calcium, may prevent glutamate release.

GSH is an important cellular antioxidant that is able to protect aconitase and mitochondrial respiration from the harmful oxidative stress of peroxynitrite like protein nitration and mitochondrial damage at complex I (Castro *et al*., 1994; Cheung *et al*., 1998; Castro *et al*., 1998). GSH itself is thereby converted to its oxidized form glutathione disulfide (GSSG), leading to a decrease in the GSH level. Hence, a lack of glutathione facilitates NO- and $ONOO^-$-induced toxicity (Bolaños *et al*., 1996; Sims *et al*., 2004; Bharath & Andersen, 2005; Hsu *et al*., 2005). For this reason, the intracellular glutathione level would be a critical factor for cellular vulnerability to $ONOO^-$. A protective effect of GSH could also be verified by administration with GSH precursors, like glutathione mono-ethyl ester (Sims *et al*., 2004) and γ-glutamylcysteinyl ethyl ester (Drake *et al*., 2002; Boyd-Kimball *et al*., 2005). Overexpression of the rate-limiting enzyme of GSH synthesis, γ-glutamylcysteine synthetase, also prevented $ONOO^-$-stimulated oxidative stress (Diaz-Hernandez *et al*., 2005). Moreover, astrocytes supply neurons with precursors for glutathione synthesis, supporting an increase in neuronal GSH level (Bolaños *et al*., 1996; Dringen *et al*., 1999a; Dringen *et al*., 1999b; Wang & Cynader, 2000). Besides reduction of GSSG to regain GSH in a NADPH-dependent reaction (Kehrer & Lund, 1994) and expression and activity of γ-glutamylcysteine synthetase and GSH synthetase (Griffith & Mulcahy, 1999; Meister & Anderson, 1983) for *de novo* synthesis of GSH, GSH level also depends on the availability of its building blocks glutamate, cysteine, and glycine. *De novo* synthesis of GSH is generally quantitatively lower than reduction of GSSG to GSH by GSSG reductase (Kehrer & Lund, 1994; Akerboom *et al*., 1982; Griffith, 1999). However, severe oxidative or nitrosative stress can reduce GSH levels,

leading to higher GSSG levels (Griffith, 1999). For this reason, the decreased glutamate levels observed in astrocytes treated with NO, may lead to decreased GSH levels contributing to attenuation of the defense mechanisms of astrocytes under nitrosative stress.

4.5.3 UDP-GlcNAc – A Useful Metabolic Marker for Impairment of the Respiratory Chain by NO

As already denoted, NO has impact on mitochondrial respiration. Amongst other mitochondrial constituents, NO was shown to inhibit cytochrome c oxidase (complex IV), the terminal enzyme of the respiratory chain, in astrocytes (Bolaños *et al*., 1994; Bolaños *et al*., 1995) and mitochondria of other cells and tissue (Brown & Cooper, 1994; Cleeter *et al*., 1994; Schweizer & Richter, 1994). Mitochondria produce more than 90 % of cellular energy and cytochrome c oxidase is responsible for about 90 % of oxygen consumption in mammals (Chance *et al*., 1979; Babcock & Wikström, 1992). Cytochrome c oxidase is the complex of the respiratory chain that is most sensitive to NO and can be inhibited even at physiological concentrations, suggesting a physiological regulatory role (Cooper, 2002; Moncada & Erusalimsky, 2002), while inhibition of other components of the mitochondrial respiratory chain, including ATP synthase, may only occur at pathological conditions (Cooper, 2002; Moncada & Erusalimsky, 2002). The precise physiological role of NO-mediated inhibition of cytochrome c oxidase in astrocytes is not clearly understood to date. Physiological levels of NO cause reversible inhibition of cytochrome c oxidase in competition with oxygen (Brown & Cooper, 1994; Cleeter *et al*., 1994; Takehara *et al*., 1995; Cassina & Radi, 1996; Poderoso *et al*., 1996). Cytochrome c oxidase is located in the mitochondrial inner membrane, and catalyzes the oxidation of cytochrome c^{2+} to cytochrome c^{3+} and the reduction of oxygen to water, and this is coupled to the translocation of protons across the membrane, establishing a protonmotive force that is used for ATP synthesis by ATP synthase (Babcock & Wikström, 1992). The enzyme contains two hemes (cytochrome a and cytochrome a_3) and two copper centers (Cu_A and Cu_B). Cytochrome a_3 and Cu_B build a binuclear center that constitutes in its reduced form (Fe^{2+}/Cu^{+}) the oxygen binding site (Babcock & Wikström, 1992). NO binds to this oxygen binding site, inhibiting cytochrome c oxidase in competition with oxygen (Wainio, 1955; Brown & Cooper, 1994; Cleeter *et al*., 1994; Schweizer & Richter, 1994). Being competitive with oxygen, the inhibitory effect of NO on cytochrome c oxidase depends on oxygen tension in the examined cells or tissue. Inhibition of cytochrome c oxidase by NO in turn, leads to enhanced production of $O_2^{\bullet -}$ due to transfer of single electrons to molecular oxygen (Palacios-Callender *et al*., 2004). This again, enables peroxynitrite formation by the

reaction between NO and $O_2^{\bullet-}$ (Poderoso *et al*., 1996; Clementi *et al*., 1998). While the effect of NO on complex IV of the mitochondrial respiratory chain is reversible, peroxynitrite exerts irreversible inhibition of complexes I (Murray *et al*., 2003; Brown & Borutaite, 2004; Pearce *et al*., 2005), II (Rubbo *et al*., 1994; Bolaños *et al*., 1995), III (Guidarelli *et al*., 2004; Pearce *et al*., 2005), of the respiratory chain, as well as ATP synthase (Cassina & Radi, 1996; Radi *et al*., 2002), via nitration of tyrosine residues and oxidation of thiol-groups. Hence, peroxynitrite converts the initial reversible inhibition of respiration into an irreversible inhibition. The activity of complex IV, on the contrary, which was shown to be reversibly inhibited by NO, was not significantly affected by peroxynitrite (Pearce *et al*., 1999; Pearce *et al*., 2002). Induction of iNOS in astrocytes by lipopolysaccharide plus interferon-γ, however caused an irreversible inhibition of complex IV, a less distinct inhibition of complex II, III, and no inhibition of complex I, concomitant with enhanced glycolysis and lactate formation (Bolaños *et al*., 1994).

In neurons, NO either administered exogenously (Brorson & Zhang, 1997; Brorson *et al*., 1997) or formed endogenously (Marks *et al*., 2005; Almeida & Bolaños, 2001) causes depolarization of mitochondrial membrane potential ($\Delta\Psi_m$), which reduces Ca^{2+} uptake, and thus decreases the ability of mitochondria to buffer cytosolic Ca^{2+} (Schweizer & Richter, 1994; Marks *et al*., 2005). The loss of $\Delta\Psi_m$ is associated with opening of the mitochondrial permeability transition pore (PTP) (Packer & Murphy, 1995; Scarlett *et al*., 1996) and release of solutes and small mitochondrial proteins, like cytochrome c, into the cytosol, initiating apoptosis (Tatton & Olanow, 1999). Preservation of $\Delta\Psi_m$ is essential for cell survival as its breakdown has been shown to represent a point where apoptosis is already irreversible (Zamzami *et al*., 1995; Beltrán *et al*., 2000). In astrocytes, however, $\Delta\Psi_m$ is maintained or even increased in presence of NO (Almeida *et al*., 2001; Takuma *et al*., 2001), an effect that was also observed in macrophages (Beltrán *et al*., 2000). This preservation may be the result of rapid activation of glycolysis. Indeed, the maintenance of $\Delta\Psi_m$ in astrocytes is eliminated when astrocytes are prevented to produce ATP via the glycolytic pathway, leading to apoptotic cell death (Almeida *et al*., 2001). To further substantiate this hypothesis, it was shown that eosinophils, which contain only a small amount of mitochondria, generate their $\Delta\Psi_m$ mainly through hydrolysis of ATP by F_1F_0-ATPase than from respiration (Peachman *et al*., 2001).

Just to mention briefly, since NO targets cysteine and other thiol groups, the intracellular GSH level is, as in the case of aconitase, also a critical factor for the resistance of the mitochondrial respiratory chain against damage due to peroxynitrite. The glutamate decrease observed in my experiments may also lessen the protective effect of GSH against

peroxynitrite induced inhibition of the respiratory chain. At the time when the GSSG:GSH level is increased under oxidative and nitrosative stress, *de novo* synthesis of GSH is required. *De novo* synthesis of GHS, however, may not proceed, when glutamine is used to replenish a part of the TCA cycle. In fact, it was shown that glutathione deficiency enhances NO- and especially peroxynitrite-induced cellular damage in the brain (Bolaños *et al*., 1996; Sims *et al*., 2004; Bharath & Andersen, 2005; Hsu *et al*., 2005).

It is suggested that the UDP-GlcNAc level gives information about the metabolic state of a cell (Zhivkov *et al*., 1975; Spiro, 1984) and alterations in its level may provide an indication of the development of metabolic disorders. UDP-GlcNAc is an ideal metabolic marker that can be easily detected in $^{1}H,^{13}C$-HSQC NMR spectra using [1-^{13}C]glucose as a precursor to follow the incorporation of the label into UDP-GlcNAc. Especially astrocytes are well suited for investigations of UDP-GlcNAc levels, since I have shown that they exhibit the highest UDP-GlcNAc concentrations in the cells investigated.

By using [1-^{13}C]glucose as labeled substrate the ^{13}C-label can be incorporated into 4 atoms of UDP-GlcNAc that are detectable with $^{1}H,^{13}C$-HSQC NMR spectra. Two of them can be unambiguously identified and assigned without being overlapped with signals of other UDP-sugars: the ^{13}C-label at the C1 position in the GlcNAc residue and the ^{13}C-label in the *N*-acetyl group of UDP-GlcNAc. The C1 atom in the GlcNAc residue gets its label directly from the administered [1-^{13}C]glucose and the *N*-acetyl group is labeled through cytosolic acetyl-CoA. The ^{13}C-label cannot be directly incorporated from [2-^{13}C]acetyl-CoA that is produced via formation of [3-^{13}C]pyruvate in glycolysis and subsequent generation of [2-^{13}C]acetyl-CoA via PDC in mitochondria, because acetyl-CoA cannot pass the mitochondrial membrane and UDP-GlcNAc synthesis occurs in the cytosol. For synthesis of cytosolic acetyl-CoA, [2-^{13}C]acetyl-CoA generated via PDC in mitochondria is introduced into the TCA cycle, where it is aligned with oxaloacetate to produce citrate. In astrocytes, the ^{13}C-label can also be introduced into the TCA cycle by replenishment with [3-^{13}C]pyruvate via pyruvate carboxylase (PC), an enzyme selectively located in astrocytes (Wallace *et al*., 1998; Jitrapakdee & Wallace, 1999; Jitrapakdee *et al*., 2008), as shown in Figure 50.

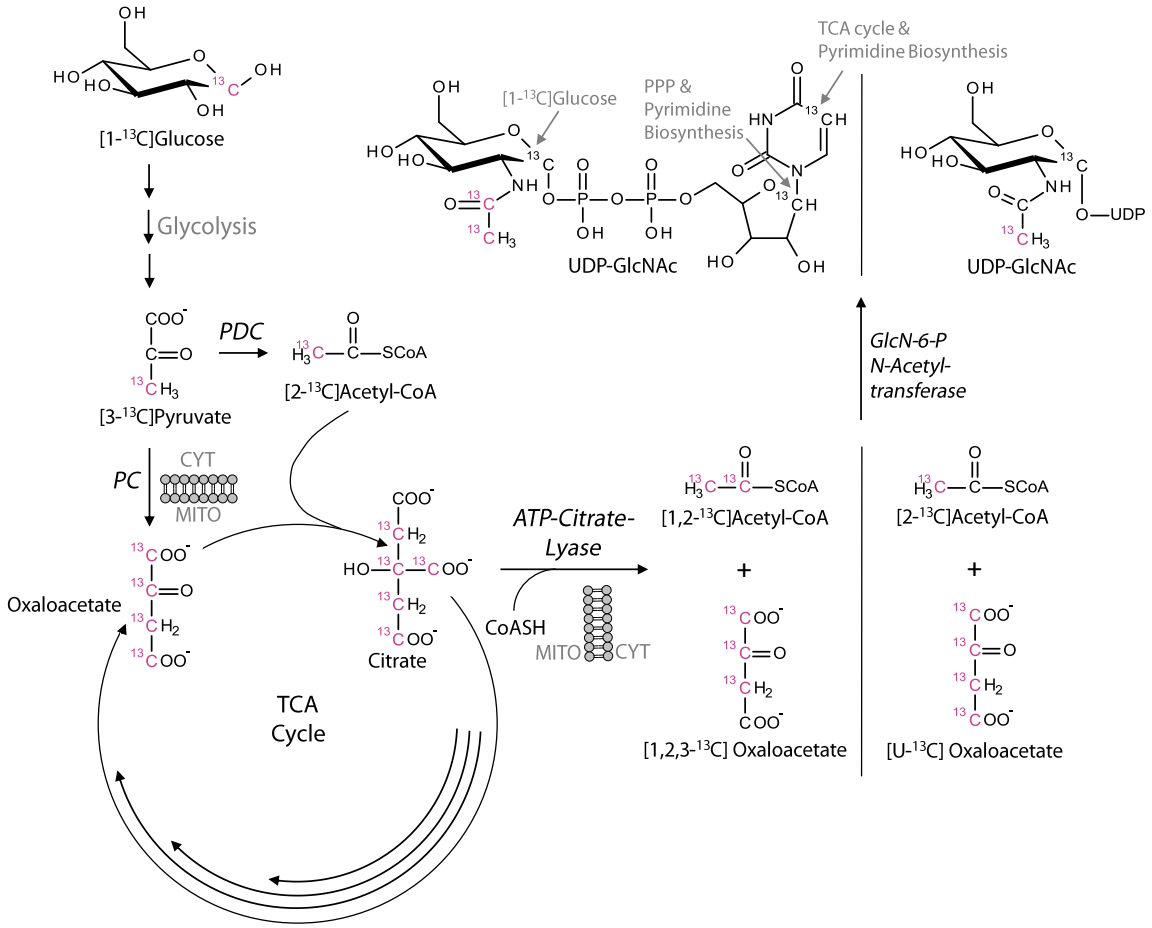

Figure 50. Incorporation of the ^{13}C-label into UDP-GlcNAc using [1-^{13}C]glucose as a precursor molecule. In glycolysis, [1-^{13}C]glucose is metabolized to [3-^{13}C]pyruvate, which is introduced into the TCA cycle either as [2-^{13}C]acetyl-CoA via PDC or as [3-^{13}C]oxaloacetate (labeling pattern not shown) via PC. After several turns through the TCA cycle the ^{13}C-label can potentially be incorporated into any C-atom of citrate, whereby one of the terminal carboxyl groups always remains unlabeled due to incorporation of [2-^{13}C]acetyl-CoA in each turn. Citrate is cleaved by ATP-citrate-lyase to acetyl-CoA and oxaloacetate. Due to the symmetry of citrate [1,2-^{13}C]acetyl-CoA and [2-^{13}C]acetyl-CoA is formed. The labeled acetyl-CoA is then transferred to UDP-GlcNAc by GlcN-6-P N-acetyl-transferase leading to introduction of the ^{13}C-label into the methyl group, as well as incorporation of the ^{13}C-label into the carbonyl C-atom of UDP-GlcNAc. Replenishment of the TCA cycle with unlabeled substances is not considered in this overview for graphical clarity. The ^{13}C-label deriving from [1-^{13}C]glucose is also incorporated directly from glucose into the C1 of the GlcNAc residue. The ^{13}C-label in the C1 of the ribose moiety is incorporated via PPP and pyrimidine biosynthesis and the C6 of uracil derives its label from aspartate formed in the TCA cycle used in de novo pyrimidine synthesis. ATP, adenosine triphosphate; CoA, coenzyme A; CYT, cytosol; GlcN, glucosamine; MITO, mitochondrion; PC, pyruvate carboxylase; PDC, pyruvate dehydrogenase complex; PPP, pentose phosphate pathway; UDP-GlcNAc, uridine diphosphate-N-acetylglucosamine; TCA, tricarboxylic acid.

In this enzymatic reaction, [3-^{13}C]pyruvate is carboxylated to the TCA cycle intermediate [3-^{13}C]oxaloacetate that condenses with [2-^{13}C]acetyl-CoA to citrate, further contributing to ^{13}C-label incorporation into citrate. After several turns through the TCA cycle the ^{13}C-label can potentially be incorporated into any C-atom of citrate, whereby one of the terminal carboxyl groups always remains unlabeled due to incorporation of [2-^{13}C]acetyl-CoA in each turn.

Citrate is then transported via CIC in exchange for malate into the cytosol, where it is cleaved by ATP-citrate-lyase to oxaloacetate and cytosolic acetyl-CoA. Considering the fact that citrate is a symmetrical molecule and one of the terminal carboxyl groups always remains

unlabeled, [2-^{13}C]acetyl-CoA and [1,2-^{13}C]acetyl-CoA will be generated in this reaction. The ^{13}C-labeled cytosolic acetyl-CoA is then incorporated into the *N*-acetyl group of UDP-GlcNAc by GlcN-6-P *N*-acetyl-transferase, leading to introduction of the ^{13}C-label into the methyl C-atom, as well as into the carbonyl C-atom of the *N*-acetyl group of UDP-GlcNAc. Compared to the ^{13}C-label in the methyl C-atom, only at least half of the carbonyl C-atoms will be labeled and the carbonyl C-atom cannot be detected with ^{1}H,^{13}C-HSQC NMR spectra because for this kind of NMR experiments a proton has to be attached to the C-atom. The ^{13}C-label is also incorporated into the C1 of the ribose moiety of UDP-GlcNAc via PPP and pyrimidine biosynthesis and into the C6 of uracil that derives its label from aspartate formed in the TCA cycle used in *de novo* pyrimidine synthesis. However, since these signal overlap with other activated sugar nucleotides in ^{1}H,^{13}C-HSQC NMR spectra these signals are not well suited to investigate UDP-GlcNAc levels in cell extracts.

A recent study in our lab has shown that the *N*-acetyl group of UDP-GlcNAc can serve as an ideal metabolic marker for impaired mitochondrial respiration using [1-^{13}C]glucose and NMR spectroscopy in neuronal HT-22 cells (Gallinger *et al*., 2011). In this study, neuronal HT-22 cells were incubated either with sodium azide, a competitive inhibitor of complex IV of the respiratory chain, or with rotenone, an inhibitor of complex I of the respiratory chain (Gallinger *et al*., 2011). Sodium azide blocks O_2 binding and electron transfer at the same site, leading to disruption of the proton gradient and subsequently ATP production comes to a halt. As a consequence of this, NADH oxidation to NAD^+ by complex I of the respiratory chain is also inhibited and NADH accumulates. NAD^+, in turn, is an essential cofactor of PDC that transforms pyruvate into acetyl-CoA. Therefore, acetyl-CoA production decreases when NAD^+ is no longer available. Furthermore, inhibition of respiration switches cells to increased glycolysis to maintain energy homeostasis due to restricted ATP production. As a result of enhanced glycolysis, more pyruvate, the end-product of glycolysis, and thus lactate is produced. Pyruvate delivers the acetyl group for the formation of acetyl-CoA, connecting glycolysis and TCA cycle. Enhanced lactate production implies that pyruvate is no longer, or rather to a lesser extent, used for production of acetyl-CoA, which can no longer enter the TCA cycle and the TCA cycle is supposed to stop under these conditions. Besides, with increased lactate production cells try to sustain the NAD^+ pool, because NADH is oxidized in this reaction. However, recovery of NAD^+ by reduction of pyruvate to lactate does only compensate the need of NAD^+ for glycolysis and cannot replenish the lack of NAD^+ caused by inhibition of complex I of the respiratory chain.

Indeed, Gallinger *et al*. observed increased glucose consumption and enhanced lactate production in neuronal HT-22 cells, when the respiratory chain was inhibited with either sodium azide or rotenone. Furthermore, they have shown that the TCA cycle has stopped due to the lack of acetyl-CoA, as the peaks of the TCA cycle intermediates citrate and malate vanished in spectra of treated cells. But most interesting, they observed a decreased incorporation of ^{13}C-labeled cytosolic acetyl-CoA into the *N*-acetyl moiety of UDP-GlcNAc. The label of the C1 atom in the GlcNAc residue was not affected by the treatment (Gallinger *et al*., 2011). It should also be noted that direct identification of ^{13}C-labeled acetyl-CoA in ^{1}H,^{13}C-HSQC spectra of cell extracts is not unambiguously possible due to severe overlap with signals of other metabolites, e.g. succinyl-CoA.

Using NMR spectroscopy and ^{13}C-labeling, UDP-GlcNAc becomes a metabolic marker that simultaneously reflects fluxes through glycolysis, TCA cycle and cytosolic acetyl-CoA formation by ATP-citrate-lyase. Furthermore, it also reflects the energy status of the cell, because mitochondrial acetyl-CoA formation by PDC depends on NAD^+ formation in the mitochondrial respiratory chain and cleavage of citrate to acetyl-CoA and oxaloacetate in the cytosol by ATP-citrate-lyase consumes ATP. Moreover, it reflects the flux of metabolites in between two cell compartments, the cytosol and the mitochondrion.

Since NO, just like sodium azide, is a known competitive inhibitor of complex IV of the respiratory chain and peroxynitrite irreversibly inhibits the complexes I, II, III, as well as ATP synthase of the respiratory chain, I assumed that incubation of astrocytes with NO leads to an altered labeling of UDP-GlcNAc. But first of all, I quantified the total concentration of unlabeled UDP-GlcNAc and other activated sugar nucleotides after treatment with NO. However, no significant changes in the concentrations between NO treated astrocytes and controls were observed. This proves that although the cells have to cope with diminished ATP production due to inhibition of the respiratory chain, the HBP, as a minor branch of glycolysis, is not constricted to ensure that glucose is exclusively passed through glycolysis to maintain ATP production. Interestingly, Almeida *et al*. observed a time-dependent decrease in Fru-6-P and an increase in fructose-1,6-bisphosphate (Fru-1,6-BP) concentrations after treatment with 1,4 µM NO for 30 – 60 min in astrocytes, but not in neurons (Almeida *et al*., 2004). The HBP branches off from glycolysis using Fru-6-P to from GlcN-6-P. A decrease in the Fru-6-P level and an increase in the Fru-1,6-BP level should therefore result in a decrease in flux through HBP and therefore minor UDP-GlcNAc formation. Cells can adjust this lower Fru-6-P supply by enhancing the activity of enzymes or by enhanced gene expression of the

enzymes of the HBP. I observed an increased mRNA expression of the HBP enzymes GFAT1, GFAT2, GlcN-6-P N-acetyltransferase, and UDP-GlcNAc pyrophosphorylase. Nevertheless, it has to be mentioned that these results are preliminary and the experiments have to be repeated for validity (see Appendix 7.4).

Quantification of UDP-GlcNAc and other activated sugar nucleotides cannot reveal the actual impact of aberrant glucose metabolism caused by NO on this metabolite, since the glucose moiety and the *N*-acetyl group of UDP-GlcNAc can be produced from other precursors than the administered glucose like glycogen, fatty acids, and TCA cycle intermediates. This was actually the case in the study of Gallinger *et al*.. Although they observed a decrease in the incorporation of ^{13}C-labeled acetyl-CoA into the *N*-acetyl moiety of UDP-GlcNAc, the total concentration of UDP-GlcNAc was unaffected, indicating that unlabeled acetyl-CoA is incorporated into the *N*-acetyl group of UDP-GlcNAc (Gallinger *et al*., 2011).
For this reason, I used [1-^{13}C]glucose to distinguish from the peaks of unlabeled UDP-GlcNAc synthesized from unlabeled precursors originating from substances other than ^{13}C-labeled glucose. But here again, no significant changes, neither of the ^{13}C-label at the C1 position in the GlcNAc residue nor of the ^{13}C-label in the *N*-acetyl group of UDP-GlcNAc were detected in 2D, as well as 1D ^{1}H,^{13}C-HSQC spectra.

The first question that raises is, if the respiratory chain is actually inhibited under these conditions. A concentration of 0,8 mM DETA-NONOate and incubation times of 12 h were used for treatments. These experimental conditions were used, because it was shown that HIF-1α protein stabilization by NO was most effectively at concentrations between 0,8 and 1,2 mM DETA-NONOate and between 6 – 12 h of DETA-NONOate treatment (Brix *et al*., 2012). It was shown that HIF-1α stabilization and ensuing expression of glycolytic genes by endothelial cell-derived NO participates in the induction of the high glycolytic activity in astrocytes (Brix *et al*., 2012). Almeida *et al*. have shown that cellular respiration is inhibited in a concentration- and time-dependent manner. They measured the amount of NO released by 0,5 mM DETA-NONOate with a NO electrode and found that 1,5 µM NO was continually released for at least 20 h in buffered Hank's solution (pH 7,4) at 37 °C (Almeida *et al*., 2001). Furthermore, they detected that cellular respiration was inhibited by 85 %, in both neurons and astrocytes, after incubation with 0,5 mM DETA-NONOate for 60 min (Almeida *et al*., 2001). Taking this into account, unless astrocytes somehow adapt to exposure of NO, the concentration of DETA-NONOate I used is within the range to inhibit cellular respiration over a time period of 12 h. As mentioned previously, the glucose concentration of 22 mM

used in my cell culture experiments exceeds the concentration in the brain (1 – 2 mM) (McNay & Gold, 1999) by far. This is potentially important, because in addition to thiols, high levels of glucose (Lizasoain *et al*., 1996) and components of common buffers (Gadelha *et al*., 1997) were shown to suppress inhibition of cellular respiration caused by peroxynitrite. Glucose prevented peroxynitrite induced inhibition of cellular respiration with an half maximal inhibitory concentration of 8 mM, however inhibition by NO was not abolished (Lizasoain *et al*., 1996), which indicates that at least complex IV of the respiratory chain should be inhibited by NO in my experiments. Inhibition of complex IV leads to a standstill of the whole respiratory chain. Furthermore, Almeida *et al*. also accomplished their experiments with a glucose concentration of 20 mM and detected a distinct inhibition of cellular respiration (Almeida *et al*., 2001).

However, the fact that I observed enhancement in glycolysis in my experiments is a clear evidence that mitochondrial respiration is inhibited in my experimental setup, because the rapid activation of glycolysis by NO is dependent on AMPK, which reacts when the AMP:ATP ratio increases during energy deficiency, resulting in activation of PFK2 and hence glycolysis. An increase in the AMP:ATP ratio, in turn, requires prior inhibition of mitochondrial respiration (Almeida *et al*., 2004). Bolaños *et al*., for instance, did not observe inhibition of respiration in astrocytes treated with 0,1 – 2 mM peroxynitrite, in the presence of 5,44 mM glucose, whereas they detected inhibition of respiration, even with lower concentrations of peroxynitrite, in neurons. But what is striking, they did not observe enhanced glycolysis in astrocytes under these conditions (Bolaños *et al*., 1995).

Gallinger *et al*. substantiated that the decrease of the ^{13}C-labeling in the *N*-acetyl group of UDP-GlcNAc after inhibition of complex IV of the respiratory chain was due to a lack of NAD^+. To proof this assertion, they incubated neuronal HT-22 cells with rotenone, an inhibitor of complex I (NADH-dehydrogenase) of the respiratory chain. The NADH-dehydrogenase catalyzes the transfer of electrons from NADH to coenzyme Q and thus oxidation of NADH to NAD^+. In contrast to inhibition of complex IV with sodium azide, inhibition of complex I does not lead to a breakdown of oxidative phosphorylation, because electron transfer at complex II is not affected. These experiments also resulted in a decrease in the intensity of the peak corresponding to the *N*-acetyl group of UDP-GlcNAc, proving that reduction of NAD^+ is indeed responsible for impaired mitochondrial acetyl-CoA formation and thus cytosolic acetyl-CoA formation from ^{13}C-labeled citrate that receives its label from condensation of oxaloacetate with mitochondrial [2-^{13}C]acetyl-CoA.

Aside from inhibition of complex IV by NO, there are also other effects that may lead to NAD^+ depletion in my experiments. Peroxynitrite can also cause DNA damage, which leads to activation of poly(ADP-ribose) polymerase-1 (PARP-1) (Zhang *et al*. 1994; Szabó & Ohshima, 1997; Tapodi *et al*., 2005), a nuclear enzyme that participates in reparation of damaged DNA by binding to DNA strand breaks, leading to formation of branched poly(ADP-ribose) polymers, a reaction that consumes NAD^+ and generates nicotinamide (Lindahl *et al*., 1995; Huber *et al*., 2004; Kim *et al*.; 2005). Restoration of NAD^+ from nicotinamide requires ATP. Activation of PARP-1 due to peroxynitrite is therefore considered to either lead to NAD^+ depletion or energy deficiency. It is suggested that PARP-1 over-activation is linked to neuronal death (Critchlow & Jackson, 1998). Mitochondrial damage and apoptotic cell death provoked by PARP-1 activation has been shown in cortical neurons after oxygen and glucose deprivation (Tanaka *et al*., 2005).

Furthermore, Brix *et al*. observed that NO treatment, identically equal to my experiments, enhanced the expression of the enzyme PDK1 in astrocytes but not in neurons (Brix *et al*., 2012). PDK1 is responsible for the regulation of the activity of PDH, the first enzyme of the PDC that transforms pyruvate into acetyl-CoA. PDK1 causes inactivation of PDH by phosphorylating the enzyme. This implies that mitochondrial acetyl-CoA is no longer or to a lesser extent synthesized, favoring the formation of lactate from pyruvate. Under these conditions acetyl-CoA can no longer enter the TCA cycle to carry out oxidative respiration thus favoring glycolysis. Inactivation of PDH should therefore also lead to a decrease of the ^{13}C-label in cytosolic acetyl-CoA and hence in the *N*-acetyl group of UDP-GlcNAc.

To assume that there is still enough NAD^+ available in astrocytes treated with NO for the generation of mitochondrial acetyl-CoA by PDC, it has to be considered that aconitase is inhibited under these conditions having impact on citrate labeling and as a consequence of this on labeling of cytosolic acetyl-CoA that again provides the ^{13}C-label in the *N*-acetyl group of UDP-GlcNAc. Since flux through the TCA cycle is impaired due to inhibition of aconitase, citrate accumulates and can no longer pass through the TCA cycle for several turns. Therefore, the ^{13}C-label cannot be incorporated into potentially any C-atom of citrate anymore. Glutamate is most likely used to replenish the TCA cycle and thus partially maintaining it. In the experiments where I pre-incubated with [1-^{13}C]glucose alone for 12 h before adding DETA-NONOate, glutamate will be itself ^{13}C-labeled to some extent. However, there will also be unlabeled glutamate used for replenishment due to newly synthesized glutamate from unlabeled glutamine present in the incubation medium. In the experiments where [1-^{13}C]glucose and DETA-NONOate were added at once, labeling of

glutamate is not expected to a greater extent. It is also unknown to which extend [3-^{13}C]pyruvate is introduced into the TCA cycle by PC. However, excluding these unknown factors, citrate will be at least mono labeled ([2-^{13}C]citrate), leading to introduction of the ^{13}C-label into at least every other acetyl-CoA molecule synthesized by ATP-citrate-lyase und subsequent incorporation of the ^{13}C-label into UDP-GlcNAc. These reflections show that it is still possible that the ^{13}C-label deriving from [1-^{13}C]glucose is still possible when NAD^+ is available to generate mitochondrial [2-^{13}C]acetyl-CoA although aconitase is inhibited and the TCA cycle is most like replenished with glutamate even if it is not ^{13}C-labeled. Figure 51 shows how the ^{13}C-label is still incorporated into the *N*-acetyl group of UDP-GlcNAc when aconitase is inhibited, as observed in my experiments, since the intensity of the signal of the *N*-acetyl group did not decrease in ^{1}H,^{13}C-HSQC NMR spectra of cell extracts of astrocytes treated with DETA-NONOate compared to controls.

I have hypothesized that citrate will most likely remain in the mitochondrion to possibly chelate Fe^{2+} ions that are released when the 4Fe-4S cluster of aconitase is disrupted by peroxynitrite. For the incorporation of the ^{13}C-label, however, citrate has to be transported into the cytosol. Nevertheless, it is still more likely that the majority of citrate remains in the mitochondrion, because formation of cytosolic acetyl-CoA occurs under the expense of ATP and citrate is usually transported into the cytosol for fatty acid synthesis when ATP is high, which is clearly not the case when the mitochondrial respiratory chain is inhibited. However, there is still enough ATP available to produce sufficient amounts of *de novo* synthesized cytosolic ^{13}C-labeled acetyl-CoA for incorporation into the *N*-acetyl group of UDP-GlcNAc. Incorporation of unlabeled acetyl-CoA deriving from degradation of fatty acids is not an alternative under these conditions. Fatty acid ß-oxidation occurs in the mitochondrion and relies on sufficient NAD^+ supply that will be short in supply due to inhibition of the mitochondrial respiration chain. Aside from that the generated unlabeled acetyl-CoA from ß-oxidation has to be metabolized the same way as cytosolic acetyl-CoA generated from [1-^{13}C]glucose does, that means introduction into the TCA cycle, transport out of the mitochondria as citrate, and cleavage to cytosolic acetyl-CoA by ATP-citrate-lyase.

Taken together, my results indicate that cytosolic ^{13}C-labeled acetyl-CoA deriving from [1-^{13}C]glucose is still generated in astrocytes treated with NO. This implies that the respiratory chain is not fully inhibited under these conditions and there is still sufficient NAD^+ available to to sustain the formation of mitochondrial [2-^{13}C]acetyl-CoA by PDC. In the study of Gallinger *et al*. the TCA cycle was completely paralyzed as evidenced by the disappearance

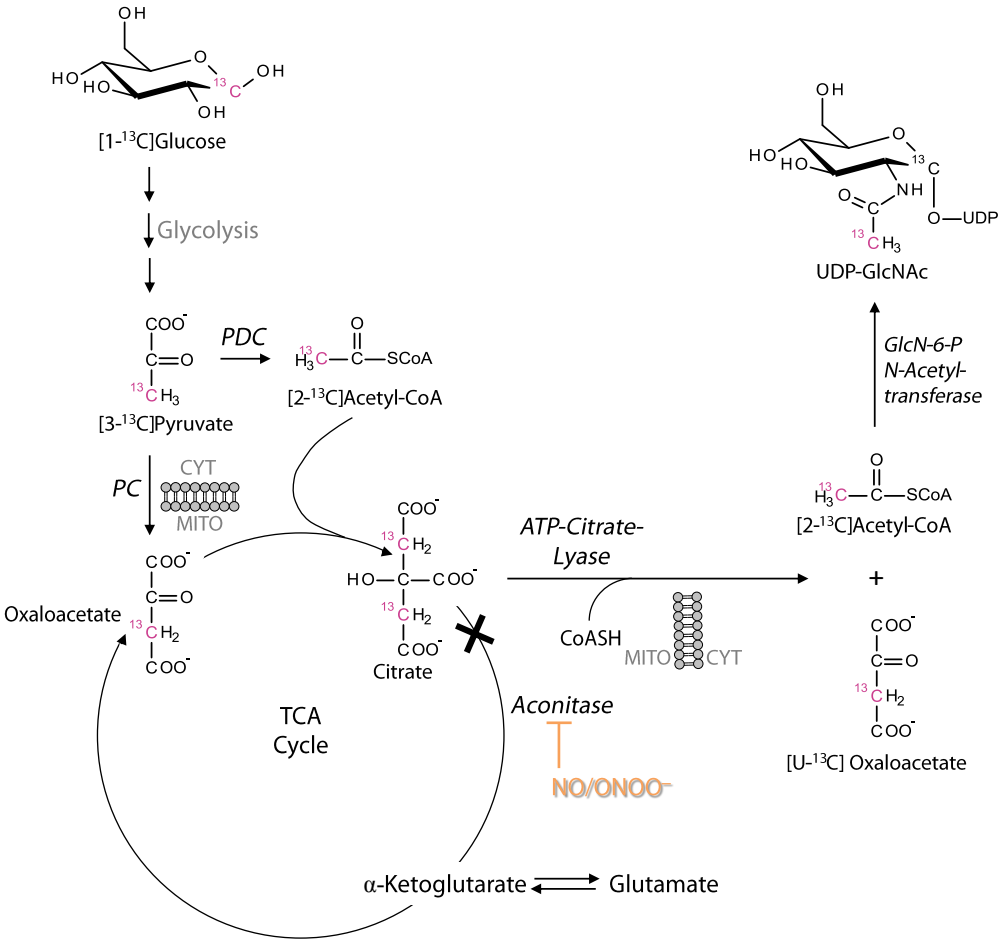

Figure 51. Incorporation of the ^{13}C-label deriving from [1-^{13}C]glucose into UDP-GlcNAc using [1-^{13}C]glucose when aconitase is inhibited by NO and/or peroxynitrite. In glycolysis, [1-^{13}C]glucose is metabolized to [3-^{13}C]pyruvate, which is introduced into the TCA cycle either as [2-^{13}C]acetyl-CoA via PDC or as [3-^{13}C]oxaloacetate via PC. Since flux through the TCA cycle is impaired due to inhibition of aconitase, citrate can no longer pass through the TCA cycle for several turns and accumulates. Therefore, the ^{13}C-label cannot be incorporated into potentially any C-atom of citrate anymore. Glutamate is most likely used to replenish the TCA cycle and thus partially maintaining it. In the experiments where I pre-incubated with [1-^{13}C]glucose alone for 12h before adding DETA-NONOate, glutamate will be itself ^{13}C-labeled to some extent. However, there will also be unlabeled glutamate used for replenishment due to newly synthesized glutamate from unlabeled glutamine present in the incubation medium. In the experiments where [1-^{13}C]glucose and DETA-NONOate were added at once, labeling of glutamate is not expected to a greater extent. It is also unknown to which extend [3-^{13}C]pyruvate is introduced into the TCA cycle by PC. However, excluding these unknown factors, citrate will be at least mono labeled ([2-^{13}C]citrate), leading to introduction of the ^{13}C-label into at least every other acetyl-CoA molecule synthesized by ATP-citrate-lyase und subsequent incorporation of the ^{13}C-label into UDP-GlcNAc. ATP, adenosine triphosphate; CoA, coenzyme A; CYT, cytosol; GlcN, glucosamine; MITO, mitochondrion; PC, pyruvate carboxylase; PDC, pyruvate dehydrogenase complex; PPP, pentose phosphate pathway; UDP-GlcNAc, uridine diphosphate-N-acetylglucosamine; TCA, tricarboxylic acid.

of the peaks of the TCA cycle intermediates citrate and malate in spectra of sodium azide treated neuronal HT-22 cells (Gallinger *et al.*, 2011). However, in my experiments, the TCA cycle was partially maintained by replenishment with glutamate which leads to preservation of NADH/H$^+$ equivalents, which would otherwise decrease, when the whole TCA cycle is blocked. NADH/H$^+$ equivalents are needed to maintain the mitochondrial membrane potential and thus NAD$^+$ generation and ATP production. Furthermore, PDH, the first enzyme of PDC, cannot be completely inactivated by enhanced expression of PDK1. The essentials of the foregoing discussion are summarized in Figure 52.

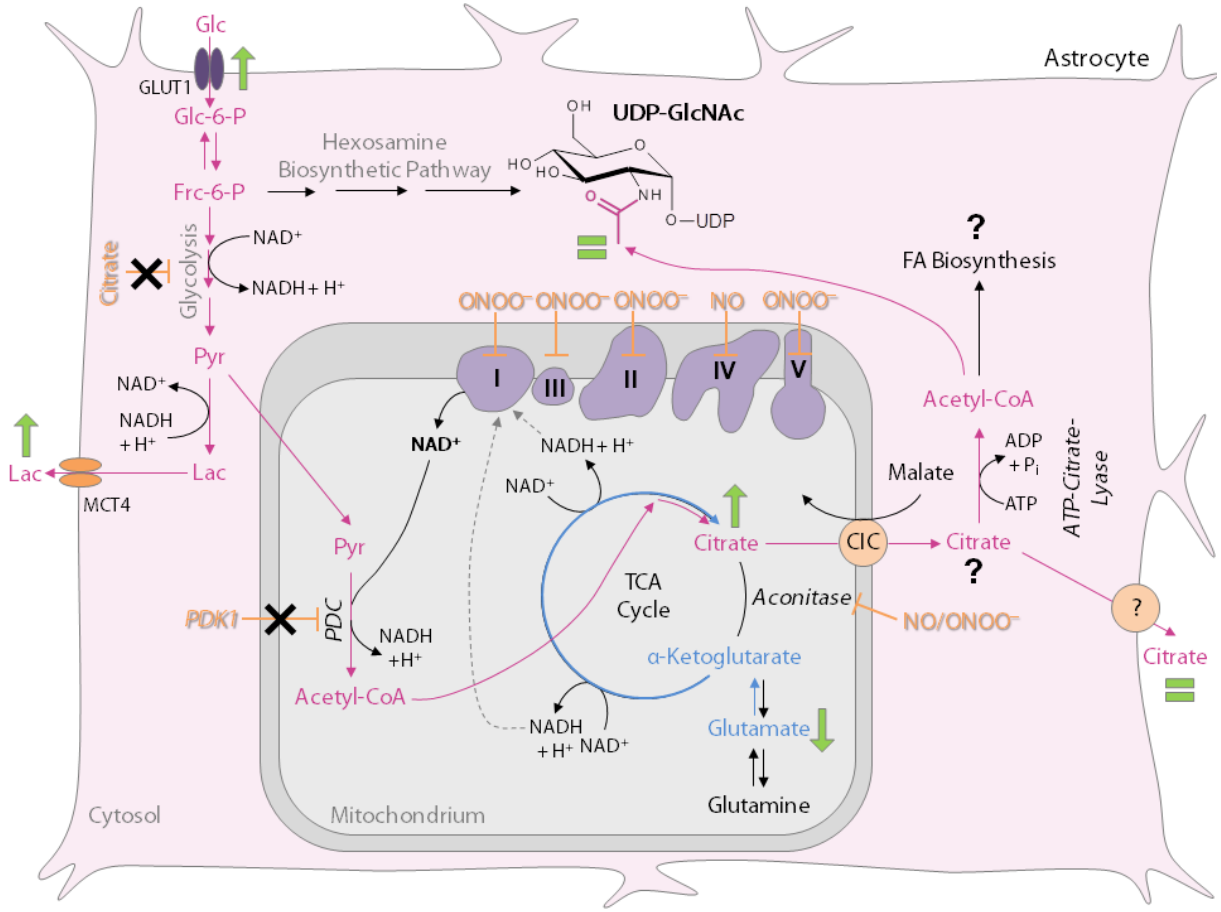

Figure 52. Impact of nitric oxide and peroxynitrite on the metabolism of astrocytes. The ^{13}C-label deriving from [1-^{13}C]glucose is still incorporated into the N-acetyl group of UDP-GlcNAc, proving that mitochondrial respiration is not fully disrupted by NO and/or $ONOO^-$. The incorporation of the ^{13}C-label was monitored using NMR-spectroscopy. Note: The exact incorporation of the ^{13}C-label into individual carbon atoms is not depicted for graphical clarity. The route of the ^{13}C-label is shown in pink. Only essential metabolites are highlighted in pink. The label can also be incorporated into carbon atoms of other molecules. In UDP-GlcNAc it is only shown that the acetyl moiety of the N-acetyl group is ^{13}C-labeled. The label is also incorporated into the carbon attached to the anomeric proton of the GlcNAc moiety, as well as into the ribose and uracil moiety of UDP-GlcNAc. Glycolysis is stimulated, as judged by increased glucose uptake (green upwards pointing arrow) and lactate release (green upwards pointing arrow), due to inhibition of the mitochondrial respiratory chain by NO and/or $ONOO^-$ to maintain energy homeostasis. Lactate formation restores the NAD^+ pool expensed by glycolysis. Besides being converted to lactate, pyruvate also enters the mitochondrion, where it is converted to acetyl-CoA by PDC to enter the TCA cycle. Aconitase is also inhibited by NO and/or $ONOO^-$, leading to citrate accumulation (green upwards pointing arrow). To maintain NADH production, glutamate is most likely used to replenish the TCA cycle (depicted in blue), further contributing to citrate accumulation. Citrate is at least in part transported into the cytosol by CIC. Since citrate release into the medium was not enhanced (green equal sign), I hypothesized that the majority of citrate may remain in the mitochondrion to possibly chelate reactive Fe^{2+} ions liberated by aconitase inhibition. Cytosolic citrate is converted to acetyl-CoA by ATP-citrate-lyase and is incorporated into the N-acetyl group of UDP-GlcNAc. The incorporation of ^{13}C-labeled acetyl-CoA into UDP-GlcNAc is not affected by NO and/or peroxynitrite (green equal sign). Inhibitors are shown in orange. Inhibition of glycolysis by citrate, as well as inactivation of PDC by PDK1 were not observed. Acetyl-CoA, acetyl-coenzyme A; ADP, adenosine diphosphate; ATP, adenosine triphosphate; CIC, citrate carrier; CoA, coenzyme A; FA, fatty acids; Fru-6-P, fructose-6-phosphate; Glc, glucose; Glc-6-P, glucose-6-phosphate; GLUT1, glucose transporter 1; Lac, lactate; MCT4, monocarboxylate transporter 4; NAD, nicotinamide adenine dinucleotide; NO, nitric oxide; $ONOO^-$, peroxynitrite; P_i, inorganic phosphate; PDC, pyruvate dehydrogenase complex; PDK1, pyruvate dehydrogenase kinase 1; Pyr, pyruvate; TCA, tricarboxylic acid; UDP-GlcNAc, uridine diphosphate-N-acetylglucosamine. (See text for further details.)

4.5.4 Conclusions and Perspectives

In summary, I have shown in compliance with earlier studies, for the first time using [1-^{13}C]glucose as a precursor for selective labeling and NMR spectroscopy as analytical method that treatment with NO switches primary cortical astrocytes into a glycolytic state as judged by increased glucose consumption and *de novo* lactate synthesis. This increase in glycolysis is most likely the response to defense against energy depletion due to inhibition of the respiratory chain by NO. A response that is solely attributed to astrocytes (Almeida *et al*., 2004), but not to neurons (Almeida *et al*., 2004). A shift of glucose metabolism towards PPP to maintain ATP production was not observed in my experiments as revealed by calculation of fractional ^{13}C-enrichment in extracellular lactate. Furthermore, that I did not observe significant alterations in the fractional ^{13}C-enrichment in extracellular lactate when astrocytes were exposed to NO may also indicate that glycogenolysis, in addition to glycolysis, is not enhanced in astrocytes incubated with NO to serve as an endogenous energy source. However, the glucose concentration (22 mM) used in my experiments exceeded the normal concentration in the brain (1 - 2 mM) (McNay & Gold, 1999) and was far from being consumed. There was probably no necessity of the astrocytes to break down their glycogen storage.

Moreover, I have shown for the first time, that citrate is accumulated in cell extracts of astrocytes treated with NO. Although NO is a known inhibitor of aconitase, the enzyme that catalyzes the reversible isomerization of citrate to isocitrate (Breusch, 1937), the direct detection of citrate accumulation in astrocytes, however, has not been shown before. Although citrate is an allosteric inhibitor of phosphofructokinase, the rate limiting enzyme of glycolysis, glycolysis is enhanced when astrocytes are exposed to NO, leading to the assumption that citrate may possibly not be transported out of the mitochondrion into the cytosol. I hypothesized that citrate accumulation in the mitochondria due to aconitase inhibition may concurrently prevent further damage of cellular components by chelating Fe^{2+} ions that are liberated due to the disassembly of the 4Fe-4S cluster of aconitase. In contrast to a previous study, where fluorocitrate was used as an inhibitor of aconitase, I did not detect an increase of citrate release into the cell culture medium, although citrate is highly accumulated inside the cell. The difference between inhibition of aconitase by NO and/or peroxynitrite and fluorocitrate is that by inhibition with fluorocitrate iron is not liberated. This may further substantiate the hypothesis that citrate remains in the mitochondrion, possibly to chelate and thus protect astrocytes from the harmful effects of Fe^{2+} ions. Previous studies have attributed the failure of neurons to compensate the NO-induced impairment of the respiratory chain by

enhancing glycolysis to inability of increasing PFK2, an enzyme that is almost absent in neurons (Almeida *et al*., 2001; Almeida *et al*., 2004). Since I assume that citrate might also play a role in protection of astrocytes from the deleterious effects of NO and/or peroxynitrite, it should be borne in mind that astrocytes, but not neurons are able to produce citrate in large amounts (Sonnewald *et al*., 1991; Westergaard *et al*., 1994).

Aside from these observations, I observed a decrease in intracellular glutamate content in astrocytes treated with NO. Due to the fact that the normal flux through the TCA cycle is blocked because of inhibition of aconitase, I assume that glutamate serves as an alternative substrate to fuel and thereby partially maintains a segment of the TCA cycle. The mitochondrial membrane potential is maintained by $NADH/H^+$ equivalents generated in the TCA cycle. If the mitochondrial respiratory chain is not completely inhibited by NO and/or peroxynitrite, partial maintenance of the TCA cycle by introduction of glutamate at the step of α-ketoglutarate at least to some extent sustains mitochondrial respiration and thus protects astrocytes against energy failure. Although NO-induced glutamate release has been reported in astrocytes (McNaught & Jenner, 2000; Bal-Price *et al*., 2002), I did not observe glutamate release from astrocytes after treatment with the NO-donor DETA-NONOate. This observation may corroborate the theory that the glutamate-pool in astrocytes is used to partially maintain the TCA cycle.

Physiological levels of NO inhibit reversibly and in competition with oxygen complex IV of the mitochondrial respiratory chain (Brown & Cooper, 1994; Cleeter *et al*., 1994; Takehara *et al*., 1995; Cassina & Radi, 1996; Poderoso *et al*., 1996). Whereas peroxynitrite irreversibly inhibits complex I (Murray *et al*., 2003; Brown & Borutaite, 2004; Pearce *et al*., 2005), II (Rubbo *et al*., 1994; Bolaños *et al*., 1995), and III (Guidarelli *et al*., 2004; Pearce *et al*., 2005) of the respiratory chain, as well as ATP synthase (Cassina & Radi, 1996; Radi *et al*., 2002). UDP-GlcNAc is an ideal metabolic marker for impaired mitochondrial respiration using [1-^{13}C]glucose and NMR spectroscopy as a recent study in our lab has shown (Gallinger *et al*., 2011). However, although mitochondrial respiration is most likely impaired in my experiments as inferred from enhanced glycolysis, incorporation of the ^{13}C-label in the *N*-acetyl group of UDP-GlcNAc was not affected. This means that ^{13}C-labeled cytosolic acetyl-CoA deriving from [1-^{13}C]glucose is still generated in astrocytes treated with NO. This observation implies that the mitochondrial respiration is not completely broken down in my experiments and NAD^+ generation by complex I of the respiratory chain is at least to a certain extent maintained. Preservation of mitochondrial respiration is most likely supported by maintenance of the mitochondrial membrane potential due to ATP production in glycolysis

and replenishment and thus partial maintenance of the TCA cycle by glutamate to deliver $NADH/H^+$ equivalents.

To conclude, astrocytes cope pretty well with the nitrosative stress induced by NO, using different cellular mechanisms, as also shown by the unchanged cell viability in my experiments.

For future studies, it would be interesting to follow astrocytic NO-altered metabolism when the glucose availability is restricted in view of the glycolytic state of the cells and hence the ability to cope with impaired mitochondrial respiration. Furthermore, it would be interesting, to calculate the fractional ^{13}C-enrichment under these conditions to examine if the glycogen stores are used to maintain energy homeostasis and if the cells switch towards PPP to maintain ATP production. To resolve at least in part the question, to which extent citrate is shuttled from the mitochondrion into the cytosol, the lipids in the chloroform phase of the M/C extracts could be quantified. If citrate is shuttled to a greater extent into the cytosol it is most likely that it is used for fatty acid synthesis. To substantiate the hypothesis that glutamate is used to replenish and thus partially maintain the TCA cycle, it would be interesting to investigate if PAG, the enzyme that catalyzes the deamination of glutamine to glutamate, exhibits higher mRNA expression or a higher activity in astrocytes treated with NO. If so, it is guaranteed, that more glutamate can be introduced into the TCA cycle. Inhibition of GS, the enzyme that catalyzes glutamine formation from glutamate, has already been shown to be inhibited in astrocytes treated with the NO-donor S-nitroso-*N*-acetylpenicillamine (Miñana *et al*., 1997). Anyway, the effect of NO should also be investigated in primary neurons and co-cultures of neurons and astrocytes using [1-^{13}C]glucose as a precursor for selective labeling and NMR spectroscopy as analytical method. It is extremely interesting to investigate citrate formation and glutamate consumption in NO-treated neurons compared to astrocytes. Maybe, the lesser extent of citrate formation in neurons is another aspect in addition to the almost absence of PFK2 why neurons fail to cope with nitrosative stress induced by NO.

Citrate is an essential metabolite in mammalian metabolism and cation chelation and citrate levels are strictly regulated. A decrease in aconitase activity is associated with neurodegenerative diseases where oxidative stress plays a role, like Parkinson's disease and Alzheimer's disease (Hinerfeld *et al*., 2004). Accumulation of iron, which may have been released after disruption of the 4Fe-4S by NO and/or peroxynitrite, was observed in the brain of people with Parkinson's disease (Salvatore *et al*., 2005). In addition, mitochondrial

aconitase is also a key target of oxidative damage during aging (Delaval *et al*., 2004; Yarian *et al*., 2006).

Protein nitration by peroxynitrite may also be involved in the development of neurological disorders. Nitration of proteins for example, may be involved in the mechanisms of the pathogenesis in Alzheimer's disease, since a number of proteins were found to be nitrated in in the brain of patients with Alzheimer's disease, correlating with amyloid-ß deposits (Sultana *et al*., 2006). The parkin protein was found to be S-nitrosylated in an *in vivo* mouse model of Parkinson's disease, as well as in the brain of patients with this disease (Chung *et al*., 2004). Furthermore, in consistency, NO production by iNOS was found to be abnormally enhanced in glia cells and a mouse model with this disorder (Liberatore *et al*., 1999; Wu *et al*., 2002). iNOS expression was also found in the brain of patients with Alzheimer's disease (Heneka *et al*., 2001; Haas *et al*., 2002) and in astrocytes exposed to amyloid-ß (Hu *et al*., 1998; Haas *et al*., 2002). Also, inhibition of complex I of the respiratory chain is associated with Parkinson's disease (Schapira *et al*., 1990a; Schapira *et al*., 1990b), whereas inhibition of complex IV is connected to Alzheimer's disease (Bennett *et al*., 1992; Kish *et al*., 1992; Mutisya *et al*., 1994), both complexes are known to be inhibited by peroxynitrite and NO, respectively. GSH is known to protect mitochondria against NO and/or peroxynitrite induced damage. GSH levels were found to be reduced in postmortem brain tissue of patients with Parkinson's disease (Jenner *et al*., 1992). Moreover, levels of human iNOS mRNA and thus NO production was found to be significantly increased in astrocytes in brains of patients with multiple sclerosis (Bö *et al*., 1994; Bagasra *et al*., 1995; Hill *et al*., 2004).

Besides being involved in the pathogenesis of many neurological disorders, it should not be disregarded that NO is also a physiological molecule by being an important intercellular messenger in the CNS that can be produced by all brain cells, including astrocytes, neurons, and endothelial cells (Garthwaite & Boulton, 1995; Murphy & Grzybicki, 1996). This physiological role was also emphasized by the finding that NO produced in endothelial cells leads to a high glycolytic activity in astrocytes via astrocytic HIF-1α activation, leading to stimulated lactate production that can serve to fuel neuronal energy needs. These findings suggest that NO plays an important role in brain energy metabolism (Brix *et al*., 2012). Since astrocytes cope well with the nitrous stress induced by NO and/or peroxynitrite and mitochondrial respiration is not completely disrupted in my experiments, it is presumable that NO deriving from endothelial cells is a physiological signal for astrocytes to enhance lactate formation for neuronal energy supply.

Also there are many studies suggesting a central role of NO in the development of neurological disorders, hitherto hardly little is known about development and mechanisms of these diseases and as well as its role in brain energy metabolism, in particular in view of the different vulnerability of astrocytes and neurons to NO. NMR spectroscopic detection of metabolites involved in the metabolism of brain cells coping with nitrous stress induced by NO using ^{13}C-labeling, facilitates the elucidation of the aberrant metabolic profile helping to understand the mechanisms involved in the development of these neurodegenerative diseases.

4.6 Metabolic Effects of Amyloid-ß on Neuronal HT-22 Cells and Primary Astrocytes

In this chapter I have shown that Aß strongly influences the rate of glycolysis in neuronal HT-22 cells and primary astrocytes. In addition, by investigating UDP-GlcNAc levels under influence of Aß, I have provided further evidence that the two major hallmarks of Alzheimer's disease - Aß containing senile plaques (LaFerla *et al*., 2007) and NFTs aggregated from hyperphosphorylated tau (Grundke-Iqbal *et al*., 1986a; Grundke-Iqbal *et al*., 1986b) - are mechanistically linked.

4.6.1 Enhanced Glycolysis in Neuronal HT-22 Cells and Astrocytes Exposed to Aß

Alzheimer's disease is commonly associated with impaired glucose uptake and metabolism as revealed by the use of FDG-PET (Mielke *et al*., 1992; Mosconi *et al*., 2008). Contrary to this, I have detected a significant increase in glucose uptake in neuronal HT-22 cells incubated with $Aß_{25-35}$. Since lactate synthesis was also significantly increased in these cells, it can be concluded that $Aß_{25-35}$ enhances glycolysis in neuronal HT-22 cells. In primary astrocytes, $Aß_{25-35}$ also led to significantly elevated lactate levels. Glucose utilization was not significantly increased in these cells, but there was a trend towards increased glucose uptake, also indicating enhanced glycolysis in these cells.

These contradictory results obtained by us are not an exception. The role of glucose metabolism in Alzheimer's disease is controversially discussed and the cause of impaired glucose uptake is not fully understood. In consistency with my results, Aß-induced increase in glucose uptake was investigated in cortical neurons (Soucek *et al*., 2003). In hippocampal neurons increased glucose uptake in the presence of Aß was detected in embryonic neurons,

but not in middle-age or old neurons (Patel & Brewer, 2003). Whereas a decrease in neuronal glucose uptake was observed in cultured rat hippocampal and cortical neurons exposed to Aß (Mark *et al*., 1997). In astrocytes the majority of reports show that glucose uptake is decreased after treatment with Aß (Parpura-Gill *et al*., 1997; Soucek *et al*., 2003; Schubert *et al*., 2009). However, in a recent study of Allaman *et al*., an increase in glucose uptake and lactate release was shown in astrocytes exposed to $Aß_{25-35}$ (Allaman *et al*., 2010).

How these discrepancies in isolated cells occur is not clear. One possible explanation may be differences in treatment of these cells, such as Aß concentration and incubation time. As deduced from the results of Patel & Brewer (Patel & Brewer, 2003), the age of the cells may also be a crucial factor. Furthermore, results from isolated cell culture experiments cannot be transferred to processes in a complex organ. Moreover, Alzheimer's disease develops over many years and metabolism of involved brain cells may change over a long period.

4.6.2 Aß Decreases UDP-GlcNAc Levels in Astrocytes

In the discussion above no explanation for the mechanism(s) leading to enhanced glycolysis was given. In the previous chapter we discussed extensively how inhibition of the mitochondrial respiratory chain by NO and/or peroxynitrite would affect UDP-GlcNAc synthesis.

Briefly, UDP-GlcNAc derives its *N*-acetyl group from cytosolic acetyl-CoA. Cytosolic acetyl-CoA can be *de novo* synthesized from glucose. Glucose is converted to pyruvate via glycolysis in the cytosol. Pyruvate then enters the mitochondrion, where it is converted to acetyl-CoA by PDC. Since acetyl-CoA cannot pass the mitochondrial membrane, it is introduced into the TCA cycle. The TCA cycle intermediate citrate is then transported out of the mitochondrion into the cytosol, where it is cleaved by ATP-citrate-lyase to oxaloacetate and cytosolic acetyl-CoA (see also Figure 51 and Figure 52 in Chapter 4.5.3). Alternatively to *de novo* synthesis, acetyl-CoA can also be generated by degradation of fatty acids. Since fatty acid ß-oxidation occurs in the mitochondrion, the acetyl-CoA generated from fatty acids, also has to be exported as citrate. Cytosolic acetyl-CoA is then incorporated into the *N*-acetyl group of UDP-GlcNAc by GlcN-6-P *N*-acetyl-transferase.

When the mitochondrial respiratory chain is inhibited, NADH oxidation to NAD^+ by complex I of the respiratory chain comes to a halt and NADH accumulates. NAD^+ is an essential cofactor of PDC that transforms pyruvate into acetyl-CoA. For this reason, acetyl-CoA production in the mitochondrion decreases when NAD^+ is no longer available. Under these conditions, acetyl-CoA can no longer enter the TCA cycle and the TCA cycle stops. As

a result, citrate is no longer produced, also leading to decreased formation of cytosolic acetyl-CoA. Cytosolic acetyl-CoA can no longer be incorporated into the *N*-acetyl group of UDP-GlcNAc and UDP-GlcNAc levels in cells are supposed to decrease. Besides, formation of acetyl-CoA via fatty acid degradation is not likely when the mitochondrial respiration chain is inhibited, because ß-oxidation also relies on sufficient NAD^+ supply.

Aß is known to trigger oxidative stress leading to inhibition of the mitochondrial respiratory chain (Behl *et al*., 1994; Miranda *et al*., 2000; Canevari *et al*., 2004). This process is not only limited to neurons and also takes place in astrocytes (Abramov *et al*., 2004; Canevari *et al*., 2004). There is strong evidence that at least one cause of tau hyperphosphorylation in neurons is mitochondrial dysfunction and that these processes are induced by Aß (Melov *et al*., 2007; Su *et al*., 2010; Garwood *et al*., 2011), indicating that tau pathology is secondary in the development of Alzheimer's disease.

To exert its toxic effects, Aß cannot only be internalized into the cytosol in the cell, but can also be transported into the mitochondrion (Pagani & Eckert, 2011) via the translocase of the outer membrane (TOM) (Hansson Petersen *et al*., 2008). Mitochondria were found to be the main target of Aß toxicity because Aß and its precursor protein were found to be accumulated in mitochondria of Alzheimer's disease brains (Devi *et al*., 2006; Pavlov *et al*., 2009). In the mitochondrion especially complex IV of the respiratory chain seems to be mostly affected by Aß. In transgenic Alzheimer's disease mice, complex IV activity, as well as protein levels were found to be decreased compared to age-matched controls (Manczak *et al*., 2006; Rhein *et al*., 2009). Direct inhibition of complex IV was also shown by dimeric $Aß_{1-42}$ in a dose-dependent manner in isolated human mitochondria (Crouch *et al*., 2005). Furthermore, decreased complex IV activity and/or expression were found in human Alzheimer's disease brains (Rapoport, 1999; Blass *et al*., 2000). Underexpression of all complexes of the respiratory chain, including ATP synthase (complexes I-V) was also detected in human Alzheimer's disease brains at the protein level (Liang *et al*., 2008).

Inhibition of the mitochondrial respiratory chain is most likely mediated by enhanced ROS production caused by Aß. Aß triggers cytokine release in astrocytes (Gitter *et al*., 1995) and activates iNOS in astrocytes leading to enhanced release of NO (Akama *et al*.,1998; Schubert *et al*., 2009). Elevated NO levels and enhanced activity of nNOS and iNOS were also detected in neuron-like PC12 cells exposed to increasing concentrations of Aß (Keil *et al*., 2004). Inhibition of intracellular Aß production by a γ-secretase inhibitor reduces NO production and normalizes cellular ATP levels, which had been reduced due to inhibition of the mitochondrial respiratory chain by Aß (Keil *et al*., 2004). Another effective source of

oxidative stress is H_2O_2. Increased H_2O_2 production has been observed in transgenic Alzheimer's disease mice and directly correlated with increased Aß levels (Manczak *et al*., 2006; Yao *et al*., 2009). Incubation with Aß also increased H_2O_2 production in astrocytes (Allaman *et al*., 2010) and neurons (Behl *et al*., 1994). As described in the previous chapter, peroxynitrite is a potent oxidant that can be formed by a reaction of NO with $O_2^{\bullet-}$ (Beckman *et al*., 1990; Radi *et al*., 1991). Peroxynitrite causes nitration of tyrosine residues. Nitrated tyrosine residues have been found in neurons and glia in Alzheimer's disease brain (Good *et al*., 1996; Smith *et al*., 1997), making peroxynitrite also accountable for oxidative stress in Alzheimer's disease. Besides, protein nitration, protein oxidation and lipid peroxidation (all harmful effects of ROS) were also detected in NFTs and Aß plaques in Alzheimer's disease brain (Perry *et al*., 2000). The ultimate consequence of these cellular dysfunctions induced by ROS formation is neuronal death (Varadarajan *et al*., 2000).

It has been shown that levels of the antioxidant GSH are depleted in astrocytes exposed to Aß (Abramov *et al*., 2003). The oxidative damage caused by Aß can be inhibited by exogenous GSH (Medina *et al*., 2002) or by up-regulation of GSH synthesis (Boyd-Kimball *et al*., 2005), as well as by the antioxidant and free radical scavenger vitamin E in primary neuronal cultures (Yatin *et al*., 2000). Since astrocytes supply neurons with precursors for GSH synthesis (Bolaños *et al*., 1996; Dringen *et al*., 1999a; Dringen *et al*., 1999b; Wang & Cynader, 2000), depletion of GSH by Aß in astrocytes will also affect neuronal GSH levels, making them more susceptible to oxidative stress. Moreover, GSH levels in rat brain have been shown to diminish with age (Liu & Choi, 2000; Zhu *et al*., 2006). Activities of antioxidant enzymes glutathione peroxidase, superoxide dismutase and catalase were also found to be significantly lower in patients with Alzheimer's disease compared to controls (Vural *et al*., 2010).

I detected significantly lower UDP-GlcNAc and UDP-GalNAc levels in primary cortical astrocytes, but not in neuronal HT-22 cells treated with $Aß_{25-35}$. On the basis of the extensive evidence that Aß induces oxidative stress in cells, I hypothesize that the decrease is caused by inhibition of the mitochondrial respiratory chain. Cytosolic acetyl-CoA can no longer be produced and incorporated into the *N*-acetyl group of UDP-GlcNAc. Since OGT is highly sensitive to varying UDP-GlcNAc concentrations (Haltiwanger *et al*., 1992; Kreppel *et al*., 1997; Kreppel & Hart, 1999), reduced UDP-GlcNAc levels by this mechanism, in turn, may be at least one possible factor contributing to decreased *O*-GlcNAcylation and thus hyperphosphorylation of tau in Alzheimer's disease.

Concomitant with the decrease in UDP-GlcNAc and UDP-GalNAc levels, I detected a significant increase in the mRNA expression of the GFAT1 isoform - the rate limiting enzyme

of the HBP - in Aß treated primary astrocytes. This increase implies that the HBP may compensate the Aß-induced reduced flux through the HBP. There was also a slight trend towards increased GFAT2 (which is less expressed than GFAT1 in astrocytes as well as neuronal HT-22 cell), GlcN-6-P *N*-acetyltransferase, and UDP-GlcNAc pyrophosphorylase mRNA levels. In accordance with the nonappearance of altered UDP-GlcNAc levels in HT-22 cell exposed to Aß, I detected no changes in the mRNA level in enzymes of the HBP. These results also provide an indication that Aß does not affect the formation of UDP-GlcNAc in these cells.

The assumption that Aß reduces UDP-GlcNAc levels in primary astrocytes is strongly substantiated by the fact that other enzymes involved in UDP-GlcNAc synthesis are dysregultated in Alzheimer's disease. PDC, the enzyme that transforms pyruvate into acetyl-CoA, as well as the TCA cycle enzyme α-KGDH complex are deficient in Alzheimer's disease brain (Sorbi *et al*., 1983; Gibson *et al*., 1998; Blass *et al*., 2001; Casley *et al*., 2002). Both enzymes are crucial for generation of cytosolic acetyl-CoA for UDP-GlcNAc synthesis in the cytosol. Last but not least expression of ATP-citrate-lyase, the enzyme responsible for acetyl-CoA generation in the cytosol, was found to be decreased in post-mortem brain tissues from Alzheimer's disease cases (Perry *et al*., 1980; Sorbi *et al*., 1983). The decrease in expression correlated with decreased acetyl-CoA production in Alzheimer's disease brains (Sorbi *et al*., 1983). ATP-citrate-Lyase activity was also found to decrease with age in rats (Nogalska *et al*., 2003).

It has to be noted that tau itself has been shown to induce oxidative stress and inhibit mitochondrial respiration (David *et al*., 2005). In particular complex I and V of the mitochondrial respiratory chain were found to be inhibited in transgenic mice accumulating hyperphosphorylated tau (Rhein *et al*., 2009). These transgenic mice also exhibited impaired ATP synthesis, higher levels of ROS, modified lipid peroxidation levels, and the up-regulation of antioxidant enzymes (David *et al*., 2005). These studies suggested that not only Aß, but also hyperphosphorylated tau can lead to oxidative stress observed in Alzheimer's disease. These findings are not contradictory to my hypothesis that impaired mitochondrial respiration leading to decreased UDP-GlcNAc levels may be one cause of decreased *O*-GlcNAcylation of tau. Aß toxicity may still precede hyperphosphorylation of tau and tau-induced oxidative stress occurs additionally later on in disease development.

Accordingly, the increase in glycolysis detected under my conditions may be an early response to prevent ATP depletion due to inhibition of the mitochondrial respiratory chain. This increase may be an early response in Alzheimer's disease, whereas impaired glucose

uptake occurs later in the disease. This assumption is substantiated by the fact that on the contrary to enzymes involved in oxidative phosphorylation and UDP-GlcNAc synthesis, enzymes of glycolysis, such as hexokinase, glyceraldehyde-3-phosphate dehydrogenase (GAPDH), pyruvate kinase, lactate dehydrogenase (LDH), and PFK were demonstrated to be increased in activity in Alzheimer's disease brains (Bigl *et al*., 1996; Bigl *et al*., 1999; Soucek *et al*., 2003).

Furthermore, I detected significantly increased Glc-1-P levels in astrocytes treated with $Aß_{25-35}$. Glc-1-P is involved in anabolic as well as catabolic cellular processes. Glc-1-P can be activated with UTP to from UDP-glucose. UDP-glucose can then be incorporated into astrocytic glycogen storage. However, UDP-glucose levels were unaltered in astrocytes treated with $Aß_{25-35}$ and it is unlikely that cells coping with oxidative stress fill up their glycogen stores. Glc-1-P can also be formed catabolically during glycogenolysis and serves as an endogenous energy source. For this reason, I assume that astrocytes break down their glycogen stores, in addition to increased glycolysis, as a response to compensate ATP depletion induced by inhibition of the mitochondrial respiratory chain. The increase in Glc-1-P concentration was not observed in neuronal HT-22 cells treated with $Aß_{25-35}$, because glycogen is almost exclusively localized in astrocytes (Cataldo & Broadwell, 1986; Magistretti *et al*., 1993). Therefore, neuronal cells should be more vulnerable to oxidative stress compared to astrocytes. However, I did not observe decreased UDP-GlcNAc levels in neuronal HT-22 cells. Although it has been shown that Aß is internalized into neurons, neuron-like cells, and other cell lines (Mohamed & Posse de Chaves, 2011), one possible explanation may be that the $Aß_{25-35}$ is not internalized into HT-22 cells due to lack of the receptors necessary. The fact that I detected enhanced glycolysis in Aß treated HT-22 cells does not support the consideration that $Aß_{25-23}$ is not internalized into HT-22 cells and there is no evidence that extracellular Aß enhances glycolysis in neurons. In accordance with my results, Abramov *et al*. also detected different responses of astrocytes and neurons to $Aß_{1-42}$ and $Aß_{25-35}$ exposure in cocultures of hippocampal neurons and astrocytes (Abramov *et al*., 2004). These authors observed that Aß caused a loss of $\Delta\Psi_m$ in astrocytes but no changes in the mitochondrial function were detected in neurons (Abramov *et al*., 2004). If this is also the case in neuronal HT-22 cells, this would be a possible explanation why I detected decreased UDP-GlcNAc levels in astrocytes but not in HT-22 cells. Furthermore, in the same study, astrocytes were identified as the major source for ROS production in Aß-treated cocultures (Abramov *et al*., 2004). Abramov *et al*. attributed the ROS production in astrocytes to activation of NADPH oxidase, an enzyme that generates superoxide (Babior, 2004) and that was found to be selectively expressed in astrocytes (Abramov *et al*., 2004). However, the

mechanism how Aß activates NADPH is not yet clarified. The involvement of NADPH oxidase in Aß-induced neurotoxicity has also been discussed before in microglia (Bianca *et al*., 1999; Qin *et al*., 2002).

There is now increasing evidence that astrocytes treated with Aß exert detrimental effects on neurons. Neurotoxicity is exacerbated or even provoked when neurons were treated with Aß in the presence of astrocytes compared to sole neuronal cultures (Paradisi *et al*., 2004; Abramov *et al*., 2004; Allaman *et al*., 2010; Garwood *et al*., 2011). One possible explanation for neuronal death due to Aß toxicity although the toxic processes take place in astrocytes is that Aß depletes GSH levels in astrocytes (Abramov *et al*., 2003). Under these circumstances, astrocytes can no longer supply neurons with precursors for GSH synthesis. As a result, neurons become incapable of protecting themselves against oxidative stress. Astrocytes, however, are more resistant against oxidative stress than neurons and cope with it by enhancing glycolytic activity and glycogen breakdown (Abramov *et al*., 2004). Another possibility how astrocytes mediate neurotoxicity is cytokine release. Aß was found to significantly increase the secretion of several inflammatory cytokines from astrocytes (Garwood *et al*., 2011). Cytokines in turn were found to activate iNOS in primary astrocytes and leads to enhanced NO release that contributes to neurotoxicity (Hu *et al*., 1998). Under the conditions I used for my experiments no enhanced cell death was detected in sole astrocytic, as well as sole neuronal HT-22 cell cultures, using trypan blue exclusion.

These results, together with the fact that I observed decreased UDP-GlcNAc levels in Aß-treated astrocytes but not in neuronal HT-22 cell emphasize the importance of astrocytes in the development of Alzheimer's disease. Further evidence that astrocytes might play a major role in Alzheimer's disease development is that they were found to accumulate close to Aß plaques (Itagaki *et al*., 1989; Kato *et al*., 1998). According to my hypothesis, that decreased UDP-GlcNAc levels may be one factor contributing to decreased *O*-GlcNAcylation requires that tau is present and also hyperphosphorylated in Alzheimer's disease. Tau was originally considered to be a neuronal protein (Binder *et al*., 1985), but more recent studies indicate that tau is also present in other cells including astrocytes and other glial cells (Papasozomenos & Binder 1987; Shin *et al*., 1991). Furthermore, tau was also found to be hyperphosphorylated in astrocytes in transgenic mice, indicating that astrocytic tauopathies also contribute to the pathogenesis of Alzheimer's disease (Ikeda *et al*., 1998; Higuchi *et al*., 2002; Lin *et al*., 2003). Therefore, decreased UDP-GlcNAc levels may actually be a cause of decreased *O*-GlcNAcylation and thus increased hyperphosphorylation in astrocytes. Furthermore, studies using cocultures of primary neurons and astrocytes have demonstrated that astrocytes treated

with Aß induce hyperphosphorylation of tau (Saez *et al*., 2004) and that astrocytes are even required for Aß-induced tau phosphorylation in neurons (Garwood *et al*., 2011). Moreover, it was shown that NO derived from astrocytes exposed to Aß is one mechanism responsible for hyperphosphorylation of tau in astrocytes (Saez *et al*., 2004). On this account it is possible that UDP-GlcNAc may also decrease in neurons cocultured with astrocytes. However, on the basis of the above described results from previous studies it is not surprising that I did not detect a decrease in the UDP-GlcNAc levels in neuronal HT-22 cells in my experiments. Figure 53 summarizes the impact of Aß on astrocytic metabolism detected in my experiments and how these effects may contribute to decreased *O*-GlcNAcylation in astrocytes.

4.6.3 Conclusions and Perspectives

In summary, I have shown that treatment with Aß leads to significantly decreased UDP-GlcNAc and UDP-GalNAc levels in primary astrocytes but not in neuronal HT-22 cells. This decrease was most likely due to inhibition of the mitochondrial respiratory chain, as well as inhibition of other enzymes involved in *de novo* synthesis of UDP-GlcNAc, such as PDC and ATP-citrate-lyase. I also detected an upregulation of glycolysis in astrocytes, possibly to maintain ATP-levels that would otherwise deplete due to inhibition of oxidative phosphorylation. In addition, astrocytes break down their glycogen stores when treated with Aß to maintain energy production as evidenced by significantly elevated Glc-1-P levels. Enhanced glycolysis was also detected in neuronal HT-22 cells, although no decrease in the UDP-GlcNAc concentration was detected which implies that mitochondrial respiration was not impaired. The reason for enhanced glycolysis in HT-22 cells cannot be resolved at this point.

I hypothesized that Aß-induced reduction in UDP-GlcNAc levels in astrocytes may be at least one possible factor contributing to decreased *O*-GlcNAcylation and thus hyperphosphorylation of tau in Alzheimer's disease. To the best of my knowledge, this is the first study that links Aß toxicity to changes in UDP-GlcNAc formation. My results further corroborate that astrocytes and neurons respond differently to treatment with Aß and that astrocytes may play a major role in the pathogenesis of Alzheimer's disease. In addition, my results also corroborate the assumption that accumulation of Aß precedes hyperphosphorylation of tau and thus NFT formation (LaFerla *et al*., 2007).

Furthermore, although enhanced NO production caused by Aß in astrocytes may lead to inhibition of the mitochondrial respiratory chain in astrocytes and thus reduced UDP-GlcNAc levels in these cells, other mechanisms must also be involved in this process, because I

investigated that treatment of astrocytes with NO alone induced no alterations in UDP-GlcNAc levels in astrocytes (see Chapter 4.5.3).

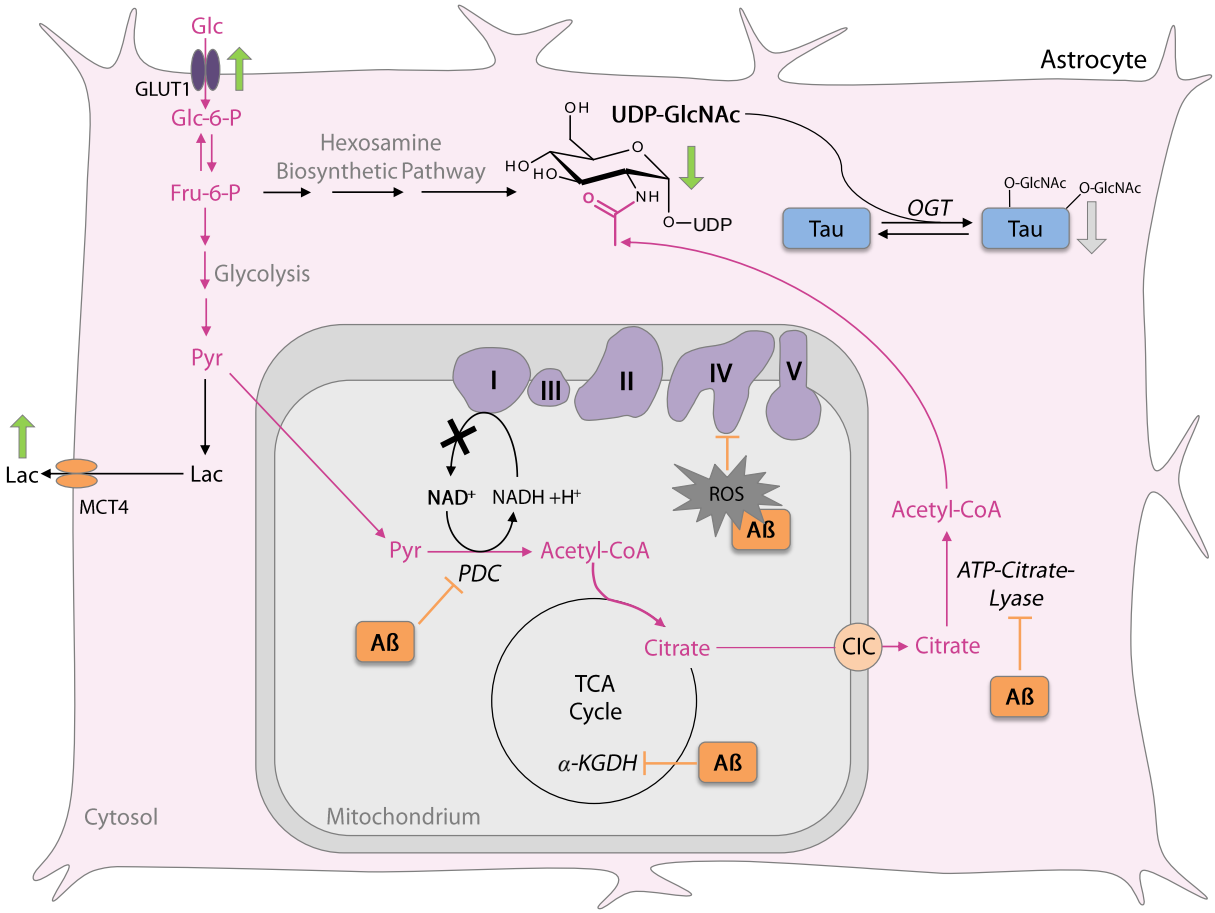

Figure 53. Aß induced impairment of UDP-GlcNAc synthesis. The route of *de novo* synthesized cytosolic acetyl-CoA from glucose is shown in pink. Glucose is metabolized via glycolysis to pyruvate. Pyruvate enters the mitochondrion and is converted to acetyl-CoA. Mitochondrial acetyl-CoA cannot leave the mitochondrion and is introduced into the TCA cycle. Citrate is then exported into the cytosol to produce cytosolic acetyl-CoA by ATP-citrate-lyase which is then incorporated into the *N*-acetyl group of UDP-GlcNAc. Aß was found to be responsible for several metabolic impairments involved in Alzheimer's disease. Note: In the graphical overview it is not distinguished between impairments directly exerted by Aß or found in brain tissue of Alzheimer's disease patients. Aß impairs in particular complex IV of the mitochondrial respiratory chain mainly by ROS production. Under inhibition of complex IV, NAD^+ production by complex I is also disrupted. NAD^+, however, is an essential cofactor for PDC. NAD^+ depletion therefore leads to termination of mitochondrial acetyl-CoA synthesis, which in turn leads to a standstill of the TCA cycle. PDC as well as the TCA cycle enzyme α-KGDH are also directly affected Aß. Citrate will no longer be produced and exported into the cytosol to be available for generation of cytosolic acetyl-CoA which is needed for synthesis of UDP-GlcNAc. ATP-citrate-lyase itself was also found to be underexpressed in Alzheimer's disease brain. The consequence of these metabolic impairments by Aß is a decrease in the UDP-GlcNAc level (green downwards pointing arrow). To cope with oxidative stress and ATP depletion, astrocytes enhance glycolysis as evidenced by increased glucose uptake (green upwards pointing arrow) and enhanced lactate synthesis (green upwards pointing arrow) in Aß-treated cells. Since OGT is highly sensitive to varying concentrations of UDP-GlcNAc, I hypothesized that a reduction of UDP-GlcNAc due to Aß toxicity may at least contribute to decreased *O*-GlcNAcylation and thus hyperphosphorylation of tau (gray upwards pointing arrow) observed in Alzheimer's disease. Aß, amyloid-ß; acetyl-CoA, acetyl-coenzyme A; ATP, adenosine triphosphate; CIC, citrate carrier; Fru-6-P, fructose-6-phosphate; Glc, glucose; Glc-6-P, glucose-6-phosphate; GLUT1, glucose transporter 1; α-KGDH, α-ketoglutarate dehydrogenase; Lac, lactate; MCT4, monocarboxylate transporter 4; NAD, nicotinamide adenine dinucleotide; O-GlcNAc, O-linked N-acetylglucosamine; OGT, O-GlcNAc transferase; PDC, pyruvate dehydrogenase complex; Pyr, pyruvate; ROS, reactive oxygen species; TCA, tricarboxylic acid; UDP-GlcNAc, uridine diphosphate-N-acetylglucosamine. (See text for further details.)

For future studies, it would be interesting to perform these experiments with ^{13}C-labeled glucose and analysis with ^{1}H,^{13}C-HSQC NMR spectroscopy. These experiments would provide further information about the mechanism of Aß-induced decrease in UDP-GlcNAc levels, such as involvement of TCA cycle or PPP. Monitoring TCA cycle intermediates in ^{1}H,^{13}C-HSQC spectra for example would give information whether the TCA cycle has stopped when cells are treated with Aß because mitochondrial acetyl-CoA is no longer produced. Besides, these experiments may reveal differences between treatments of astrocytes with NO compared to Aß with regard to inhibition of the mitochondrial respiratory chain and decreased UDP-GlcNAc formation. Inhibition of aconitase by NO leading to citrate accumulation in astrocytes was extensively discussed in the previous chapter. Since Aß treatment leads to NO formation, it would be interesting to monitor citrate levels in Aß treated neurons and astrocytes, especially as inactivation of aconitase by Aß has been shown in neuronal cell lines (Longo *et al*., 2000).

Since I have detected a significant increase in the mRNA expression of GFAT1 in astrocytes but not in neuronal HT-22 cells treated with Aß, it would also be interesting to quantify the mRNA levels of other enzymes involved in synthesis of UDP-GlcNAc and *O*-GlcNAcylation, especially ATP-citrate-lyase, PDC, and OGT under these conditions.

Last but not least since several studies have shown that astrocytes are necessary to induce tau hyperphosphorylation it would be deeply interesting to investigate Aß-induced changes on UDP-GlcNAc levels in neurons cocultured with astrocytes. One might expect that UDP-GlcNAc levels decrease under these conditions. However, to achieve more physiologically conditions these experiments should be carried out with primary neurons.

5 Materials and Methods

All chemicals, consumables, and equipment used are listed in Appendix 7.6.

5.1 Cell Lines and Cell Culture Conditions

The immortalized mouse hippocampal cell line HT-22 (Maher & Davis, 1996), human embryonic kidney 293 (HEK293) cells, Madin-Darby bovine kidney (MDBK) cells and primary cortical astrocytes were cultured as adherent cultures in Dulbecco's modified Eagle's medium (DMEM; high glucose (25 mM), with L-glutamine (4 mM)) supplemented with 10 % fetal calf serum (FCS), 1 mM sodium pyruvate, and 100 U/mL penicillin and 100 µg/mL streptomycin. Chinese hamster ovarian cells (CHO) were cultured in DMEM HAM's F12 (1:1) supplemented with 5 % FCS, and 100 U/mL penicillin and 100 µg/mL streptomycin. All cells were kept at 37 °C in a humidified atmosphere of 5 % CO_2 in air. Cells of all cell lines were routinely seeded in 75 cm^2 flasks with filter-vented caps at a density of approximately $1 \cdot 10^5$ cells/mL in 15 mL medium.

HEK293, MDBK, and CHO cells were subcultured by trypsinization. The culture medium was removed and cells were washed twice with phosphate buffered saline (PBS; pH 7,4). 1 mL 0,25 % Trypsin-EDTA (1:250; 1x) was added and cells were incubated for 5 min at room temperature. Detached cells were resuspended in 14 mL fresh culture medium. For the new subculture, 1 mL of this suspension was diluted in 14 mL fresh culture medium. HT-22 cells were subcultured by shaking of the cells without using Trypsin-EDTA. For the new subculture, 1 mL of resuspended HT-22 cells was diluted in 14 mL fresh culture medium. Cells were subcultured all 3 – 4 days.

For cryoconservation HT-22, HEK293, and MDBK cells (70 – 80 % confluent) were detached as described above. Cells were pelleted by centrifugation (200 x g; 5 min). Supernatant was aspirated and the pellet was resuspended in 3 mL freezing medium (40 % standard culture medium, 50 % FCS, 10 % DMSO sterile filtered), resulting in a concentration of approximately $1\text{-}10 \cdot 10^6$ cells/mL depending on confluency and cell line. 1 mL aliquots of cell suspension were transferred into cryovials. Cells were frozen overnight at - 80 °C before transferred into liquid nitrogen. CHO cells were cryoconserved using the same procedure, but

the freezing medium consisted of 68 % standard culture medium, 20 % FCS, and 12 % sterile filtered DMSO.

For revitalization, cryovials were quickly thawed in a 37 °C water bath. The cold cell suspension was transferred into 10 mL of appropriate cold (7 °C) culture medium. Cells were pelleted by centrifugation (200 x g; 5 min). The cell pellet was diluted into 15 mL of fresh culture medium and transferred into a cell culture flask.

Cells were regularly tested for mycoplasma contamination using the Venor® GeM Mycoplasma Detection Kit for conventional PCR (Minerva Biolabs) according to the manufacturer's protocol. No contamination of cells was detected at any time.

HT-22 and CHO cells were kindly provided by PD Dr. rer. nat. Olaf Jöhren, Institute of Experimental and Clinical Pharmacology and Toxicology, University of Lübeck. MDBK cells were kindly provided by Dr. rer. nat. Olaf Isken, Institute of Virology and Cell Biology, University of Lübeck. HEK293 cells were kindly provided by the Institute for Medical Microbiology and Hygiene, University of Lübeck.

5.2 Preparation of Primary Cortical Astrocytes

Primary cultures of cerebral cortical astrocytes were prepared as previously described (McCarthy & de Vellis, 1980; Sorg & Magistretti, 1991; Sorg & Magistretti, 1992). Astrocytes were prepared from the brain of 1 – 2 day old D1 C57/Bl16 mice. Mice were decapitated with a scissor. The brain was uncovered by cutting the head skin and the skull with a scissor along the midline to the nose. To expose the whole brain, the cut skull was bent apart by applying slight pressure or by using the scissors blades. The brain was removed by using a spatula. The olfactory bulb and the cerebellum were removed and the two hemispheres were split. The hippocampus and the white matter (*Substantia alba*) were removed. The meninges and blood vessels were carefully peeled from the cortical lobes with thin forceps using second forceps for fixation of the cortex. The cortices were immediately pooled into a small sterile petri dish on ice containing 3 mL dissection medium (DMEM high glucose (25 mM), with L-glutamine (4 mM); 10 % FCS; 1 % Antibiotic-Antimicotic). For dissociation, cortices were gently passed through needles of different gauges (20G, 21G, 25G; 3 x each) into a 5 mL syringe. The cell suspension was diluted with dissection medium

(45 mL per brain) and 35 mL were used for seeding the cells into 175 cm^2 cell culture flasks. All cells were kept at 37 °C in a humidified atmosphere of 5 % CO_2 in air. Medium was exchanged every 3 - 4 days. Experiments were performed after 21 (± 2) days in culture.
Primary cortical astrocytes were kindly prepared by Christine Eichholz, Institute of Experimental and Clinical Pharmacology and Toxicology, University of Lübeck.

5.3 Incubation Conditions

All incubation experiments have been performed with cells cultured in 175 cm^2 culture flasks or 10 cm diameter petri dishes. If not specified otherwise, experiments were carried out in 175 cm^2 culture flasks.

To improve the adherence of HT-22 cells, cultureware was coated with poly-L-ornithine prior to incubation. Poly-L-ornithine solution (0,015 g/L) was diluted 1:10 with sterile water. 4,5 mL were used for 10 cm diameter petri dishes and 13 mL for 175 cm^2 culture flasks. Petri dishes or culture flasks were incubated overnight at 37 °C. The coating solution was removed and dishes/flasks were washed with PBS. All other cells were incubated without poly-L-ornithine coating.

Unless otherwise indicated, cells were seeded at a density of $1 \cdot 10^5$ cells/mL 48 h before incubation and were incubated at 60 – 70 % confluence. 10 mL of cell suspension were used for experiments in 10 cm diameter petri dishes and 35 mL for 175 cm^2 culture flasks.

5.3.1 Comparison M/C and PCA Cell Extracts

These experiments were carried out with HT-22 cells in 10 cm diameter petri dishes. The medium was removed, cells were washed twice with 7,5 mL PBS and 10 mL fresh standard growth medium was added. Cells were incubated for 24 h. The medium was removed, cells were washed twice with 7,5 mL PBS and trypsinated using 1 mL 0,25 % Trypsin-EDTA (1:250; 1x) as described above. Cells were resuspended in 10 mL standard growth medium. To obtain the same conditions, cells of two 10 cm diameter petri dishes were pooled and cells were counted in a hemocytometer using trypan blue exclusion. Cells were centrifuged (200 x g; 5 min) and the pellet was washed twice with 200 mL ice-cold PBS (pH 7,4). The cell suspension was divided into two and cells were centrifuged (200 x g; 5 min). One pellet

was used for PCA extraction and the other for M/C extraction. Both extraction methods were performed in parallel. Simultaneous experiments were carried out in collaboration with Dr. rer. nat. Anika Hellberg, Institute of Chemistry, University of Lübeck. Cell extracts were prepared as described in Chapter 5.4.1 and Chapter 5.4.2.
In a separate set of experiments HT-22 cells were incubated in the same way as described above, but were extracted with a modified PCA extraction termed as PCA (mild conditions). Extraction procedure is described in Chapter 5.4.3.

5.3.2 Quantification of Activated Sugar Nucleotide Levels in Different Cells

HT-22, CHO, MDBK, and HEK293 were directly seeded in standard growth media at a concentration of $1 \cdot 10^5$ cells/mL. 35 mL cell suspension was used for each experiment. Cells were let grown for 72 h before M/C extraction was carried out.

Primary cortical astrocytes were used after 21 (± 2) days in culture. The medium was changed and cells were incubated with fresh standard growth medium for the corresponding time.

5.3.3 Hexosamine Treatment

100 mM stock solutions of hexosamines (GlcN, GalN, and ManN) were prepared in sterile PBS (pH 7,4) and were stored at 7 °C.
These experiments were performed with HT-22 and CHO cells. Growth medium was removed and cells were washed twice with 10 mL PBS. 35 µL of the 100 mM stock solutions of hexosamines were diluted in 35 mL standard growth medium und cells were incubated for 24 h. HT-22 and CHO cells incubated for 24 h with standard growth medium without addition of hexosamines served as controls. Cell extracts were obtained by M/C extraction (Chapter 5.4.1).

5.3.4 Galactose Treatment

These experiments were performed with HT-22 and CHO cells grown in 10 cm diameter petri dishes. DMEM (without glucose, without L-glutamine) was supplemented with 4 mM L-glutamine and 10 % FCS. For different incubation conditions, concentrations of 10 mM glucose, 5 mM galactose + 5 mM glucose, 5 mM galactose, or 10 mM galactose in medium

were prepared. DMEM HAM's F12 (1:1) was not available without glucose, thus DMEM was used for both HT-22 and CHO cells.
The growth medium was removed and cells were washed twice with 10 mM PBS (pH 7,4). Different incubation media were added and cells were incubated for 24 h. Cell extracts were obtained by M/C extraction (Chapter 5.4.1).

5.3.5 Limited Glucose Availability

These experiments were performed with HT-22 cells. DMEM (without glucose, without L-glutamine) was supplemented with 4 mM L-glutamine, 10 % FCS, and 1 mM sodium pyruvate.
For different incubation conditions, concentrations of 25 mM glucose, 18 mM glucose, 12 mM glucose, or 6 mM glucose in medium were prepared. Cells were directly seeded at a concentration $1 \cdot 10^5$ cells/mL. 35 mL cell suspension was used. Cells were let grown for 72 h before M/C extraction was carried out.

5.3.6 Glucose Deprivation

HT-22 cells and primary astrocytes were used for these experiments. DMEM (without glucose, without L-glutamine) was supplemented with 4 mM L-glutamine. These experiments were carried out without supplementation of FCS, because FCS contains undefined varying concentrations of glucose. The growth medium was removed and cells were washed twice with 10 mM PBS (pH 7,4). Cells were incubated for 12 h and 18 h with the incubation medium containing no glucose. As controls, cells were incubated with standard growth medium. Cell extracts were obtained by M/C extraction (Chapter 5.4.1).

5.3.7 Treatment with Nitric Oxide

For these experiments primary cortical astrocytes were used. DMEM (without glucose, without L-glutamine) was supplemented with 22 mM [1-^{13}C]glucose, 4 mM L-glutamine, 10 % FCS, and 1 mM sodium pyruvate.
The growth medium was removed and cells were washed twice with 10 mM PBS (pH 7,4). 20 mL of incubation medium were added to the primary astrocytes and cells were incubated for 12 h. After 12 h, 2,6 mg DETA-NONOate (final concentration 0,8 mM) was diluted in a small volume of medium and added to the cells for further 12 h. As controls, 2,98 mg Sulfo-

NONOate (final concentration 0,8 mM) was added for 12 h after 12 h preincubation with [1-^{13}C]glucose. Sulfo-NONOate is a NO-donor that does not produce NO at physiological pH. As an additional control astrocytes were incubated for 24 h with medium containing [1-^{13}C]glucose alone.

The same experiments were also carried out using unlabeled glucose instead of [1-^{13}C]glucose.

In addition, experiments where [1-^{13}C]glucose and DETA-NONOate, or Sulfo-NONOate were added at once to the incubation medium were carried out. Incubation time for these experiments was 12 h. For controls, cells were incubated with [1-^{13}C]glucose alone for 12 h. This experimental setup was chosen, to exclude that preincubation with [1-^{13}C]glucose leads to less distinct differences in the metabolic profiles, since [1-^{13}C]glucose is incorporated into the metabolites before NO is added.

Medium samples (200 µL) were taken before and after incubation.

M/C extracts of cells, as well as culture medium were analyzed by NMR spectroscopy.

5.3.8 Incubation with Amyloid-ß

A 2,5 mM stock solution of Aß$_{25-35}$ (100 x) in sterile water was prepared and kept at - 20 °C before use. The amino acid sequence is as follows: H-Gly-Ser-Asn-Lys-Gly-Ala-Ile-Ile-Gly-Leu-Met-OH. In the part of the Aß$_{25-35}$ fragment the amino acid sequence is identical in human and mouse.

These experiments were performed with HT-22 cells and primary astrocytes. Growth medium was removed and cells were washed twice with 10 mL PBS. 350 µL of the 2,5 mM stock solution (100 x) of Aß$_{25-35}$ in sterile water was diluted in 35 mL standard growth medium (final concentration 25 µM) und cells were incubated for 24 h. HT-22 cells and primary astrocytes incubated for 24 h with standard growth medium served as controls. Cell extracts were obtained by M/C extraction (Chapter 5.4.1).

Medium samples (200 µL) were taken before and after incubation.

5.4 Extraction Procedures

The incubation medium was removed and cells were washed with 10 mL PBS (pH 7,4). Cells were harvested by trypsinization with 0,25 % Trypsin-EDTA (1:250; 1x). 1mL Trypsin-EDTA was used for cells incubated in 10 cm diameter petri dishes and 2 mL were used for

cells incubated in 175 cm^2 cell culture flasks. Detached cells were resuspended in 10 mL DMEM (without glucose, without L-glutamine) supplemented with 10 % FCS. A small aliquot was used for counting using trypan blue as a vital stain for quantification. Cells were centrifuged (200 x g; 5 min) and the pellet containing approximately 10^6-10^7 cells was used for extraction.

Primary astrocytes do not detach easily by trypsinization. Astrocytes were therefore washed with PBS (pH 7,4) containing 1 mM EDTA before trypsinization. 2 mL 0,25 % Trypsin-EDTA (1:250; 1x) were added and cells were incubated for 5 min at 37 °C. Cells that still remained attached to the culture flask bottom were detached by scraping them off with a cell scraper.

5.4.1 Methanol/Chloroform Extraction

Both lipid and water-soluble cell extract fractions were obtained using a dual-phase extraction method based on methanol/chloroform/water (1:1:1; v/v/v) as originally described by Tyagi *et al*., 1996. The exact protocol used here was described by Glunde *et al*., 2004.

Pelleted cells were washed twice with 10 mL room-temperature PBS (pH 7,4), and transferred into a glass centrifuge tube. 4 mL of ice cold methanol were added to the pelleted cells and vortexed vigorously. The cells were kept on ice for 10 min. 4 mL of chloroform were added, vortexed and kept on ice for 10 min. Finally, 4 mL of water were added and the samples were vortexed vigorously. All procedures were performed on ice. Samples were left overnight at 4 ºC for phase separation.

Samples were centrifuged at 3200 × g at 4 ºC for 45 min. The two phases were separated carefully. The upper methanol/water phase contains the water soluble metabolites, such as UDP-GlcNAc and other activated sugar nucleotides. Methanol was removed by rotary evaporation. The remaining water phase was lyophilized after freezing in liquid nitrogen and stored at - 20 ºC. The lower chloroform phase containing the cellular lipids was discarded.

5.4.2 Perchloric Acid Extraction

3 mL PCA (0,9 M) were added to the pelleted cells and the cell material was resuspended by pipetting up and down. The cell suspension was centrifuged (2000 x g; 10 min; 4 °C) and the supernatant was neutralized with KOH (2,7 M). Precipitated $KClO_4$ was removed by centrifugation (2000 x g; 5 min; 4 °C), and the supernatant was lyophilized after freezing in liquid nitrogen and stored at – 20 °C.

Usually the concentrations are quantified with respect to the protein content when PCA extraction is used. However, for better comparison with M/C extracts the number of cells was counted before extraction as described above and concentrations were normalized to cell number.

5.4.3 Perchloric Acid Extraction (mild conditions)

The PCA extraction (mild conditions) was performed according to the protocol of Kochanowsky *et al*., 2006 with slight modifications. The main differences to the standard PCA extraction were the use of a less concentrated PCA solution, carrying out the whole procedure on ice, and using cold solutions.

185 µL of cold PCA (0,5 M) was added to the cell pellet and the cell material was resuspended by pipetting up and down. Samples were incubated for 2 min on ice and then centrifuged (3220 x g; 5 min; 4 °C). The supernatant was neutralized with a cold solution consisting of 42 µL KOH (2,5 M) and K_2HPO_4 (1,5 M). Samples were incubated for 2 min on ice. Precipitated $KClO_4$ was removed by centrifugation (3220 x g; 5 min; 4 °C). Supernatants were filtered through a 0,22 µm filter and then lyophilized after freezing in liquid nitrogen.

Samples were stored at – 20 °C before use.

5.5 Treatment of Pure Compounds with Perchloric Acid and Methanol/Chloroform

1 mM solutions of UDP-GlcNAc, UDP-GalNAc, UDP-Glc, UDP-Gal, UDP-GlcUA, CMP-NeuNAc, GDP-Man, and GDP-Fuc were prepared. The solutions were divided into 200 µL aliquots and then lyophilized after freezing at - 80 °C.

The lyophilized residues were used a) as references, b) for treatment with PCA, and c) for treatment with methanol/chloroform.

a) References: NMR samples were directly prepared from the lyophilized residue as described in Chapter 5.7.1.
b) PCA treatment: 3 mL PCA (0,9 M) was added to the lyophilized residue and the solution was left for 5 min before neutralization with KOH (2,7 M). Precipitated $KClO_4$ was removed by centrifugation (2000 x g; 5 min; 4 °C), and the supernatant was lyophilized after freezing at – 80 °C.

c) Methanol/chloroform treatment: 4 mL of ice cold methanol were added to the lyophilized residue and vortexed vigorously. The solution was kept on ice for 10 min. 4 mL of chloroform were added, vortexed and kept on ice for 10 min. Finally, 4 mL of water were added and the samples were vortexed vigorously. All procedures were performed on ice and samples were left overnight at 4 ºC for phase separation. The samples were centrifuged at 3200 × g at 4 ºC for 45 min. The two phases were separated carefully. Only the upper methanol/water phase was utilized. Methanol was removed by rotary evaporation and the remaining water phase was lyophilized after freezing in liquid nitrogen.

All samples were stored at - 20 °C before use.

5.6 Formation and Hydrolysis of Cyclo-Phosphates

5.6.1 Metal Ion Catalyzed Formation of Glc-1,2-cyclo-P and Gal-1,2-cyclo-P

A solution containing a concentration of 2,5 mM $ZnCl_2$ and 1 mM UDP-Glc/UDP-Gal was prepared in H_2O (volume 200 µL). The reaction batch was incubated for 24 h at RT.

The samples were lyophilized and stored at – 20 °C until NMR analysis.

5.6.2 Acid Hydrolysis of Glc-1,2-cyclo-P and Gal-1,2-cyclo-P

Lyophilized samples of Glc-1,2-cyclo-P and Gal-1,2-cyclo-P, respectively, obtained by treatment of the respective UDP-hexoses with $ZnCl_2$, were dissolved in 200 µL 0,1 M HCl and heated up to 100 °C for 5 min. The reaction was stopped by placing the samples on ice. The samples were neutralized to pH 7,0 with 0,1 M NaOH and lyophilized.

Samples were stored at - 20 °C until NMR analysis.

5.7 NMR Spectroscopy

5.7.1 Sample Preparation

Lyophilized residues of medium, PCA or M/C cell extracts, and pure compounds were redissolved in 200 µL 100 mM sodium-phosphate buffer (pH 7,4) in D_2O containing 1 mM 3-(trimethylsilyl)propionic-2,2,3,3-d_4 acid (TSP) as an internal concentration standard and chemical shift reference. NMR samples were transferred into 3 mm NMR tubes.

5.7.2 Data Acquisition - Cell Extracts

If not stated otherwise, all experiments were performed on a Bruker Avance DRX or AV III 500 MHz NMR spectrometer equipped with a TCI cryogenic probe operating at 499,80 MHz for protons and 125,69 MHz for carbons. All spectra were obtained at a temperature of 298 K. The deuterium signal in D_2O present in the samples was used for the field frequency lock for the magnetic field of the spectrometer. Bruker Topspin 2.1 and 3.0 were used for data acquisition.

Fully relaxed ^{1}H-NMR spectra of water-soluble cell extracts were obtained using a 30° flip angle. For each spectrum 32768 time-domain data points (zero-filled to 65536 data points before Fourier transform) were collected using 1024 scans, an acquisition time of 2,72 s, and 4 dummy scans. To ensure that spectra were completely relaxed for quantification, a relaxation delay of 10 s was chosen. The spectral width was set to 12 ppm (6010 Hz).

2D ^{1}H,^{13}C-HSQC spectra were recorded with 2048 (F2) x 256 (F1) data points using 64 scans per increment, a relaxation delay of 2 s, an acquisition time of 0,14 s, and 16 dummy scans. The spectral widths were set to 15 ppm (7500 Hz) in F2 and 200 ppm (25142 Hz) in F1 dimension.

1D ^{1}H,^{13}C-HSQC spectra were acquired with 16384 time-domain data points using 5120 scans, a relaxation delay of 0.1s, an acquisition time of 1.36 s, and 16 dummy scans. The spectral width was set to 12 ppm (6010 Hz). The ^{13}C offset (O2) was set to 97.62 ppm (12271 Hz) for the C1 proton of UDP-GlcNAc.

5.7.3 Data Acquisition - Media Samples

Fully relaxed ^{1}H-NMR spectra of water-soluble cell extracts were obtained using a 30° flip angle. For each spectrum 32768 time-domain data points (zero-filled to 65536 data points

before Fourier transform) were collected using 64 scans, an acquisition time of 2,72 s, and 4 dummy scans. To ensure that spectra were completely relaxed for quantification, a relaxation delay of 10 s was chosen. The spectral width was set to 12 ppm.

5.7.4 Data Acquisition – Pure Compounds and References

Fully relaxed ^{1}H-NMR spectra of pure compounds or reference substances were obtained by collecting 32768 time-domain data points (zero-filled to 65536 data points before Fourier transform), an acquisition time of 2,72 s, and 4 dummy scans. Spectra of the pure compounds treated with PCA and methanol/chloroform as described in Chapter 5.5, were acquired using 2048 scans. For spectra of reference substances that were used for signal assignment 64 scans were sufficient. When quantification was required, spectra were acquired using a 30° flip angle and a relaxation delay of 10 s. Other spectra, where quantification was not necessary, were obtained using a 90° flip angle and a relaxation delay of 1 s. The spectral width was set to 12 ppm (6010 Hz).

For the verification of Gal-2-P formation by treatment of UDP-Gal with PCA, a ^{31}P-decoupled ^{1}H-NMR spectrum was acquired using inverse gated decoupling. Experiments were performed on a Bruker Avance DPX 250 MHz NMR spectrometer equipped with a 5 mm inverse broadband probe with z-gradient operating at 250,13 MHz for protons and 101,26 MHz for phosphorus. The spectra were obtained with the following acquisition parameters: 90° flip angle, 16384 time-domain data points (zero-filled to 32768 data points before Fourier transform), 12288 scans, 2,34 s acquisition time, 2 dummy scans, and 1 s relaxation delay. The spectral width was set to 14 ppm (3501 Hz). The ^{31}P-decoupled spectrum was compared to a ^{1}H-NMR spectrum where coupling of ^{1}H to ^{31}P is visible using the same acquisition parameters.

5.7.5 Processing and Spectral Analysis

All NMR spectra were processed and analyzed using Bruker Topspin 2.1 and 3.0 software. All spectra were manually phased and an exponential window function with a line broadening of 1 Hz was applied. Baselines were initially corrected automatically. To ensure correct integration, partial manual baseline correction was accomplished in spectral regions were signal integration was performed. Chemical shifts were referenced to TSP at 0 ppm. J-coupling constants were measured from the splitting of the resonance signals in ^{1}H-NMR spectra. All signals were integrated manually.

The peak assignment of metabolites in the spectra of cell extracts and media samples was done using data from the human metabolome database (http://www.hmdb.ca; Wishart *et al*., 2009) or by comparison with spectra of authentic compounds.

The signal integrals of the anomeric protons (H1) of UDP-GlcNAc at 5,52 ppm, UDP-GalNAc at 5,55 ppm, UDP-Glc at 5,61 ppm, UDP-Gal at 5,65 ppm, Gal-1-P at 5,50 ppm, GalN-1-P at 5,69 ppm, Glc-1-P at 5,46 ppm and the signal integral of the ethyl resonances of glutamate at C4 at 2,35 ppm were determined in cell extracts. For quantification of UDP-Glc and UDP-Gal only the outer doublets of the signals were integrated, because the signal of UDP-GlcUA overlaps with the inner doublets of the doublet of doublet of UDP-Glc and UDP-Gal. The concentration calculated was doubled afterwards, giving maximal accuracy in this particular case. The concentration of UDP-GlcUA was calculated by the difference of UDP-Hex(NAc) and the sum of UDP-GlcNAc, UDP-GalNAc, UDP-Glc, and UDP-Gal. UDP-Hex(NAc) stands for the sum of all activated sugar nucleotides as determined by signal integration over the whole range of signals from anomeric protons of activated sugar nucleotides resonating in this area. In medium samples, signal integrals of the protons of methyl group of lactate at 1,33 ppm and of the anomeric proton of the α anomer of glucose at 5,24 ppm were determined. The concentration obtained by integration of the signal of the α anomer of glucose was subsequently extrapolated to total glucose (α anomer plus ß anomer).

The concentration of each metabolite in cell extracts was determined by comparison of the peak integration from the metabolites with that of the internal standard and normalization to the number of cells according to the following equation:

$$[\text{metabolite}] = \frac{I_{\text{metabolite}} \cdot n_{TSP}}{I_{TSP} \cdot \text{cell number}} \qquad \text{(eqn 1)}$$

In this equation, [metabolite] stands for the intracellular concentration of the metabolite of interest expressed in [fmol/cell]. $I_{metabolite}$ is the signal integral of the metabolite of interest divided by the number of protons, and n_{TSP} is the amount of TSP used in mol ($2 \cdot 10^{-7}$ mol). I_{TSP} is the signal integral of TSP divided by the number of protons. The number of cells in each sample (cell number) was counted before extraction.

Glucose uptake and lactate release quantified from media samples was calculated similarly with equation 1. The amount of each metabolite present in the NMR sample (200 µL volume) was determined in mol. This amount was then extrapolated to the total amount of each

metabolite present in the whole volume of medium used for incubation (35 mL and 20 mL, respectively). This amount was then divided by the number of cells. Glucose and lactate concentrations were determined in the cell culture medium before and after incubation. The difference gives the glucose uptake and lactate release expressed in [pmol/cell].

Fractional ^{13}C-enrichment in C3 of lactate was determined from ^{1}H-NMR spectra by referencing the concentration (or signal integral) of ^{13}C-labeled lactate ([^{1}H-^{13}C]) to the sum of unlabeled lactate plus ^{13}C-labeled lactate ([^{1}H-^{12}C] + [^{1}H-^{13}C]) according to equation 2:

$$^{13}\text{C-enrichment [\%]} = \frac{[^{1}\text{H-}^{13}\text{C}]}{[^{1}\text{H-}^{12}\text{C}]+[^{1}\text{H-}^{13}\text{C}]} \cdot 100 \qquad \text{(eqn 2)}$$

The values were corrected for 1,1 % natural abundance of ^{13}C.

5.8 Determination of mRNA Expression

5.8.1 Cell Lysis and Total RNA Isolation

The mRNA expression of HBP enzymes GFAT1, GFAT2, GlcN-6-P *N*-acetyltransferase, and UDP-GlcNAc pyrophosphorylase was tested using qRT-PCR.

HT-22 cells were cultured and incubated in 10 cm diameter dishes as described in Chapter 5.3.5 and Chapter 5.3.8. The incubation medium was removed and cells were washed with 5 mL PBS (pH 7,4). 2x Nucleic Acid Purification Lysis Solution, was diluted with an equal volume of calcium/magnesium-free PBS to give 1x lysis buffer. 4,5 mL of 1x lysis buffer was added to the cells. Cells were scraped off with a cell scraper and samples were homogenized by pipetting up and down.

Astrocytes were cultured and incubated in 175 cm^2 culture flasks as described in Chapter 5.3.7 and Chapter 5.3.8. Cells were trypsinated and resuspended in 10 mL DMEM (without glucose, without L-glutamine) supplemented with 10 % FCS as described in Chapter 5.4. 300 µL of this cell suspension were used for RNA lysis. Cells suspension was centrifuged (200 x g; 5 min) and 500 µL of 1x lysis buffer was added to the cells. Cells were homogenized by pipetting up and down.

Samples were stored at - 20 °C until use.

Total RNA isolation was then performed using the 6100 Nucleic Acid Prepstation and RNA Cell program according to the manufacturer's protocol. RNA yield was determined with the NanoDrop ND-1000 Spectrophotometer.

RNA samples were stored at - 80 °C until use.

5.8.2 cDNA Synthesis

4,5 µL of RNA solution was used for preparation of cDNA using the Cloned AMV First Strand Synthesis Kit according to the manufacturer's protocol. Primer, dNTP mix, and RNA were combined according to Table 4. To denature RNA and primer the reaction mix was incubated at 65 °C for 5 min and then placed on ice.

Table 4. RNA and primer denature mix.

Component	Amount
dNTP Mix (10 mM)	1 µL
Oligo$(dT)_{20}$ (50 µM)	0,5 µL
total RNA	4,5 µL

A second master reaction mix was prepared on ice as specified below (Table 5). The master mix was vortexed gently and 4 µL were added to each sample. The reaction mix was incubated for 60 min at 50 °C.

Table 5. cDNA master reaction mix.

Component	Amount
5x cDNA Synthesis Buffer	2 µL
DTT (0,1 M)	0,5 µL
RNaseOUT™ (40 U/µL)	0,5 µL
DEPC-treated water	0,5 µL
Cloned AMV RT (15 units/µL)	0,5 µL

The reaction was terminated by incubating at 85 °C for 5 min. cDNA samples were diluted 1:1 with DEPC-treated water and stored at - 20 °C until use.

5.8.3 qRT-PCR

Gene specific primers for GFAT1, GFAT2, GlcN-6-P *N*-acetyltransferase, and UDP-GlcNAc pyrophosphorylase were designed using the Primer Express program (Table 6). qRT-PCR was performed on the ABI Prism 7000 Sequence Detection System using Platinum SYBR Green qPCR Supermix according to the manufacturer's protocol. 23 µL of the master mix specified below (Table 7) were pipetted into each well of a PCR plate. 2 µL of cDNA were added and the reactions were run as shown in Table 8.

Table 6. Gene-specific forward (-F) and reverse (-R) primers used for qRT-PCR experiments.

Primer pair	Primer sequence
GFAT1-F	5'-TCCATGCAAGAGAGACGCAAA-3'
GFAT1-R	5'-CGCCAGCTTCTGGATTTCATC-3'
GFAT2-F	5'-AAGGAGATCTTCGAGCAGCCA-3'
GFAT2-R	5'-AAATGGTCCTTCAAGCCACCC-3'
GlcN-6-P *N*-acetyltransferase-F	5'-AACCCGATGAAACTCCCATG-3'
GlcN-6-P *N*-acetyltransferase-R	5'-TCAAAACCAAGCCTTCTCCAG-3'
UDP-GlcNAc pyrophosphorylase-F	5'-GATGGACGGCTGCTGTTCAAT-3'
UDP-GlcNAc pyrophosphorylase-R	5'-TGGTGCTGCAACTGAGGTTCA-3'

Table 7. Reaction mix for qRT-PCR.

Component	Amount
Platinum® SYBR® Green qPCR SuperMix	12,5 µL
Forward primer (10 pmol/µL)	0,75 µL
Reverse primer (10 pmol/µL)	0,75 µL
DEPC-treated water	9 µL
cDNA	2 µL

Table 8. Real-time qRT-PCR program (including melting curve analysis).

Cycles	Temperature [°C]	Time [s]
1	50 °C	120
1	95 °C	120
40	95 °C	15
	60 °C	60
1	95 °C	15
1	60 °C	20
1	95 °C	15

For quantification, the copy number of each gene was calculated by a standard curve. mRNA expression values were normalized to total RNA.

5.9 Statistical Analysis

Data of incubation experiments were obtained from at least three independent experiments. All data are expressed as the mean ± standard deviation. Statistical significance between experiments of control and treated groups was tested by performing an unpaired student's *t*-test. *P* values of $P < 0.05$ were considered to be significant.

6 References

Abeijon C1, Mandon EC, Hirschberg CB. Transporters of nucleotide sugars, nucleotide sulfate and ATP in the Golgi apparatus. *Trends Biochem Sci* 22(6), 203-207 (1997).

Abraham S, Fitch WM, Chaikoff IL. Mannose metabolism and the demonstration of mannokinase and phosphomannoisomerase activities in the lactating rat mammary gland. *Arch Biochem Biophys* 93, 278-282 (1961).

Abramov AY, Canevari L, Duchen MR. Beta-amyloid peptides induce mitochondrial dysfunction and oxidative stress in astrocytes and death of neurons through activation of NADPH oxidase. *J Neurosci* 24(2), 565-575 (2004).

Abramov AY, Canevari L, Duchen MR. Changes in intracellular calcium and glutathione in astrocytes as the primary mechanism of amyloid neurotoxicity. *J Neurosci* 23(12), 5088-5095 (2003).

Akama KT, Albanese C, Pestell RG, Van Eldik LJ. Amyloid β-peptide stimulates nitric oxide production in astrocytes through an NFκB-dependent mechanism. *Proc Natl Acad Sci U S A* 95(10), 5795–5800 (1998).

Akerboom TP, Bilzer M, Sies H. The relationship of biliary glutathione disulfide efflux and intracellular glutathione disulfide content in perfused rat liver. *J Biol Chem* 257(8), 4248-4252 (1982).

Akimoto Y, Comer FI, Cole RN, Kudo A, Kawakami H, Hirano H, Hart GW. Localization of the *O*-GlcNAc transferase and *O*-GlcNAc-modified proteins in rat cerebellar cortex. *Brain Re*s 966(2), 194-205 (2003).

Akimoto Y, Hart GW, Wells L, Vosseller K, Yamamoto K, Munetomo E, Ohara-Imaizumi M, Nishiwaki C, Nagamatsu S, Hirano H, Kawakami H. Elevation of the post-translational modification of proteins by *O*-linked *N*-acetylglucosamine leads to deterioration of the glucose-stimulated insulin secretion in the pancreas of diabetic Goto-Kakizaki rats. *Glycobiology* 17(2), 127-140 (2007).

Akimoto Y, Kreppel LK, Hirano H, Hart GW. Hyperglycemia and the *O*-GlcNAc transferase in rat aortic smooth muscle cells: elevated expression and altered patterns of *O*-GlcNAcylation. *Arch Biochem Biophys* 389(2), 166-175 (2001).

Akiyama H, Barger S, Barnum S, Bradt B, Bauer J, Cole GM, Cooper NR, Eikelenboom P, Emmerling M, Fiebich BL, Finch CE, Frautschy S, Griffin WS, Hampel H, Hull M, Landreth G, Lue L, Mrak R, Mackenzie IR, McGeer PL, O'Banion MK, Pachter J, Pasinetti G, Plata-Salaman C, Rogers J, Rydel R, Shen Y, Streit W, Strohmeyer R, Tooyoma I, Van Muiswinkel FL, Veerhuis R, Walker D, Webster S, Wegrzyniak B, Wenk G, Wyss-Coray T. Inflammation and Alzheimer's disease. *Neurobiol Aging* 21(3), 383-421 (2000).

Al-Chalabi A, Miller CC. Neurofilaments and neurological disease. *Bioessays* 25(4), 346-355 (2003).

Alexander GE, Chen K, Pietrini P, Rapoport SI, Reiman EM. Longitudinal PET Evaluation of Cerebral Metabolic Decline in Dementia: A Potential Outcome Measure in Alzheimer's Disease Treatment Studies. *Am J Psychiatry* 159(5), 738-745 (2002).

Allaman I, Gavillet M, Bélanger M, Laroche T, Viertl D, Lashuel HA, Magistretti PJ. Amyloid-ß aggregates cause alterations of astrocytic metabolic phenotype: impact on neuronal viability. *J Neurosci* 30(9), 3326-3338 (2010).

Almeida A, Almeida J, Bolaños JP, Moncada S. Different responses of astrocytes and neurons to nitric oxide: The role of glycolytically generated ATP in astrocyte protection. *Proc Natl Acad Sci U S A* 98(26), 15294–15299 (2001a).

Almeida A, Bolaños JP. A transient inhibition of mitochondrial ATP synthesis by nitric oxide synthase activation triggered apoptosis in primary cortical neurons. *J Neurochem* 77(2), 676-90 (2001).

Almeida A, Moncada S, Bolaños JP. Nitric oxide switches on glycolysis through the AMP protein kinase and 6-phosphofructo-2-kinase pathway. *Nat Cell Biol* 6(1), 45-51 (2004).

Andersson U, Leighton B, Young ME, Blomstrand E, Newsholme EA. Inactivation of aconitase and oxoglutarate dehydrogenase in skeletal muscle *in vitro* by superoxide anions and/or nitric oxide. *Biochem Biophys Res Commun* 249(2), 512-516 (1998).

Andrali SS, Qian Q, Ozcan S. Glucose mediates the translocation of NeuroD1 by *O*-linked glycosylation. *J Biol Chem* 282(21), 15589-15596 (2007).

Andreozzi F, D'Alessandris C, Federici M, Laratta E, Del Guerra S, Del Prato S, Marchetti P, Lauro R, Perticone F, Sesti G. Activation of the hexosamine pathway leads to phosphorylation of insulin receptor substrate-1 on Ser307 and Ser612 and impairs the

phosphatidylinositol 3-kinase/Akt/mammalian target of rapamycin insulin biosynthetic pathway in RIN pancreatic beta-cells. *Endocrinology* 145(6), 2845-2857 (2004).

Angata T, Varki A. Chemical diversity in the sialic acids and related alpha-keto acids: an evolutionary perspective. *Chem Rev* 102(2), 439-469 (2002).

Arnold CS, Johnson GV, Cole RN, Dong DL, Lee M, Hart GW. The microtubule-associated protein tau is extensively modified with *O*-linked *N*-acetylglucosamine. *J Biol Chem* 271(46), 28741-28744 (1996).

Arriagada PV, Growdon JH, Hedley-Whyte ET, Hyman BT. Neurofibrillary tangles but not senile plaques parallel duration and severity of Alzheimer's disease. *Neurology* 42(3 Pt 1), 631-639 (2004).

Atochin DN, Demchenko IT, Astern J, Boso AE, Piantadosi CA, Huang PL. Contributions of endothelial and neuronal nitric oxide synthases to cerebrovascular responses to hyperoxia. J *Cereb Blood Flow Metab* 23(10), 1219-26 (2003).

Atochin DN, Huang PL. Endothelial nitric oxide synthase transgenic models of endothelial dysfunction. *Pflugers Arch* 460(6), 965-74 (2010).

Avila J, Lucas JJ, Perez M, Hernandez F. Role of tau protein in both physiological and pathological conditions. *Physiol Rev* 84(2), 361-384 (2004).

Azzouz N, de Macedo CS, Ferguson MA, Smith TK, Schwarz RT. Mannosamine can replace glucosamine in glycosylphosphatidylinositols of *Plasmodium falciparum in vitro*. *Mol Biochem Parasitol* 142(1), 12-24 (2005).

Babcock GT, Wikström M. Oxygen activation and the conservation of energy in cell respiration. *Nature* 356(6367), 301-309 (1992).

Babior BM. NADPH oxidase. *Curr Opin Immunol* 16(1), 42-47 (2004).

Bagasra O, Michaels FH, Zheng YM, Bobroski LE, Spitsin SV, Fu ZF, Tawadros R, Koprowski H. Activation of the inducible form of nitric oxide synthase in the brains of patients with multiple sclerosis. *Proc Natl Acad Sci U S A* 92(26), 12041-12045 (1995).

Ball LE, Berkaw MN, Buse MG. Identification of the major site of *O*-linked ß-*N*-acetylglucosamine modification in the C terminus of insulin receptor substrate-1. *Mol Cell Proteomics* 5(2), 313-323 (2006).

Ballard FJ. Purification and properties of galactokinase from pig liver. *Biochem J* 98(1), 347-352 (1966).

Ballatore C, Lee VM, Trojanowski JQ. Tau-mediated neurodegeneration in Alzheimer's disease and related disorders. *Nat Rev Neurosci* 8(9), 663-672 (2007).

Bal-Price A, Brown GC. Inflammatory neurodegeneration mediated by nitric oxide from activated glia-inhibiting neuronal respiration, causing glutamate release and excitotoxicity. *J Neurosci* 21(17), 6480-6491 (2001).

Bal-Price A, Moneer Z, Brown GC. Nitric oxide induces rapid, calcium-dependent release of vesicular glutamate and ATP from cultured rat astrocytes. *Glia* 40(3), 312-323 (2002).

Bannon JH, Mc Gee MM. Understanding the role of aneuploidy in tumorigenesis. *Biochem Soc Trans* 37(Pt 4), 910-913 (2009).

Barker JE, Bolaños JP, Land JM, Clark JB, Heales SJ. Glutathione protects astrocytes from peroxynitrite-mediated mitochondrial damage: implications for neuronal/astrocytic trafficking and neurodegeneration. *Dev Neurosci* 18(5-6), 391-396 (1996).

Baron AD, Zhu JS, Zhu JH, Weldon H, Maianu L, Garvey WT. Glucosamine induces insulin resistance in vivo by affecting GLUT 4 translocation in skeletal muscle. Implications for glucose toxicity. *J Clin Invest* 96(6), 2792-2801 (1995).

Barone BB, Yeh HC, Snyder CF, Peairs KS, Stein KB, Derr RL, Wolff AC, Brancati FL. Long-term all-cause mortality in cancer patients with preexisting diabetes mellitus: a systematic review and meta-analysis. *JAMA* 300(23), 2754-2764 (2008).

Bates TE, Loesch A, Burnstock G, Clark JB. Immunocytochemical evidence for a mitochondrially located nitric oxide synthase in brain and liver. *Biochem Biophys Res Commun* 213(3), 896-900 (1995).

Bates TE, Loesch A, Burnstock G, Clark JB. Mitochondrial nitric oxide synthase: a ubiquitous regulator of oxidative phosphorylation? *Biochem Biophys Res Commun* 218(1), 40-44 (1996).

Beckman JS, Beckman TW, Chen J, Marshall PA, Freeman BA. Apparent hydroxyl radical production by peroxynitrite: implications for endothelial injury from nitric oxide and superoxide. *Proc Natl Acad Sci U S A* 87(4), 1620-1624 (1990).

Beffert U, Aumont N, Dea D, Lussier-Cacan S, Davignon J, Poirier J. Beta-amyloid peptides increase the binding and internalization of apolipoprotein E to hippocampal neurons. *J Neurochem* 70(4), 1458-1466 (1998).

Behl C, Davis JB, Lesley R, Schubert D. Hydrogen peroxide mediates amyloid beta protein toxicity. *Cell* 77(6), 817-827 (1994).

Beinert H, Kennedy MC, Stout CD. Aconitase as Iron-Sulfur Protein, Enzyme, and Iron-Regulatory Protein. *Chem Rev* 96(7), 2335-2374 (1996).

Belfiore F, Iannello S. Insulin resistance in obesity: metabolic mechanisms and measurement methods. *Mol Genet Metab* 65(2), 121-128 (1998).

Bell GI, Burant CF, Takeda J, Gould GW. Structure and function of mammalian facilitative sugar transporters. *J Biol Chem* 268(26), 19161-19164 (1993).

Beltrán B, Mathur A, Duchen MR, Erusalimsky JD, Moncada S. The effect of nitric oxide on cell respiration: A key to understanding its role in cell survival or death. *Proc Natl Acad Sci U S A* 97(26), 14602-14607 (2000).

Bennett MC, Diamond DM, Stryker SL, Parks JK, Parker WD Jr. Cytochrome oxidase inhibition: a novel animal model of Alzheimer's disease. *J Geriatr Psychiatry Neurol* 5(2), 93-101 (1992).

Bertram L, Blacker D, Mullin K, Keeney D, Jones J, Basu S, Yhu S, McInnis MG, Go RC, Vekrellis K, Selkoe DJ, Saunders AJ, Tanzi RE. Evidence for genetic linkage of Alzheimer's disease to chromosome 10q. *Science* 290(5500), 2302-1303 (2000).

Bharath S, Andersen JK. Glutathione depletion in a midbrain-derived immortalized dopaminergic cell line results in limited tyrosine nitration of mitochondrial complex I subunits: implications for Parkinson's disease. *Antioxid Redox Signal* 7(7-8), 900-10 (2005).

Bhat PJ. Galactose-1-phosphate is a regulator of inositol monophosphatase: a fact or a fiction? *Med Hypotheses* 60(1), 123-128 (2003).

Bianca VD, Dusi S, Bianchini E, Dal Prà I, Rossi F. Beta-amyloid activates the $O_2^{\bullet -}$ forming NADPH oxidase in microglia, monocytes, and neutrophils. A possible inflammatory mechanism of neuronal damage in Alzheimer's disease. *J Biol Chem* 274(22), 15493-15499 (1999).

Bigl M, Bleyl AD, Zedlick D, Arendt T, Bigl V, Eschrich K. Changes of activity and isozyme pattern of phosphofructokinase in the brains of patients with Alzheimer's disease. *J Neurochem* 67(3), 1164-1171 (1996).

Bigl M, Brückner MK, Arendt T, Bigl V, Eschrich K. Activities of key glycolytic enzymes in the brains of patients with Alzheimer's disease. *J Neural Transm* 106(5-6), 499-511 (1999).

Binder LI, Frankfurter A, Rebhun LI. The distribution of tau in the mammalian central nervous system. *J Cell Biol* 101(4), 1371-1378 (1985).

Bisaccia F, De Palma A, Palmieri F. Identification and purification of the tricarboxylate carrier from rat liver mitochondria. *Biochim Biophys Acta* 977(2), 171-176 (1989).

Blanchard J. Evaluation of the relative efficacy of various techniques for deproteinizing plasma samples prior to high-performance liquid chromatographic analysis. *J Chromatogr* 226(2), 455-460 (1981).

Blass JP, Sheu RK, Gibson GE. Inherent abnormalities in energy metabolism in Alzheimer disease. Interaction with cerebrovascular compromise. *Ann N Y Acad Sci* 903, 204-221 (2000).

Bligh EG, Dyer WJ. A rapid method of total lipid extraction and purification. *Can J Biochem Physiol* 37(8), 911-917 (1959).

Bö L, Dawson TM, Wesselingh S, Mörk S, Choi S, Kong PA, Hanley D, Trapp BD. Induction of nitric oxide synthase in demyelinating regions of multiple sclerosis brains. *Ann Neurol* 36(5), 778-86 (1994).

Boland K, Manias K, Perlmutter DH. Specificity in recognition of amyloid-ß peptide by the serpin-enzyme complex receptor in hepatoma cells and neuronal cells. *J Biol Chem* 270(47), 28022-28028 (1995).

Bolaños JP, Heales SJ, Land JM, Clark JB. Effect of peroxynitrite on the mitochondrial respiratory chain: differential susceptibility of neurones and astrocytes in primary culture. *J Neurochem* 64(5), 1965-1972 (1995).

Bolaños JP, Heales SJ, Peuchen S, Barker JE, Land JM, Clark JB. Nitric oxide-mediated mitochondrial damage: a potential neuroprotective role for glutathione. *Free Radic Biol Med* 21(7):995-1001 (1996).

Bolaños JP, Peuchen S, Heales SJ, Land JM, Clark JB. Nitric oxide-mediated inhibition of the mitochondrial respiratory chain in cultured astrocytes. *J Neurochem* 63(3), 910-916 (1994).

Borchelt DR, Thinakaran G, Eckman CB, Lee MK, Davenport F, Ratovitsky T, Prada CM, Kim G, Seekins S, Yager D, Slunt HH, Wang R, Seeger M, Levey AI, Gandy SE, Copeland NG, Jenkins NA, Price DL, Younkin SG, Sisodia SS. Familial Alzheimer's disease-linked presenilin 1 variants elevate Aß1-42/1-40 ratio *in vitro* and *in vivo*. *Neuron* 17(5), 1005-1013 (1996).

Bouzier AK, Thiaudiere E, Biran M, Rouland R, Canioni P, Merle M. The Metabolism of [3-^{13}C]Lactate in the Rat Brain Is Specific of a Pyruvate Carboxylase-Deprived Compartment. *J Neurosci* 75(2), 480-486 (2000).

Boyd-Kimball D, Sultana R, Abdul HM, Butterfield DA. Gamma-glutamylcysteine ethyl ester-induced up-regulation of glutathione protects neurons against Aß(1-42)-mediated oxidative stress and neurotoxicity: implications for Alzheimer's disease. *J Neurosci Res* 79(5), 700-6 (2005).

Bradbury MW. Transport of iron in the blood-brain-cerebrospinal fluid system. *J Neurochem* 69(2), 443-54 (1997).

Brand A, Richter-Landsberg C, Leibfritz D. Multinuclear NMR studies on the energy metabolism of glial and neuronal cells. *Dev Neurosci*. 15(3-5), 289-98 (1993).

Brandt R, Hundelt M, Shahani N. Tau alteration and neuronal degeneration in tauopathies: mechanisms and models. *Biochim Biophys Acta* 1739(2-3), 331-354 (2005).

Breusch FL. Citric acid in tissue metabolism. *Physiol Chem* 250, 262-280 (1937).

Brix B, Mesters JR, Pellerin L, Jöhren O. Endothelial Cell-Derived Nitric Oxide Enhances Aerobic Glycolysis in Astrocytes via HIF-1α-Mediated Target Gene Activation. *J Neurosci* 32(28), 9727-9735 (2012).

Brockhausen I, Schachter H, Stanley P. O-GalNAc Glycans. In: Varki A, Cummings RD, Esko JD, *et al*., editors. Essentials of Glycobiology. 2nd edition. Cold Spring Harbor (NY): Cold Spring Harbor Laboratory Press. Chapter 9 (2009).

Brorson JR, Sulit RA, Zhang H. Nitric oxide disrupts Ca^{2+} homeostasis in hippocampal neurons. *J Neurochem* 68(1), 95-105 (1997).

Brorson JR, Zhang H. Disrupted $[Ca^{2+}]_i$ homeostasis contributes to the toxicity of nitric oxide in cultured hippocampal neurons. J Neurochem 69(5), 1882-1889 (1997).

Brown AM, Baltan Tekkök S, Ransom BR. Energy transfer from astrocytes to axons: the role of CNS glycogen. *Neurochem Int* 45(4), 529-36 (2004).

Brown DH. Action of phosphoglucomutase on D-glucosamine-6-phosphate. *J Biol Chem* 204(2), 877-889 (1953).

Brown GC, Borutaite V. Inhibition of mitochondrial respiratory complex I by nitric oxide, peroxynitrite and S-nitrosothiols. *Biochim Biophys Acta* 1658(1-2), 44-9 (2004).

Brown GC, Cooper CE. Nanomolar concentrations of nitric oxide reversibly inhibit synaptosomal respiration by competing with oxygen at cytochrome oxidase. *FEBS Lett* 356(2-3), 295-298 (1994).

Brown GC. Nitric oxide regulates mitochondrial respiration and cell functions by inhibiting cytochrome oxidase. *FEBS Lett* 369(2-3), 136-139 (1995).

Buse MG, Robinson KA, Marshall BA, Hresko RC, Mueckler MM. Enhanced *O*-GlcNAc protein modification is associated with insulin resistance in GLUT1-overexpressing muscles. *Am J Physiol Endocrinol Metab* 283(2), E241-E250 (2002).

Buse MG. Hexosamines, insulin resistance, and the complications of diabetes: current status. *Physiol Endocrinol Metab* 290(1), E1-E8 (2006).

Cahoy JD, Emery B, Kaushal A, Foo LC, Zamanian JL, Christopherson KS, Xing Y, Lubischer JL, Krieg PA, Krupenko SA, Thompson WJ, Barres BA. A transcriptome database for astrocytes, neurons, and oligodendrocytes: a new resource for understanding brain development and function. *J Neurosci* 28(1), 264-278 (2008).

Caldwell SA, Jackson SR, Shahriari KS, Lynch TP, Sethi G, Walker S, Vosseller K, Reginato MJ. Nutrient sensor *O*-GlcNAc transferase regulates breast cancer tumorigenesis through targeting of the oncogenic transcription factor FoxM1. *Oncogene* 29(19), 2831-2842 (2010).

Canevari L, Abramov AY, Duchen MR. Toxicity of amyloid beta peptide: tales of calcium, mitochondria, and oxidative stress. *Neurochem Res* 29(3), 637-650 (2004).

Casadesus G, Moreira PI, Nunomura A, Siedlak SL, Bligh-Glover W, Balraj E, Petot G, Smith MA, Perry G. Indices of metabolic dysfunction and oxidative stress. *Neurochem Res* 32(4-5), 717-722 (2007).

Casley CS, Canevari L, Land JM, Clark JB, Sharpe MA. Beta-amyloid inhibits integrated mitochondrial respiration and key enzyme activities. *J Neurochem* 80(1), 91-100 (2002).

Cassina A, Radi R. Differential inhibitory action of nitric oxide and peroxynitrite on mitochondrial electron transport. *Arch Biochem Biophys* 328(2), 309-16 (1996).

Castro L, Rodriguez M, Radi R. Aconitase is readily inactivated by peroxynitrite, but not by its precursor, nitric oxide. *J Biol Chem* 269(47), 29409-29415 (1994).

Castro LA, Robalinho RL, Cayota A, Meneghini R, Radi R. Nitric oxide and peroxynitrite-dependent aconitase inactivation and iron-regulatory protein-1 activation in mammalian fibroblasts. *Arch Biochem Biophys* 359(2), 215-24 (1998).

Cataldo AM, Broadwell RD. Cytochemical identification of cerebral glycogen and glucose-6-phosphatase activity under normal and experimental conditions: I. Neurons and glia. *J Electron Microsc Tech* 3(4), 413–437 (1986).

Chachami G, Paraskeva E, Mingot JM, Braliou GG, Görlich D, Simos G. Transport of hypoxia-inducible factor HIF-1alpha into the nucleus involves importins 4 and 7. *Biochem Biophys Res Commun* 390(2), 235-40 (2009).

Chance B, Sies H, Boveris A. Hydroperoxide metabolism in mammalian organs. *Physiol Rev* 59(3), 527-605 (1979).

Chang S, Duerr B, Serif G. An epimerase-reductase in L-fucose synthesis. J Biol Chem 263(4), 1693-1697 (1988).

Chao CC, Hu S, Ehrlich L, Peterson PK. Interleukin-1 and tumor necrosis factor-alpha synergistically mediate neurotoxicity: involvement of nitric oxide and of *N*-methyl-D-aspartate receptors. *Brain Behav Immun* 9(4), 355-365 (1995).

Cheema-Dhadli S, Halperin ML. Effect of palmitoyl-CoA and beta-oxidation of fatty acids on the kinetics of mitochondrial citrate transporter. *Can J Biochem* 54(2), 171-177 (1976).

Chen YQ, Su M, Walia RR, Hao Q, Covington JW, Vaughan DE. Sp1 sites mediate activation of the plasminogen activator inhibitor-1 promoter by glucose in vascular smooth muscle cells. *J Biol Chem* 273(14), 8225-8231 (1998).

Cheng HM, Xiong H, Xiong J, Tsubota K. Metabolic studies of galactosemic cataract. *Exp Eye Res* 51(4), 345-349 (1990).

Cheung PY, Danial H, Jong J, Schulz R. Thiols protect the inhibition of myocardial aconitase by peroxynitrite. *Arch Biochem Biophys* 350(1), 104-108 (1998).

Cheung WD, Hart GW. AMP-activated Protein Kinase and p38 MAPK Activate *O*-GlcNAcylation of Neuronal Proteins during Glucose Deprivation. *J Biol Chem* 283(19), 13009–13020 (2008).

Choi YK, Kim CK, Lee H, Jeoung D, Ha KS, Kwon YG, Kim KW, Kim YM. Carbon monoxide promotes VEGF expression by increasing HIF-1alpha protein level via two distinct mechanisms, translational activation and stabilization of HIF-1alpha protein. *J Biol Chem* 285(42), 32116-32125 (2010).

Chung KK, Thomas B, Li X, Pletnikova O, Troncoso JC, Marsh L, Dawson VL, Dawson TM. S-nitrosylation of parkin regulates ubiquitination and compromises parkin's protective function. *Science* 304(5675), 1328-1331 (2004).

Chuquet J, Quilichini P, Nimchinsky EA, Buzsáki G. Predominant enhancement of glucose uptake in astrocytes versus neurons during activation of the somatosensory cortex. *J Neurosci* 30(45), 15298-15303 (2010).

Clark RJ, McDonough PM, Swanson E, Trost SU, Suzuki M, Fukuda M, Dillmann WH. Diabetes and the accompanying hyperglycemia impairs cardiomyocyte calcium cycling through increased nuclear *O*-GlcNAcylation. *J Biol Chem* 278(45), 44230-44307 (2003).

Cleeter MW, Cooper JM, Darley-Usmar VM, Moncada S, Schapira AH. Reversible inhibition of cytochrome c oxidase, the terminal enzyme of the mitochondrial respiratory chain, by nitric oxide. Implications for neurodegenerative diseases. *FEBS Lett* 345(1), 40-45 (1994).

Clementi E, Brown GC, Feelisch M, Moncada S. Persistent inhibition of cell respiration by nitric oxide: crucial role of S-nitrosylation of mitochondrial complex I and protective action of glutathione. *Proc Natl Acad Sci U S A* 95(13), 7631-7636 (1998).

Clodfelder-Miller B, De Sarno P, Zmijewska AA, Song L, Jope RS. Physiological and pathological changes in glucose regulate brain Akt and glycogen synthase kinase-3. *J Biol Chem* 280(48), 39723-39731 (2005).

Coates SW, Gurney T Jr, Sommers LW, Yeh M, Hirschberg CB. Subcellular localization of sugar nucleotide synthetases. *J Biol Chem* 255(19), 9225-9229 (1980).

Coen M, Hong YS, Clayton TA, Rohde CM, Pearce JT, Reily MD, Robertson DG, Holmes E, Lindon JC, Nicholson JK. The mechanism of galactosamine toxicity revisited; a metabonomic study. *J Proteome Res* 6(7), 2711-2719 (2007).

Cohen JS, Lyon RC, Chen C, Faustino PJ, Batist G, Shoemaker M, Rubalcaba E, Cowan KH. Differences in phosphate metabolite levels in drug-sensitive and -resistant human breast cancer cell lines determined by ^{31}P magnetic resonance spectroscopy. *Cancer Res* 46(8), 4087-4090 (1986).

Cole RN, Hart GW. Glycosylation sites flank phosphorylation sites on synapsin I: *O*-linked *N*-acetylglucosamine residues are localized within domains mediating synapsin I interactions. *J Neurochem* 73(1), 418-428 (1999).

Comb DG, Watson DR, Roseman S. The sialic acids. IX. Isolation of cytidine 5'-monophospho-N-acetylneuraminic acid from Escherichia coli K-235. *J Biol Chem* 241(23), 5637-42 (1966).

Comer FI, Vosseller K, Wells L, Accavitti MA, Hart GW. Characterization of a mouse monoclonal antibody specific for *O*-linked *N*-acetylglucosamine. *Anal Biochem* 293(2), 169-177 (2001).

Comtesse N, Maldener E, Meese E. Identification of a nuclear variant of MGEA5, a cytoplasmic hyaluronidase and a ß-N-acetylglucosaminidase. *Biochem Biophys Res Commun* 283(3), 634-640 (2001).

Considine RV, Cooksey RC, Williams LB, Fawcett RL, Zhang P, Ambrosius WT, Whitfield RM, Jones R, Inman M, Huse J, McClain DA. Hexosamines regulate leptin production in human subcutaneous adipocytes. *J Clin Endocrinol Metab* 85(10), 3551-3556 (2000).

Cooksey RC, Hebert LF Jr, Zhu JH, Wofford P, Garvey WT, McClain DA. Mechanism of hexosamine-induced insulin resistance in transgenic mice overexpressing glutamine:fructose-

6-phosphate amidotransferase: decreased glucose transporter GLUT4 translocation and reversal by treatment with thiazolidinedione. *Endocrinology* 140(3), 1151-1157 (1999).

Cooksey RC, McClain DA. Transgenic Mice Overexpressing the Rate-Limiting Enzyme for Hexosamine Synthesis in Skeletal Muscle or Adipose Tissue Exhibit Total Body Insulin Resistance. *Ann N Y Acad Sci* 967, 102-111 (2002).

Cooper CE. Nitric oxide and cytochrome oxidase: substrate, inhibitor or effector? *Trends Biochem Sci* 27(1), 33-9 (2002).

Cooper CE. Nitric oxide and iron proteins. *Biochim Biophys Acta* 1411(2-3), 290-309 (1999).

Copeland RJ, Bullen JW, Hart GW. Cross-talk between GlcNAcylation and phosphorylation: roles in insulin resistance and glucose toxicity. *Am J Physiol Endocrinol Metab* 295(1), E17-E28 (2008).

Corbett RJ, Nunnally RL, Giovanella BC, Antich PP. Characterization of the ^{31}P nuclear magnetic resonance spectrum from human melanoma tumors implanted in nude mice. *Cancer Res* 47(19), 5065-5069 (1987).

Critchlow SE, Jackson SP. DNA end-joining: from yeast to man. *Trends Biochem Sci* 23(10), 394-8 (1998).

Crook ED, Zhou J, Daniels M, Neidigh JL, McClain DA. Regulation of glycogen synthase by glucose, glucosamine, and glutamine:fructose-6-phosphate amidotransferase. *Diabetes* 44(3), 314-320 (1995).

Crouch PJ, Blake R, Duce JA, Ciccotosto GD, Li QX, Barnham KJ, Curtain CC, Cherny RA, Cappai R, Dyrks T, Masters CL, Trounce IA. Copper-dependent inhibition of human cytochrome c oxidase by a dimeric conformer of amyloid-ß$_{1-42}$. *J Neurosci* 25(3), 672-679 (2005).

Cryer PE, Davis SN, Shamoon H. Hypoglycemia in diabetes. *Diabetes Care* 26(6), 1902-1912 (2003).

Cummings RD, Roth S. The discovery of a lipid-linked glucuronide and its synthesis by chicken liver. *J Biol Chem* 257(4), 1755-64 (1982).

Dahlgren KN, Manelli AM, Stine WB Jr, Baker LK, Krafft GA, LaDu MJ. Oligomeric and fibrillar species of amyloid-beta peptides differentially affect neuronal viability. *J Biol Chem* 277(35), 32046-32053 (2002).

D'Andrea MR, Nagele RG, Wang HY, Peterson PA, Lee DH. Evidence that neurones accumulating amyloid can undergo lysis to form amyloid plaques in Alzheimer's disease. *Histopathology* 38(2), 120-134 (2001).

Dang CV. Rethinking the Warburg effect with Myc micromanaging glutamine metabolism. *Cancer Res* 70(3), 859-862 (2010).

Daniels MC, Ciaraldi TP, Nikoulina S, Henry RR, McClain DA. Glutamine:fructose-6-phosphate amidotransferase activity in cultured human skeletal muscle cells: relationship to glucose disposal rate in control and non-insulin-dependent diabetes mellitus subjects and regulation by glucose and insulin. *J Clin Invest* 97(5), 1235-1241 (1996).

Datta A. Regulatory role of adenosine triphosphate on hog kidney *N*-acetyl-D-glucosamine 2-epimerase. *Biochemistry* 9(17), 3363-3370 (1970).

Daude N, Ellie E, Reichardt JK, Petry KG. *In vivo* and *in vitro* expression of rat galactose-1-phosphate uridyltransferase (GALT) in the developing central and peripheral nervous system. *Brain Res Dev Brain Res* 94(2), 190-196 (1996b).

Daude N, Lestage J, Reichardt JK, Petry KG. Expression of galactose-1-phosphate uridyltransferase in the anterior pituitary of rat during the estrous cycle. *Neuroendocrinology* 64(1), 42-48 (1996a).

David DC, Hauptmann S, Scherping I, Schuessel K, Keil U, Rizzu P, Ravid R, Dröse S, Brandt U, Müller WE, Eckert A, Götz J. Proteomic and functional analyses reveal a mitochondrial dysfunction in P301L tau transgenic mice. *J Biol Chem* 280(25), 23802-23814 (2005).

Davidson EA, Blumenthal HJ, Roseman S. Glucosamine metabolism. II. Studies on glucosamine 6-phosphate N-acetylase. J Biol Chem 226(1), 125-133 (1957).

De Jongh WA, Bro C, Ostergaard S, Regenberg B, Olsson L, Nielsen J. The roles of galactitol, galactose-1-phosphate, and phosphoglucomutase in galactose-induced toxicity in Saccharomyces cerevisiae. *Biotechnol Bioeng* 101(2), 317-326 (2008).

De la Monte SM, Tong M, Lester-Coll N, Plater M Jr, Wands JR. Therapeutic rescue of neurodegeneration in experimental type 3 diabetes: relevance to Alzheimer's disease. *J Alzheimers Dis* 10(1), 89-109 (2006).

De la Torre JC. Alzheimer's disease is a vasocognopathy: a new term to describe its nature. *Neurol Res* 26(5), 517-524 (2004).

Deberardinis RJ, Sayed N, Ditsworth D, Thompson CB. Brick by brick: metabolism and tumor cell growth. *Curr Opin Genet Dev* 18(1), 54-61 (2008).

Decker K, Keppler D. Galactosamine hepatitis: key role of the nucleotide deficiency period in the pathogenesis of cell injury and cell death. *Rev Physiol Biochem Pharmacol* (71), 77-106 (1974).

Dedkova EN, Blatter LA. Modulation of mitochondrial Ca^{2+} by nitric oxide in cultured bovine vascular endothelial cells. *Am J Physiol Cell Physiol* 289(4), C836-845 (2005).

DeHaven JE, Robinson KA, Nelson BA, Buse MG. A novel variant of glutamine: fructose-6-phosphate amidotransferase-1 (GFAT1) mRNA is selectively expressed in striated muscle. *Diabetes* 50(11), 2419-2424 (2001).

Delacourte A, Buée L. Tau pathology: a marker of neurodegenerative disorders. *Curr Opin Neurol* 13(4), 371-376 (2000).

Delaval E, Perichon M, Friguet B. Age-related impairment of mitochondrial matrix aconitase and ATP-stimulated protease in rat liver and heart. *Eur J Biochem* 271(22), 4559-4564 (2004).

Dennis JW, Granovsky M, Warren CE. Glycoprotein glycosylation and cancer progression. *Biochim Biophys Acta* 1473(1), 21-34 (1999).

Denton RM, Randle PJ. Citrate and the regulation of adipose-tissue phosphofructokinase. *Biochem J* 100(2), 420-423 (1996).

Devi L, Prabhu BM, Galati DF, Avadhani NG, Anandatheerthavarada HK. Accumulation of amyloid precursor protein in the mitochondrial import channels of human Alzheimer's disease brain is associated with mitochondrial dysfunction. *J Neurosci* 26(35), 9057-9068 (2006).

Dias WB, Hart GW. *O*-GlcNAc modification in diabetes and Alzheimer's disease. *Mol Biosyst* 3(11), 766-772 (2007).

Diaz-Hernandez JI, Almeida A, Delgado-Esteban M, Fernandez E, Bolaños JP. Knockdown of glutamate-cysteine ligase by small hairpin RNA reveals that both catalytic and modulatory subunits are essential for the survival of primary neurons. *J Biol Chem* 280(47), 38992-39001 (2005).

Dienel GA, Hertz L. Glucose and lactate metabolism during brain activation. *J Neurosci Res* 66(5), 824–838 (2001).

Dong DL, Hart GW. Purification and characterization of an *O*-GlcNAc selective N-acetyl-beta-D-glucosaminidase from rat spleen cytosol. *J Biol Chem* 269(30), 19321-19330 (1994).

Dong DL, Xu ZS, Chevrier MR, Cotter RJ, Cleveland DW, Hart GW. Glycosylation of mammalian neurofilaments. Localization of multiple *O*-linked *N*-acetylglucosamine moieties on neurofilament polypeptides L and M. *J Biol Chem* 268(22), 16679-16687 (1993).

Dong DL, Xu ZS, Hart GW, Cleveland DW. Cytoplasmic *O*-GlcNAc modification of the head domain and the KSP repeat motif of the neurofilament protein neurofilament-H. *J Biol Chem* 271(34), 20845-20852 (1996).

Donnell GN, Bergren WR, Perry G, Koch R. Galactose-1-phosphate in galactosemia. Pediatrics 31, 802-810 (1963).

Dorfmueller HC, Borodkin VS, Schimpl M, Shepherd SM, Shpiro NA, van Aalten DM. GlcNAcstatin: a picomolar, selective *O*-GlcNAcase inhibitor that modulates intracellular *O*-glcNAcylation levels. *J Am Chem Soc* 128(51), 16484-16485 (2006).

Drake J, Kanski J, Varadarajan S, Tsoras M, Butterfield DA. Elevation of brain glutathione by gamma-glutamylcysteine ethyl ester protects against peroxynitrite-induced oxidative stress. *J Neurosci Res* 68(6):776-84 (2002).

Dringen R, Gebhardt R, Hamprecht B. Glycogen in astrocytes: possible function as lactate supply for neighboring cells. *Brain Res* 623(2), 208-214 (1993).

Dringen R, Kussmaul L, Gutterer JM, Hirrlinger J, Hamprecht B. The glutathione system of peroxide detoxification is less efficient in neurons than in astroglial cells. *J Neurochem* 72(6), 2523-2530 (1999a).

Dringen R, Pfeiffer B, Hamprecht B. Synthesis of the antioxidant glutathione in neurons: supply by astrocytes of CysGly as precursor for neuronal glutathione. *J Neurosci* 19(2), 562-9 (1999b).

Du XL, Edelstein D, Dimmeler S, Ju Q, Sui C, Brownlee M. Hyperglycemia inhibits endothelial nitric oxide synthase activity by posttranslational modification at the Akt site. *J Clin Invest* 108(9), 1341-1348 (2001).

Du XL, Edelstein D, Rossetti L, Fantus IG, Goldberg H, Ziyadeh F, Wu J, Brownlee M. Hyperglycemia-induced mitochondrial superoxide overproduction activates the hexosamine pathway and induces plasminogen activator inhibitor-1 expression by increasing Sp1 glycosylation. *Proc Natl Acad Sci U S A* 97(22), 12222-12226 (2000).

Dube DH, Bertozzi CR. Glycans in cancer and inflammation--potential for therapeutics and diagnostics. *Nat Rev Drug Discov* 4(6), 477-488 (2005).

Duggleby RG, Chao YC, Huang JG, Peng HL, Chang HY. Sequence differences between human muscle and liver cDNAs for UDPglucose pyrophosphorylase and kinetic properties of the recombinant enzymes expressed in Escherichia coli. *Eur J Biochem* 235(1-2), 173-179 (1996).

Dwyer DS, Vannucci SJ, Simpson IA. Expression, regulation, and functional role of glucose transporters (GLUTs) in brain. *Int Rev Neurobiol* 51, 159-188 (2002).

Eddy AA. Plasminogen activator inhibitor-1 and the kidney. *Am J Physiol Renal Physiol* 283(2), F209-220 (2002).

Englard S, Seifter S. Precipitation techniques. *Methods Enzymol* 182, 285-300 (1990).

Esko JD, Kimata K, Lindahl U. Proteoglycans and Sulfated Glycosaminoglycans. In: Varki A, Cummings RD, Esko JD, *et al*., editors. Essentials of Glycobiology. 2nd edition. Cold Spring Harbor (NY): Cold Spring Harbor Laboratory Press. Chapter 16 (2009).

Federici M, Menghini R, Mauriello A, Hribal ML, Ferrelli F, Lauro D, Sbraccia P, Spagnoli LG, Sesti G, Lauro R. Insulin-dependent activation of endothelial nitric oxide synthase is impaired by *O*-linked glycosylation modification of signaling proteins in human coronary endothelial cells. *Circulation* 106(4), 466-472 (2002).

Fehm HL, Kern W, Peters A. The selfish brain: competition for energy resources. *Prog Brain Res* 153, 129-140 (2006).

Ferguson MAJ, Kinoshita T, Hart GW. Glycosylphosphatidylinositol Anchors. In: Varki A, Cummings RD, Esko JD, *et al*., editors. Essentials of Glycobiology. 2nd edition. Cold Spring Harbor (NY): Cold Spring Harbor Laboratory Press. Chapter 11 (2009).

Fernyhough P, Gallagher A, Averill SA, Priestley JV, Hounsom L, Patel J, Tomlinson DR. Aberrant neurofilament phosphorylation in sensory neurons of rats with diabetic neuropathy. *Diabetes* 48(4), 881-889 (1999).

Fernyhough P, Schmidt RE. Neurofilaments in diabetic neuropathy. *Int Rev Neurobiol* 50, 115-144 (2002).

Ferreira A, Rapoport M. The synapsins: beyond the regulation of neurotransmitter release. *Cell Mol Life Sci* 59(4), 589-595 (2002).

Ferreras C, Hernández ED, Martínez-Costa OH, Aragón JJ. Subunit interactions and composition of the fructose 6-phosphate catalytic site and the fructose 2,6-bisphosphate allosteric site of mammalian phosphofructokinase. *J Biol Chem* 284(14), 9124-31 (2009).

Field MC, Medina-Acosta E, Cross GA. Inhibition of glycosylphosphatidylinositol biosynthesis in *Leishmania mexicana* by mannosamine. *J Biol Chem* 268(13), 9570-9577 (1993).

Folch J, Lees M, Sloane-Stanley GH. A simple method for the isolation and purification of total lipides from animal tissues. *J Biol Chem* 226(1), 497-509 (1957).

Förstermann U, Münzel T. Endothelial nitric oxide synthase in vascular disease: from marvel to menace. *Circulation* 113(13), 1708-1714 (2006).

Förstermann U, Pollock JS, Schmidt HH, Heller M, Murad F. Calmodulin-dependent endothelium-derived relaxing factor/nitric oxide synthase activity is present in the particulate and cytosolic fractions of bovine aortic endothelial cells. *Proc Natl Acad Sci U S A* 88(5), 1788–1792 (1991).

Francisco H, Kollins K, Varghis N, Vocadlo D, Vosseller K, Gallo G. *O*-GLcNAc post-translational modifications regulate the entry of neurons into an axon branching program. *Dev Neurobiol* 69(2-3), 162-173 (2009).

Freedman JE, Sauter R, Battinelli EM, Ault K, Knowles C, Huang PL, Loscalzo J. Deficient platelet-derived nitric oxide and enhanced hemostasis in mice lacking the NOSIII gene. *Circ Res* 84(12), 1416-21 (1999).

Freeze HH. Genetic defects in the human glycome. *Nat Rev Genet* 7(7), 537-551 (2006).

Fréminet A. Carbohydrate and amino acid metabolism during acute hypoxia in rats: blood and heart metabolites. *Comp Biochem Physiol* 70(3), 427-433 (1981).

Frozza RL, Horn AP, Hoppe JB, Simão F, Gerhardt D, Comiran RA, Salbego CG. A comparative study of ß-amyloid peptides Aß1-42 and Aß25-35 toxicity in organotypic hippocampal slice cultures. *Neurochem Res* 34(2), 295-303 (2009).

Fuster MM, Esko JD. The sweet and sour of cancer: glycans as novel therapeutic targets. *Nat Rev Cancer* 5(7), 526-542 (2005).

Gadelha FR, Thomson L, Fagian MM, Costa AD, Radi R, Vercesi AE. Ca^{2+}-independent permeabilization of the inner mitochondrial membrane by peroxynitrite is mediated by membrane protein thiol cross-linking and lipid peroxidation. *Arch Biochem Biophys* 345(2), 243-50 (1997).

Gallinger A, Biet T, Pellerin L, Peters T. Insights into neuronal cell metabolism using NMR spectroscopy: uridyl diphosphate N-acetyl-glucosamine as a unique metabolic marker. Angew *Chem Int Ed Engl* 50(49):11672-4 (2011).

Gan JC. Metabolism of D-mannosamine in bovine thyroid gland slices. *Biochim Biophys Acta* 385(2), 412-420 (1975).

Gao Y, Miyazaki J, Hart GW. The transcription factor PDX-1 is post-translationally modified by *O*-linked *N*-acetylglucosamine and this modification is correlated with its DNA binding activity and insulin secretion in min6 beta-cells. *Arch Biochem Biophys* 415(2), 155-163 (2003).

Gao Y, Wells L, Comer FI, Parker GJ, Hart GW. Dynamic *O*-glycosylation of nuclear and cytosolic proteins: cloning and characterization of a neutral, cytosolic beta-*N*-acetylglucosaminidase from human brain. *J Biol Chem* 276(13), 9838-9845 (2001).

Gardner AM, Xu FH, Fady C, Jacoby FJ, Duffey DC, Tu Y, Lichtenstein A. Apoptotic vs. nonapoptotic cytotoxicity induced by hydrogen peroxide. *Free Radic Biol Med* 22(1-2), 73-83 (1997).

Gardner PR, Nguyen DD, White CW. Aconitase is a sensitive and critical target of oxygen poisoning in cultured mammalian cells and in rat lungs. *Proc Natl Acad Sci U S A* 91(25), 12248-12252 (1994).

Garthwaite J, Boulton CL. Nitric Oxide Signaling in the Central Nervous System. *Annu Rev Physiol* (57), 683-706 (1995).

Garwood CJ, Pooler AM, Atherton J, Hanger DP, Noble W. Astrocytes are important mediators of Aβ-induced neurotoxicity and tau phosphorylation in primary culture. *Cell Death Dis* 2, e167 (2011).

Gatenby RA, Gillies RJ. Why do cancers have high aerobic glycolysis? *Nat Rev Cancer* 4(11), 891-899 (2004).

Gawlitzek M, Valley U, Wagner R. Ammonium ion and glucosamine dependent increases of oligosaccharide complexity in recombinant glycoproteins secreted from cultivated BHK-21 cells. *Biotechnol Bioeng* 57(5), 518-28 (1998).

Gerozissis K. Brain insulin, energy and glucose homeostasis; genes, environment and metabolic pathologies. *Eur J Pharmacol* 585(1), 38-49 (2008).

Ghafourifar P, Richter C. Nitric oxide synthase activity in mitochondria. *FEBS Lett* 418(3), 291-296 (1997).

Gibson GE, Sheu KF, Blass JP. Abnormalities of mitochondrial enzymes in Alzheimer disease. *J Neural Transm* 105(8-9), 855-870 (1998).

Ginsburg V. Formation of guanosine diphosphate L-fucose from guanosine diphosphate D-mannose. J Biol Chem 235, 2196-2201 (1960).

Ginsburg V. Studies on the biosynthesis of guanosine diphosphate L-fucose. *J Biol Chem* 236, 2389-2393 (1961).

Gitter BD, Cox LM, Rydel RE, May PC. Amyloid beta peptide potentiates cytokine secretion by interleukin-1 beta-activated human astrocytoma cells. *Proc Natl Acad Sci U S A* 92(23), 10738-10741 (1995).

Gitzelmann R. Galactose-1-phosphate in the pathophysiology of galactosemia. *Eur J Pediatr* 154(7 Suppl 2), S45-49 (1995).

Gjedde A, Marrett S. Glycolysis in Neurons, Not Astrocytes, Delays Oxidative Metabolism of Human Visual Cortex During Sustained Checkerboard Stimulation *in Vivo*. *J Cereb Blood Flow Metab* 21, 1384–1392 (2001).

Glunde K, Jie C, Bhujwalla ZM. Molecular causes of the aberrant choline phospholipid metabolism in breast cancer. *Cancer Res* 64(12), 4270-4276 (2004).

Goedert M, Jakes R, Qi Z, Wang JH, Cohen P. Protein phosphatase 2A is the major enzyme in brain that dephosphorylates tau protein phosphorylated by proline-directed protein kinases or cyclic AMP-dependent protein kinase. *J Neurochem* 65(6), 2804-2807 (1995).

Goldberg HJ, Whiteside CI, Hart GW, Fantus IG. Posttranslational, reversible *O*-glycosylation is stimulated by high glucose and mediates plasminogen activator inhibitor-1 gene expression and Sp1 transcriptional activity in glomerular mesangial cells. *Endocrinology* 147(1), 222-231 (2006).

Gong CX, Liu F, Grundke-Iqbal I, Iqbal K. Impaired brain glucose metabolism leads to Alzheimer neurofibrillary degeneration through a decrease in tau *O*-GlcNAcylation. *J Alzheimers Dis* 9(1), 1-12 (2006).

Gong CX, Shaikh S, Wang JZ, Zaidi T, Grundke-Iqbal I, Iqbal K. Phosphatase activity toward abnormally phosphorylated tau: decrease in Alzheimer disease brain. *J Neurochem* 65(2), 732-738 (1995).

Good PF, Werner P, Hsu A, Olanow CW, Perl DP. Evidence of neuronal oxidative damage in Alzheimer's disease. *Am J Pathol* 149(1), 21-28 (1996).

Goodman Y, Mattson MP. Secreted forms of beta-amyloid precursor protein protect hippocampal neurons against amyloid beta-peptide-induced oxidative injury. *Exp Neurol* 128(1), 1-12 (1994).

Gouras GK, Tsai J, Naslund J, Vincent B, Edgar M, Checler F, Greenfield JP, Haroutunian V, Buxbaum JD, Xu H, Greengard P, Relkin NR. Intraneuronal Aß42 accumulation in human brain. *Am J Pathol* 156(1), 15-20 (2000).

Govindaraju V, Young K, Maudsley AA. Proton NMR chemical shifts and coupling constants for brain metabolites. NMR Biomed 13(3), 129-153 (2000).

Gracy RW, Noltmann EA. Studies on phosphomannose isomerase. I. Isolation, homogeneity measurements, and determination of some physical properties. *J Biol Chem* 243(11), 3161-3168 (1968).

Grande S, Palma A, Luciani AM, Rosi A, Guidoni L, Viti V. Glycosidic intermediates identified in ^{1}H MR spectra of intact tumour cells may contribute to the clarification of aspects of glycosylation pathways. *NMR Biomed* 24(1), 68-79 (2011).

Gregory GA, Welsh FA, Yu AC, Chan PH. Fructose-1,6-bisphosphate reduces ATP loss from hypoxic astrocytes. *Brain Res* 516(2), 310-312 (1990).

Gribbestad IS, Petersen SB, Fjøsne HE, Kvinnsland S, Krane J. ^{1}H NMR spectroscopic characterization of perchloric acid extracts from breast carcinomas and non-involved breast tissue. *NMR Biomed* 7(4), 181-194 (1994).

Griffith LS, Mathes M, Schmitz B. ß-amyloid precursor protein is modified with *O*-linked *N*-acetylglucosamine. *J Neurosci Res* 41(2), 270-278 (1995).

Griffith OW, Mulcahy RT. The enzymes of glutathione synthesis: gamma-glutamylcysteine synthetase. *Adv Enzymol Relat Areas Mol Biol* 73, 209-267, xii (1999).

Griffith OW. Biologic and pharmacologic regulation of mammalian glutathione synthesis. *Free Radic Biol Med* 27(9-10), 922-35 (1999).

Grundke-Iqbal I, Iqbal K, Quinlan M, Tung YC, Zaidi MS, Wisniewski HM. Microtubule-associated protein tau. A component of Alzheimer paired helical filaments. *J Biol Chem* 261(13), 6084-6089 (1986b).

Grundke-Iqbal I, Iqbal K, Tung YC, Quinlan M, Wisniewski HM, Binder LI. Abnormal phosphorylation of the microtubule-associated protein τ (tau) in Alzheimer cytoskeletal pathology. *Proc Natl Acad Sci U S A* 83(13), 4913-4917 (1986a).

Gry M, Rimini R, Strömberg S, Asplund A, Pontén F, Uhlén M, Nilsson P. Correlations between RNA and protein expression profiles in 23 human cell lines. *BMC Genomics* 10, 365 (2009).

Gu Y, Mi W, Ge Y, Liu H, Fan Q, Han C, Yang J, Han F, Lu X, Yu W. GlcNAcylation plays an essential role in breast cancer metastasis. *Cancer Res* 70(15), 6344-6351 (2010).

Guidarelli A, Fiorani M, Cantoni O. Enhancing effects of intracellular ascorbic acid on peroxynitrite-induced U937 cell death are mediated by mitochondrial events resulting in enhanced sensitivity to peroxynitrite-dependent inhibition of complex III and formation of hydrogen peroxide. *Biochem J* 378(Pt 3), 959-966 (2004).

Guilherme A, Czech MP. Stimulation of IRS-1-associated phosphatidylinositol 3-kinase and Akt/protein kinase B but not glucose transport by beta1-integrin signaling in rat adipocytes. *J Biol Chem* 273(50), 33119-33122 (1998).

Haas J, Storch-Hagenlocher B, Biessmann A, Wildemann B. Inducible nitric oxide synthase and argininosuccinate synthetase: co-induction in brain tissue of patients with Alzheimer's dementia and following stimulation with beta-amyloid 1-42 in vitro. *Neurosci Lett* 322(2), 121-125 (2002).

Haass C, Selkoe DJ. Soluble protein oligomers in neurodegeneration: lessons from the Alzheimer's amyloid beta-peptide. *Nat Rev Mol Cell Biol* 8(2), 101-112 (2007).

Haberland C, Perou M, Brunngraber EG, Hof H. The neuropathology of galactosemia. A histopathological and biochemical study. *J Neuropathol Exp Neurol* 30(3), 431-447 (1971).

Hagen T, Taylor CT, Lam F, Moncada S. Redistribution of intracellular oxygen in hypoxia by nitric oxide: effect on HIF1α. *Science* 302(5652), 1975-1978 (2003).

Hakomori S. Glycosylation defining cancer malignancy: new wine in an old bottle. *Proc Natl Acad Sci U S A* 99(16), 10231-10233 (2002).

Hall CN, Garthwaite J. What is the real physiological NO concentration *in vivo*? *Nitric Oxide* 21(2), 92-103 (2009).

Haltiwanger RS, Blomberg MA, Hart GW. Glycosylation of nuclear and cytoplasmic proteins. Purification and characterization of a uridine diphospho-N-acetylglucosamine:polypeptide beta-N-acetylglucosaminyltransferase. *J Biol Chem* 267(13), 9005-9013 (1992).

Haltiwanger RS, Grove K, Philipsberg GA. Modulation of *O*-linked N-acetylglucosamine levels on nuclear and cytoplasmic proteins in vivo using the peptide *O*-GlcNAc-beta-*N*-acetylglucosaminidase inhibitor *O*-(2-acetamido-2-deoxy-D-glucopyranosylidene)amino-*N*-phenylcarbamate. *J Biol Chem* 273(6), 3611-3617 (1998).

Han D, Canali R, Garcia J, Aguilera R, Gallaher TK, Cadenas E. Sites and mechanisms of aconitase inactivation by peroxynitrite: modulation by citrate and glutathione. *Biochemistry* 44(36), 11986-11996 (2005).

Hansen RG, Freedland RA, Scott HM. Lactose metabolism. V. The uridine nucleotides in galactose toxicity. *J Biol Chem* 219(1):391-397 (1956).

Hansen SH, Frank SR, Casanova JE. Cloning and characterization of human phosphomannomutase, a mammalian homologue of yeast SEC53. *Glycobiology* 7(6), 829-834 (1997).

Hansson Petersen CA, Alikhani N, Behbahani H, Wiehager B, Pavlov PF, Alafuzoff I, Leinonen V, Ito A, Winblad B, Glaser E, Ankarcrona M. The amyloid beta-peptide is imported into mitochondria via the TOM import machinery and localized to mitochondrial cristae. *Proc Natl Acad Sci U S A* 105(35), 13145-13150 (2008).

Hardie DG, Ross FA, Hawley SA. AMPK: a nutrient and energy sensor that maintains energy homeostasis. *Nat Rev Mol Cell Biol* 13(4), 251-262 (2012).

Harr SD, Simonian NA, Hyman BT. Functional alterations in Alzheimer's disease: decreased glucose transporter 3 immunoreactivity in the perforant pathway terminal zone. *J Neuropathol Exp Neurol* 54(1), 38-41 (1995).

Hart GW, Housley MP, Slawson C. Cycling of *O*-linked ß-*N*-acetylglucosamine on nucleocytoplasmic proteins. *Nature* 446(7139), 1017-1022 (2007).

Hassel B, Sonnewald U, Unsgård G, Fonnum F. NMR spectroscopy of cultured astrocytes: effects of glutamine and the gliotoxin fluorocitrate. *J Neurochem* 62(6), 2187-2194 (1994).

Hassel B, Sonnewald U. Effects of potassium and glutamine on metabolism of glucose in astrocytes. *Neurochem Res* 27(1-2), 167-71 (2002).

Hausladen A, Fridovich I. Superoxide and peroxynitrite inactivate aconitases, but nitric oxide does not. *J Biol Chem* 269(47), 29405-29408 (1994).

Hawkins M, Barzilai N, Liu R, Hu M, Chen W, Rossetti L. Role of the glucosamine pathway in fat-induced insulin resistance. *J Clin Invest* 99(9), 2173-2182 (1997).

Hawkins PT, Berrie CP, Morris AJ, Downes CP. Inositol 1,2-cyclic 4,5-trisphosphate is not a product of muscarinic receptor-stimulated phosphatidylinositol 4,5-bisphosphate hydrolysis in rat parotid glands. *Biochem J* 243(1), 211-218 (1987).

Haworth JC, Ford JD, Ho HK. The effect of galactose toxicity on growth of the developing rat brain. *Brain Res* 21(3), 385-390 (1970).

Heales SJ, Bolaños JP, Land JM, Clark JB. Trolox protects mitochondrial complex IV from nitric oxide-mediated damage in astrocytes. *Brain Res* 668(1-2), 243-5 (1994).

Heart E, Choi WS, Sung CK. Glucosamine-induced insulin resistance in 3T3-L1 adipocytes. *Am J Physiol Endocrinol Metab* 278(1), E103-112 (2000).

Hebert LF, Daniels MC , Zhou J, Crook ED, Turner RL, Simmons ST, Neidigh JL, Zhu JS, Baron AD, McClain DA. Overexpression of glutamine:fructose-6-phosphate amidotransferase in transgenic mice leads to insulin resistance. *J Clin Invest* 98(4), 930-936 (1996).

Heckel D, Comtesse N, Brass N, Blin N, Zang KD, Meese E. Novel immunogenic antigen homologous to hyaluronidase in meningioma. *Hum Mol Genet* 7(12), 1859-1872 (1998).

Hellwig-Bürgel T, Rutkowski K, Metzen E, Fandrey J, Jelkmann W. Interleukin-1beta and tumor necrosis factor-alpha stimulate DNA binding of hypoxia-inducible factor-1. *Blood* 94(5), 1561-1567 (1999).

Heneka MT, Wiesinger H, Dumitrescu-Ozimek L, Riederer P, Feinstein DL, Klockgether T. Neuronal and glial coexpression of argininosuccinate synthetase and inducible nitric oxide synthase in Alzheimer disease. *J Neuropathol Exp Neurol* 60(9), 906-916 (2001).

Higuchi M, Ishihara T, Zhang B, Hong M, Andreadis A, Trojanowski J, Lee VM. Transgenic mouse model of tauopathies with glial pathology and nervous system degeneration. *Neuron* 35(3), 433-446 (2002).

Hill KE, Zollinger LV, Watt HE, Carlson NG, Rose JW. Inducible nitric oxide synthase in chronic active multiple sclerosis plaques: distribution, cellular expression and association with myelin damage. *J Neuroimmunol* 151(1-2), 171-179 (2004).

Hinderlich S, Nöhring S, Weise C, Franke P, Stäsche R, Reutter W. Purification and characterization of *N*-acetylglucosamine kinase from rat liver--comparison with UDP-*N*-acetylglucosamine 2-epimerase/N-acetylmannosamine kinase. *Eur J Biochem* 252(1), 133-139 (1998).

Hinderlich S, Stäsche R, Zeitler R, Reutter W. A bifunctional enzyme catalyzes the first two steps in *N*-acetylneuraminic acid biosynthesis of rat liver. Purification and characterization of UDP-*N*-acetylglucosamine 2-epimerase/*N*-acetylmannosamine kinase. *J Biol Chem* 272(39), 24313-24318 (1997).

Hinerfeld D, Traini MD, Weinberger RP, Cochran B, Doctrow SR, Harry J, Melov S. Endogenous mitochondrial oxidative stress: neurodegeneration, proteomic analysis, specific

respiratory chain defects, and efficacious antioxidant therapy in superoxide dismutase 2 null mice. *J Neurochem* 88(3), 657-667 (2004).

Holden HM, Rayment I, Thoden JB. Structure and function of enzymes of the Leloir pathway for galactose metabolism. *J Biol Chem* 278(45), 43885-43888 (2003).

Hollingsworth MA, Swanson BJ. Mucins in cancer: protection and control of the cell surface. *Nat Rev Cancer* 4(1), 45-60 (2004).

Holt GD, Hart GW. The subcellular distribution of terminal N-acetylglucosamine moieties. Localization of a novel protein-saccharide linkage, O-linked GlcNAc. J Biol Chem 261, 8049-8057 (1986).

Hölzl G, Dörmann P. Structure and function of glycoglycerolipids in plants and bacteria. *Prog Lipid Res* 46(5), 225-243 (2007).

Hresko RC, Heimberg H, Chi MM, Mueckler M. Glucosamine-induced insulin resistance in 3T3-L1 adipocytes is caused by depletion of intracellular ATP. *J Biol Chem* 273(32), 20658-20668 (1998).

Hsu M, Srinivas B, Kumar J, Subramanian R, Andersen J. Glutathione depletion resulting in selective mitochondrial complex I inhibition in dopaminergic cells is via an NO-mediated pathway not involving peroxynitrite: implications for Parkinson's disease. *J Neurochem* 92(5), 1091-1103 (2005).

Hu J, Akama KT, Krafft GA, Chromy BA, Van Eldik LJ. Amyloid-beta peptide activates cultured astrocytes: morphological alterations, cytokine induction and nitric oxide release. *Brain Res* 785(2), 195-206 (1998).

Hu Y, Belke D, Suarez J, Swanson E, Clark R, Hoshijima M, Dillmann WH. Adenovirus-mediated overexpression of *O*-GlcNAcase improves contractile function in the diabetic heart. *Circ Res* 96(9), 1006-1013 (2005).

Huang LE, Gu J, Schau M, Bunn HF. Regulation of hypoxia-inducible factor 1α is mediated by an O_2-dependent degradation domain via the ubiquitin-proteasome pathway. *Proc Natl Acad Sci U S A* 95(14), 7987–7992 (1998).

Huang LE, Willmore WG, Gu J, Goldberg MA, Bunn HF. Inhibition of hypoxia-inducible factor 1 activation by carbon monoxide and nitric oxide. Implications for oxygen sensing and signaling. *J Biol Chem* 274(13), 9038-9044 (1999).

Huber A, Bai P, de Murcia JM, de Murcia G. PARP-1, PARP-2 and ATM in the DNA damage response: functional synergy in mouse development. *DNA Repair (Amst)* 3(8-9), 1103-1108 (2004).

Huizing M, Ruitenbeek W, van den Heuvel LP, Dolce V, Iacobazzi V, Smeitink JA, Palmieri F, Trijbels JM. Human mitochondrial transmembrane metabolite carriers: tissue distribution and its implication for mitochondrial disorders. *J Bioenerg Biomembr* 30(3), 277-84 (1998).

Ida N, Masters CL, Beyreuther K. Rapid cellular uptake of Alzheimer amyloid ßA4 peptide by cultured human neuroblastoma cells. *FEBS Lett* 394(2), 174-178 (1996).

Ikeda K, Akiyama H, Arai T, Nishimura T. Glial tau pathology in neurodegenerative diseases: their nature and comparison with neuronal tangles. *Neurobiol Aging* 19(1 Suppl), S85-91 (1998).

Inoue K, Zhuang L, Ganapathy V. Human Na^+-coupled citrate transporter: primary structure, genomic organization, and transport function. *Biochem Biophys Res Commun* 299(3), 465-71 (2002a).

Inoue K, Zhuang L, Maddox DM, Smith SB, Ganapathy V. Structure, function, and expression pattern of a novel sodium-coupled citrate transporter (NaCT) cloned from mammalian brain. *J Biol Chem* 277(42), 39469-39476 (2002b).

Ischiropoulos H, Zhu L, Chen J, Tsai M, Martin JC, Smith CD, Beckman JS. Peroxynitrite-mediated tyrosine nitration catalyzed by superoxide dismutase. *Arch Biochem Biophys* 298(2), 431-437 (1992).

Ishihara H, Heath EC. The metabolism of L-fucose. IV. The biosynthesis of guanosine diphosphate L-fucose in porcine liver. *J Biol Chem* 243(6), 1110-1115 (1968b).

Ishihara H, Massaro DJ, Heath EC. The metabolism of L-fucose. III. The enzymatic synthesis of ß-L-fucose 1-phosphate. *J Biol Chem* 243(6), 1103-1109 (1968a).

Itagaki S, McGeer PL, Akiyama H, Zhu S, Selkoe D. Relationship of microglia and astrocytes to amyloid deposits of Alzheimer disease. *J Neuroimmunol* 24(3), 173-182 (1989).

Ivan M, Kondo K, Yang H, Kim W, Valiando J, Ohh M, Salic A, Asara JM, Lane WS, Kaelin WG Jr. HIFalpha targeted for VHL-mediated destruction by proline hydroxylation: implications for O2 sensing. *Science* 292(5516), 464-468 (2001).

Jaakkola P, Mole DR, Tian YM, Wilson MI, Gielbert J, Gaskell SJ, von Kriegsheim A, Hebestreit HF, Mukherji M, Schofield CJ, Maxwell PH, Pugh CW, Ratcliffe PJ. Targeting of HIF-alpha to the von Hippel-Lindau ubiquitylation complex by O2-regulated prolyl hydroxylation. *Science* 292(5516), 468-472 (2001).

Jackson SP, Tjian R. *O*-glycosylation of eukaryotic transcription factors: implications for mechanisms of transcriptional regulation. *Cell* 55(1), 125-133 (1988).

Jacobsen KT, Iverfeldt K. *O*-GlcNAcylation increases non-amyloidogenic processing of the amyloid-β precursor protein (APP). *Biochem Biophys Res Commun* 404(3), 882-886 (2011).

James LR, Fantus IG, Goldberg H, Ly H, Scholey JW. Overexpression of GFAT activates PAI-1 promoter in mesangial cells. *Am J Physiol Renal Physiol* 279(4), F718-727 (2000).

Jenner P, Dexter DT, Sian J, Schapira AH, Marsden CD. Oxidative stress as a cause of nigral cell death in Parkinson's disease and incidental Lewy body disease. *Ann Neurol* 32, S82-S87 (1992).

Jitrapakdee S, St Maurice M, Rayment I, Cleland WW, Wallace JC, Attwood PV. Structure, mechanism and regulation of pyruvate carboxylase. *Biochem J* 413(3), 369-387 (2008).

Jitrapakdee S, Wallace JC. Structure, function and regulation of pyruvate carboxylase. *Biochem J* 340(Pt 1), 1-16 (1999).

Kalaria RN, Harik SI. Reduced glucose transporter at the blood-brain barrier and in cerebral cortex in Alzheimer disease. *J Neurochem* 53(4), 1083-1088 (1989).

Kalckar HM, Maxwell ES, Strominger JL. Some properties of uridine diphosphoglucose dehydrogenase. *Arch Biochem Biophys* 65(1), 2-10 (1956).

Kallio PJ, Wilson WJ, O'Brien S, Makino Y, Poellinger L. Regulation of the hypoxia-inducible transcription factor 1alpha by the ubiquitin-proteasome pathway. *J Biol Chem* 274(10), 6519-6525 (1999).

Kamemura K, Hayes BK, Comer FI, Hart GW. Dynamic interplay between *O*-glycosylation and *O*-phosphorylation of nucleocytoplasmic proteins: alternative glycosylation/phosphorylation of THR-58, a known mutational hot spot of c-Myc in lymphomas, is regulated by mitogens. *J Biol Chem* 277(21), 19229-19235 (2002).

Kamura T, Sato S, Iwai K, Czyzyk-Krzeska M, Conaway RC, JW Conaway. Activation of hif1alpha ubiquitination by a reconstituted von hippel-lindau (vhl) tumor suppressor complex. *Proc Natl Acad Sci U S A* 97(19), 10430-10435 (2000).

Kang JG, Park SY, Ji S, Jang I, Park S, Kim HS, Kim SM, Yook JI, Park YI, Roth J, Cho JW. *O*-GlcNAc protein modification in cancer cells increases in response to glucose deprivation through glycogen degradation. *J Biol Chem* 284(50), 34777-34784 (2009).

Karlsson KA. Microbial recognition of target-cell glycoconjugates. *Curr Opin Struct Biol* 5(5), 622-635 (1995).

Kasuno K, Takabuchi S, Fukuda K, Kizaka-Kondoh S, Yodoi J, Adachi T, Semenza GL, Hirota K. Nitric oxide induces hypoxia-inducible factor 1 activation that is dependent on MAPK and phosphatidylinositol 3-kinase signaling. *J Biol Chem* 279(4), 2550-2558 (2004).

Kato S, Gondo T, Hoshii Y, Takahashi M, Yamada M, Ishihara T. Confocal observation of senile plaques in Alzheimer's disease: senile plaque morphology and relationship between senile plaques and astrocytes. *Pathol Int* 48(5), 332-340 (1998).

Katyal SL, Barilaro L, Hanin I. Lipid composition of different areas of murine brain: effects of lipid extraction procedures. *Lipids* 20(3), 201-203 (1985).

Kawamura T, Ishimoto N, Ito E. Enzymatic synthesis of uridine diphosphate N-acetyl-D-mannosaminuronic acid. *J Biol Chem* 254(17), 8457-8465 (1979).

Kawamura T, Kimura M, Yamamori S, Ito E. Enzymatic formation of uridine diphosphate N-acetyl-D-mannosamine. *J Biol Chem* 253(10), 3595-3601 (1978).

Kehrer JP, Lund LG. Cellular reducing equivalents and oxidative stress. *Free Radic Biol Med* 17(1), 65-75 (1994).

Keil U, Bonert A, Marques CA, Scherping I, Weyermann J, Strosznajder JB, Müller-Spahn F, Haass C, Czech C, Pradier L, Müller WE, Eckert A. Amyloid beta-induced changes in nitric oxide production and mitochondrial activity lead to apoptosis. *J Biol Chem* 279(48), 50310-50320 (2004).

Kelleher JA, Chan TY, Chan PH, Gregory GA. Protection of astrocytes by fructose 1,6-bisphosphate and citrate ameliorates neuronal injury under hypoxic conditions. *Brain Res* 726(1-2), 167-173 (1996).

Kelly WG, Dahmus ME, Hart GW. RNA polymerase II is a glycoprotein. Modification of the COOH-terminal domain by *O*-GlcNAc. *J Biol Chem* 268(14), 10416-10424 (1993).

Kent TA, Emptage MH, Merkle H, Kennedy MC, Beinert H, Münck E. Mössbauer studies of aconitase. Substrate and inhibitor binding, reaction intermediates, and hyperfine interactions of reduced 3Fe and 4Fe clusters. *J Biol Chem* 260(11), 6871-6881 (1985).

Keppler D, Decker K. Studies on the mechanism of galactosamine-1-phosphate and its inhibition of UDP-glucose pyrophosphorylase. *Eur J Biochem* 10(2), 219-225 (1969).

Keppler D, Fröhlich J, Reutter W, Wieland O, Decker K. Changes in uridine nucleotides during liver perfusion with D-galactosamine. *FEBS Lett* 4(4), 278-280 (1969).

Keppler D, Lesch R, Reutter W, Decker K. Experimental hepatitis induced by D-galactosamine. *Exp Mol Pathol* 9(2), 279-290 (1968).

Keppler DO, Pausch J, Decker K. Selective uridine triphosphate deficiency induced by D-galactosamine in liver and reversed by pyrimidine nucleotide precursors. Effect on ribonucleic acid synthesis. *J Biol Chem* 249(1), 211-216 (1974).

Keppler DO, Rudigier JF, Bischoff E, Decker KF. The trapping of uridine phosphates by D-galactosamine. D-glucosamine, and 2-deoxy-D-galactose. A study on the mechanism of galactosamine hepatitis. *Eur J Biochem* 17(2), 246-253 (1970).

Keppler DO. Uridine triphosphate deficiency, growth inhibition, and death in ascites hepatoma cells induced by a combination of pyrimidine biosynthesis inhibition with uridylate trapping. *Cancer Res* 37(3), 911-917 (1977).

Keun HC, Beckonert O, Griffin JL, Richter C, Moskau D, Lindon JC, Nicholson JK. Cryogenic probe ^{13}C NMR spectroscopy of urine for metabonomic studies. *Anal Chem* 74(17), 4588-4593 (2002).

Khidekel N, Ficarro SB, Clark PM, Bryan MC, Swaney DL, Rexach JE, Sun YE, Coon JJ, Peters EC, Hsieh-Wilson LC. Probing the dynamics of *O*-GlcNAc glycosylation in the brain using quantitative proteomics. *Nat Chem Biol* 3(6), 339-348 (2007).

Khorana HG, Tener GM, Wright RS, Moffatt JG. Cyclic Phosphates. III. Some General Observations on the Formation and Properties of Five-, Six- and Seven-membered Cyclic Phosphate Esters. *J Am Chem Soc* 79(2), 430–436 (1957).

Kim J, Shao Y, Kim SY, Kim S, Song HK, Jeon JH, Suh HW, Chung JW, Yoon SR, Kim YS, Choi I. Hypoxia-induced IL-18 increases hypoxia-inducible factor-1α expression through a Rac1-dependent NF-κB pathway. *Mol Biol Cell* 19(2), 433-444 (2008).

Kim MY, Zhang T, Kraus WL. Poly(ADP-ribosyl)ation by PARP-1: 'PAR-laying' NAD^+ into a nuclear signal. *Genes Dev* 19(17), 1951-1967 (2005).

Kimelberg HK, Pang S, Treble DH. Excitatory amino acid-stimulated uptake of 22 Na^+ in primary astrocyte cultures. *J Neurosci* 9(4), 1141-1149 (1989).

Kish SJ, Bergeron C, Rajput A, Dozic S, Mastrogiacomo F, Chang LJ, Wilson JM, DiStefano LM, Nobrega JN. Brain cytochrome oxidase in Alzheimer's disease. *J Neurochem* 59(2), 776-779 (1992).

Kitano T, Nisimaru N, Shibata E, Iwasaka H, Noguchi T, Yamada K. Lactate utilization as an energy substrate in ischemic preconditioned rat brain slices. *Life Sci* 72(4-5), 557-564 (2002).

Klein WL, Krafft GA, Finch CE. Targeting small Aß oligomers: the solution to an Alzheimer's disease conundrum? *Trends Neurosci* 24(4), 219-224 (2001).

Kleinert H, Pautz A, Linker K, Schwarz PM. Regulation of the expression of inducible nitric oxide synthase. *Eur J Pharmacol* 500(1-3), 255-66 (2004).

Knowles RG, Moncada S. Nitric oxide synthases in mammals. *Biochem J* 298 (Pt 2). 249-58 (1994).

Knull HR, Taylor WF, Wells WW. Effects of energy metabolism on in vivo distribution of hexokinase in brain. *J Biol Chem* 248(15), 5414-5417 (1973).

Kobzik L, Stringer B, Balligand JL, Reid MB, Stamler JS. Endothelial type nitric oxide synthase in skeletal muscle fibers: mitochondrial relationships. *Biochem Biophys Res Commun* 211(2), 375-81 (1995).

Kochanowski N, Blanchard F, Cacan R, Chirat F, Guedon E, Marc A, Goergen JL. Intracellular nucleotide and nucleotide sugar contents of cultured CHO cells determined by a fast, sensitive, and high-resolution ion-pair RP-HPLC. *Anal Biochem* 348(2), 243-251 (2006).

Kokesh FC, Cameron DA, Kakuda Y, Kuras PV. Hydrolysis of α-D-glucopyranose 1,2-cyclic phosphate: the effect of pH and temperature on the product distribution, and the position of

opening of the phosphate diester ring in formation of D-glucose 2-phosphate. *Carbohydr Res* 62(2), 289–300 (1978).

Kolset SO, Prydz K, Pejler G. Intracellular proteoglycans. *Biochem J* 379(Pt 2), 217-227 (2004).

Kornfeld R. Studies on L-Glutamine D-Fructose 6-Phosphate Amidotransferase I. Feedback Inhibition by Uridine Diphosphate-*N*-Acetylglucosamine. *J Biol Chem* 242(13), 3135-3141 (1967).

Kornfeld RH, Ginsburg V. Control of synthesis of guanosine 5'-diphosphate D-mannose and guanosine 5'-diphosphate L-fucose in bacteria. *Biochim Biophys Acta* 117(1), 79-87 (1966).

Kornfeld S, Kornfeld R, Neufeld EF, O'Brief PJ. The Feedback Control of Sugar Nucleotide Biosynthesis in Liver. *Proc Natl Acad Sci U S A* 52(2), 371-379 (1964).

Kozak LP, Wells WW. Studies on the metabolic determinants of D-galactose-induced neurotoxicity in the chick. *J Neurochem* 18(11), 2217-2228 (1971).

Kreppel LK, Blomberg MA, Hart GW. Dynamic glycosylation of nuclear and cytosolic proteins. Cloning and characterization of a unique *O*-GlcNAc transferase with multiple tetratricopeptide repeats. *J Biol Chem* 272, 9308-9315 (1997).

Kreppel LK, Hart GW. Regulation of a cytosolic and nuclear *O*-GlcNAc transferase. Role of the tetratricopeptide repeats. *J Biol Chem* 274(45), 32015-32022 (1999).

Krug E, Zweibaum A, Schulz-Holstege C, Keppler D. D-glucosamine-induced changes in nucleotide metabolism and growth of colon-carcinoma cells in culture. *Biochem J* 217(3), 701-708 (1984).

Krzeslak A, Pomorski L, Lipinska A. Elevation of nucleocytoplasmic beta-*N*-acetylglucosaminidase (*O*-GlcNAcase) activity in thyroid cancers. *Int J Mol Med* 25(4), 643-648 (2010).

Kubo T, Kumagae Y, Miller CA, Kaneko I. Beta-amyloid racemized at the Ser26 residue in the brains of patients with Alzheimer disease: implications in the pathogenesis of Alzheimer disease. *J Neuropathol Exp Neurol* 62(3), 248-259 (2003).

Kubo T, Nishimura S, Kumagae Y, Kaneko I. *In vivo* conversion of racemized ß-amyloid ([D-Ser 26]Aß1-40) to truncated and toxic fragments ([D-Ser 26]Aß25-35/40) and fragment presence in the brains of Alzheimer's patients. *J Neurosci Res* 70(3), 474-483 (2002).

Kuhl DE, Metter EJ, Riege WH, Phelps ME. Effects of human aging on patterns of local cerebral glucose utilization determined by the [18F]fluorodeoxyglucose method. *J Cereb Blood Flow Metab* 2(2), 163-171 (1982).

LaFerla FM, Green KN, Oddo S. Intracellular amyloid-beta in Alzheimer's disease. *Nat Rev Neurosci* 8(7), 499-50 (2007).

Lai K, Langley SD, Khwaja FW, Schmitt EW, Elsas LJ. GALT deficiency causes UDP-hexose deficit in human galactosemic cells. *Glycobiology* 13(4), 285-294 (2003).

Lairson LL, Henrissat B, Davies GJ, Withers SG. Glycosyltransferases: structures, functions, and mechanisms. *Annu Rev Biochem* 77, 521-555 (2008).

Lau KS, Dennis JW. *N*-Glycans in cancer progression. *Glycobiology* 18(10), 750-760 (2008).

Lauble H, Kennedy MC, Emptage MH, Beinert H, Stout CD. The reaction of fluorocitrate with aconitase and the crystal structure of the enzyme-inhibitor complex. *Proc Natl Acad Sci U S A* 93(24), 13699–13703 (1996).

Lawrence SM, Huddleston KA, Pitts LR, Nguyen N, Lee YC, Vann WF, Coleman TA, Betenbaugh MJ. Cloning and expression of the human N-acetylneuraminic acid phosphate synthase gene with 2-keto-3-deoxy-D-glycero- D-galacto-nononic acid biosynthetic ability. *J Biol Chem* 275(23), 17869-17877 (2000).

Le Belle JE, Harris NG, Williams SR, Bhakoo KK. A comparison of cell and tissue extraction techniques using high-resolution ^{1}H-NMR spectroscopy. *NMR Biomed* 15(1), 37-44 (2002).

Ledo A, Barbosa RM, Gerhardt GA, Cadenas E, Laranjinha J. Concentration dynamics of nitric oxide in rat hippocampal subregions evoked by stimulation of the NMDA glutamate receptor. *Proc Natl Acad Sci U S A* 102(48), 17483-17488 (2005).

Lee MK, Xu Z, Wong PC, Cleveland DW. Neurofilaments are obligate heteropolymers *in vivo*. *J Cell Biol* 122(6), 1337-1350 .

Lefebvre T, Caillet-Boudin ML, Buée L, Delacourte A, Michalski JC. *O*-GlcNAc glycosylation and neurological disorders. *Adv Exp Med Biol* 535, 189-202 (2003).

Lefebvre T, Guinez C, Dehennaut V, Beseme-Dekeyser O, Morelle W, Michalski JC. Does *O*-GlcNAc play a role in neurodegenerative diseases? *Expert Rev Proteomics* 2(2), 265-275 (2005).

Lehman DM, Fu DJ, Freeman AB, Hunt KJ, Leach RJ, Johnson-Pais T, Hamlington J, Dyer TD, Arya R, Abboud H, Göring HH, Duggirala R, Blangero J, Konrad RJ, Stern MP. A single nucleotide polymorphism in MGEA5 encoding *O*-GlcNAc-selective N-acetyl-beta-D glucosaminidase is associated with type 2 diabetes in Mexican Americans. *Diabetes* 54(4), 1214-1221 (2005).

Leloir LF, Cardini CE, Olavarria JM. Phosphorylation of acetylhexosamines. *Arch Biochem Biophys* 74(1), 84-91 (1958).

Leloup C, Arluison M, Lepetit N, Cartier N, Marfaing-Jallat P, Ferré P, Pénicaud L. Glucose transporter 2 (GLUT 2): expression in specific brain nuclei. *Brain Res* 638(1-2), 221-226 (1994).

Li X, Lu F, Wang JZ, Gong CX. Concurrent alterations of *O*-GlcNAcylation and phosphorylation of tau in mouse brains during fasting. *Eur J Neurosci* 23(8), 2078-2086 (2006).

Liang WS, Reiman EM, Valla J, Dunckley T, Beach TG, Grover A, Niedzielko TL, Schneider LE, Mastroeni D, Caselli R, Kukull W, Morris JC, Hulette CM, Schmechel D, Rogers J, Stephan DA. Alzheimer's disease is associated with reduced expression of energy metabolism genes in posterior cingulate neurons. *Proc Natl Acad Sci U S A* 105(11), 4441-4446 (2008).

Liberatore GT, Jackson-Lewis V, Vukosavic S, Mandir AS, Vila M, McAuliffe WG, Dawson VL, Dawson TM, Przedborski S. Inducible nitric oxide synthase stimulates dopaminergic neurodegeneration in the MPTP model of Parkinson disease. *Nat Med* 5(12), 1403-1409 (1999).

Lim CK. Sample preparation for high-performance liquid chromatography in the clinical laboratory. *Trend Anal Chem* 7(9), 340-345 (1988).

Lin WL, Lewis J, Yen SH, Hutton M, Dickson DW. Filamentous tau in oligodendrocytes and astrocytes of transgenic mice expressing the human tau isoform with the P301L mutation. *Am J Pathol* 162(1), 213-218 (2003).

Lin Y, Sun Z. Current views on type 2 diabetes. *J Endocrinol* 204(1), 1-11 (2010).

Lindahl T, Satoh MS, Poirier GG, Klungland A. Post-translational modification of poly(ADP-ribose) polymerase induced by DNA strand breaks. *Trends Biochem Sci* 20(10), 405-11 (1995).

Lipinski P, Starzynski RR, Drapier JC, Bouton C, Bartlomiejczyk T, Sochanowicz B, Smuda E, Gajkowska A, Kruszewski M. Induction of iron regulatory protein 1 RNA-binding activity by nitric oxide is associated with a concomitant increase in the labile iron pool: implications for DNA damage. *Biochem Biophys Res Commun* 327(1), 349-355 (2005).

Liu F, Grundke-Iqbal I, Iqbal K, Gong CX. Contributions of protein phosphatases PP1, PP2A, PP2B and PP5 to the regulation of tau phosphorylation. *Eur J Neurosci* 22(8), 1942-1950 (2005).

Liu F, Iqbal K, Grundke-Iqbal I, Hart GW, Gong CX. *O*-GlcNAcylation regulates phosphorylation of tau: a mechanism involved in Alzheimer's disease. *Proc Natl Acad Sci U S A* 101(29), 10804-10809 (2004b).

Liu F, Shi J, Tanimukai H, Gu J, Gu J, Grundke-Iqbal I, Iqbal K, Gong CX. Reduced *O*-GlcNAcylation links lower brain glucose metabolism and tau pathology in Alzheimer's disease. *Brain* 132(Pt 7), 1820-1832 (2009b).

Liu K, Paterson AJ, Zhang F, McAndrew J, Fukuchi K, Wyss JM, Peng L, Hu Y, Kudlow JE. Accumulation of protein *O*-GlcNAc modification inhibits proteasomes in the brain and coincides with neuronal apoptosis in brain areas with high *O*-GlcNAc metabolism. *J Neurochem* 89(4), 1044-1055 (2004a).

Liu R, Choi J. Age-associated decline in gamma-glutamylcysteine synthetase gene expression in rats. *Free Radic Biol Med* 28(4), 566-574 (2000).

Liu Y, Liu F, Grundke-Iqbal I, Iqbal K, Gong CX. Brain glucose transporters, *O*-GlcNAcylation and phosphorylation of tau in diabetes and Alzheimer's disease. *J Neurochem* 111(1), 242-249 (2009a).

Liu Y, Liu F, Iqbal K, Grundke-Iqbal I, Gong CX. Decreased glucose transporters correlate to abnormal hyperphosphorylation of tau in Alzheimer disease. *FEBS Lett* 582(2), 359-364 (2008).

Lizasoain I, Moro MA, Knowles RG, Darley-Usmar V, Moncada S. Nitric oxide and peroxynitrite exert distinct effects on mitochondrial respiration which are differentially blocked by glutathione or glucose. *Biochem J* 314 (Pt 3), 877-80 (1996).

Longo VD, Viola KL, Klein WL, Finch CE. Reversible inactivation of superoxide-sensitive aconitase in $A\beta_{1-42}$-treated neuronal cell lines. *J Neurochem* 75(5), 1977-1985 (2000).

Lopez MF, Kristal BS, Chernokalskaya E, Lazarev A, Shestopalov AI, Bogdanova A, Robinson M. High-throughput profiling of the mitochondrial proteome using affinity fractionation and automation. *Electrophoresis* 21(16), 3427-3440 (2000).

Lovatt D, Sonnewald U, Waagepetersen HS, Schousboe A, He W, Lin JH, Han X, Takano T, Wang S, Sim FJ, Goldman SA, Nedergaard M. The transcriptome and metabolic gene signature of protoplasmic astrocytes in the adult murine cortex. *J Neurosci* 27(45), 12255-12266 (2007).

Love DC, Hanover JA. The hexosamine signaling pathway: deciphering the "*O*-GlcNAc code". *Sci STKE* 2005(312), re13 (2005).

Love DC, Kochan J, Cathey RL, Shin SH, Hanover JA. Mitochondrial and nucleocytoplasmic targeting of *O*-linked GlcNAc transferase. *J Cell Sci* 116(Pt 4), 647-654 (2003).

Lowe JB, Marth JD. A genetic approach to Mammalian glycan function. *Annu Rev Biochem* 72, 643-691 (2003).

Lubas WA, Frank DW, Krause M, Hanover JA. *O*-Linked GlcNAc transferase is a conserved nucleocytoplasmic protein containing tetratricopeptide repeats. *J Biol Chem* 272(14), 9316-9324 (1997).

Lubas WA, Hanover JA. Functional expression of *O*-linked GlcNAc transferase. Domain structure and substrate specificity. *J Biol Chem* 275(15), 10983-10988 (2000).

Luchansky SJ, Yarema KJ, Takahashi S, Bertozzi CR. GlcNAc 2-epimerase can serve a catabolic role in sialic acid metabolism. *J Biol Chem* 278(10), 8035-8042 (2003).

Lüdemann N, Clement A, Hans VH, Leschik J, Behl C, Brandt R. *O*-glycosylation of the tail domain of neurofilament protein M in human neurons and in spinal cord tissue of a rat model of amyotrophic lateral sclerosis (ALS). *J Biol Chem* 280(36), 31648-31658 (2005).

Lynch TP, Ferrer CM, Jackson SR, Shahriari KS, Vosseller K, Reginato MJ. Critical role of *O*-Linked β-*N*-acetylglucosamine transferase in prostate cancer invasion, angiogenesis, and metastasis. *J Biol Chem* 287(14), 11070-11081 (2012).

Maccioni HJ, Giraudo CG, Daniotti JL. Understanding the stepwise synthesis of glycolipids. *Neurochem Res* 27(7-8), 629-636 (2002).

Macfarlane WM, McKinnon CM, Felton-Edkins ZA, Cragg H, James RF, Docherty K. Glucose stimulates translocation of the homeodomain transcription factor PDX1 from the cytoplasm to the nucleus in pancreatic beta-cells. *J Biol Chem* 274(2), 1011-1016 (1999).

Maddaiah VT, Madsen NB. Kinetics of purified liver phosphorylase. *J Biol Chem* 241(17), 3873-3881 (1966).

Magistretti PJ, Pellerin L, Rothman DL, Shulman RG. Energy on Demand. *Science* 283(5401), 496-497 (1999).

Magistretti PJ, Pellerin L. Cellular mechanisms of brain energy metabolism and their relevance to functional brain imaging. *Philos Trans R Soc Lond B Biol Sci* 354(1387), 1155–1163 (1999).

Magistretti PJ, Sorg O, Martin JL. Regulation of glycogen metabolism in astrocytes: physiological, pharmacological, and pathological aspects. In: Astrocytes: pharmacology and function (Murphy S. cd), San Diego: Academic, 243-265 (1993).

Magistretti PJ. Neuron-glia metabolic coupling and plasticity. *J Exp Biol* 209(Pt 12), 2304-2311 (2006).

Maher P, Davis JB. The role of monoamine metabolism in oxidative glutamate toxicity. *J Neurosci* 16(20), 6394-6401 (1996).

Majumdar G, Harrington A, Hungerford J, Martinez-Hernandez A, Gerling IC, Raghow R, Solomon S. Insulin dynamically regulates calmodulin gene expression by sequential *O*-glycosylation and phosphorylation of Sp1 and its subcellular compartmentalization in liver cells. *J Biol Chem* 281(6), 3642-3650 (2006).

Maley F, Maley GF. The enzymic conversion of glucosamine to galactosamine. *Biochim Biophys Acta* 31(2), 577-578 (1959).

Maley F, Tarentino AL, McGarrahan JF, Delgiacco R. The metabolism of D-galactosamine and *N*-acetyl-D-galactosamine in rat liver. *Biochem J* 107(5), 637-644 (1968).

Maley F. The synthesis of UDP-galactosamine and UDP-N-acetylgalactosamine. *Biochem Biophys Res Commun* 39(3), 371-378 (1970).

Manczak M, Anekonda TS, Henson E, Park BS, Quinn J, Reddy PH. Mitochondria are a direct site of Aß accumulation in Alzheimer's disease neurons: implications for free radical generation and oxidative damage in disease progression. *Hum Mol Genet* 15(9), 1437-1449 (2006).

Manning G, Whyte DB, Martinez R, Hunter T, Sudarsanam S. The protein kinase complement of the human genome. *Science* 298(5600), 1912-1934 (2002).

Marcillac F, Brix B, Repond C, Jöhren O, Pellerin L. Nitric oxide induces the expression of the monocarboxylate transporter MCT4 in cultured astrocytes by a cGMP-independent transcriptional activation. *Glia* 59(12), 1987-1995 (2011).

Mark RJ, Pang Z, Geddes JW, Uchida K, Mattson MP. Amyloid beta-peptide impairs glucose transport in hippocampal and cortical neurons: involvement of membrane lipid peroxidation. *J Neurosci* 17(3), 1046-1054 (1997).

Markesbery WR. Oxidative stress hypothesis in Alzheimer's disease. *Free Radic Biol Med* 23(1), 134-147 (1997).

Marks JD, Boriboun C, Wang J. Mitochondrial nitric oxide mediates decreased vulnerability of hippocampal neurons from immature animals to NMDA. *J Neurosci* 25(28), 6561-75 (2005).

Marshall S, Bacote V, Traxinger PR. Complete inhibition of glucose-induced desensitization of the glucose transport system by inhibitors of mRNA synthesis. Evidence for rapid turnover of glutamine:fructose-6-phosphate amidotransferase. *J Biol Chem* 266, 10155-10161 (1991b).

Marshall S, Bacote V, Traxinger PR. Discovery of a metabolic pathway mediating glucose-induced desensitization of the glucose transport system. Role of hexosamine biosynthesis in the induction of insulin resistance. *J Biol Chem* 266, 4706-4712 (1991a).

Marshall S, Garvey WT, Traxinger PR. New insights into the metabolic regulation of insulin resistance: role of glucose and amino acids. *FASEB J* 5, 3031-3036 (1991c).

Marshall S, Nadeau O, Yamasaki K. Dynamic actions of glucose and glucosamine on hexosamine biosynthesis in isolated adipocytes: differential effects on glucosamine 6-phosphate, UDP-N-acetylglucosamine, and ATP levels. *J Biol Chem* 279(34), 35313-35319 (2004).

Martinez-Hernandez A, Bell KP, Norenberg MD. Glutamine synthetase: glial localization in brain. *Science* 195(4284), 1356-1358 (1977).

Maru I, Ohta Y, Murata K, Tsukada Y. Molecular cloning and identification of *N*-acyl-D-glucosamine 2-epimerase from porcine kidney as a renin-binding protein. *J Biol Chem* 271(27), 16294-16299 (1996).

Matasova LV, Popova TN. Aconitate hydratase of mammals under oxidative stress. *Biochemistry (Mosc)* 73(9), 957-964 (2008).

Matthews JA, Belof JL, Acevedo-Duncan M, Potter RL. Glucosamine-induced increase in Akt phosphorylation corresponds to increased endoplasmic reticulum stress in astroglial cells. *Mol Cell Biochem* 298(1-2), 109-123 (2007).

Maxwell PH. Hypoxia-inducible factor as a physiological regulator. *Exp Physiol* 90(6), 791–797 (2005).

McCarthy KD, de Vellis J. Preparation of separate astroglial and oligodendroglial cell cultures from rat cerebral tissue. *J Cell Biol* 85(3), 890-902 (1980).

McClain DA, Crook ED. Hexosamines and insulin resistance. *Diabetes* 45(8), 1003-1009 (1996).

McClain DA, Lubas WA, Cooksey RC, Hazel M, Parker GW, Love DC, Hanover JA. Altered glycan-dependent signaling induces insulin resistance and hyperleptinemia. *Proc Natl Acad Sci U S A* 99(16), 10695-10699 (2002).

McDowall RD. Sample preparation for biomedical analysis. *J Chromatogr* 492, 3-58 (1989).

McKnight GL, Mudri SL, Mathewes SL, Traxinger RR, Marshall S, Sheppard PO, O'Hara PJ. Molecular cloning, cDNA sequence, and bacterial expression of human glutamine:fructose-6-phosphate amidotransferase. *J Biol Chem* 267(35), 25208-25212 (1992).

McNaught KS, Jenner P. Extracellular accumulation of nitric oxide, hydrogen peroxide, and glutamate in astrocytic cultures following glutathione depletion, complex I inhibition, and/or lipopolysaccharide-induced activation. *Biochem Pharmacol* 60(7), 979-988 (2000).

McNay EC, Gold PE. Extracellular glucose concentrations in the rat hippocampus measured by zero-net-flux: effects of microdialysis flow rate, strain, and age. *J Neurochem* 72(2), 785-90 (1999).

Medina S, Martínez M, Hernanz A. Antioxidants inhibit the human cortical neuron apoptosis induced by hydrogen peroxide, tumor necrosis factor alpha, dopamine and beta-amyloid peptide 1-42. *Free Radic Res* 36(11), 1179-1184 (2002).

Meister A, Anderson ME. Glutathione. *Annu Rev Biochem* 52, 711-760 (1983).

Melino G, Bernassola F, Catani MV, Rossi A, Corazzari M, Sabatini S, Vilbois F, Green DR. Nitric oxide inhibits apoptosis via AP-1-dependent CD95L transactivation. *Cancer Res* 60(9), 2377-2383 (2000).

Melov S, Adlard PA, Morten K, Johnson F, Golden TR, Hinerfeld D, Schilling B, Mavros C, Masters CL, Volitakis I, Li QX, Laughton K, Hubbard A, Cherny RA, Gibson B, Bush AI. Mitochondrial Oxidative Stress Causes Hyperphosphorylation of Tau. *PLoS ONE* 2(6), e536 (2007).

Menon S, Stahl M, Kumar R, Xu GY, Sullivan F. Stereochemical course and steady state mechanism of the reaction catalyzed by the GDP-fucose synthetase from Escherichia coli. *J Biol Chem* 274(38), 26743-26750 (1999).

Mergia E, Friebe A, Dangel O, Russwurm M, Koesling D. Spare guanylyl cyclase NO receptors ensure high NO sensitivity in the vascular system. *J Clin Invest* 116(6), 1731-1737 (2006).

Michaelis T, Merboldt KD, Hänicke W, Gyngell ML, Bruhn H, Frahm J. On the identification of cerebral metabolites in localized ^{1}H NMR spectra of human brain *in vivo*. *NMR Biomed* 4(2), 90-98 (1991).

Michalski JC, Klein A. Glycoprotein lysosomal storage disorders: alpha- and beta-mannosidosis, fucosidosis and alpha-*N*-acetylgalactosaminidase deficiency. *Biochim Biophys Acta* 1455(2-3), 69-84 (1999).

Mielke R, Herholz K, Grond M, Kessler J, Heiss WD. Differences of regional cerebral glucose metabolism between presenile and senile dementia of Alzheimer type. *Neurobiol Aging* 13(1), 93-98 (1992).

Mikesh LM, Ueberheide B, Chi A, Coon JJ, Syka JE, Shabanowitz J, Hunt DF. The utility of ETD mass spectrometry in proteomic analysis. *Biochim Biophys Acta* 1764(12), 1811-1822 (2006).

Miller CC, Ackerley S, Brownlees J, Grierson AJ, Jacobsen NJ, Thornhill P. Axonal transport of neurofilaments in normal and disease states. *Cell Mol Life Sci* 59(2), 323-330 (2002).

Miñana MD, Kosenko E, Marcaida G, Hermenegildo C, Montoliu C, Grisolía S, Felipo V. Modulation of glutamine synthesis in cultured astrocytes by nitric oxide. *Cell Mol Neurobiol* 17(4), 433-45 (1997).

Miranda S, Opazo C, Larrondo LF, Muñoz FJ, Ruiz F, Leighton F, Inestrosa NC. The role of oxidative stress in the toxicity induced by amyloid beta-peptide in Alzheimer's disease. *Prog Neurobiol* 62(6), 633-648 (2000).

Mitrovic B, Ignarro LJ, Montestruque S, Smoll A, Merrill JE. Nitric oxide as a potential pathological mechanism in demyelination: its differential effects on primary glial cells *in vitro*. *Neuroscience* 61(3), 575-585 (1994).

Moeller JR, Ishikawa T, Dhawan V, Spetsieris P, Mandel F, Alexander GE, Grady C, Pietrini P, Eidelberg D. The metabolic topography of normal aging. *J Cereb Blood Flow Metab* 16(3), 385-398 (1996).

Mohamed A, Posse de Chaves E. Aβ internalization by neurons and glia. *Int J Alzheimers Dis* 2011, 127984 (2011).

Möller HJ, Graeber MB. The case described by Alois Alzheimer in 1911. Historical and conceptual perspectives based on the clinical record and neurohistological sections. *Eur Arch Psychiatry Clin Neurosci* 248(3), 111-122 (1998).

Monauni T, Zenti MG, Cretti A, Daniels MC, Targher G, Caruso B, Caputo M, McClain D, Del Prato S, Giaccari A, Muggeo M, Bonora E, Bonadonna RC. Effects of glucosamine infusion on insulin secretion and insulin action in humans. *Diabetes* 49(6), 926-935 (2000).

Moncada S, Erusalimsky JD. Does nitric oxide modulate mitochondrial energy generation and apoptosis? *Nat Rev Mol Cell Biol* 3(3), 214-220 (2002).

Moncada S, Palmer RM, Higgs EA. Nitric oxide: physiology, pathophysiology, and pharmacology. *Pharmacol Rev* 43(2), 109-42 (1991).

Mooradian AD, Chung HC, Shah GN. GLUT-1 expression in the cerebra of patients with Alzheimer's disease. *Neurobiol Aging* 18(5), 469-74 (1997).

Morgan PM, Sala RF, Tanner ME. Eliminations in the Reactions Catalyzed by UDP-*N*-Acetylglucosamine 2-Epimerase. *J Am Chem Soc* 119(43), 10269–10277 (1997).

Morrish F, Isern N, Sadilek M, Jeffrey M, Hockenbery DM. c-Myc activates multiple metabolic networks to generate substrates for cell-cycle entry. *Oncogene* 28(27), 2485-2491 (2009).

Mosconi L, Pupi A, De Leon MJ. Brain glucose hypometabolism and oxidative stress in preclinical Alzheimer's disease. *Ann N Y Acad Sci* 1147, 180-195 (2008).

Moseley HN, Lane AN, Belshoff AC, Higashi RM, Fan TW. A novel deconvolution method for modeling UDP-N-acetyl-D-glucosamine biosynthetic pathways based on ^{13}C mass isotopologue profiles under non-steady-state conditions. *BMC Biol* 9(37) (2011).

Munch-Petersen A. Reversible enzymatic synthesis of guanosine diphosphate mannose from guanosine triphosphate and mannose-1-phosphate. *Acta Chem Scand* 10, 928-934 (1956).

Munoz DG, Feldman H. Causes of Alzheimer's disease. *CMAJ* 162(1), 65-72 (2000).

Murphy S, Grzybicki D. Glial NO: Normal and Pathological Roles. *Neuroscientist* 2(2), 90-99 (1996).

Murray J, Taylor SW, Zhang B, Ghosh SS, Capaldi RA. Oxidative damage to mitochondrial complex I due to peroxynitrite: identification of reactive tyrosines by mass spectrometry. *J Biol Chem* 278(39), 37223-37230 (2003).

Mutisya EM, Bowling AC, Beal MF. Cortical cytochrome oxidase activity is reduced in Alzheimer's disease. *J Neurochem* 63(6), 2179-2184 (1994).

Nagele RG, D'Andrea MR, Lee H, Venkataraman V, Wang HY. Astrocytes accumulate Aß42 and give rise to astrocytic amyloid plaques in Alzheimer disease brains. *Brain Res* 971(2), 197-209 (2003).

Nakajima K, Kitazume S, Angata T, Fujinawa R, Ohtsubo K, Miyoshi E, Taniguchi N. Simultaneous determination of nucleotide sugars with ion-pair reversed-phase HPLC. Glycobiology 20(7), 865-871 (2010).

Nelson BA, Robinson KA, Buse MG. Defective Akt activation is associated with glucose- but not glucosamine-induced insulin resistance. *Am J Physiol Endocrinol Metab* 282(3), E497-506 (2002).

Nelson BA, Robinson KA, Buse MG. High glucose and glucosamine induce insulin resistance via different mechanisms in 3T3-L1 adipocytes. *Diabetes* 49(6), 981-991 (2000).

Nerlich AG, Sauer U, Kolm-Litty V, Wagner E, Koch M, Schleicher ED. Expression of glutamine:fructose-6-phosphate amidotransferase in human tissues: evidence for high variability and distinct regulation in diabetes. *Diabetes* 47(2), 170-178 (1998).

Nicholson JK, Wilson ID. High Resolution Proton Magnetic Resonance Spectroscopy of Biological Fluids. *Prog Nucl Magn Reson Spectrosc* 21, 449-501 (1989).

Niehues R, Hasilik M, Alton G, Körner C, Schiebe-Sukumar M, Koch HG, Zimmer KP, Wu R, Harms E, Reiter K, von Figura K, Freeze HH, Harms HK, Marquardt T. Carbohydrate-deficient glycoprotein syndrome type Ib. Phosphomannose isomerase deficiency and mannose therapy. *J Clin Invest* 101(7), 1414-1420 (1998).

Niimi M, Ogawara T, Yamashita T, Yamamoto Y, Ueyama A, Kambe T, Okamoto T, Ban T, Tamanoi H, Ozaki K, Fujiwara T, Fukui H, Takahashi EI, Kyushiki H, Tanigami A. Identification of GFAT1-L, a novel splice variant of human glutamine: fructose-6-phosphate amidotransferase (GFAT1) that is expressed abundantly in skeletal muscle. *J Hum Genet* 46(10), 566-571 (2001).

Niwa K, Kazama K, Younkin SG, Carlson GA, Iadecola C. Alterations in cerebral blood flow and glucose utilization in mice overexpressing the amyloid precursor protein. *Neurobiol Dis* 9(1), 61-68 (2002).

Nogalska A, Pankiewicz A, Goyke E, Swierczynski J. The age-related inverse relationship between ob and lipogenic enzymes genes expression in rat white adipose tissue. *Exp Gerontol* 38(4), 415-422 (2003).

Novelli G, Reichardt JK. Molecular basis of disorders of human galactose metabolism: past, present, and future. *Mol Genet Metab* 71(1-2), 62-65 (2000).

Nunez HA, Barker R. The metal ion catalyzed decomposition of nucleoside diphosphate sugars. *Biochemistry* 15(17), 3843-3847 (1976).

Nussbaum RL, Ellis CE. Alzheimer's disease and Parkinson's disease. *N Engl J Med* 348(14), 1356-1364 (2003).

O'Donnell N, Zachara NE, Hart GW, Marth JD. *Ogt*-Dependent X-Chromosome-Linked Protein Glycosylation Is a Requisite Modification in Somatic Cell Function and Embryo Viability. *Mol Cell Biol* 24(4), 1680-1690 (2004).

O'Connor JV, Nunez HA, Barker R. α and ß-glycopyranosyl phosphates and 1.2-phosphates. Assignments of conformations in solution by ^{13}C and ^{1}H NMR. *Biochemistry* 18(3), 500-507 (1979).

Oetke C, Hinderlich S, Brossmer R, Reutter W, Pawlita M, Keppler OT. Evidence for efficient uptake and incorporation of sialic acid by eukaryotic cells. *Eur J Biochem* 268(16), 4553-4561 (2001).

Ohtsubo K, Marth JD. Glycosylation in cellular mechanisms of health and disease. *Cell* 126(5), 855-867 (2006).

Oki T, Yamazaki K, Kuromitsu J, Okada M, Tanaka I. cDNA cloning and mapping of a novel subtype of glutamine:fructose-6-phosphate amidotransferase (GFAT2) in human and mouse. *Genomics* 57(2), 227-234 (1999).

Oliver IT. Inhibitor studies on uridine diphosphoglucose pyrophosphorylase. *Biochim Biophys Acta* 52, 75-81 (1961).

Oths PJ, Mayer RM, Floss HG. Stereochemistry and mechanism of the GDP-mannose dehydratase reaction. *Carbohydr Res* 198(1), 91-100 (1990).

Packer MA, Murphy MP. Peroxynitrite formed by simultaneous nitric oxide and superoxide generation causes cyclosporin-A-sensitive mitochondrial calcium efflux and depolarisation. *Eur J Biochem* 234(1), 231-239 (1995).

Pagani L, Eckert A. Amyloid-Beta interaction with mitochondria. *Int J Alzheimers Dis* 2011, 925050 (2011).

Palacios-Callender M, Quintero M, Hollis VS, Springett RJ, Moncada S. Endogenous NO regulates superoxide production at low oxygen concentrations by modifying the redox state of cytochrome c oxidase. *Proc Natl Acad Sci U S A* 101(20), 7630-7605 (2004).

Paladini AC, Leloir LF. Studies on uridine-diphosphate-glucose. *Biochem J* 51(3), 426–430 (1952).

Palmer RM, Ferrige AG, Moncada S. Nitric oxide release accounts for the biological activity of endothelium-derived relaxing factor. *Nature* 327(6122), 524-6 (1987).

Palmieri F, Biasaccia F, Izcobazzi V, Indiveri C, Zara V. Mitochondrial substrate carriers. Biochim Biophys Acta 1992. 1101(2), 223-227 (1992).

Palmieri F, Pierri CL. Mitochondrial metabolite transport. *Essays Biochem* 47, 37-52 (2010).

Palmieri F, Stipani I, Quagliariello E, Klingenberg M. Kinetic study of the tricarboxylate carrier in mitochondria. *Eur J Biochem* 26(4), 587–594 (1972).

Palmieri F. The mitochondrial transporter family (SLC25): physiological and pathological implications. *Pflügers Arch* 447(5), 689-709 (2004).

Pan X, Wilson M, Mirbahai L, McConville C, Arvanitis TN, Griffin JL, Kauppinen RA, Peet AC. *In vitro* metabonomic study detects increases in UDP-GlcNAc and UDP-GalNAc, as early phase markers of cisplatin treatment response in brain tumor cells. *J Proteome Res* 10(8), 3493-3500 (2011).

Panneerselvam K, Etchison JR, Freeze HH. Human fibroblasts prefer mannose over glucose as a source of mannose for N-glycosylation. Evidence for the functional importance of transported mannose. *J Biol Chem* 272(37), 23123-23129 (1997).

Panneerselvam K, Freeze HH. Mannose enters mammalian cells using a specific transporter that is insensitive to glucose. *J Biol Chem* 271(16), 9417-9421 (1996).

Papasozomenos SC, Binder LI. Phosphorylation determines two distinct species of Tau in the central nervous system. *Cell Motil Cytoskeleton* 8(3), 210-226 (1987).

Paradisi S, Sacchetti B, Balduzzi M, Gaudi S, Malchiodi-Albedi F. Astrocyte modulation of *in vitro* beta-amyloid neurotoxicity. Glia 46(3), 252-260 (2004).

Pardridge WM. Blood-brain barrier transport of glucose, free fatty acids, and ketone bodies. *Adv Exp Med Biol* 291, 43-53 (1991).

Park LC, Zhang H, Sheu KF, Calingasan NY, Kristal BS, Lindsay JG, Gibson GE. Metabolic impairment induces oxidative stress, compromises inflammatory responses, and inactivates a key mitochondrial enzyme in microglia. *J Neurochem* 72(5), 1948-1958 (1999).

Park SY, Ryu J, Lee W. *O*-GlcNAc modification on IRS-1 and Akt2 by PUGNAc inhibits their phosphorylation and induces insulin resistance in rat primary adipocytes. *Exp Mol Med* 37(3), 220-229 (2005).

Park YK, Ahn DR, Oh M, Lee T, Yang EG, Son M, Park H. Nitric oxide donor, (+/-)-S-nitroso-N-acetylpenicillamine, stabilizes transactive hypoxia-inducible factor-1alpha by inhibiting von Hippel-Lindau recruitment and asparagine hydroxylation. *Mol Pharmacol* 74(1), 236-245 (2008).

Parker G, Taylor R, Jones D, McClain D. Hyperglycemia and inhibition of glycogen synthase in streptozotocin-treated mice: role of O-linked N-acetylglucosamine. *J Biol Chem* 279(20), 20636-20642 (2004).

Parker GJ, Lund KC, Taylor RP, McClain DA. Insulin resistance of glycogen synthase mediated by *O*-linked *N*-acetylglucosamine. *J Biol Chem* 278(12), 10022-10027 (2003).

Parpura-Gill A, Beitz D, Uemura E. The inhibitory effects of beta-amyloid on glutamate and glucose uptakes by cultured astrocytes. *Brain Res* 754(1-2), 65-71 (1997).

Patel JR, Brewer GJ. Age-related changes in neuronal glucose uptake in response to glutamate and beta-amyloid. *J Neurosci Res* 72(4), 527-536 (2003).

Patel M, Day BJ, Crapo JD, Fridovich I, McNamara JO. Requirement for superoxide in excitotoxic cell death. *Neuron* 16(2), 345-55 (1996).

Paterson AJ, Kudlow JE. Regulation of glutamine:fructose-6-phosphate amidotransferase gene transcription by epidermal growth factor and glucose. *Endocrinology* 136(7), 2809-2816 (1995).

Patti ME, Virkamäki A, Landaker EJ, Kahn CR, Yki-Järvinen H. Activation of the hexosamine pathway by glucosamine *in vivo* induces insulin resistance of early postreceptor insulin signaling events in skeletal muscle. *Diabetes* 48(8), 1562-1571 (1999).

Paueksakon P, Revelo MP, Ma LJ, Marcantoni C, Fogo AB. Microangiopathic injury and augmented PAI-1 in human diabetic nephropathy. *Kidney Int* 61(6), 2142-2148 (2002).

Pauwels PJ, Opperdoes FR, Trouet A. Effects of antimycin, glucose deprivation, and serum on cultures of neurons, astrocytes, and neuroblastoma cells. *J Neurochem* 44(1), 143-148 (1985).

Pavlov PF, Hansson Petersen C, Glaser E, Ankarcrona M. Mitochondrial accumulation of APP and Aß: significance for Alzheimer disease pathogenesis. *J Cell Mol Med* 13(10), 4137-4145 (2009).

Peachman KK, Lyles DS, Bass DA. Mitochondria in eosinophils: functional role in apoptosis but not respiration. *Proc Natl Acad Sci U S A* 98(4), 1717-1722 (2001).

Pearce LL, Kanai AJ, Birder LA, Pitt BR, Peterson J. The catabolic fate of nitric oxide: the nitric oxide oxidase and peroxynitrite reductase activities of cytochrome oxidase. *J Biol Chem*. 277(16), 13556-13562 (2002).

Pearce LL, Kanai AJ, Epperly MW, Peterson J. Nitrosative stress results in irreversible inhibition of purified mitochondrial complexes I and III without modification of cofactors. *Nitric Oxide* 13(4), 254-263 (2005).

Pearce LL, Pitt BR, Peterson J. The peroxynitrite reductase activity of cytochrome c oxidase involves a two-electron redox reaction at the hemea_3-Cu_B site. *J Biol Chem* 274(50), 35763-35767 (1999).

Pellerin L, Bouzier-Sore AK, Aubert A, Serres S, Merle M, Costalat R, Magistretti PJ. Activity-dependent regulation of energy metabolism by astrocytes: an update. *Glia* 55(12), 1251-1262 (2007).

Pellerin L, Magistretti PJ. Glutamate uptake into astrocytes stimulates aerobic glycolysis: a mechanism coupling neuronal activity to glucose utilization. *Proc Natl Acad Sci U S A.* 91(22), 10625-10629 (1994).

Pellerin L, Magistretti PJ. How to balance the brain energy budget while spending glucose differently. *J Physiol* 546, 325 (2003).

Pellerin L, Magistretti PJ. Sweet sixteen for ANLS. *J Cereb Blood Flow Metab* 32(7), 1152-1166 (2012).

Pellerin L, Pellegri G, Bittar PG, Charnay Y, Bouras C, Martin JL, Stella N, Magistretti PJ. Evidence supporting the existence of an activity-dependent astrocyte-neuron lactate shuttle. *Dev Neurosci* 20(4-5), 291-299 (1998).

Pels Rijcken WR, Ferwerda W, Van den Eijnden DH, Overdijk B. Influence of D-galactosamine on the synthesis of sugar nucleotides and glycoconjugates in rat hepatocytes. Glycobiology 5(5), 495-502 (1995).

Peng L, Zhang X, Hertz L. High extracellular potassium concentrations stimulate oxidative metabolism in a glutamatergic neuronal culture and glycolysis in cultured astrocytes but have no stimulatory effect in a GABAergic neuronal culture. *Brain Res* 663(1), 168‑172 (1994).

Perry EK, Perry RH, Tomlinson BE, Blessed G, Gibson PH. Coenzyme A-acetylating enzymes in Alzheimer's disease: possible cholinergic 'compartment' of pyruvate dehydrogenase. *Neurosci Lett* 18(1), 105-110 (1980).

Perry G, Nunomura A, Hirai K, Takeda A, Aliev G, Smith MA. Oxidative damage in Alzheimer's disease: the metabolic dimension. *Int J Dev Neurosci* 18(4-5), 417-421 (2000).

Perry G, Nunomura A, Raina AK, Aliev G, Siedlak SL, Harris PL, Casadesus G, Petersen RB, Bligh-Glover W, Balraj E, Petot GJ, Smith MA. A metabolic basis for Alzheimer disease. *Neurochem Res* 28(10), 1549-1552 (2003).

Peters A, Schweiger U, Pellerin L, Hubold C, Oltmanns KM, Conrad M, Schultes B, Born J, Fehm HL. The selfish brain: competition for energy resources. *Neurosci Biobehav Rev* 28(2), 143-180 (2004).

Petry K, Greinix HT, Nudelman E, Eisen H, Hakomori S, Levy HL, Reichardt JK. Characterization of a novel biochemical abnormality in galactosemia: deficiency of glycolipids containing galactose or N-acetylgalactosamine and accumulation of precursors in brain and lymphocytes. *Biochem Med Metab Biol* 46(1), 93-104 (1991).

Petry KG, Reichardt JK. The fundamental importance of human galactose metabolism: lessons from genetics and biochemistry. *Trends Genet* 14(3), 98-102 (1998).

Pihlaja R, Koistinaho J, Malm T, Sikkilä H, Vainio S, Koistinaho M. Transplanted astrocytes internalize deposited ß-amyloid peptides in a transgenic mouse model of Alzheimer's disease. *Glia* 56(2), 154-163 (2008).

Pike CJ, Walencewicz-Wasserman AJ, Kosmoski J, Cribbs DH, Glabe CG, Cotman CW. Structure-activity analyses of beta-amyloid peptides: contributions of the beta 25-35 region to aggregation and neurotoxicity. *J Neurochem* 64(1), 253-265 (1995).

Piras R, Cabib E. Microscale Identification of Several Sugar Phosphates by Paper Chromatography and Electrophoresis. *Anal Chem* 35(6), 755-760 (1963).

Piras R. Synthesis of some aldose 2-phosphates. *Arch Biochem Biophys* 103, 291-292 (1963).

Planel E, Miyasaka T, Launey T, Chui DH, Tanemura K, Sato S, Murayama O, Ishiguro K, Tatebayashi Y, Takashima A. Alterations in glucose metabolism induce hypothermia leading to tau hyperphosphorylation through differential inhibition of kinase and phosphatase activities: implications for Alzheimer's disease. *J Neurosci* 24(10), 2401-2411 (2004).

Poderoso JJ, Carreras MC, Lisdero C, Riobó N, Schöpfer F, Boveris A. Nitric oxide inhibits electron transfer and increases superoxide radical production in rat heart mitochondria and submitochondrial particles. *Arch Biochem Biophys* 328(1), 85-92 (1996).

Poulos TL. Soluble guanylate cyclase. *Curr Opin Struct Biol* 16(6), 736-43 (2006).

Prapong T, Buss J, Hsu WH, Heine P, West Greenlee H, Uemura E. Amyloid beta-peptide decreases neuronal glucose uptake despite causing increase in GLUT3 mRNA transcription and GLUT3 translocation to the plasma membrane. *Exp Neurol* 174(2), 253-258 (2002).

Prihar HS, Behrman EJ. Chemical synthesis of ß-L-fucopyranosyl phosphate and ß-L-rhamnopyranosyl phosphate. *Biochemistry* 12(5), 997-1002 (1973).

Qin L, Liu Y, Cooper C, Liu B, Wilson B, Hong JS. Microglia enhance beta-amyloid peptide-induced toxicity in cortical and mesencephalic neurons by producing reactive oxygen species. *J Neurochem* 83(4), 973-983 (2002).

Radi R, Beckman JS, Bush KM, Freeman BA. Peroxynitrite oxidation of sulfhydryls. The cytotoxic potential of superoxide and nitric oxide. *J Biol Chem* 266(7), 4244-4250 (1991).

Radi R, Cassina A, Hodara R, Quijano C, Castro L. Peroxynitrite reactions and formation in mitochondria. *Free Radic Biol Med* 33(11), 1451-64 (2002).

Raff MC, Mirsky R, Fields KL, Lisak RP, Dorfman SH, Silberberg DH, Gregson NA, Leibowitz S, Kennedy MC. Galactocerebroside is a specific cell-surface antigenic marker for oligodendrocytes in culture. *Nature* 274(5673), 813-816 (1978).

Raisys VA, Winzler RJ. Metabolism of exogenous D-mannosamine. *J Biol Chem* 245(12), 3203-3208 (1970).

Ralton JE, Milne KG, Güther ML, Field RA, Ferguson MA. The mechanism of inhibition of glycosylphosphatidylinositol anchor biosynthesis in Trypanosoma brucei by mannosamine. *J Biol Chem* 268(32), 24183-24189 (1993).

Randle PJ. Regulatory interactions between lipids and carbohydrates: the glucose fatty acid cycle after 35 years. *Diabetes Metab Rev* 14(4), 263-283 (1998).

Rapoport SI. Functional brain imaging in the resting state and during activation in Alzheimer's disease. Implications for disease mechanisms involving oxidative phosphorylation. *Ann N Y Acad Sci* 893, 138-153 (1999).

Reaven GM. Role of insulin resistance in human disease. *Diabetes* 37(12), 1595-1607 (1988).

Rhein V, Song X, Wiesner A, Ittner LM, Baysang G, Meier F, Ozmen L, Bluethmann H, Dröse S, Brandt U, Savaskan E, Czech C, Götz J, Eckert A. Amyloid-beta and tau synergistically impair the oxidative phosphorylation system in triple transgenic Alzheimer's disease mice. *Proc Natl Acad Sci U S A* 106(47), 20057-20062 (2009).

Riobó NA, Melani M, Sanjuan N, Fiszman ML, Gravielle MC, Carreras MC, Cadenas E, Poderoso JJ. The modulation of mitochondrial nitric-oxide synthase activity in rat brain development. *J Biol Chem* 8, 277(45):42447-42455. (2002).

Robertson LA, Moya KL, Breen KC. The potential role of tau protein *O*-glycosylation in Alzheimer's disease. *J Alzheimers Dis* 6(5), 489-495 (2004).

Robinson KA, Ball LE, Buse MG. Reduction of *O*-GlcNAc protein modification does not prevent insulin resistance in 3T3-L1 adipocytes. *Am J Physiol Endocrinol Metab* 292(3), E884-890 (2007).

Robinson KA, Sens DA, Buse MG. Pre-exposure to glucosamine induces insulin resistance of glucose transport and glycogen synthesis in isolated rat skeletal muscles. Study of mechanisms in muscle and in rat-1 fibroblasts overexpressing the human insulin receptor. *Diabetes* 42(9), 1333-1346 (1993).

Robinson KA, Weinstein ML, Lindenmayer GE, Buse MG. Effects of diabetes and hyperglycemia on the hexosamine synthesis pathway in rat muscle and liver. *Diabetes* 44(12), 1438-1446 (1995).

Rome LH, Hill DF. Lysosomal degradation of glycoproteins and glycosaminoglycans. Efflux and recycling of sulphate and N-acetylhexosamines. *Biochem J* 235(3), 707-713 (1986).

Roos MD, Su K, Baker JR, Kudlow JE. *O*-glycosylation of an Sp1-derived peptide blocks known Sp1 protein interactions. *Mol Cell Biol* 17(11), 6472-6480 (1997).

Rossetti L, Hawkins M, Chen W, Gindi J, Barzilai N. *In vivo* glucosamine infusion induces insulin resistance in normoglycemic but not in hyperglycemic conscious rats. *J Clin Invest* 96(1), 132-140 (1995).

Rothstein JD, Dykes-Hoberg M, Pardo CA, Bristol LA, Jin L, Kuncl RW, Kanai Y, Hediger MA, Wang Y, Schielke JP, Welty DF. Knockout of glutamate transporters reveals a major role for astroglial transport in excitotoxicity and clearance of glutamate. *Neuron* 16(3), 675-686 (1996).

Rubbo H, Denicola A, Radi R. Peroxynitrite inactivates thiol-containing enzymes of *Trypanosoma cruzi* energetic metabolism and inhibits cell respiration. *Arch Biochem Biophys* 308(1), 96-102 (1994).

Saavedra L, Mohamed A, Ma V, Kar S, de Chaves EP. Internalization of beta-amyloid peptide by primary neurons in the absence of apolipoprotein E. *J Biol Chem* 282(49), 35722-35732 (2007).

Saez TE, Pehar M, Vargas M, Barbeito L, Maccioni RB. Astrocytic nitric oxide triggers tau hyperphosphorylation in hippocampal neurons. *In Vivo* 18(3), 275-280 (2004).

Sala RF, Morgan PM, Tanner ME. Enzymatic Formation and Release of a Stable Glycal Intermediate: The Mechanism of the Reaction Catalyzed by UDP-*N*-Acetylglucosamine 2-Epimerase. *J Am Chem Soc* 118(12), 3033–3034 (1996).

Salkovic-Petrisic M, Hoyer S. Central insulin resistance as a trigger for sporadic Alzheimer-like pathology: an experimental approach. *J Neural Transm Suppl* (72), 217-233 (2007).

Salvatore MF, Fisher B, Surgener SP, Gerhardt GA, Rouault T. Neurochemical investigations of dopamine neuronal systems in iron-regulatory protein 2 (IRP-2) knockout mice. *Brain Res Mol Brain Res* 139(2), 341-347 (2005).

Sandau KB, Fandrey J, Brüne B. Accumulation of HIF-1alpha under the influence of nitric oxide. *Blood* 97(4), 1009-1015 (2001).

Sandau KB, Faus HG, Brüne B. Induction of hypoxia-inducible-factor 1 by nitric oxide is mediated via the PI 3K pathway. *Biochem Biophys Res Commun* 278(1), 263-267 (2000).

Santolini J. The molecular mechanism of mammalian NO-synthases: a story of electrons and protons. *J Inorg Biochem* 105(2), 127-41 (2011).

Sastry PS, Rao KS. Apoptosis and the nervous system. *J Neurochem* 74(1):1-20 (2000).

Scarlett JL, Packer MA, Porteous CM, Murphy MP. Alterations to glutathione and nicotinamide nucleotides during the mitochondrial permeability transition induced by peroxynitrite. *Biochem Pharmacol* 52(7), 1047-55 (1996).

Schapira AH, Cooper JM, Dexter D, Clark JB, Jenner P, Marsden CD. Mitochondrial complex I deficiency in Parkinson's disease. *J Neurochem* 54(3), 823-827 (1990a).

Schapira AH, Mann VM, Cooper JM, Dexter D, Daniel SE, Jenner P, Clark JB, Marsden CD. Anatomic and disease specificity of NADH CoQ1 reductase (complex I) deficiency in Parkinson's disease. *J Neurochem* 55(6), 2142-2145 (1990b).

Scharnbeck H, Schaffner F, Keppler D, Decker K. Ultrastructural studies on the effect of choline orotate on galactosamine induced hepatic injury in rats. *Exp Mol Pathol* 16(1), 33-46 (1972).

Schofield CJ, Zhang Z. Structural and mechanistic studies on 2-oxoglutarate-dependent oxygenases and related enzymes. *Curr Opin Struct Biol* 9(6), 722-731 (1999).

Schousboe A, Westergaard N, Waagepetersen HS, Larsson OM, Bakken IJ, Sonnewald U. Trafficking between glia and neurons of TCA cycle intermediates and related metabolites. *Glia* 21(1), 99-105 (1997).

Schubert D, Soucek T, Blouw B. The induction of HIF-1 reduces astrocyte activation by amyloid beta peptide. *Eur J Neurosci* 29(7), 1323-1334 (2009).

Schubert D. Glucose metabolism and Alzheimer's disease. *Ageing Res Rev* 4(2), 240-257 (2005).

Schwarz V, Goldberg L, Komrower GM, Holzel A. Some disturbances of erythrocyte metabolism in galactosaemia. *Biochem J* 62(1), 34-40 (1956).

Schwarzkopf M, Knobeloch KP, Rohde E, Hinderlich S, Wiechens N, Lucka L, Horak I, Reutter W, Horstkorte R. Sialylation is essential for early development in mice. *Proc Natl Acad Sci U S A* 99(8), 5267-5270 (2002).

Schweizer M, Richter C. Nitric oxide potently and reversibly deenergizes mitochondria at low oxygen tension. *Biochem Biophys Res Commun* 204(1), 169-75 (1994).

Seidel B, Stanarius A, Wolf G. Differential expression of neuronal and endothelial nitric oxide synthase in blood vessels of the rat brain. *Neurosci Lett* 239(2-3), 109-12 (1997).

Sellick CA, Knight D, Croxford AS, Maqsood AR, Stephens GM, Goodacre R, Dickson AJ. Evaluation of extraction processes for intracellular metabolite profiling of mammalian cells: matching extraction approaches to cell type and metabolite targets. *Metabolomics* 6(3), 427-438 (2010).

Semenza GL. Hypoxia, clonal selection, and the role of HIF-1 in tumor progression. *Crit Rev Biochem Mol Biol* 35(2), 71-103 (2000).

Semenza GL. Regulation of mammalian O_2 homeostasis by hypoxia-inducible factor 1. *Annu Rev Cell Dev Biol* 15, 551-578 (1999).

Serkova NJ, Glunde K. Metabolomics of cancer. *Methods Mol Biol* 520, 273-295 (2009).

Serkova NJ, Hasebroock KM, Kraft SL. Magnetic resonance spectroscopy of living tissues. *Methods Mol Biol* 520, 315-27 (2009).

Shafi R, Iyer SPN, Ellies LG, O'Donnell N, Marek KW, Chui D, Hart GW, Marth JD. The *O*-GlcNAc transferase gene resides on the X chromosome and is essential for embryonic stem cell viability and mouse ontogeny. *Proc Natl Acad Sci U S A* 97(11), 5735–5739 (2000).

Shankar GM, Li S, Mehta TH, Garcia-Munoz A, Shepardson NE, Smith I, Brett FM, Farrell MA, Rowan MJ, Lemere CA, Regan CM, Walsh DM, Sabatini BL, Selkoe DJ. Amyloid-beta protein dimers isolated directly from Alzheimer's brains impair synaptic plasticity and memory. *Nat Med* 14(8), 837-842 (2008).

Shin RW, Iwaki T, Kitamoto T, Tateishi J. Hydrated autoclave pretreatment enhances tau immunoreactivity in formalin-fixed normal and Alzheimer's disease brain tissues. *Lab Invest* 64(5), 693-702 (1991).

Sijens PE, van Echteld CJ, Neijt JP, Schipper J, Dunki Jacobs PB, de Graaf PW, Seijkens D. ^{31}P NMR study of the impact of dietary manipulation on tumor metabolism and response to methotrexate. *NMR Biomed* 2(1), 12-18 (1989).

Silver IA, Erecińska M. Energetic demands of the Na^+/K^+ ATPase in mammalian astrocytes. *Glia* 21(1), 35-45 (1997).

Simpson IA, Chundu KR, Davies-Hill T, Honer WG, Davies P. Decreased concentrations of GLUT1 and GLUT3 glucose transporters in the brains of patients with Alzheimer's disease. *Ann Neurol* 35(5), 546-551 (1994).

Sims NR, Nilsson M, Muyderman H. Mitochondrial glutathione: a modulator of brain cell death. *J Bioenerg Biomembr* 36(4), 329-33 (2004).

Singh LP, Crook ED. The effects of glucose and the hexosamine biosynthesis pathway on glycogen synthase kinase-3 and other protein kinases that regulate glycogen synthase activity. *J Investig Med* 48(4), 251-258 (2000).

Slawson C, Copeland RJ, Hart GW. *O*-GlcNAc signaling: a metabolic link between diabetes and cancer? *Trends Biochem Sci* 35(10), 547-555 (2010).

Slawson C, Hart GW. Dynamic interplay between *O*-GlcNAc and *O*-phosphate: the sweet side of protein regulation. *Curr Opin Struct Biol* 13(5), 631-636 (2003).

Slawson C, Hart GW. *O*-GlcNAc signalling: implications for cancer cell biology. *Nat Rev Cancer* 11(9), 678-684 (2011).

Slawson C, Housley MP, Hart GW. *O*-GlcNAc cycling: how a single sugar post-translational modification is changing the way we think about signaling networks. *J Cell Biochem* 97(1), 71-83 (2006).

Slawson C, Pidala J, Potter R. Increased *N*-acetyl-beta-glucosaminidase activity in primary breast carcinomas corresponds to a decrease in *N*-acetylglucosamine containing proteins. *Biochim Biophys Acta* 1537(2), 147-157 (2001).

Slawson C, Zachara NE, Vosseller K, Cheung WD, Lane MD, Hart GW. Perturbations in *O*-linked ß-*N*-acetylglucosamine protein modification cause severe defects in mitotic progression and cytokinesis. *J Biol Chem* 280(38), 32944-32956 (2005).

Slepak T, Tang M, Addo F, Lai K. Intracellular galactose-1-phosphate accumulation leads to environmental stress response in yeast model. *Mol Genet Metab* 86(3), 360-371 (2005).

Slepak TI, Tang M, Slepak VZ, Lai K. Involvement of endoplasmic reticulum stress in a novel Classic Galactosemia model. *Mol Genet Metab* 92(1-2), 78-87 (2007).

Smith MA, Richey Harris PL, Sayre LM, Beckman JS, Perry G. Widespread peroxynitrite-mediated damage in Alzheimer's disease. *J Neurosci* 17(8), 2653-2657 (1997).

Smith PL, Myers JT, Rogers CE, Zhou L, Petryniak B, Becker DJ, Homeister JW, Lowe JB. Conditional control of selectin ligand expression and global fucosylation events in mice with a targeted mutation at the FX locus. *J Cell Biol* 158(4), 801-815 (2002).

Snyder SW, Ladror US, Wade WS, Wang GT, Barrett LW, Matayoshi ED, Huffaker HJ, Krafft GA, Holzman TF. Amyloid-beta aggregation: selective inhibition of aggregation in mixtures of amyloid with different chain lengths. *Biophys J* 67(3), 1216-1228 (1994).

Sogawa K, Numayama-Tsuruta K, Ema M, Abe M, Abe H, Fujii-Kuriyama Y. Inhibition of hypoxia-inducible factor 1 activity by nitric oxide donors in hypoxia. *Proc Natl Acad Sci U S A* 95(13), 7368-7373 (1998).

Sokoloff L. Chapter 2: The brain as a chemical machine. *Progr Brain Res* 94, 19-33 (1992).

Sokoloff L. Mapping local functional activity by measurement of local cerebral glucose utilization in the central nervous system of animals and man. *Harvey Lect* 79, 77-143 (1983-1984).

Sokoloff L. Relation Between Physiological Function And Energy Metabolism In The Central Nervous System. *J Neurochem* 29(1), 13-26 (1977).

Sola-Penna M, Da Silva D, Coelho WS, Marinho-Carvalho MM, Zancan P. Regulation of mammalian muscle type 6-phosphofructo-1-kinase and its implication for the control of the metabolism. *IUBMB Life* 62(11), 791-796 (2010).

Sonnewald U, Risan AG, Hole HB, Westergaard N, Qu H. Citrate, beneficial or deleterious in the CNS? *Neurochem Res* 27(1-2), 155-9 (2002).

Sonnewald U, Westergaard N, Krane J, Unsgård G, Petersen SB, Schousboe A. First direct demonstration of preferential release of citrate from astrocytes using [^{13}C]NMR spectroscopy of cultured neurons and astrocytes. *Neurosci Lett* 128(2), 235-239 (1991).

Sorbi S, Bird ED, Blass JP. Decreased pyruvate dehydrogenase complex activity in Huntington and Alzheimer brain. *Ann Neurol* 13(1), 72-78 (1983).

Sorg O, Magistretti PJ. Characterization of the glycogenolysis elicited by vasoactive intestinal peptide, noradrenaline and adenosine in primary cultures of mouse cerebral cortical astrocytes. *Brain Res* 563(1-2), 227-233 (1991).

Sorg O, Magistretti PJ. Vasoactive intestinal peptide and noradrenaline exert long-term control on glycogen levels in astrocytes: blockade by protein synthesis inhibition. *J Neurosci* 12(12), 4923-4931 (1992).

Soucek T, Cumming R, Dargusch R, Maher P, Schubert D. The regulation of glucose metabolism by HIF-1 mediates a neuroprotective response to amyloid beta peptide. *Neuron* 39(1), 43-56 (2003).

Spik G, Six P, Montreuil J. Chemical and enzymic degradations of nucleoside mono- and diphosphate sugars. I. Determination of the degradation rate during the glycosyltransferase assays. *Biochim Biophys Acta* 584(2), 203-215 (1979).

Spiro MJ. Effect of diabetes on the sugar nucleotides in several tissues of the rat. *Diabetologia* 26(1), 70-75 (1984).

Stachlewitz RF, Seabra V, Bradford B, Bradham CA, Rusyn I, Germolec D, Thurman RG. Glycine and uridine prevent D-galactosamine hepatotoxicity in the rat: role of Kupffer cells. *Hepatology* 29(3), 737-745 (1999).

Stamler JS. Redox signaling: nitrosylation and related target interactions of nitric oxide. *Cell* 78(6), 931-936 (1994).

Stanarius A, Töpel I, Schulz S, Noack H, Wolf G. Immunocytochemistry of endothelial nitric oxide synthase in the rat brain: a light and electron microscopical study using the tyramide signal amplification technique. *Acta Histochem* 99(4), 411-29 (1997).

Stanley P, Schachter H, Taniguchi N. N-Glycans. In: Varki A, Cummings RD, Esko JD, *et al*., editors. Essentials of Glycobiology. 2nd edition. Cold Spring Harbor (NY): Cold Spring Harbor Laboratory Press. Chapter 8 (2009).

Strominger JL, Smith MS. Uridine diphosphoacetylglucosamine pyrophosphorylase. *J Biol Chem* 234(7), 1822-1827 (1959).

Stubbs KA, Zhang N, Vocadlo DJ. A divergent synthesis of 2-acyl derivatives of PUGNAc yields selective inhibitors of *O*-GlcNAcase. *Org Biomol Chem* 4(5), 839-845 (2006).

Su B, Wang X, Lee HG, Tabaton M, Perry G, Smith MA, Zhu X. Chronic oxidative stress causes increased tau phosphorylation in M17 neuroblastoma cells. *Neurosci Lett* 468(3), 267-271 (2010).

Sullivan FX, Kumar R, Kriz R, Stahl M, Xu GY, Rouse J, Chang XJ, Boodhoo A, Potvin B, Cumming DA. Molecular cloning of human GDP-mannose 4,6-dehydratase and reconstitution of GDP-fucose biosynthesis in vitro. *J Biol Chem* 273(14), 8193-8202 (1998).

Sultana R, Poon HF, Cai J, Pierce WM, Merchant M, Klein JB, Markesbery WR, Butterfield DA. Identification of nitrated proteins in Alzheimer's disease brain using a redox proteomics approach. *Neurobiol Dis* 22(1), 76-87 (2006).

Sun J, Aluvila S, Kotaria R, Mayor JA, Walters DE, Kaplan RS. Mitochondrial and Plasma Membrane Citrate Transporters: Discovery of Selective Inhibitors and Application to Structure/Function Analysis. *Mol Cell Pharmacol* 2(3), 101-110 (2010).

Sweeney C, Mackintosh D, Mason RM. UDP-sugar metabolism in Swarm rat chondrosarcoma chondrocytes. *Biochem J* 290(Pt 2), 563-570 (1993).

Szabó C, Ohshima H. DNA damage induced by peroxynitrite: subsequent biological effects. *Nitric Oxide* 1(5), 373-85 (1997).

Tagliabracci VS, Heiss C, Karthik C, Contreras CJ, Glushka J, Ishihara M, Azadi P, Hurley TD, DePaoli-Roach AA, Roach PJ. Phosphate incorporation during glycogen synthesis and Lafora disease. *Cell Metab* 13(3), 274-282 (2011).

Takahashi S, Ohsawa T, Miura R, Miyake Y. Purification of high molecular weight (HMW) renin from porcine kidney and direct evidence that the HMW renin is a complex of renin with renin binding protein (RnBP). *J Biochem* 93(1), 265-274 (1983).

Takehara Y, Kanno T, Yoshioka T, Inoue M, Utsumi K. Oxygen-dependent regulation of mitochondrial energy metabolism by nitric oxide. *Arch Biochem Biophys* 323(1), 27-32 (1995).

Takuma K, Phuagphong P, Lee E, Mori K, Baba A, Matsuda T. Anti-apoptotic effect of cGMP in cultured astrocytes: inhibition by cGMP-dependent protein kinase of mitochondrial permeable transition pore. *J Biol Chem* 276(51), 48093-48099 (2001).

Tallent MK, Varghis N, Skorobogatko Y, Hernandez-Cuebas L, Whelan K, Vocadlo DJ, Vosseller K. *In vivo* modulation of *O*-GlcNAc levels regulates hippocampal synaptic plasticity through interplay with phosphorylation. *J Biol Chem* 284(1), 174-181 (2009).

Tanaka S, Takehashi M, Iida S, Kitajima T, Kamanaka Y, Stedeford T, Banasik M, Ueda K. Mitochondrial impairment induced by poly(ADP-ribose) polymerase-1 activation in cortical neurons after oxygen and glucose deprivation. *J Neurochem* 95(1), 179-90 (2005).

Taniguchi N, Miyoshi E, Gu J, Honke K, Matsumoto A. Decoding sugar functions by identifying target glycoproteins. *Curr Opin Struct Biol* 16(5), 561-566 (2006).

Tanner ME. The enzymes of sialic acid biosynthesis. *Bioorg Chem* 33(3), 216-228 (2005).

Tansey FA, Farooq M, Cammer W. Glutamine Synthetase in Oligodendrocytes and Astrocytes: New Biochemical and Immunocytochemical Evidence. *J Neurochem* 56(1), 266-272 (1991).

Tapodi A, Debreceni B, Hanto K, Bognar Z, Wittmann I, Gallyas F Jr, Varbiro G, Sumegi B. Pivotal role of Akt activation in mitochondrial protection and cell survival by poly(ADP-ribose)polymerase-1 inhibition in oxidative stress. *J Biol Chem* 280(42), 35767-35775 (2005).

Tatoyan A, Giulivi C. Purification and characterization of a nitric-oxide synthase from rat liver mitochondria. *J Biol Chem* 273(18), 11044-11048 (1998).

Tatton WG, Olanow CW. Apoptosis in neurodegenerative diseases: the role of mitochondria. *Biochim Biophys Acta* 1410(2), 195-213 (1999).

Taylor RP, Geisler TS, Chambers JH, McClain DA. Up-regulation of *O*-GlcNAc transferase with glucose deprivation in HepG2 cells is mediated by decreased hexosamine pathway flux. *J Biol Chem* 284(6), 3425-3432 (2009).

Taylor RP, Parker GJ, Hazel MW, Soesanto Y, Fuller W, Yazzie MJ, McClain DA. Glucose deprivation stimulates *O*-GlcNAc modification of proteins through up-regulation of *O*-linked *N*-acetylglucosaminyltransferase. *J Biol Chem* 283(10), 6050-6057 (2008).

Tomiya N, Ailor E, Lawrence SM, Betenbaugh MJ, Lee YC. Determination of nucleotides and sugar nucleotides involved in protein glycosylation by high-performance anion-exchange chromatography: sugar nucleotide contents in cultured insect cells and mammalian cells. *Anal Biochem* 293(1), 129-137 (2001).

Tonetti M, Sturla L, Bisso A, Benatti U, De Flora A. Synthesis of GDP-L-fucose by the human FX protein. J Biol Chem 271(44), 27274-27279 (1996).

Tong WH, Rouault TA. Metabolic regulation of citrate and iron by aconitases: role of iron-sulfur cluster biogenesis. *Biometals* 20(3-4), 549-64 (2007).

Torres CR, Hart GW. Topography and polypeptide distribution of terminal *N*-acetylglucosamine residues on the surfaces of intact lymphocytes. Evidence for *O*-linked GlcNAc. *J Biol Chem* 259, 3308-3317 (1984).

Traving C, Schauer R. Structure, function and metabolism of sialic acids. *Cell Mol Life Sci* 54(12):1330-1349 (1998).

Traxinger RR, Marshall S. Coordinated regulation of glutamine:fructose-6-phosphate amidotransferase activity by insulin, glucose, and glutamine. Role of hexosamine biosynthesis in enzyme regulation. *J Biol Chem* 266, 10148-10154 (1991).

Tretter L, Adam-Vizi V. Inhibition of Krebs cycle enzymes by hydrogen peroxide: A key role of α-ketoglutarate dehydrogenase in limiting NADH production under oxidative stress. *J Neurosci* 20(24), 8972-8979 (2000).

Trujillo JL, Gan JC. Glycoprotein biosynthesis. VI. Regulation of uridine diphosphate N-acetyl-D-glucosamine metabolism in bovine thyroid gland slices. *Biochim Biophys Acta* 304(1), 32-41 (1973).

Tsacopoulos M, Magistretti PJ. Metabolic coupling between glia and neurons. *J Neurosci* 16(3), 877-85 (1996).

Tyagi RK, Azrad A, Degani H, Salomon Y. Simultaneous extraction of cellular lipids and water-soluble metabolites: evaluation by NMR spectroscopy. *Magn Reson Med* 35(2), 194-200 (1996).

Uyeda K. Phosphofructokinase. *Adv Enzymol Relat Areas Mol Biol* 48, 193-244 (1979).

Van Rinsum J, Van Dijk W, Hooghwinkel GJ, Ferwerda W. Subcellular localization and tissue distribution of sialic acid precursor-forming enzymes. *Biochem J* 210(1), 21-28 (1983).

Van Uden P, Kenneth NS, Rocha S. Regulation of hypoxia-inducible factor-1alpha by NF-κB. *Biochem J* 412(3), 477-484 (2008).

Vander Heiden MG, Cantley LC, Thompson CB. Understanding the Warburg effect: the metabolic requirements of cell proliferation. *Science* 324(5930), 1029-1033 (2009).

Vannucci SJ, Maher F, Simpson IA. Glucose transporter proteins in brain: Delivery of glucose to neurons and glia. *Glia* 21(1), 2-21 (1997).

Varadarajan S, Yatin S, Aksenova M, Butterfield DA. Review: Alzheimer's amyloid beta-peptide-associated free radical oxidative stress and neurotoxicity. *J Struct Biol* 130(2-3), 184-208 (2000).

Varki A, Cummings R, Esko J, *et al*., editors. Essentials of Glycobiology. Cold Spring Harbor (NY): Cold Spring Harbor Laboratory Press. Chapter 6, Monosaccharide Metabolism (1999).

Varki A, Sharon N. Historical Background and Overview. In: Varki A, Cummings RD, Esko JD, *et al*., editors. Essentials of Glycobiology. 2nd edition. Cold Spring Harbor (NY): Cold Spring Harbor Laboratory Press. Chapter 1 (2009).

Varki A. Sialic acids as ligands in recognition phenomena. *FASEB J* 11(4), 248-255 (1997).

Veerababu G, Tang J, Hoffman RT, Daniels MC, Hebert LF, Crook ED, Cooksey RC, McClain DA. Overexpression of glutamine: fructose-6-phosphate amidotransferase in the liver of transgenic mice results in enhanced glycogen storage, hyperlipidemia, obesity, and impaired glucose tolerance. *Diabetes* 49(12), 2070-2078 (2000).

Vesce S, Bezzi P, Volterra A. Synaptic Transmission with the Glia. *News Physiol Sci* 16, 178-184 (2001).

Vimr E, Lichtensteiger C. To sialylate, or not to sialylate: that is the question. *Trends Microbiol* 10(6), 254-257 (2002).

Virkamäki A, Yki-Järvinen H. Allosteric regulation of glycogen synthase and hexokinase by glucosamine-6-phosphate during glucosamine-induced insulin resistance in skeletal muscle and heart. *Diabetes* 48(5), 1101-1107 (1999).

Vizi ES. Stimulation, by inhibition of (Na^+-K^+-Mg^{2+})-activated, ATP-ase, of acetylcholine release in cortical slices from rat brain. *J Physiol* 226, 95-117 (1972).

Vocadlo DJ, Hang HC, Kim EJ, Hanover JA, Bertozzi CR. A chemical approach for identifying *O*-GlcNAc-modified proteins in cells. *Proc Natl Acad Sci U S A* 100(16), 9116-9121 (2003).

Vogelsberg-Ragaglia V, Schuck T, Trojanowski JQ, Lee VM. PP2A mRNA expression is quantitatively decreased in Alzheimer's disease hippocampus. *Exp Neurol* 168(2), 402-412 (2001).

Vosseller K, Hansen KC, Chalkley RJ, Trinidad JC, Wells L, Hart GW, Burlingame AL. Quantitative analysis of both protein expression and serine / threonine post-translational modifications through stable isotope labeling with dithiothreitol. *Proteomics* 5(2), 388-398 (2005).

Vosseller K, Sakabe K, Wells L, Hart GW. Diverse regulation of protein function by *O*-GlcNAc: a nuclear and cytoplasmic carbohydrate post-translational modification. *Curr Opin Chem Biol* 6(6), 851-857 (2002a).

Vosseller K, Trinidad JC, Chalkley RJ, Specht CG, Thalhammer A, Lynn AJ, Snedecor JO, Guan S, Medzihradszky KF, Maltby DA, Schoepfer R, Burlingame AL. *O*-linked *N*-acetylglucosamine proteomics of postsynaptic density preparations using lectin weak affinity chromatography and mass spectrometry. *Mol Cell Proteomics* 5(5), 923-934 (2006).

Vosseller K, Wells L, Lane MD, Hart GW. Elevated nucleocytoplasmic glycosylation by *O*-GlcNAc results in insulin resistance associated with defects in Akt activation in 3T3-L1 adipocytes. *Proc Natl Acad Sci U S A* 99(8), 5313-5318 (2002b).

Vural H, Demirin H, Kara Y, Eren I, Delibas N. Alterations of plasma magnesium, copper, zinc, iron and selenium concentrations and some related erythrocyte antioxidant enzyme activities in patients with Alzheimer's disease. *J Trace Elem Med Biol* 24(3), 169-173 (2010).

Waagepetersen HS, Bakken IJ, Larsson OM, Sonnewald U, Schousboe A. Comparison of lactate and glucose metabolism in cultured neocortical neurons and astrocytes using ^{13}C-NMR spectroscopy. *Dev Neurosci* 20(4-5), 310-320 (1998).

Wadey AL, Muyderman H, Kwek PT, Sims NR. Mitochondrial glutathione uptake: characterization in isolated brain mitochondria and astrocytes in culture. *J Neurochem* 109 (Suppl 1), 101-108 (2009).

Wainio WW. Reactions of cytochrome oxidase. *J Biol Chem* 212(2), 723-33 (1955).

Walgren JLE, Vincent TS, Schey KL, Buse MG. High glucose and insulin promote *O*-GlcNAc modification of proteins, including α-tubulin. *Am J Physiol Endocrinol Metab* 284(2), E424-E434 (2003).

Walker DG, Khan HH. Some properties of galactokinase in developing rat liver. *Biochem J* 108(2), 169-175 (1968).

Wallace JC, Jitrapakdee S, Chapman-Smith A. Pyruvate carboxylase. *Int J Biochem Cell Biol* 30(1), 1-5 (1998).

Walz W, Mukerji S. Lactate release from cultured astrocytes and neurons: A comparison. *Glia* 1(6), 366–370 (1988).

Wang GL, Jiang BH, Rue EA, Semenza GL. Hypoxia-inducible factor 1 is a basic-helix-loop-helix-PAS heterodimer regulated by cellular O2 tension. *Proc Natl Acad Sci U S A* 92(12), 5510–5514 (1995).

Wang GL, Semenza GL. Desferrioxamine induces erythropoietin gene expression and hypoxia-inducible factor 1 DNA-binding activity: implications for models of hypoxia signal transduction. *Blood* 82(12), 3610-3615 (1993).

Wang XF, Cynader MS. Astrocytes provide cysteine to neurons by releasing glutathione. *J Neurochem* 74(4), 1434-42 (2000).

Wang Z, Udeshi ND, Slawson C, Compton PD, Sakabe K, Cheung WD, Shabanowitz J, Hunt DF, Hart GW. Extensive crosstalk between *O*-GlcNAcylation and phosphorylation regulates cytokinesis. *Sci Signal* 3(104), ra2 (2010).

Weckbecker G, Keppler DO. Dual role of hexose-1-phosphate uridylyltransferase in galactosamine metabolism. *Eur J Biochem* 128(1), 163-168 (1982).

Weigert C, Klopfer K, Kausch C, Brodbeck K, Stumvoll M, Häring HU, Schleicher ED. Palmitate-induced activation of the hexosamine pathway in human myotubes: increased expression of glutamine:fructose-6-phosphate aminotransferase. *Diabetes* 52(3), 650-656 (2003).

Weisdorf S, Hendrich K, Buchthal S, Wike J, Bratt G, Merkle H, Garwood M, Uğurbil K. Hepatic D-galactosamine toxicity studied with localized *in vivo* ^{31}P magnetic resonance spectroscopy in intact rats. *Magn Reson Med* 21(2), 178-190 (1991).

Wells L, Vosseller K, Cole RN, Cronshaw JM, Matunis MJ, Hart GW. Mapping sites of *O*-GlcNAc modification using affinity tags for serine and threonine post-translational modifications. *Mol Cell Proteomics* 1(10),791-804 (2002).

Wells L, Vosseller K, Hart GW. A role for *N*-acetylglucosamine as a nutrient sensor and mediator of insulin resistance. *Cell Mol Life Sci* 60(2), 222-228 (2003).

Wells L, Vosseller K, Hart GW. Glycosylation of nucleocytoplasmic proteins: signal transduction and *O*-GlcNAc. *Science* 291(5512), 2376-2378 (2001).

Westergaard N, Sonnewald U, Unsgård G, Peng L, Hertz L, Schousboe A. Uptake, release, and metabolism of citrate in neurons and astrocytes in primary cultures. *J Neurochem* 62(5), 1727-33 (1994).

Wice BM, Trugnan G, Pinto M, Rousset M, Chevalier G, Dussaulx E, Lacroix B, Zweibaum A. The intracellular accumulation of UDP-N-acetylhexosamines is concomitant with the inability of human colon cancer cells to differentiate. *J Biol Chem* 260(1), 139-146 (1985).

Willker W, Engelmann J, Brand A, Leibfritz D. Metabolite identification in cell extracts and culture media by proton-detected 2D-H, C-NMR spectroscopy. *J Magn Reson Anal* 2, 21-32 (1996).

Wilquet V, De Strooper B. Amyloid-beta precursor protein processing in neurodegeneration. *Curr Opin Neurobio*l 14(5), 582-588 (2004).

Wilson DB, Hogness DS. The Enzymes of the Galactose Operon in *Escherichia coli*. I. Purification and characterization of uridine diphosphogalactose 4-epimerase. *J Biol Chem* 239, 2469-2481 (1964).

Winchester B. Lysosomal metabolism of glycoproteins. *Glycobiology* 15(6), 1R-15R (2005).

Wishart DS, Knox C, Guo AC, Eisner R, Young N, Gautam B, Hau DD, Psychogios N, Dong E, Bouatra S, Mandal R, Sinelnikov I, Xia J, Jia L, Cruz JA, Lim E, Sobsey CA, Shrivastava S, Huang P, Liu P, Fang L, Peng J, Fradette R, Cheng D, Tzur D, Clements M, Lewis A, De Souza A, Zuniga A, Dawe M, Xiong Y, Clive D, Greiner R, Nazyrova A, Shaykhutdinov R, Li L, Vogel HJ, Forsythe I. HMDB: a knowledgebase for the human metabolome. *Nucleic Acids Res* 37(Database issue), D603-610 (2009).

Wlodek D, Gonzales M. Decreased energy levels can cause and sustain obesity. *J Theor Biol* 225(1), 33-44 (2003).

Wolfe MS. Secretase as a target for Alzheimer's disease. *Curr Top Med Chem* 2(4), 371-383 (2002).

Wolfgang MJ, Lane MD. Control of energy homeostasis: role of enzymes and intermediates of fatty acid metabolism in the central nervous system. *Annu Rev Nutr* 26, 23-44 (2006).

Wu DC, Jackson-Lewis V, Vila M, Tieu K, Teismann P, Vadseth C, Choi DK, Ischiropoulos H, Przedborski S. Blockade of microglial activation is neuroprotective in the 1-methyl-4-phenyl-1,2,3,6-tetrahydropyridine mouse model of Parkinson disease. *J Neurosci* 22(5), 1763-1771 (2002).

Xu WL, von Strauss E, Qiu CX, Winblad B, Fratiglioni L. Uncontrolled diabetes increases the risk of Alzheimer's disease: a population-based cohort study. *Diabetologia* 52(6), 1031-1039 (2009).

Yamamoto H, Matsumoto K, Araki E, Miyamoto E. New aspects of neurotransmitter release and exocytosis: involvement of Ca^{2+}/calmodulin-dependent phosphorylation of synapsin I in insulin exocytosis. *J Pharmacol Sci* 93(1), 30-34 (2003).

Yang WH, Kim JE, Nam HW, Ju JW, Kim HS, Kim YS, Cho JW. Modification of p53 with *O*-linked *N*-acetylglucosamine regulates p53 activity and stability. *Nat Cell Biol* 8(10), 1074-1083 (2006).

Yang X, Ongusaha PP, Miles PD, Havstad JC, Zhang F, So WV, Kudlow JE, Michell RH, Olefsky JM, Field SJ, Evans RM. Phosphoinositide signalling links *O*-GlcNAc transferase to insulin resistance. *Nature* 451(7181), 964-969 (2008).

Yankner BA, Duffy LK, Kirschner DA. Neurotrophic and neurotoxic effects of amyloid beta protein: reversal by tachykinin neuropeptides. *Science* 250(4978), 279-282 (1990).

Yao J, Irwin RW, Zhao L, Nilsen J, Hamilton RT, Brinton RD. Mitochondrial bioenergetic deficit precedes Alzheimer's pathology in female mouse model of Alzheimer's disease. Proc Natl Acad Sci U S A 106(34), 14670-14675 (2009).

Yao PJ, Coleman PD. Reduction of *O*-linked *N*-acetylglucosamine-modified assembly protein-3 in Alzheimer's disease. *J Neurosci* 18(7), 2399-2411 (1998).

Yarian CS, Toroser D, Sohal RS. Aconitase is the main functional target of aging in the citric acid cycle of kidney mitochondria from mice. *Mech Ageing Dev* 127(1), 79-84 (2006).

Yatin SM, Varadarajan S, Butterfield DA. Vitamin E Prevents Alzheimer's Amyloid beta-Peptide (1-42)-Induced Neuronal Protein Oxidation and Reactive Oxygen Species Production. *J Alzheimers Dis* 2(2), 123-131 (2000).

Yi W, Clark PM, Mason DE, Keenan MC, Hill C, Goddard WA 3rd, Peters EC, Driggers EM, Hsieh-Wilson LC. Phosphofructokinase 1 glycosylation regulates cell growth and metabolism. *Science* 337(6097), 975-980 (2012).

Yki-Järvinen H, Daniels MC, Virkamäki A, Mäkimattila S, DeFronzo RA, McClain D. Increased glutamine:fructose-6-phosphate amidotransferase activity in skeletal muscle of patients with NIDDM. *Diabetes* 45(3), 302-307 (1996).

Yki-Järvinen H, Virkamäki A, Daniels MC, McClain D, Gottschalk WK. Insulin and glucosamine infusions increase *O*-linked *N*-acetyl-glucosamine in skeletal muscle proteins *in vivo*. Metabolism 47(4), 449-455 (1998).

Yodoya E, Wada M, Shimada A, Katsukawa H, Okada N, Yamamoto A, Ganapathy V, Fujita T. Functional and molecular identification of sodium-coupled dicarboxylate transporters in rat primary cultured cerebrocortical astrocytes and neurons. *J Neurochem* 97(1), 162-73 (2006).

Yogeeswaran G, Salk PL. Metastatic potential is positively correlated with cell surface sialylation of cultured murine tumor cell lines. *Science* 212(4502), 1514-1516 (1981).

Younkin SG. The role of Aß42 in Alzheimer's disease. *J Physiol Paris* 92(3-4), 289-292 (1998).

Yousefi S, Higgins E, Daoling Z, Pollex-Krüger A, Hindsgaul O, Dennis JW. Increased UDP-GlcNAc:Gal beta 1-3GaLNAc-R (GlcNAc to GaLNAc) beta-1, 6-N-acetylglucosaminyltransferase activity in metastatic murine tumor cell lines. Control of polylactosamine synthesis. *J Biol Chem* 266(3), 1772-1782 (1991).

Yu C, Nwabuisi-Heath E, Laxton K, Ladu MJ. Endocytic pathways mediating oligomeric Aß42 neurotoxicity. Mol Neurodegener 5(1), article 19 (2010).

Yurchenco PD, Atkinson PH. Equilibration of fucosyl glycoprotein pools in HeLa cells. *Biochemistry* 16(5), 944-953 (1977).

Zachara NE, Hart GW. *O*-GlcNAc a sensor of cellular state: the role of nucleocytoplasmic glycosylation in modulating cellular function in response to nutrition and stress. *Biochim Biophys Acta* 1673(1-2), 13-28 (2004).

Zachara NE, O'Donnell N, Cheung WD, Mercer JJ, Marth JD, Hart GW. Dynamic *O*-GlcNAc modification of nucleocytoplasmic proteins in response to stress. A survival response of mammalian cells. *J Biol Chem* 279(29), 30133-30142 (2004).

Zamzami N, Marchetti P, Castedo M, Zanin C, Vayssière JL, Petit PX, Kroemer G. Reduction in mitochondrial potential constitutes an early irreversible step of programmed lymphocyte death in vivo. *J Exp Med* 181(5), 1661-1672 (1995).

Zapata G, Vann WF, Aaronson W, Lewis MS, Moos M. Sequence of the cloned Escherichia coli K1 CMP-N-acetylneuraminic acid synthetase gene. *J Biol Chem* 264(25),14769-14774 (1989).

Zeng G, Nystrom FH, Ravichandran LV, Cong LN, Kirby M, Mostowski H, Quon MJ. Roles for insulin receptor, PI3-kinase, and Akt in insulin-signaling pathways related to production of nitric oxide in human vascular endothelial cells. *Circulation* 101(13), 1539-1545 (2000).

Zhang J, Dawson VL, Dawson TM, Snyder SH. Nitric oxide activation of poly(ADP-ribose) synthetase in neurotoxicity. *Science* 263(5147), 687-689 (1994).

Zhivkov V, Tosheva R, Zhivkova Y. Concentration of uridine diphosphate sugars in various tissues of vertebrates. *Comp Biochem Physiol B* 51(4), 421-4 (1975).

Zhou L, Zhu DY. Neuronal nitric oxide synthase: structure, subcellular localization, regulation, and clinical implications. *Nitric Oxide* 20(4), 223-30 (2009).

Zhu W, Leber B, Andrews DW. Cytoplasmic *O*-glycosylation prevents cell surface transport of E-cadherin during apoptosis. *EMBO J* 20(21), 5999-6007 (2001).

Zhu Y, Carvey PM, Ling Z. Age-related changes in glutathione and glutathione-related enzymes in rat brain. *Brain Res* 1090(1), 35-44 (2006).

Zou L, Zhu-Mauldin X, Marchase RB, Paterson AJ, Liu J, Yang Q, Chatham JC. Glucose deprivation-induced increase in protein *O*-GlcNAcylation in cardiomyocytes is calcium-dependent. *J Biol Chem* 287(41), 34419-34431 (2012).

Zou M, Martin C, Ullrich V. Tyrosine nitration as a mechanism of selective inactivation of prostacyclin synthase by peroxynitrite. *Biol Chem* 378(7), 707-713 (1997).

Zwingmann C, Leibfritz D. Regulation of glial metabolism studied by ^{13}C-NMR. *NMR Biomed* 16(6-7), 370-99 (2003).

7 Appendix

7.1 Chemical Structures of Activated Sugar Nucleotides

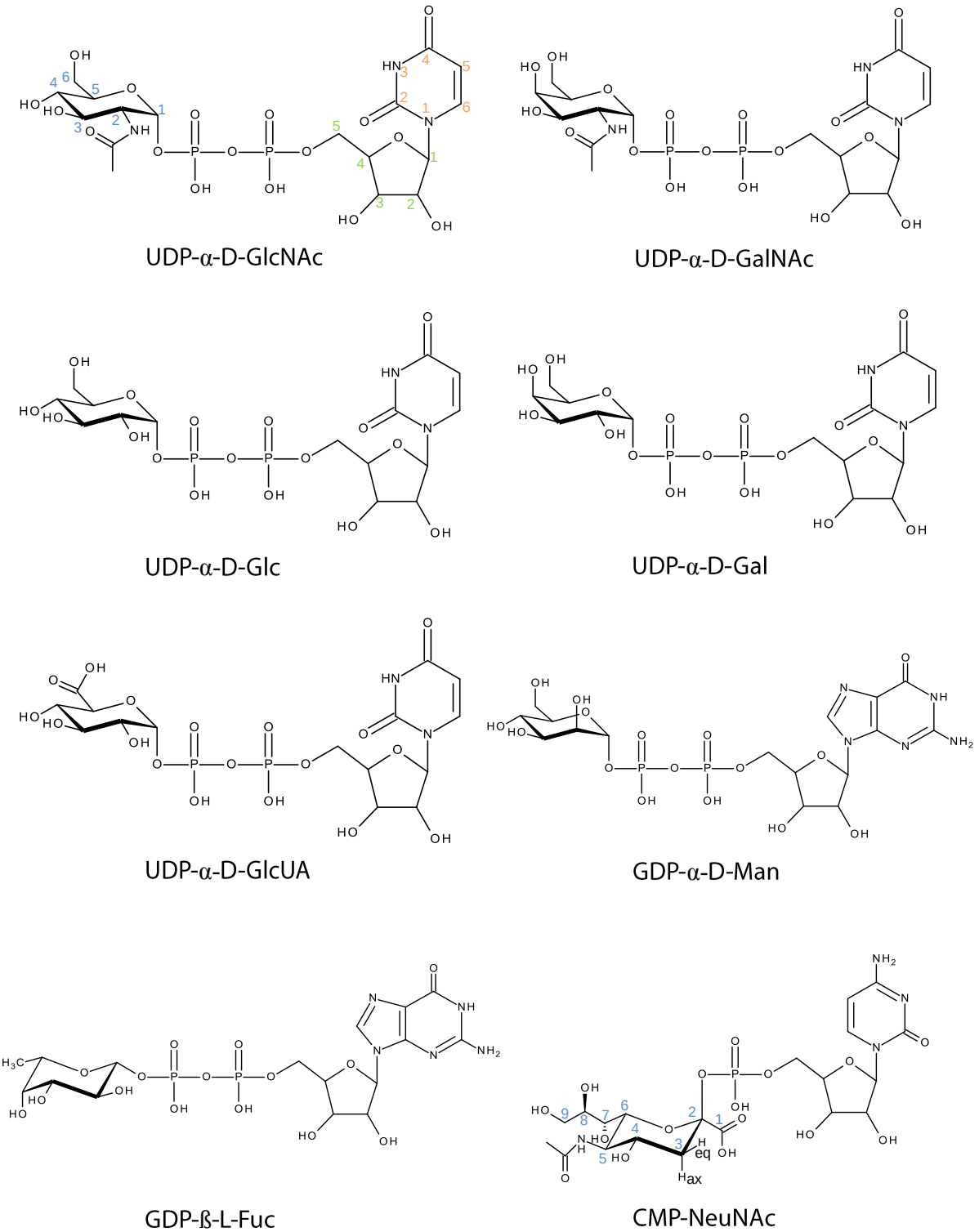

Figure 54. Chemical structures of uridine diphosphate-α-D-*N*-acetylglucosamine (UDP-α-D-GlcNAc), uridine diphosphate-α-D-*N*-acetylgalactosamine (UDP-α-D-GalNAc), uridine diphosphate-α-D-*N*-acetylglucose (UDP-α-D-Glc), uridine diphosphate-α-D-*N*-acetylgalactose (UDP-α-D-Gal), uridine diphosphate-α-D-glucuronic acid (UDP-α-D-GlcUA), guanosine diphosphate-α-D-mannose (GDP-α-D-Man), guanosine diphosphate-ß-L-fucose (GDP-ß-L-Fucose), and cytidine monophosphate-*N*-acetyl neuraminic acid (CMP-NeuNAc) with exemplary numbering of the pyranose (blue), ribose (green), and uracil (orange) moiety.

7.2 Proton and Carbon Chemical Shift and Coupling Constants of Metabolites Detected in M/C Cell Extracts and Culture Media

Table 9. Selected proton (^{1}H) and carbon (^{13}C) chemical shifts (δ) and coupling constants (J) of metabolites and compounds used in this thesis for signal assignment and quantification. The values have been obtained from ^{1}H- or 2D-^{1}H,^{13}C-HSQC-NMR spectra. All metabolites were measured in 100 mM Na-phosphate buffer (pH 7) in D_2O at 298 K. Signals were referenced to TSP as internal reference.

Metabolite	δ (ppm) ^{13}C	δ (ppm) ^{1}H	J (Hz); Multiplicity
Acetate			
C2/ H2	26,11	1,92	
Alanine (Ala)			
C3/H3	18,96	1,49	
Aspartate (Asp)			
C3/H3	39,48	2,82	
C3/H3'		2,71	
Citrate	48,41	2,69	
		2,55	
CMP-NeuNAc			
H3(ax)		1,66	J = 5,7, 11,68, 12,91 (ddd)
L-Fucose			
H1(α)		4,56	$^{3}J_{H1,H2}$ = 7,97 (d)
H1(ß)		5,21	$^{3}J_{H1,H2}$ = 3,91 (d)
Gal-1-P			
H1(α)		5,50	$^{3}J_{H1,H2}$ = 3,68; $^{3}J_{H1,P}$ = 7,43 (dd)
Gal-2-P			
H1(α)		5,37	$^{3}J_{H1,H2}$ = 3,95 (d)
H2		4,20	J = 3,80 (dd)
Gal-1,2-cyclo-P			
H1(α)		5,87	$^{3}J_{H1,H2}$ = 4,89 (d)
GalN-1-P			
H1(α)		5,69	$^{3}J_{H1,H2}$ = 3,46; $^{3}J_{H1,P}$ = 7,31 (dd)
GDP-ß-L-fucose			
H1(ß)		4,92	$^{3}J_{H1,H2}$ = $^{3}J_{H1,P}$ = 8,14 (dd/t)
H3 ribose		4,54	n.d. (m)
GDP-α-D-Mannose		5,52	$^{3}J_{H1,H2}$ = 1,57; $^{3}J_{H1,P}$ = 7,83 (dd)
H1(α)			
Glc-1-P			
H1(α)		5,46	$^{3}J_{H1,H2}$ = 3,51; $^{3}J_{H1,P}$ = 7,35 (dd)
Glc-2-P			
H1(α)		5,34	$^{3}J_{H1,H2}$ = 3,65 (d)
Glc-1,2-cyclo-P			
H1(α)		5,82	$^{3}J_{H1,H2}$ = 4,85; $^{3}J_{H1,P}$ = 2,05 (dd)

Metabolite	δ (ppm) ^{13}C	^{1}H	J (Hz); Multiplicity
GlcUA-2-P			
H1(α)		5,36	$^{3}J_{H1,H2}$ = 3,43 (d)
GlcUA-1,2-cyclo-P			
H(α)		5,83	n.d. (dd)
Glucose			
H1(α)		5,24	$^{3}J_{H1,H2}$ = 3,74 (d)
H1(ß)		4,65	$^{3}J_{H1,H2}$ = 7,93 (d)
Glutamate (Glu)			
C3/H3	29,77	2,07	
C4/H4	36,21	2,35	
Glutamine (Gln)			
C3/H3	29,08	2,17	
C4/H4	33,71	2,46	
Lactate			
H2(CH)	71,15	4,12	
H3(CH_3)	22,91	1,33	
NeuNAc			
H3(ax)		1,83	$^{3}J_{H3ax,H4}$ = 12,18 (t)
UDP-α-D-Gal			
H1(α)		5,65	$^{3}J_{H1,H2}$ = 3,62; $^{3}J_{H1,P}$ = 7,21 (dd)
UDP- α-D-GalNAc			
C1/H1(α)	97,73	5,55	$^{3}J_{H1,H2}$ = 3,43; $^{3}J_{H1,P}$ = 7,23 (dd)
N-Ac	25,22	2,09	
UDP-α-D Glc			
H1(α)		5,61	$^{3}J_{H1,H2}$ = 3,54 ; $^{3}J_{H1,P}$ = 7,26 (dd)
UDP-α-D-GlcNAc			
C1/H1(α)	97,61	5,52	$^{3}J_{H1,H2}$ = 3,26; $^{3}J_{H1,P}$ = 7,31 (dd)
N-Ac	25,21	2,08	
C1/H1 ribose	91,27	5,99	
C6/H6 uracil	105,35	5,98	
UDP-α-D-GlcUA			
H1(α)		5,63	$^{3}J_{H1,H2}$ = 3,36; $^{3}J_{H1,P}$ = 7,59 (dd)

7.3 ^{1}H-NMR spectra of UDP-GlcUA, GDP-Man, CMP-NeuNAc, and GDP- FUC after M/C and PCA extraction

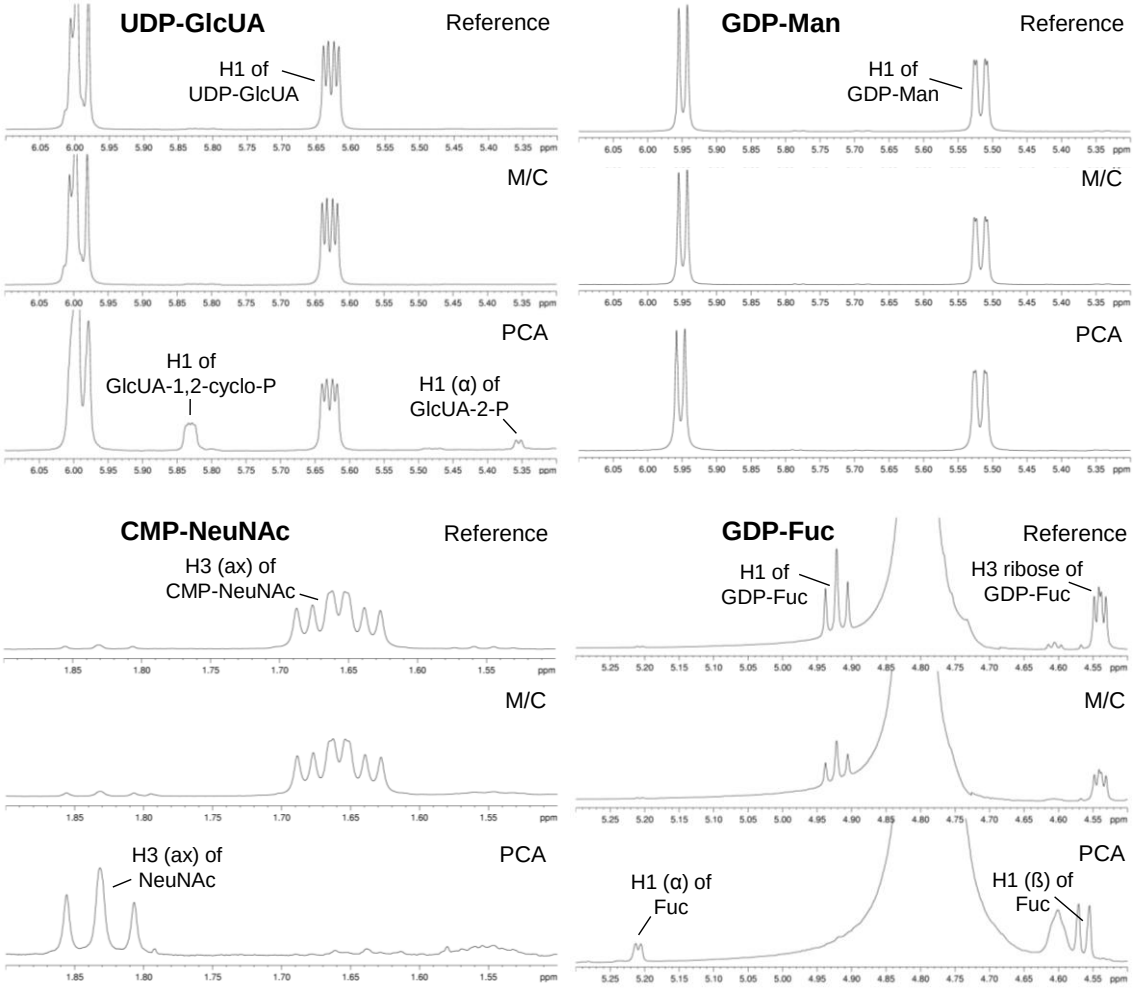

Figure 55. ^{1}H-NMR spectra of the pure compounds UDP-GlcUA, GDP-Man, CMP-NeuNAc, and GDP-Fuc. The expanded regions of the spectra show the signals of the anomeric protons (H1) of UDP-GlcUA, GDP-Man, and GDP-Fuc and the signal of the H3 of CMP-NeuNAc, respectively, in reference spectra and after treatment with M/C or PCA. In the case of UDP-GlcUA, CMP-NeuNAc, and GDP-Fuc the signals of the decomposition products after PCA treatment are assigned. GDP-Man is stable against PCA treatment. CMP-NeuNAc, cytidine 5-monophosphate-*N*-acetylneuraminic acid; Fuc, fucose; GDP-Fuc, guanosine diphosphate-fucose; GDP-Man, guanosine diphosphate-mannose; GlcUA-1,2-cyclo-P, glucuronic acid-1,2-cyclo-phosphate; GlcUA-2-P, glucuronic acid-2-phosphate; NeuNAc, *N*-acetylneuraminic acid; UDP-GlcUA, uridine diphosphate-glucoronic acid.

7.4 Nitric Oxide: Alterations in mRNA Expression of Enzymes of the HBP

The effect of NO on the mRNA expression of genes of the HBP was tested in primary cortical astrocytes by qRT-PCR. Higher mRNA levels of all genes tested in astrocytes treated with the NO-donor DETA-NONOate (0,8 mM) for 12 h were detected compared to untreated controls. However, these results are not conclusive and have to be repeated for validity, but may give a hint that overexpression of the genes of the HBP might contribute to the maintenance of the

UDP-GlcNAc level in astrocytes coping with nitrous stress. It is therefore of interest to further investigate in future studies the effect of NO on genes of the HBP.

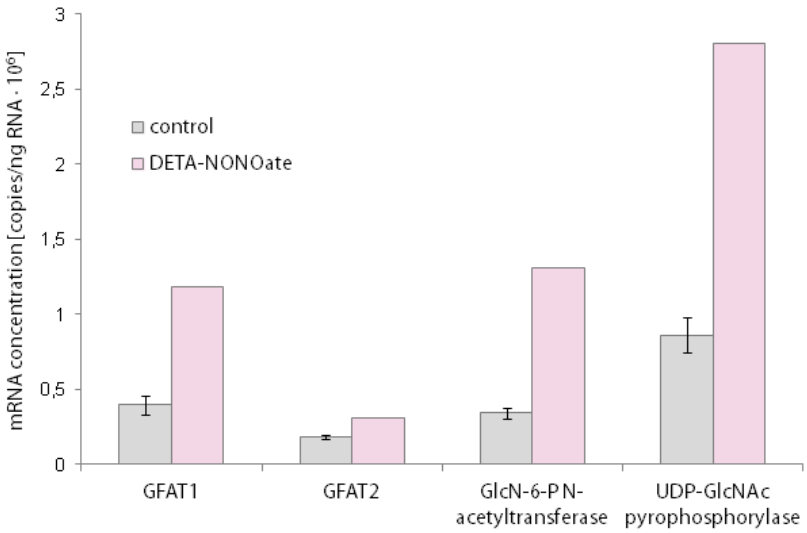

Figure 56. mRNA expression levels of the enzymes of the HBP obtained by qRT-PCR in astrocytes after treatment with 0,8 mM DETA-NONOate (n = 1) for 12 h compared to untreated controls (n = 3). Values are mean ± standard deviation for controls. DETA-NONOate, (Z)-1-[N-(2-aminoethyl)-N-(2-ammonioethyl)amino] diazen-1-ium-1,2-diolate; GFAT, *Glutamine-fructose-6-P aminotransferase*; GlcN, glucosamine; UDP-GlcNAc, uridine diphosphate-*N*-acetylglucosamine.

7.5 Pulse Programs

^{1}H- NMR Spectra (zg)

```
;zg
;avance-version (06/11/09)
;1D sequence
;
;$CLASS=HighRes
;$DIM=1D
;$TYPE=
;$SUBTYPE=
;$COMMENT=


#include <Avance.incl>


"acqt0=-p1*2/3.1416"


1 ze
2 30m
```

```
  d1
  p1 ph1
  go=2 ph31
  30m mc #0 to 2 F0(zd)
exit


ph1=0 2 2 0 1 3 3 1
ph31=0 2 2 0 1 3 3 1


;pl1 : f1 channel - power level for pulse (default)
;p1 : f1 channel -  high power pulse
;d1 : relaxation delay; 1-5 * T1
;NS: 1 * n, total number of scans: NS * TD0



;$Id: zg,v 1.10 2009/07/02 16:40:47 ber Exp $
```

^{1}H-NMR Spectra (30°-Pulse; zg 30)

```
;zg30
;avance-version (10/02/09)
;1D sequence
;using 30 degree flip angle
;
;$CLASS=HighRes
;$DIM=1D
;$TYPE=
;$SUBTYPE=
;$COMMENT=
;$RECOMMEND=y


#include <Avance.incl>


"acqt0=-p1*0.66/3.1416"


1 ze
2 30m
  d1
  p1*0.33 ph1
  go=2 ph31
  30m mc #0 to 2 F0(zd)
exit


ph1=0 2 2 0 1 3 3 1
```

```
ph31=0 2 2 0 1 3 3 1


;pl1 : f1 channel - power level for pulse (default)
;p1 : f1 channel -  90 degree high power pulse
;d1 : relaxation delay; 1-5 * T1
;NS: 1 * n, total number of scans: NS * TD0



;$Id: zg30,v 1.11 2010/02/10 16:23:03 ber Exp $
```

1D $^{1}H,^{13}C$-HSQC-NMR Spectra (hsqcgpnd1d)

```
;hsqcgpnd1d
;avance-version (11/02/24)
;HSQC
;1D H-1/X correlation via double inept transfer
;using gradient pulses for selection
;use as setup for pulseprogram 'invigptp'
;
;$CLASS=HighRes
;$DIM=1D
;$TYPE=
;$SUBTYPE=
;$COMMENT=


#include <Avance.incl>
#include <Grad.incl>
#include <Delay.incl>


"p2=p1*2"
"p4=p3*2"
"d4=1s/(cnst2*4)"


"DELTA1=p16+d16"
"DELTA2=d4-p16-d16-de+p1*2/PI-8u"
```

```
"acqt0=0"
baseopt_echo


1 ze
2 30m
  d1
  (p1 ph1)
  d4
  (center (p2 ph2) (p4 ph6):f2 )
  d4
  (p1 ph3) (p3 ph7):f2
  DELTA1 UNBLKGRAD
  (p4 ph8):f2
  4u
  p16:gp1
  d16
  (p3 ph9):f2
  4u
  p16:gp2
  d16
  (p3 ph10):f2
  4u
  (p2 ph4)
  4u
  (ralign (p1 ph3) (p3 ph11):f2 )
  d4
  (center (p2 ph5) (p4 ph12):f2 )
  4u
  p16:gp3
  d16
  DELTA2
  4u BLKGRAD
  go=2 ph31
```

```
  30m mc #0 to 2 F0(zd)
exit


ph1=0
ph2=0
ph3=1
ph4=0 0 2 2
ph5=0
ph6=0
ph7=1 1 1 1 3 3 3 3
ph8=0
ph9=3
ph10=0
ph11=0 2
ph12=0
ph31=0 2 0 2 2 0 2 0



;pl1 : f1 channel - power level for pulse (default)
;pl2 : f2 channel - power level for pulse (default)
;p1 : f1 channel -  90 degree high power pulse
;p2 : f1 channel - 180 degree high power pulse
;p3 : f2 channel -  90 degree high power pulse
;p4 : f2 channel - 180 degree high power pulse
;p16: homospoil/gradient pulse
;d1 : relaxation delay; 1-5 * T1
;d4 : 1/(4J)XH
;d16: delay for homospoil/gradient recovery
;cnst2: = J(XH)
;NS: 1 * n, total number of scans: NS * TD0
;DS: 16

;use gradient ratio:      gp 1 : gp 2 : gp 3
;                           80 :   30 : 20.1    for C-13
```

; 80 : 30 : 8.1 for N-15

;for z-only gradients:
;gpz1: 80%
;gpz2: 30%
;gpz3: 20.1% for C-13, 8.1% for N-15

;use gradient files:
;gpnam1: SMSQ10.100
;gpnam2: SMSQ10.100
;gpnam3: SMSQ10.100

;$Id: hsqcgpnd1d,v 1.3.4.1 2011/02/24 17:26:41 ber Exp $

2D $^{1}H,^{13}C$-HSQC-NMR Spectra (hsqcedetgpsisp2.2)

```
;hsqcedetgpsisp2.2
;avance-version (11/02/24)
;HSQC
;2D H-1/X correlation via double inept transfer
;   using sensitivity improvement
;phase sensitive using Echo/Antiecho-TPPI gradient selection
;with decoupling during acquisition
;using trim pulses in inept transfer
;with multiplicity editing during selection step
;using shaped pulses for all 180degree pulses on f2 - channel
;with gradients in back-inept
;
;A.G. Palmer III, J. Cavanagh, P.E. Wright & M. Rance, J. Magn.
;   Reson. 93, 151-170 (1991)
;L.E. Kay, P. Keifer & T. Saarinen, J. Am. Chem. Soc. 114,
;   10663-5 (1992)
;J. Schleucher, M. Schwendinger, M. Sattler, P. Schmidt, O. Schedletzky,
;   S.J. Glaser, O.W. Sorensen & C. Griesinger, J. Biomol. NMR 4,
;   301-306 (1994)
;W. Willker, D. Leibfritz, R. Kerssebaum & W. Bermel, Magn. Reson.
;   Chem. 31, 287-292 (1993)
;
;$CLASS=HighRes
;$DIM=2D
;$TYPE=
;$SUBTYPE=
;$COMMENT=
```

```
#include <Avance.incl>
#include <Grad.incl>
#include <Delay.incl>


"p2=p1*2"
"d4=1s/(cnst2*4)"
"d11=30m"


"d0=3u"

"in0=inf1/2"


"DELTA=d21-cnst17*p24/2-p16-d16-p2-d0*2"
"DELTA1=p16+d16-p1*0.78+de+8u"
"DELTA2=d4-larger(p2,p14)/2"
"DELTA3=d24-cnst17*p24/2-p19-d16"
"DELTA4=d4-larger(p2,p14)/2-p16-d16"
"DELTA5=d21-cnst17*p24/2"


"acqt0=0"
baseopt_echo


1 ze
  d11 pl12:f2
2 d1 do:f2
3 (p1 ph1)
  DELTA2 pl0:f2
  4u
  (center (p2 ph1) (p14:sp3 ph6):f2 )
  4u
  DELTA2 pl2:f2 UNBLKGRAD
  p28 ph1
  4u
  (p1 ph2) (p3 ph3):f2
  d0
  (p2 ph7)
  d0
  p16:gp1*EA
  d16
  DELTA
  4u
  (center (p2 ph1) (p24:sp7 ph4):f2 )
  4u
  DELTA5 pl2:f2
  (center (p1 ph1) (p3 ph4):f2 )
```

```
 p19:gp3
 d16
 DELTA3
 (center (p2 ph1) (p24:sp7 ph1):f2 )
 DELTA3
 p19:gp3
 d16 pl2:f2
 (center (p1 ph2) (p3 ph5):f2 )
 p16:gp4
 d16
 DELTA4 pl0:f2
 (center (p2 ph1) (p14:sp3 ph1):f2 )
 DELTA4
 p16:gp4
 d16
 (p1 ph1)
 DELTA1
 (p2 ph1)
 4u
 p16:gp2
 d16 pl12:f2
 4u BLKGRAD
 go=2 ph31 cpd2:f2
 d1 do:f2 mc #0 to 2
   F1EA(calgrad(EA) & calph(ph5, +180), caldel(d0, +in0) & calph(ph3, +180) & calph(ph6,
+180) & calph(ph31, +180))
exit


ph1=0
ph2=1
ph3=0 2
ph4=0 0 2 2
ph5=1 1 3 3
ph6=0
ph7=0 0 2 2
ph31=2 0 0 2


;pl0 : 0W
;pl1 : f1 channel - power level for pulse (default)
;pl2 : f2 channel - power level for pulse (default)
;pl12: f2 channel - power level for CPD/BB decoupling
;sp3: f2 channel - shaped pulse (180degree inversion)
;spnam3: Crp60,0.5,20.1
;sp7: f2 channel - shaped pulse (180degree refocussing)
;spnam7: Crp60comp.4
;p1 : f1 channel -  90 degree high power pulse
;p2 : f1 channel - 180 degree high power pulse
;p3 : f2 channel -  90 degree high power pulse
;p14: f2 channel - 180 degree shaped pulse for inversion
;     = 500usec for Crp60,0.5,20.1
```

```
;p16: homospoil/gradient pulse
;p19: gradient pulse 2                          [500 usec]
;p24: f2 channel - 180 degree shaped pulse for refocussing
;     = 2msec for Crp60comp.4
;p28: f1 channel - trim pulse
;d0 : incremented delay (2D)                    [3 usec]
;d1 : relaxation delay; 1-5 * T1
;d4 : 1/(4J)XH
;d11: delay for disk I/O                        [30 msec]
;d16: delay for homospoil/gradient recovery
;d21: set d21 according to multiplicity selection
;       1/(2J(XH))  XH, XH3 positive, XH2 negative
;d24: 1/(8J)XH for all multiplicities
;     1/(4J)XH for XH
;cnst2: = J(XH)
;cnst17: = -0.5 for Crp60comp.4
;inf1: 1/SW(X) = 2 * DW(X)
;in0: 1/(2 * SW(X)) = DW(X)
;nd0: 2
;NS: 1 * n
;DS: >= 16
;td1: number of experiments
;FnMODE: echo-antiecho
;cpd2: decoupling according to sequence defined by cpdprg2
;pcpd2: f2 channel - 90 degree pulse for decoupling sequence


;use gradient ratio:     gp 1 : gp 2 : gp 3 : gp 4
;                          80 : 20.1 :   11 :   -5    for C-13
;                          80 :  8.1 :   11 :   -5    for N-15

;for z-only gradients:
;gpz1: 80%
;gpz2: 20.1% for C-13, 8.1% for N-15
;gpz3: 11%
;gpz4: -5%

;use gradient files:
;gpnam1: SMSQ10.100
;gpnam2: SMSQ10.100
;gpnam3: SMSQ10.100
;gpnam4: SMSQ10.100


;cnst17: Factor to compensate for coupling evolution during a pulse
;       (usually +1). A positive factor indicates that coupling
;       evolution continues during the pulse, whereas a negative
;       factor is necessary if the coupling is (partially) refocussed.



;$Id: hsqcedetgpsisp2.2,v 1.8.2.1 2011/02/24 17:26:39 ber Exp $
```

^{31}P-decoupled ^{1}H-NMR Spectra (zgig)

```
;zgig
;avance-version (07/04/03)
;1D sequence with inverse gated decoupling
;
;$CLASS=HighRes
;$DIM=1D
;$TYPE=
;$SUBTYPE=
;$COMMENT=


#include <Avance.incl>


"d11=30m"


"acqt0=-p1*2/3.1416"


1 ze
  d11 pl12:f2
2 30m do:f2
  d1
  p1 ph1
  go=2 ph31 cpd2:f2
  30m do:f2 mc #0 to 2 F0(zd)
exit


ph1=0 2 2 0 1 3 3 1
ph31=0 2 2 0 1 3 3 1


;pl1 : f1 channel - power level for pulse (default)
;pl12: f2 channel - power level for CPD/BB decoupling
;p1 : f1 channel -  high power pulse
;d1 : relaxation delay; 1-5 * T1
;d11: delay for disk I/O                  [30 msec]
;NS: 1 * n, total number of scans: NS * TD0
;cpd2: decoupling according to sequence defined by cpdprg2
;pcpd2: f2 channel - 90 degree pulse for decoupling sequence



;$Id: zgig,v 1.10 2009/07/02 16:40:47 ber Exp $
```

7.6 List of Chemicals and Materials

7.6.1 Chemicals

Table 10. List of chemicals used in alphabetical order.

Chemical	Description	Manufacturer
[1-^{13}C]glucose	D-Glucose (1-^{13}C, 98-99 %)	Cambridge Isotope laboratories, Inc.
Amyloid-ß Protein (25-35)	Trifluoroacetate salt	Bachem
Antibiotic-Antimicotic	100x	Invitrogen
Chloroform	pro analysi (p.a.)	Fluka
CMP-NeuNAc	Cytidine-5′-monophospho-ß-sialic acid disodium salt	Calbiochem
D_2O	Deuterium oxide 100% (99,97% D)	Euriso-top
DEPC		
DETA-NONOate	(Z)-1-[N-(2-aminoethyl)-N-(2-ammonioethyl)amino]diazen-1-ium-1,2-diolate (≥ 97 %)	Enzo Life Sciences
DMSO	Dimethyl sulfoxide	Serva
EDTA	Ethylenediaminetetraacetic acid tetrasodium tetrahydrate salt	Merck
FCS	Fetal Calf Serum	Biochrom AG
Galactosamine	D-(+)-Galactosamine hydrochloride (≥ 99 %)	Fluka
Galactose	D(+)-Galactose for microbiology (≥ 99 %)	Fluka
GDP-Fuc	Guanosine 5′-diphospho-β-L-fucose sodium salt (≥ 85 %)	Sigma-Aldrich
GDP-Man	Guanosine 5′-diphospho-D-mannose sodium salt (≥ 97 %)	Sigma-Aldrich
Glucosamine	D-(+)-Glucosamine hydrochloride (≥ 99 %)	Fluka
Glucose	D-(+)-Glucose; anhydrous	Merck
K_2HPO_4	Dipotassium phosphate	Sigma
KOH	Potassium hydroxide pellets, anhydrous	Merck
L-Glutamine		Merck
Mannosamine	D-Mannosamine hydrochloride (≥ 98,0 %)	Fluka
Methanol	p.a.	Roth
$Na_2HPO_4 \cdot 2\ H_2O$	Disodium hydrogen phosphate dihydrate; p.a. (≥ 99 %)	Merck
$NaH_2PO_4 \cdot 2\ H_2O$	Sodium dihydrogen phosphate dihydrate; p.a. (≥ 99,5 %)	Merck
$NaH_2PO_4 \cdot H_2O$	Sodium dihydrogen phosphate monohydrate; p.a.	Merck
Nucleic Acid Purification Lysis Solution	2x	Applied Biosystems
PCA	Perchloric acid; p.a. (70 - 72 %)	Fluka
Penicillin-Streptomycin Solution	100x; 10,000 units/mL of penicillin and 10,000 µg/mL of streptomycin	PAA

Chemical	Description	Manufacturer
Poly-L-ornithine	Poly-L-ornithine hydrobromide	Sigma-Aldrich
RNA Elution Solution		Applied Biosystems
RNA Purification Wash solution 1		Applied Biosystems
RNA Purification Wash solution 2		Applied Biosystems
Sodium pyruvate solution	100 mM	PAA
Sulfo-NONOate	(E)-1-sulfonatodiazen-1-ium-1,2-diolate disodium salt (≥ 90 %)	Enzo Life Sciences
Trypan blue	0,4 % solution	Gibco®
Trypsin-EDTA	1:250; 1x	PAA
TSP	3-(trimethylsilyl)propionic-2,2,3,3-d4 acid (98 % D)	Cambridge Isotope laboratories, Inc.
UDP-Gal	Uridine 5′-diphosphogalactose disodium salt	Calbiochem
UDP-GalNAc	Uridine 5′-diphospho-*N*-acetylgalactosamine disodium salt (≥ 98 %)	Sigma
UDP-Glc	Uridine 5′-diphosphoglucose disodium salt hydrate (≥ 98 %)	Sigma
UDP-GlcNAc	Uridine 5′-diphospho-*N*-acetylglucosamine sodium salt (≥ 98 %)	Sigma
UDP-GlcUA	Uridine 5′-diphosphoglucuronic acid trisodium salt (98 - 100 %)	Sigma-Aldrich
$ZnCl_2$	Zink chloride	Merck

7.6.2 Buffers and Solutions

Table 11. Buffer recipes.

Description	Composition
10x PBS (pH 7,4)	2,6 g $NaH_2PO_4 \cdot H_2O$ 14,4 g $Na_2HPO_4 \cdot 2\ H_2O$ 88 g NaCl were dissolved in 1 L H_2O and sterilized by autoclaving; pH adjustment was not necessary after dilution to 1x PBS
PBS + 1mM EDTA	37,22 mg EDTA disodium salt dihydrate were dissolved in 100 mL PBS. The solution was sterile filtered before use.
100 mM Sodium-phosphate buffer (pH 7) in D_2O	2.949 g $NaH_2PO_4 \cdot 2\ H_2O$ 5.518 g $Na_2HPO_4 \cdot 2\ H_2O$ were dissolved in 500 mL water
DEPC-treated water	0,1% DEPC (v/v) was dissolved in H_2O and sterilized by autoclaving

7.6.3 Cell Culture Media

Table 12. Cell culture media used.

Description	Manufacturer
DMEM high glucose (25 mM), with L-glutamine (4 mM)	PAA
DMEM without glucose, without L-glutamine	PAA
DMEM HAM's F12 (1:1)	PAA

7.6.4 Kits

Table 13. Kits.

Description	Manufacturer
Cloned AMV First Strand Synthesis Kit	Invitrogen
Platinum SYBR Green qPCR Supermix	Invitrogen
Venor® GeM Mycoplasma Detection Kit	Minerva Biolabs

7.6.5 Primers for real-time qRT-PCR

Table 14. Gene-specific forward (-F) and reverse (-R) primers used for qRT-PCR experiments.

Primer pair	Primer sequence	Manufacturer
GFAT1-F	5'-TCCATGCAAGAGAGACGCAAA-3'	Invitrogen
GFAT1-R	5'-CGCCAGCTTCTGGATTTCATC-3'	Invitrogen
GFAT2-F	5'-AAGGAGATCTTCGAGCAGCCA-3'	Invitrogen
GFAT2-R	5'-AAATGGTCCTTCAAGCCACCC-3'	Invitrogen
GlcN-6-P *N*-acetyltransferase-F	5'-AACCCGATGAAACTCCCATG-3'	Invitrogen
GlcN-6-P *N*-acetyltransferase-R	5'-TCAAAACCAAGCCTTCTCCAG-3'	Invitrogen
UDP-GlcNAc pyrophosphorylase-F	5'-GATGGACGGCTGCTGTTCAAT-3'	Invitrogen
UDP-GlcNAc pyrophosphorylase-R	5'-TGGTGCTGCAACTGAGGTTCA-3'	Invitrogen

7.6.6 Equipment

Table 15. List of equipment in alphabetical order.

Instrument	Name	Manufacturer
Autoclav	ELV 3850	Tuttnauer Systec
	Laboklav	HSP
Bench	Labgard NU-440-400E Class II Biological Safety Cabinets	Nuaire
Camera	Powershot A95	Canon

Instrument	Name	Manufacturer
Centrifuges	Centrifuge 5810 Centrifuge 5415D Heraeus Pico 17 Centrifuge	Eppendorf Eppendorf Thermo Electron Cooperation
Hemocytometer	Neubauer improved; depth 0,100 mm	Marienfeld
Incubator	IR Autoflow CO_2 water-jacketed incubator	Nuaire
Lyophilizer	Beta A Alpha 1-2 LD Plus	Christ Christ
Microscale	MC 210 S	Sartorius
Microscope	Axiovert 25	Zeiss
NMR sample changer	SampleXpress Bruker	Bruker
NMR spectrometer (250 MHz)	Bruker Avance DPX 250 5 mm inverse broadband probe with z-gradient	Bruker
NMR spectrometer (500 MHz)	Bruker Avance DRX 500 Bruker Avance III 500 TCI cryogenic probe	Bruker
PCR cycler	TGradient Thermoblock	Biometra
pH-electrode	Hamilton Spintrode	Hamilton
Real-time PCR instrument	ABI Prism 7000 Sequence Detection System	Applied Biosystems
RNA purification instrument	6100 Nucleic Acid Prepstation	Applied Biosystems
Rotary evaporator		
Spectrophotometer	NanoDrop ND-1000 Spectrophotometer	Peqlab
Vortex mixer	IKA® Vortex Genius 3	IKA

7.6.7 Consumables

Table 16. List of consumables and glassware.

Description	Manufacturer
75 cm^2 cell culture flasks; filter-vented cap	Sarstedt
175 cm^2 cell culture flasks; filter-vented cap	Sarstedt
10 cm diameter petri dishes	Sarstedt
Serological pipettes; plugged, sterile, non-pyrogenic (5 mL, 10 mL, 25 mL)	Sarstedt
Syringes (1 mL, 5 mL, 10 mL)	B.Braun
Needles of different gauges (20G, 21G, 25)	B.Braun
0,22 µM Filter; (Millex®-GV 0,22 µm Filter Unit	Millipore
Cell scrapers; thin, flexible, 2-position blades, 25 cm	Sarstedt
Rotilabo®-syringe filters; sterile, 0,22 µm	Roth
Tubes with screw cap; sterile, non-pyrogenic (15 mL, 20 mL)	Sarstedt
Nunc® CryoTubes®; cryogenic vial, 1,0 mL, internal thread	Nunc

Description	Manufacturer
Glassware:	
3 mm NMR Tubes for Bruker MATCH holder	Hilgenberg
Glass evaporating flasks (25 mL; NS 29/32)	Schott Duran
Glass centrifuge tubes (10 mL)	Schott Duran

Acknowledgment

First of all, I would like to gratefully thank Prof. Dr. Thomas Peters for giving me the opportunity to work on my doctoral thesis under his supervision and for introducing me into this interesting and exciting research project. I would like to acknowledge his support and advice while at the same time giving me the opportunity to develop my own ideas for my doctoral thesis. I would also like to thank him for revision of the manuscript and for the possibility to present parts of my results at international conferences.

A special thank goes to Prof. Dr. Olaf Jöhren for a very successful cooperation during my thesis and for being the second referee of my thesis. In this regard I would like to thank Christine Eichholz for providing the astrocytes I used in my research and for the helpful assistance with the qRT-PCR experiments.

I would also like to thank Prof. Dr. Norbert Tautz for his willingness to chair the examination board.

Prof. Dr. Luc Pellerin I would like to thank for the fruitful discussions about brain cell metabolism and his advice for further experimental work.

I would like to thank all members of the Institute of Chemistry at the University of Lübeck for their continuous help and support in many respects:

Many thanks goes to Dr. Thorsten Biet for his excellent supervision and his ongoing assistance with NMR spectroscopic experiments.

Dr. Anika Hellberg I would like to thank for the introduction into the project and for the nice teamwork.

Dr. Hanne Peters I would like to thank for her continuing assistance in the lab and many productive discussions.

I would like to thank Prof. Dr. Karsten Seeger for many fruitful discussions, advice, and for the interest in my research topic.

I would like to thank Tobias Schöne, who was assigned to my project during his bachelor thesis, for many productive discussions, experimental progress and for the fun-times working late in the lab (including all catchy tunes).

Lena Lisbeth Grimm, Sophie Weißbach, Anna Tomhardt, Sarah Schöning, and Mila Leuthold I would like to thank for the excellent teamwork - even far beyond the end of workday. I like to remember our “Kolleginnenkochen“, “Modischen Mittwoch“, “Reich und Schön Party“, the pub quiz, and many more.

Finally, I would like to thank all members of the group (Dr. Brigitte Fiege, Dr. Nora Begemann, Dr. Rosa Pulz, Dr. Thomas Weimar, Thies Köhli, Willy Hellebrandt, Christiane Blunk, Petra Lipp, and others) for providing such a pleasant working atmosphere.

Last but not least, I cordially thank my parents Barbara Döpkens and Dr. Joachim Döpkens and Niels Eckstein who have loved and supported me during the whole journey of my education and doctoral thesis. Without them I would not have been able to complete this work.

This study was financially supported by Deutsche Forschungsgemeinschaft (DFG Clinical Research Group “Selfish Brain“).

Publications

Journals

Wijnen JP1, Jiang L, Greenwood TR, Cheng M, Döpkens M, Cao MD, Bhujwalla ZM, Krishnamachary B, Klomp DW, Glunde K. Silencing of the glycerophosphocholine phosphodiesterase GDPD5 alters the phospholipid metabolite profile in a breast cancer model in vivo as monitored by ^{31}P MRS. *NMR Biomed* 27(6), 692-699 (2014).

Döpkens M, Greenwood TR, Vesuna F, Raman V, Leibfritz D, Glunde K. GDPD5 inhibition alters the choline phospholipid metabolite profile of breast cancer cells toward a less malignant metabolic profile. *BSI* 1(1), 3-15 (2012).

Cao MD, Döpkens M, Krishnamachary B *et al.* Glycerophosphodiester phosphodiesterase domain containing 5 (GDPD5) expression correlates with malignant choline phospholipid metabolite profiles in human breast cancer. *NMR Biomed* 25(9), 1033-1042 (2012).

Oral Presentations

Döpkens M, Blackwell TR, Vesuna F, Raman V, Krishnamachary B, Bhujwalla ZM, Leibfritz D, and Glunde K. Silencing of GDPD5 increases glycerophosphocholine levels in human breast cancer cells and may provide an anticancer target. Joint Annual Meeting ISMRM (International Society for Magnetic Resonance in Medicine)-ESMRMB, Stockholm, Sweden, May 1 – 7, 2010.

Poster

Döpkens M*, Gallinger A*, Biet T, Pellerin L, Peters T. Insight into neural cell metabolism by NMR- employing UDP-GlcNAc as a metabolic marker. * these authors contributed equally, EUROMAR 2011 Magnetic Resonance Conferecne/33rd Discussion Meeting of the MR Spectroscopy Division of the German Society of Chemistry (GDCh), Frankfurt am Main, Germany, August 21 - 25, 2011.

Döpkens M*, Gallinger A*, Biet T, Pellerin L, Peters T. Insight into neural cell metabolism by NMR- employing UDP-GlcNAc as a metabolic marker. * these authors contributed equally, ISMRM (International Society for Magnetic Resonance in Medicine) 19th Annual Meeting & Exhibition, Montréal, Québec, Canada, May 7 - 13, 2011.

Döpkens M, Gallinger A, Biet T, Pellerin L, Peters T. ^{15}N-NMR spectroscopic studies on UDP-GlcNAc as a metabolic marker in neuronal HT-22 cells. 32nd Discussion Meeting and Joint Benelux/German MR Conference of the German Society of Chemistry (GDCh), Muenster, Germany, September 20 – 23, 2010.

Gallinger A*, Döpkens M*, Biet T, Pellerin L, Peters T. UDP-GlcNAc as a metabolic marker in neuronal cell – facile detection by NMR. * these authors contributed equally, 2nd Selfish Brain Conference – New Research on the Neurobiology of Ingestive Behavior, Luebeck, Germany, May 27 – 28, 2010.

Döpkens M, Blackwell TR, Vesuna F, Raman V, Krishnamachary B, Bhujwalla ZM, Leibfritz D, and Glunde K. Magnetic resonance spectroscopy detects silencing of the novel anticancer target GDPD5 in human breast cancer cells. AACR (American Association for Cancer Research) 101st Annual Meeting, Washington, DC, USA, April 17 – 21, 2010. (presented by Glunde K on my behalf)